HAL
open science

GRANULAR PLATFORM REINFORCED BY GEOSYNTHETICS ABOVE CAVITIES : Laboratory experiments and numerical modeling of load transfer mechanisms

Minh Tuan Pham

To cite this version:

Minh Tuan Pham. GRANULAR PLATFORM REINFORCED BY GEOSYNTHETICS ABOVE CAVITIES : Laboratory experiments and numerical modeling of load transfer mechanisms. Materials Science [cond-mat.mtrl-sci]. Université Grenoble Alpes, 2019. English. NNT : 2019GREAI025 . tel-02171246

HAL Id: tel-02171246

https://theses.hal.science/tel-02171246

Submitted on 2 Jul 2019

HAL is a multi-disciplinary open access archive for the deposit and dissemination of scientific research documents, whether they are published or not. The documents may come from teaching and research institutions in France or abroad, or from public or private research centers.

L'archive ouverte pluridisciplinaire **HAL**, est destinée au dépôt et à la diffusion de documents scientifiques de niveau recherche, publiés ou non, émanant des établissements d'enseignement et de recherche français ou étrangers, des laboratoires publics ou privés.

Communauté UNIVERSITÉ Grenoble Alpes

THÈSE

Pour obtenir le grade de

DOCTEUR DE LA COMMUNAUTE UNIVERSITE GRENOBLE ALPES

Spécialité : **Ingénierie – Matériaux, Mécanique, Energétique, Environnement, Procédés, Production**

Arrêté ministériel : 25 mai 2016

Présentée par

Minh Tuan PHAM

Thèse dirigée par **Daniel DIAS** et
codirigée par **Laurent BRIANÇON**

préparée au sein du **Laboratoire 3SR**
dans **l'École Doctorale IMEP2**

GRANULAR PLATFORM REINFORCED BY GEOSYNTHETICS ABOVE CAVITIES
Laboratory experiments and numerical modeling of load transfer mechanisms

Thèse soutenue publiquement le **04 Avril 2019,**
devant le jury composé de :

M. Daniel DIAS
Professeur, Université Grenoble Alpes, Directeur de thèse
M. Laurent BRIANÇON
Maître de Conférences, INSA de Lyon, Co-directeur de thèse
M. Nicola MORACI
Professeur, Mediterranean University of Reggio Calabria, Rapporteur
M. Shijin FENG
Professeur, Tongji University, Rapporteur
M. Pascal VILLARD
Professeur, Université Grenoble Alpes, Présidente du Jury
M. Philippe DELMAS
Professeur, CNAM, Examinateur
Mme. Orianne JENCK
Maître de Conférences, Université Grenoble Alpes, Examinateur
Mme. Claire SILVANI
Maître de Conférences, INSA de Lyon, Examinateur
M. Abdelkader ABDELOUHAB
Docteur-Ingénieur, Texinov, Invité

GRANULAR PLATFORM REINFORCED BY GEOSYNTHETICS ABOVE CAVITIES

Laboratory experiments and numerical modeling of load transfer mechanisms

By

PHẠM MINH TUẤN

(Email: pmtuanbk@gmail.com)

[PhD thesis defended on April 4, 2019 at INSA de Lyon, France]

ACKNOWLEDGMENTS

What can you do for three years? An interesting question with many answers, and for me, one of the most amazing things is having a wonderful trip to France. My unexpected journey began due to contact from Grenoble, which gave a hint on a charming country in the West. Of course, this was not a relaxed tour for me, but I have never regretted my choice.

Indeed, I have encountered many difficulties during my doctorate, and I cannot finish my work alone. I am enormously grateful to my supervisor, *Professor Daniel Dias* for his guidance and encouragement with all aspects of this study. Besides, I wish to express my sincere appreciation to my co-supervisor *Doctor Laurent Briançon*, a kind person, a visionary manager and a master in geosynthetic investigations, for guiding me directly at the LabCom PITAGOR and for his endless support. My both supervisors invested a great deal of time in my doctorate; I genuinely appreciate their enthusiasm for answering all my questions. Working with them helps me improve myself, let me find joys in doing research, truthfully.

This research described in this thesis was performed from February 2016 to December 2018, in the framework of the new French Laboratory of Technical Innovations applied to Reinforcement Geosynthetics (PITAGOR) funded in December 2015 by the French National Research Agency (ANR-15-LCV3-0003). Thanks are also due to the Ministry of Education and Training of Vietnam, who awarded a scholarship for my thesis. During three years, I have much enjoyed and benefited from the exceptional environment that exists in the GEOMAS laboratory, where I stay during my doctorate. Primarily, I very much appreciated the technicians, who helped me substantially for the laboratory tests. I owe my Vietnamese friends for their help with the difficulties in life.

Researching over the years at a place far away 10 000 km from home is not easy. To be honest, after working time, living with my own family in a country of *Tour Eiffel* is a beautiful experience. I would like to send my greatest thanks to my parents, my mother-in-law, who dare to fly for thirteen hours to visit me, to my wife *Hạnh* as she comes to stay with me, be on my side, in the most challenging times and of course, to my children, *Léo* and *Léa*. One day, you will be able to read this sentence to know you are the motivation to finish this work.

From Lyon, a city of lights.

Dành tặng bố mẹ, vợ và hai con Léo, Léa của tôi!

SUMMARY

The progressive development of the territory leads to the exploitation of new areas, which are currently being abandoned because they come up with risks to the safety of users. This is particularly the case for areas of potential collapse that are related to the presence of underground cavities. Among the many preventative solutions, geosynthetic reinforcement prevents localized collapse. This solution is widely used for both its economic and environmental benefits, as well as for its ease and speed of setting up. However, the existing design methods for granular platforms reinforced by geosynthetic are based on various simplifying assumptions and do not take the complexity of the problem into account. These methods do not consider, for example, the influence of how the cavity is opened, the expansion of granular soil above the cavity, or the real stress distribution on the geosynthetic after opening the cavity.

The present study tries to improve the design methods by analyzing mechanisms developed inside the reinforced granular platform on the basis of an experimental study coupled with numerical simulations.

An experimental device was developed to simulate the opening of a cavity under a platform reinforced by geosynthetic. This device allows simulating two types of opening: a trapdoor or a concentric opening, for various heights of platforms. The mechanisms are studied by measuring the deflection of the geosynthetic, the settlement at the surface and the stress distribution applied on the geosynthetic. A Finite element model was calibrated on the experimental results then used to analyze mechanisms finely for many configurations.

This experimental and numerical study allows improving the understanding of the stress distribution, the soil expansion above the cavity and experimentally validated the influence of the opening mode on the mechanisms. Based on these results, proposals are formulated to improve the design of geosynthetic-reinforced platforms subject to localized collapse.

RÉSUMÉ

L'aménagement progressif du territoire conduit à l'exploitation de nouvelles zones, actuellement délaissées, car présentant des risques pour la sécurité des usagers. C'est notamment le cas des zones d'effondrements potentiels qui sont liées à la présence de cavités souterraines. Parmi les nombreuses solutions préventives, le renforcement géosynthétique permet de prévenir les risques d'effondrements localisés. Cette solution de renforcement est largement utilisée à la fois pour ses avantages économiques et environnementaux, que pour sa facilité et rapidité de mise en œuvre. Néanmoins, les méthodes de conception existantes des plateformes granulaires renforcées par géosynthétiques sont fondées sur diverses hypothèses simplificatrices et ne prennent pas en compte toute la complexité du problème. En effet, ces méthodes ne considèrent pas, par exemple, l'influence du mode d'ouverture de la cavité, le foisonnement du sol granulaire au droit de la cavité ou encore la distribution de charge sur le géosynthétique après ouverture de la cavité.

La présente étude tente d'améliorer les méthodes de dimensionnement en analysant les mécanismes développés dans la plateforme granulaire renforcée sur la base d'une campagne expérimentale couplée à des modélisations numériques.

Un dispositif expérimental a été développé pour simuler l'ouverture d'une cavité sous une plateforme renforcée par géosynthétique. Ce dispositif permet de simuler deux modes d'ouverture : une trappe qui s'abaisse ou une ouverture concentrique, pour différentes hauteurs de plateformes. Les mécanismes de renforcement sont étudiés en mesurant la déflexion du géosynthétique, le tassement en surface et la distribution de contrainte verticale qui s'applique sur le géosynthétique. Un modèle numérique par éléments finis a été calibré sur les résultats expérimentaux puis utilisé pour analyser finement les mécanismes pour de nombreuses configurations.

Cette étude expérimentale et numérique a permis d'améliorer la compréhension des mécanismes de transfert de charge et de foisonnement dans la zone effondrée et de valider expérimentalement l'influence du mode d'ouverture sur les mécanismes. Sur la base de ces résultats, des propositions sont formulées pour améliorer le dimensionnement des plateformes renforcées par géosynthétiques soumises à des effondrements localisés.

TABLE OF CONTENTS

ACKNOWLEDGEMENTS ..... **i**

SUMMARY ..... **iii**

RÉSUMÉ ..... **iv**

TABLE OF CONTENTS ..... **v**

LIST OF FIGURES ..... **x**

LIST OF TABLES ..... **xiv**

NOMENCLATURE ..... **xv**

CHAPTER 1. INTRODUCTION **1**

1.1. GEOSYNTHETIC-REINFORCED SOILS 2

1.1.1. General definition of geosynthetics *2*

1.1.2. Geosynthetic-reinforced soils applications *4*

1.2. OVERVIEW OF GEOSYNTHETIC-REINFORCED EMBANKMENT SPANNING CAVITIES 6

1.3. PROJECTS OF REINFORCED EMBANKMENT SPANNING CAVITIES 8

1.3.1. High-speed railway, LGV Est, Lorraine, France (Tencate, 2010) *8*

1.3.2. Public park, Arras, France (Texinov, 2018a) *9*

1.3.3. Football field, Barcelona, Spain (Tencate, 2010) *10*

1.3.4. Embankment on mining area, Estonia (Texinov, 2018b) *11*

1.3.5. Discussion on the design methods *12*

1.4. OBJECTIVES AND SCOPE OF THESIS 13

1.5. THESIS OUTLINE 14

CHAPTER 2. LITERATURE REVIEW **15**

2.1. INTRODUCTION 16

2.2. SOIL ARCHING THEORIES 16

2.2.1. Terzaghi *16*

2.2.2. Handy *18*

2.2.3. Vardoulakis *19*

2.2.5. Arching theories comparison *20*

2.3. REINFORCED STRUCTURE MECHANISMS 22

2.3.1. Membrane effect and friction behavior *22*

2.3.2. Load acting on the geosynthetic sheet *23*

2.3.3. Soil expansion *23*

2.4. EXISTING ANALYTICAL METHODS 24

2.4.1. British Standard (2010) *24*
2.4.1.1. Principles *24*
2.4.1.2. Design *26*
2.4.2. French recommendations *27*
2.4.2.1. RAFAEL *27*
2.4.2.2. New recommendations XP G 38063-2 ..... *29*
2.4.3. EBGEO (1997, 2011) *33*
2.4.3.1. Principles *33*
2.4.3.2. Design *34*
2.4.4. Design methods comparison *38*
2.4.5. Other methods and summary *42*
2.4.5.1. Specific developments *42*
2.4.5.2. Summary *43*
2.5. KEY EXPERIMENTAL STUDIES 44
2.5.1. Experimental testing of arching effect by Costa et al., 2009 ..... *44*
2.5.2. Arching effect study by Pardo and Sáez, 2014 ..... *46*
2.5.3. Laboratory tests of soil arching by Rui et al., 2016a *47*
2.5.4. Model tests of interaction between soil and geosynthetics of Zhu et al., 2012 ..... *48*
2.5.5. Experimental and numerical tests on geosynthetic of Huang et al., 2015 ..... *50*
2.5.6. Full-scale experiment of cavity by Huckert et al., 2016 ..... *52*
2.5.7. Other experimental studies *53*
2.5.8. Summary of experimental studies *54*
2.6. NUMERICAL ANALYSIS 56
2.6.1. Finite element method *57*
2.6.2. Key numerical studies *58*
2.6.2.1. Experimentation and numerical simulation of Schwerdt et al., 2004 ..... *58*
2.6.2.2. Finite element models of Potts (2007) *60*
2.6.2.3. Numerical approach by Villard et al. (2016) *62*
2.6.2.4. Numerical approach of Yu and Bathurst (2017) *63*
2.6.2.5. Other numerical studies *66*
2.6.3. Summary of numerical studies *68*
2.7. CONCLUSIONS 70

CHAPTER 3. LABORATORY EXPERIMENT 73

3.1. INTRODUCTION 74
3.2. LABORATORY TEST 74
3.2.1. Description *74*
3.2.2. Model setup *75*

3.3.2.1. Device *75*
3.2.2.2. Tested soils *76*
3.2.2.3. Tested geosynthetics *77*
3.2.3. Monitoring *78*
3.2.3.1. Displacement sensors *78*
3.2.3.2. Tactile pressure sensor *80*
3.2.4. Test program *83*
3.2.4.1. Platform set-up *83*
3.2.4.2. Displacement measurement procedure *83*
3.2.4.3. Stress measurement procedure *83*
3.2.5. Analysis procedures *84*
3.2.5.1. Soil expansion *84*
3.2.5.2. Shape of collapsed soils *86*
3.2.5.3. Load distribution *87*
3.2.5.4. Efficiency of load transfer *88*
3.3. RESULTS AND ANALYZES 89
3.3.1. Settlement and deflection *89*
3.3.2. Influence of experimental conditions *91*
3.3.2.1. Repeatability *91*
3.3.2.2. Opening methods *91*
3.3.2.3. H/D ratio *92*
3.3.3. Expansion analysis *94*
3.3.3.1. Shape of deformed zone *94*
3.3.3.2. Comparison of coefficients estimated by different methods *95*
3.3.3.3. Influence of density *97*
3.3.3.4. Conclusion on the expansion coefficient *98*
3.3.4. Load transfer mechanisms over evolving cavity (Program 1) *99*
3.3.4.1. Load transfer on anchorage areas *99*
3.3.4.2. Comparison between cavity area and anchorage area *101*
3.3.5. Load transfer mechanisms over existing cavity (Program 2) *105*
3.4. IMPROVEMENT TO BRING TO THE EXPERIMENTATION 108
3.5. CONCLUSIONS 109

CHAPTER 4. NUMERICAL SIMULATIONS 111

4.1. INTRODUCTION 112
4.2. FINITE ELEMENT ANALYSIS 112
4.2.1. Numerical modeling *112*
4.2.1.1. Basic concept *112*

4.2.1.2. Soil constitutive models *114*
4.2.1.3. Materials *115*
4.2.1.4. Geosynthetics elements *116*
4.2.1.5. Interface elements *116*
4.2.2. Numerical analysis of the physical model *117*
4.2.2.1. Initial and boundary conditions *117*
4.2.2.2. Cavities opening methods *118*
4.2.2.3. Calculation phases *118*
4.2.3. Sensitivity analysis of input parameters *118*
4.2.3.1. Overlying soil characteristics *119*
4.2.3.2. Tensile stiffness of geosynthetics *120*
4.3. KINEMATIC ANALYSIS OF EMBANKMENTS 122
4.3.1. Surface settlement *122*
4.3.2. Geosynthetic deflection *124*
4.3.3. Influence of the soil constitutive model *128*
4.4. SOIL EXPANSION ANALYSIS 129
4.4.1. Expansion coefficient *129*
4.4.2. Effect of geometrical configurations *134*
4.5. LOAD TRANSFER ANALYSIS 136
4.5.1. Load transfer on cavity area *136*
4.5.2. Efficiency of the load transfer *141*
4.5.3. Effect of the cavity diameter *143*
4.5.4. Effect of the surcharges *146*
4.6. CONCLUSIONS 149

CHAPTER 5. RESULTS DISCUSSION 151

5.1. INTRODUCTION 152
5.2. LOAD DISTRIBUTION 152
5.2.1. Shape of the load distribution *152*
5.2.2. Earth pressure coefficient *153*
5.2.3. Load transfer efficiency *154*
5.3. DEFLECTION BEHAVIORS 155
5.3.1. Shape of subsidence zone *155*
5.3.2. Influences on vertical displacements *155*
5.3.3. Geosynthetic strain *155*
5.3.4. Equal settlement plane *156*
5.4. SOIL EXPANSION COEFFICIENT 156
5.5. DESIGN PROCEDURE 157

5.5.1. Cavity characteristics estimation *157*

5.5.2. Mechanical parameters measurement *158*

5.5.3. Geosynthetic tensile stiffness determination *158*

CHAPTER 6. CONCLUSIONS 159

6.1. EXPERIMENTAL APPROACH 160

6.2. NUMERICAL APPROACH 160

6.3. RECOMMENDATIONS 161

REFERENCES 163

APPENDIX A 171

APPENDIX B 175

LIST OF FIGURES

FIGURE 1.1. GEOSYNTHETICS FUNCTIONS (IGS, 2018A) 3

FIGURE 1.2. REINFORCED SOIL APPLICATIONS 5

FIGURE 1.3. LOAD DISTRIBUTION IN PILED EMBANKMENTS (VAN EEKELEN, 2015) 6

FIGURE 1.4. DIFFERENT CAUSES OF CAVITIES (URETEK) 7

FIGURE 1.5. TYPICAL CROSS-SECTION THROUGH THE REINFORCED TRACK STRUCTURE, LGV EST, LORRAINE, FRANCE (TENCATE, 2010) 9

FIGURE 1.6. CROSS SECTION DETAILS THROUGH THE REINFORCED FOUNDATION, BARCELONA, SPAIN (TENCATE, 2010) 11

FIGURE 1.7. EUROPEAN ROUTE E20, TALLINN-NARVA SECTION, ESTONIA (TEXINOV, 2018B) 12

FIGURE 2.1. THE PRINCIPLE OF THE ARCHING EFFECT (TERZAGHI, 1943) 17

FIGURE 2.2. STATE OF THE STRESS AT A BOUNDARY POINT OF THE SLIDING MASS REPRESENTED IN MOHR CIRCLE (HANDY, 1985) 19

FIGURE 2.3. STRESS APPLIED TO THE CAVITY IN DIFFERENT METHODS OF CALCULATION 21

FIGURE 2.4. MEMBRANE EFFECT (BRIANÇON AND VILLARD, 2008) 22

FIGURE 2.5. DEFINITION OF EFFICIENCY BASED ON W_S AND F_G 23

FIGURE 2.6. CONCEPTUAL ROLE (BS8006, 2010) 25

FIGURE 2.7. DESCRIPTION OF PARAMETERS FOR DESIGN METHOD (BS8006, 2010) 25

FIGURE 2.8. MECHANISM AT THE EDGE OF THE CAVITY (BRIANÇON AND VILLARD, 2008) 30

FIGURE 2.9. EQUILIBRIUM OF AN ELEMENTARY SECTION: $U_A \leq U_0$ (A) AND $U_A > U_0$ (B), VILLARD AND BRIANÇON (2008) 30

FIGURE 2.10. DESIGNATIONS 33

FIGURE 2.11. MODEL CONFIGURATION OF COSTA ET AL. (2009) 45

FIGURE 2.12. TRAPDOOR DEVICE SCHEME OF PARDO AND SÁEZ (2014) 46

FIGURE 2.13. LOAD DISTRIBUTION ON RIGID SUPPORT OF THE BOX (PARDO AND SÁEZ, 2014) 47

FIGURE 2.14. TEST SETUP (RUI ET AL., 2016A) 48

FIGURE 2.15. LAYOUT OF MODEL TESTS (ZHU ET AL., 2012) 49

FIGURE 2.16. ILLUSTRATION OF FIRST (A) AND SECOND (B) TEST STRATEGIES (ZHU ET AL., 2012) 50

FIGURE 2.17. PHOTO OF TEST BY HUANG ET AL., 2015 51

FIGURE 2.18. SCHEMA OF FULL-SCALE EXPERIMENT (HUCKERT ET AL., 2016) 52

FIGURE 2.19. ANALYTICAL AND EXPERIMENTAL GEOSYNTHETIC STRAIN (HUCKERT ET AL., 2016) 52

FIGURE 2.20. MODEL OF THE LAYERS FOR THE PLAXIS CALCULATIONS (SCHWERDT ET AL., 2004) 59

FIGURE 2.21. EXPERIMENT TEST SET-UP (POTTS, 2007)..... 61

FIGURE 2.22. KEY RESULTS OF NUMERICAL SIMULATIONS (VILLARD ET AL., 2016) 63

FIGURE 2.23. SIMULATION WORKS OF YU AND BATHURST (2017) 65

FIGURE 3.1. EXPERIMENTAL DEVICE 76

FIGURE 3.2. OPENING METHODS: TRAPDOOR PROCEDURE (A), AND PROGRESSIVE PROCEDURE (B) 76

FIGURE 3.3. TESTED GEOSYNTHETICS 77

FIGURE 3.4. LOCATION OF DISPLACEMENT MONITORING SENSORS 79

FIGURE 3.5. PHOTOGRAPHS OF DISPLACEMENT SENSORS 79

FIGURE 3.6. INTERFACE OF SOFTWARE FOR DISPLACEMENT MEASUREMENT 80

FIGURE 3.7. PHOTOGRAPH OF TPS ON THE ANCHORAGE AREA OF THE CAVITY..... 81

FIGURE 3.8. LOCATIONS OF TPS AT THE ANCHORAGE, THE BORDER AND THE CENTER OF CAVITY 81

FIGURE 3.9. LOCATION OF TPS BEFORE AND AFTER THE CAVITY OPENING 82

FIGURE 3.10. CHAMELEON TVP SOFTWARE INTERFACE 82

FIGURE 3.11. ILLUSTRATION OF VOLUMES OF SOIL SETTLEMENT AND GEOSYNTHETIC DEFLECTION 86

FIGURE 3.12. TWO PARTS OF DEFORMATION CURVES..... 86

FIGURE 3.13. SHAPE OF COLLAPSED SOIL 87

FIGURE 3.14. SELECTED AREAS ON TPS (1-5) 87

FIGURE 3.15. A TYPICAL COMPARISON OF DEFLECTED GEOSYNTHETIC (FINE SAND & WOVEN GSY) 90

FIGURE 3.16. GEOSYNTHETIC DEFLECTION OF WOVEN GEOSYNTHETIC TESTS 92

FIGURE 3.17. GEOSYNTHETIC DEFLECTION OF NONWOVEN GEOSYNTHETIC TESTS..... 92

FIGURE 3.18. SURFACE SETTLEMENT OF WOVEN GEOSYNTHETIC TESTS 93

FIGURE 3.19. ESTIMATION OF EQUAL SETTLEMENT PLANE FOR WOVEN GEOSYNTHETIC 93

FIGURE 3.20. SURFACE SETTLEMENT OF NONWOVEN GEOSYNTHETIC TESTS 94

FIGURE 3.21. ESTIMATION OF THE EQUAL SETTLEMENT PLANE FOR NONWOVEN GEOSYNTHETIC 94

FIGURE 3.22. SHAPE FORMS OF EMBANKMENT: T – TRUNCATED SHAPE, C – CYLINDRICAL SHAPE 95

FIGURE 3.23. COMPARISON BETWEEN TWO MODELS TO FIT THE CURVES OF MEASUREMENT DATA 96

FIGURE 3.24. COMPARISON OF CE VALUES ESTIMATED USING TWO DIFFERENT METHODS FOR MODE A TESTS..... 97

FIGURE 3.25. COMPARISON OF CE VALUES COMPUTED USING TWO DIFFERENT METHODS FOR MODE B TESTS 97

FIGURE 3.26. CE VALUES OF COARSE SAND TESTED MODE B, H/D = 0.5, AND WOVEN GSY.....98

FIGURE 3.27. EFFICIENCY OF TESTS WITH AN H/D VALUE OF 0.5 AND WOVEN GEOSYNTHETICS 100

FIGURE 3.28. TPS LOCATED AT THE BORDER OF THE CAVITY.....101

FIGURE 3.29. STRESS VARIATION MEASURED BY TPS PLACED AT CAVITY BORDER 101

FIGURE 3.30. STRESS VARIATION MEASURED BY TPS COMPARING TO DIFFERENT LOCATIONS.....102

FIGURE 3.31. INCREASE OF STRESS AFTER CAVITY OPENING (PROGRAM 1).....103

FIGURE 3.32. COMPARISON OF STRESS RATIO BETWEEN PROGRAM 2 (MODE A).....105

FIGURE 3.33. COMPARISON OF STRESS RATIO BETWEEN PROGRAM 2 (MODE B).....105

FIGURE 3.34. COMPARISON OF LOAD DISTRIBUTION BETWEEN PROGRAM 1 AND 2 (MODE A).....106

FIGURE 3.35. COMPARISON OF LOAD DISTRIBUTION BETWEEN PROGRAM 1 AND 2 (MODE B).....106

FIGURE 3.36. SHAPES OF DEFLECTED GEOSYNTHETIC OF MODE B (PROGRAM 2) 107

FIGURE 3.37. STRETCHING OF GEOSYNTHETICS ON TEST TABLE 108

FIGURE 4.1. GEOMETRICAL CONFIGURATION FOR THE NUMERICAL CALCULATION 113

FIGURE 4.2. POSITIONS OF INTERFACE ELEMENTS USED IN THE NUMERICAL MODELING.....117

FIGURE 4.3. VARIATION OF SURFACE SETTLEMENT AND DEFLECTED GEOSYNTHETICS DUE TO CHANGING OF DILATANCY ANGLE AND EARTH PRESSURE COEFFICIENT.....120

FIGURE 4.4. VARIATION OF CE DUE TO CHANGING OF DILATANCY ANGLE AND EARTH PRESSURE COEFFICIENT.....120

FIGURE 4.5. VARIATION OF SURFACE SETTLEMENT AND DEFLECTED GEOSYNTHETICS DUE TO CHANGING OF GEOSYNTHETIC STIFFNESS.....121

FIGURE 4.6. VARIATION OF CE DUE TO CHANGING OF GEOSYNTHETIC STIFFNESS 121

FIGURE 4.7. COMPARISON OF SURFACE SETTLEMENT BETWEEN EXPERIMENTAL AND NUMERICAL RESULTS.....122

FIGURE 4.8. COMPARISON OF SURFACE SETTLEMENT BETWEEN EXPERIMENTAL AND NUMERICAL RESULTS.....123

FIGURE 4.9. COMPARISON OF DEFLECTED GEOSYNTHETICS BETWEEN EXPERIMENTAL AND NUMERICAL RESULTS 125

FIGURE 4.10. COMPARISON BETWEEN EXPERIMENTAL AND NUMERICAL RESULTS FOR THE MAXIMUM GEOSYNTHETICS DEFLECTION 126

FIGURE 4.11. COMPARISON OF GEOSYNTHETIC STRAINS AT CAVITY AREA BETWEEN TWO MODES OF CAVITY OPENING (FINE SAND AND WOVEN GEOSYNTHETIC).....127

FIGURE 4.12. EQUAL SETTLEMENT PLANE CALCULATED BY PLAXIS 128

FIGURE 4.13. DIFFERENCE OF THE MAXIMAL VERTICAL DISPLACEMENTS OF SURFACE SETTLEMENT AND GEOSYNTHETICS ...129

FIGURE 4.14. COMPARISON OF CE BETWEEN EXPERIMENTAL AND NUMERICAL RESULTS 130

FIGURE 4.15. CHANGE IN VOID RATIO WITHIN THE OVERLYING SOILS OVER REINFORCEMENT SYSTEMS (FINE SAND & WOVEN GSY) 132

FIGURE 4.16. AVERAGE VALUES OF VOID RATIO IN THE COLLAPSED SOIL 132

FIGURE 4.17. CHANGE IN DEVIATORIC STRAIN WITHIN THE OVERLYING SOILS OVER REINFORCEMENT SYSTEMS (FINE SAND & WOVEN GSY) 133

FIGURE 4.18. VARIATION OF SURFACE SETTLEMENT (A) AND DEFLECTED GEOSYNTHETICS (B) DUE TO CHANGING OF CAVITY DIAMETER, CASES OF FINE SAND 134

FIGURE 4.19. VARIATION OF CE DUE TO CHANGING OF CAVITY DIAMETER 135

FIGURE 4.20. NUMERICAL LOAD DISTRIBUTION ON CAVITY CALCULATED FOR FINE SAND TESTS 137

FIGURE 4.21. NUMERICAL LOAD DISTRIBUTION ON CAVITY CALCULATED FOR COARSE SAND TESTS 138

FIGURE 4.22. PRINCIPAL STRESS WITHIN THE FINE SAND OVER WOVEN GEOSYNTHETIC 139

FIGURE 4.23. PRINCIPAL STRESS WITHIN THE FINE SAND OVER WOVEN GEOSYNTHETIC WITH EVOLUTIONS OF THE TWO CAVITY OPENING 139

FIGURE 4.24. ESTIMATION OF THE STRESS RATIOS OF FINE SAND OVER GSY AFTER CAVITY OPENING 140

FIGURE 4.25. COMPARISON OF THE LOAD TRANSFER EFFICIENCY BETWEEN EXPERIMENTAL, DEM AND FEM RESULTS, CASES OF FINE SAND TESTS 142

FIGURE 4.26. NUMERICAL LOAD TRANSFER EFFICIENCY, CASES OF COARSE SAND TESTS 142

FIGURE 4.27. COMPARISON OF FINAL LOAD APPLIED ON GEOSYNTHETICS BETWEEN ANCHORAGE AND CAVITY AREAS 143

FIGURE 4.28. VARIATION OF THE LOAD DISTRIBUTION DUE TO THE CAVITY DIAMETER VARIATION: MODE A 144

FIGURE 4.29. VARIATION OF THE LOAD DISTRIBUTION DUE TO THE CAVITY DIAMETER VARIATION: MODE B 145

FIGURE 4.30. VARIATION OF THE LOAD TRANSFER EFFICIENCY DUE TO THE CAVITY DIAMETER VARIATION 146

FIGURE 4.31. SURCHARGE APPLIED ON OVERLYING SOIL ABOVE EXISTING CAVITY 147

FIGURE 4.32. COMPARISON BETWEEN THE FINAL LOAD ACTING ON GEOSYNTHETIC (FINE SAND AND PROGRAM 2) 147

FIGURE 4.33. COMPARISON OF THE LOAD DISTRIBUTION OBTAINED BY THE NUMERICAL MODELS BETWEEN PROGRAM 1 AND PROGRAM 2 148

FIGURE 5.1. COMPARISON OF STRESS RATIOS BETWEEN THE EXPERIMENT OF MODE A AND TERZAGHI'S THEORY 153

LIST OF TABLES

TABLE 2.1. CHARACTERISTICS OF FILL SOILS IN THE COMPARISON 20

TABLE 2.2. DESIGN PARAMETERS OF BRITISH STANDARD (2010) 26

TABLE 2.3. DESCRIPTION OF THE DESIGN PARAMETER OF RAFAEL METHOD 29

TABLE 2.4. DESIGN PARAMETERS OF EBGEO STANDARD (2011) 37

TABLE 2.5. PHYSICAL CHARACTERISTICS OF THE CURRENT DESIGN METHODS 38

TABLE 2.6. PARAMETERS FOR THE COMPARISON OF DESIGN METHODS 39

TABLE 2.7. RESULTS OF DESIGN METHODS IN CASE OF H/D = 0.5 40

TABLE 2.8. RESULTS OF DESIGN METHODS IN CASE OF H/D = 1.0 41

TABLE 2.9. SUMMARY OF MAIN CURRENT OUTCOMES OF EXPERIMENT STUDIES 55

TABLE 2.10. SURFACE SETTLEMENT AND MATERIAL DEFLECTION VALUES ARE TAKEN FROM MEASUREMENT AND PLAXIS (SCHWERDT ET AL., 2004) 59

TABLE 2.11. SUMMARY OF MAIN CURRENT OUTCOMES OF NUMERICAL STUDIES 69

TABLE 3.1. TESTED SOIL CHARACTERISTICS 77

TABLE 3.2. GEOSYNTHETIC CHARACTERISTICS 77

TABLE 3.3. WOVEN GEOSYNTHETIC TEST RESULTS 89

TABLE 3.4. NONWOVEN GEOSYNTHETIC TEST RESULTS 90

TABLE 3.5. REPEATABILITY TESTS 91

TABLE 3.6. COEFFICIENT OF DETERMINATION COMPARISON BETWEEN TWO MODELS 95

TABLE 3.7. STRESS VARIATION IN FINE SAND TESTS CALCULATED FROM ANCHORAGE AREAS TESTS 99

TABLE 3.8. STRESS VARIATION IN COARSE SAND TESTS CALCULATED FROM ANCHORAGE AREAS TESTS 100

TABLE 3.9. EFFICIENCY OF LOAD TRANSFER 104

TABLE 4.1. PARAMETERS FOR THE MOHR-COULOMB CONSTITUTIVE MODEL 115

TABLE 4.2. PARAMETERS FOR THE HARDENING SOIL CONSTITUTIVE MODEL FOR FINE SAND 115

TABLE 4.3. PARAMETERS FOR INTERFACES ELEMENTS 117

TABLE 4.4. VALUES OF CE CALCULATED BY NUMERICAL AND EXPERIMENT TESTS 131

TABLE 5.1. SUMMARY OF INFLUENCED FACTORS ON LOAD TRANSFER EFFICIENCY 154

TABLE 5.2. AVERAGE EXPANSION COEFFICIENT WITH THE CAVITY DIAMETER = 0.5 M 156

NOMENCLATURE

2-D	-	Two-dimensional space
3-D	-	Three-dimensional space
a, a'_1, a'_2	-	Interaction coefficients relating to the soil/reinforcement bond angle
f_{fs}	-	Partial load factor for soil
f_M		Vertical displacement of the geosynthetic at point M
f_d	-	Partial load factor for externally applied load
f_{ms}	-	Partial material factor
f_n	-	Partial factor governing the economic ramifications of failure
f_p	-	Partial factor applied to the pull-out resistance of the reinforcement
c', c_k	*kPa*	Cohesion
Cc	-	Curvature coefficient
Ce, Ce_1, Ce_2	-	Expansion coefficient
Cu	-	Uniformity coefficient
D	*m*	Cavity diameter
D_{50}	-	Intercept for 50% of cumulative mass
Dc	*m*	Inner diameter of cylinder
dg	*m*	Maximal deflection of geosynthetics (m)
D_{max}	*mm*	Maximum size of the grains
D_R	-	Relative density
D_s	*m*	Diameter of surface deformation
ds	*m*	Maximal surface settlement
E	*%*	Efficiency of load transfer
e_0	-	Void ratio
E_{50}	*MPa*	Secant modulus
$E_{cmd,d}$	*kN/m*	Design value of actions for geosynthetic cross machine direction
e_{max}	-	Void ratio of the soil at its loosest condition

$E_{md,d}$	*kN/m*	Design value of actions for geosynthetic machine direction
e_{min}	-	Void ratio of the soil at its densest condition
E_{oed}	*MPa*	Oedometer modulus
E_{ur}	*MPa*	Unloading/reloading stiffness
E_Y, E_i	*MPa*	Young's modulus
H, H_1, H_2	*m*	Embankment height (m)
H/D	-	Ratio between embankment height and cavity diameter
$H_{cmd,d}$	*kN/m*	Design value of horizontal tensile forces for geosynthetic cross machine direction
$H_{md,d}$	*kN/m*	Design value of horizontal tensile forces for geosynthetic machine direction
HS	-	Horizontal sensor (displacement sensor)
J	*kN/m*	Tensile stiffness per unit width of geosynthetic fabric
J_{cmd}	*kN/m*	Transverse axial stiffness for geosynthetic cross machine direction
J_{md}	*kN/m*	Axial stiffness for geosynthetic machine direction
K	-	Stress ratio between horizontal and vertical stress
K_a	-	Active pressure coefficient
L	*m*	Diameter/width of the void
L_A	*m*	Anchorage length
m	-	Power for stress-level dependency of stiffness
Mode A	-	Trapdoor/downward opening
Mode B	-	Progressive opening
Model 1	-	Parabolic curve for both geosynthetics and surface soil (expansion coefficient)
Model 2	-	Combination of the polynomial curve for geosynthetics and a Gaussian model for the surface soil (expansion coefficient)
N	-	Nonwoven geosynthetics
p, w_s	*kN/m²*	Surcharge
Program 1	-	Intermittent procedure to measure load distribution
Program 2	-	Continuous procedure to measure load distribution

Q, q, q_0	*kN/m²*	Total loads applied to the geosynthetic sheet
q_k	*kN/m²*	Live load
R^2	-	Coefficient of determination
s	*m*	Surface settlement
SC	-	Coarse sand
SF	-	Fine sand
T_1		Tensile force transmitted to anchorage area
T_A	*kN/m*	Tensile force in geosynthetic at the point A
T_H	*kN/m*	Horizontal tensile force in geosynthetic
T_M	*kN/m*	Tensile force in geosynthetic at point M
T_{max}	*kN/m*	Maximum tensile force per unit width of geosynthetic fabric
TPS	-	Tactile pressure sensor
U_0	*m*	Relative displacement from which friction mobilization becomes maximum
U_A	*m*	Horizontal displacement of the geosynthetic at point A
U_L	*m*	Overlap length
VS	-	Vertical sensor (laser sensor)
W	-	Woven geosynthetics
W_s	*kN*	Weight of cylindrical part of the soil sited over the cavity
X_{cmd}	*kN/m*	Load component factor for geosynthetic cross machine direction
X_{md}	*kN/m*	Load component factor for geosynthetic machine direction
θ_d, θ_k	°	Angle of the collapsed soil
$\sigma_{v,G,k}$	*kN/m²*	Normal stress in case of failure model without lateral reaction
$\sigma_{v,Q,k}$	*kN/m²*	Normal stress in case of failure model with lateral reaction
φ_A	°	Angle of the change in the orientation at geosynthetic edge
φ_{lower}	°	Lower interface angle between soil and geosynthetic
φ_{upper}	°	Upper interface angle between soil and geosynthetic
β	-	parameter characteristic of the change in orientation of the sheet at the point A

ε	*%*	Geosynthetic strain
ε_M	*%*	Sheet strain at the point M
ε_{max}	*%*	Maximum allowable strain in the reinforcement
λ	-	Coefficient dependent on the support direction
υ, υ_i	-	Possition's ratio
ϕ'	°	Friction angle of granular material
ψ	°	Dilatancy angle of soil
ω	-	Axial stiffness ratio
γ_s	kN/m^3	Unit weight of solids
γ	kN/m^3	Unit weight of soil
γ_K	kN/m^3	Unit weight of overlying soil
ρ	Mg/m^3	Density of soil
f	*m*	Deflection of geosynthetic
x	*m*	Initial horizontal position of point M
α	-	Angle at the geosynthetic boundary can be estimated by radius of cavity depression and deflection of geosynthetics
δ	°	Interface friction angle

CHAPTER 1. INTRODUCTION

Today, there is a significant increase in the constructions such as highways or railways to improve the infrastructure. However, in many areas, poor soils can seriously affect the use of structures or threaten safety. Forming by karstic phenomena or mining exploitation, underground cavities present a high risk to the stability and longevity of the structure. Many solutions such as piles, injection grouting or geosynthetics are widely used to withstand the formation of cavities and protect the structures.

In this chapter, a general definition of geosynthetics is described, and several applications in common geotechnical problems are presented. Then, an overview of the geosynthetic reinforcing embankment over cavities is specified, the principle of the solution is explained. Four fundamental constructions in Europe where the main problem was solved by geosynthetic reinforcement are presented to prove its application.

Finally, the objectives and scope are addressed to describe the aim of this study. A research plan and specific devices, which are used in the laboratory, are presented.

1.1. GEOSYNTHETIC-REINFORCED SOILS

1.1.1. General definition of geosynthetics

Geosynthetics are synthetic products that are specially manufactured to solve geosynthetic problems. Due to the polymeric nature, geosynthetic is suitable to be used in the ground with a high level of durability. By comparing to the traditional materials, geosynthetics have many capabilities including the long durability, simple design, rapid construction, consistent performance, and minor environmental impact. Geosynthetics are commonly used in civil engineering as a primary function or dual functions: separation, filtration, drainage, erosion control, and reinforcement.

- ***Separation:*** geosynthetic can be used as a separator to isolate layers of soil that have different characteristics (*Figure 1.1a*). For example, geotextile can be used between a fine-grained subgrade and the granular layer below an embankment.
- ***Filtration:*** geosynthetic material can prevent soils but allow water to move from migrating into the adjacent material, like a sand filter (*Figure 1.1b*).
- ***Drainage:*** geosynthetics can be used as a system of drains by allowing water to drain from low permeability soils (*Figure 1.1c*).

- ***Erosion control:*** geosynthetic act to limit the soil erosion caused by rainfall or surface water because it prevents the movement of soil particles from the fluid flow (*Figure 1.1d*).

- ***Reinforcement:*** geosynthetics can be used as a reinforcement element to improve the strength and mechanical properties of soils (*Figure 1.1e*). Geosynthetic-reinforced soils include several products which are relatively soft structures made of fibers can be produced as woven, non-woven or knitted, and geogrids, the more rigid appearance, can be formed by cable knitting, coating or extrusion. Currently, design and construction of geosynthetic-reinforced soils structures are commonly applied to many geotechnical engineering projects by the basic principle is to increase the shear strength of soils.

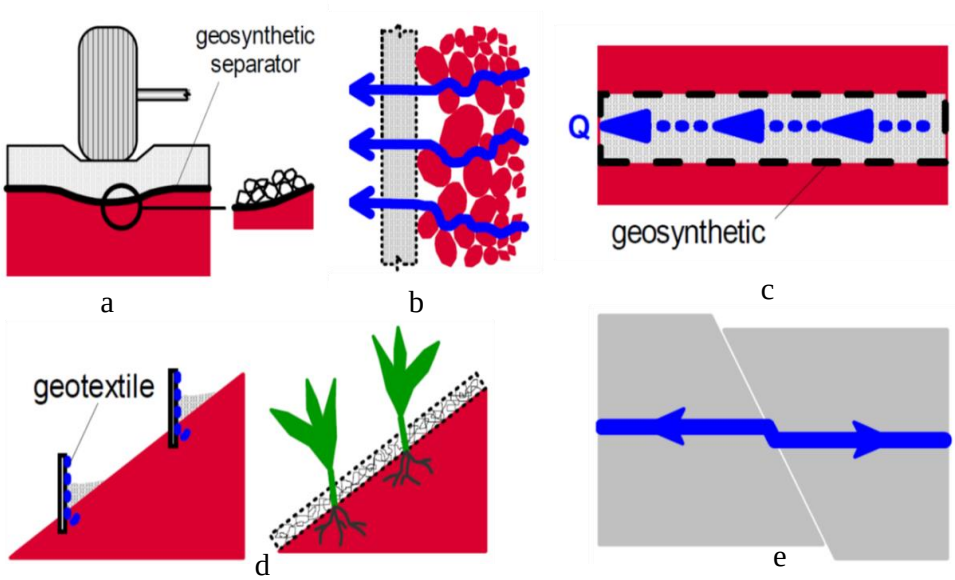

Figure 1.1. Geosynthetics functions (IGS, 2018a)

Moreover, geosynthetics are also used in other applications. They are used for asphalt pavement reinforcement, flexible concrete formworks, and sandbags. The geosynthetic materials can be used to limit the migration of fluid or to protect the surface of pavement structures from cracking in airports or roadways.

Based on the method of manufacture, the main product categories of geosynthetic can be listed as geotextiles, geogrids, geonets, geomembranes, geofoam, geocells, geocomposite, and geosynthetic clay liners.

- ***Geotextiles:*** the oldest product of geosynthetics can be supplied in two primary types: the woven and the nonwoven geotextiles differenced by the method of manufacture.

Geotextiles are applied for separation, filtration, drainage, erosion control and reinforcement.

- ***Geogrids:*** the materials have an open grid-form appearance. Their principle application is to reinforce or stabilize the soil. They can be used for retaining walls, steep slopes, dams, and levees.
- ***Geonets:*** the material formed by a continuous extrusion of parallel sets of polymeric ribs at a constant acute angle. An open-grid form material has an in-plane porosity that allows the movement of fluid or gas.
- ***Geomembranes:*** the continuous flexible sheets produced from one or more synthetic materials. The primary function of this product is to act as an impermeable layer for fluid or gas containment.
- ***Geofoam:*** the blocks created from polystyrene foam to be used for thermal insulation or a layer to reduce the earth pressure applied on rigid walls.
- ***Geocells:*** the geosynthetics act as a network of cells in the form of the mattress to limit the lateral movement of the soils, which are filled inside the cells.
- ***Geocomposites:*** a combination of two or more geosynthetic or material types in a factory fabricated system. This specific product provides the best creative efforts of the engineer and manufacturer.
- ***Geosynthetic clay liners:*** a kind of geocomposites that manufactured with a bentonite clay liner encased by one or more layers of geotextiles or geomembranes. This product is used as a barrier for liquid or gas in landfill liner applications.

1.1.2. Geosynthetic-reinforced soils applications

Among many mechanical reinforcement solutions, geosynthetic-reinforced soils is a widely used solution due to many advantages such as easy and quick installation, an economical implementation or a small environmental impact. Geosynthetic reinforcement solution is usually used as a single layer, or multiple layers to ensure the stability and the durability of geotechnical structures. This solution is used for a variety of reinforced soil applications.

- ***Reinforced slopes:*** A group of geosynthetic layers is placed on the slopes to provide stability and reduce the deformations. This solution can protect the construction of the slopes at any height and any slope angle (*Figure 1.2a*).
- ***Retaining walls:*** The presence of geosynthetic reinforcement allows stable walls to be constructed to a wide range of heights during the placing and compacting the reinforced fill (*Figure 1.2b*).

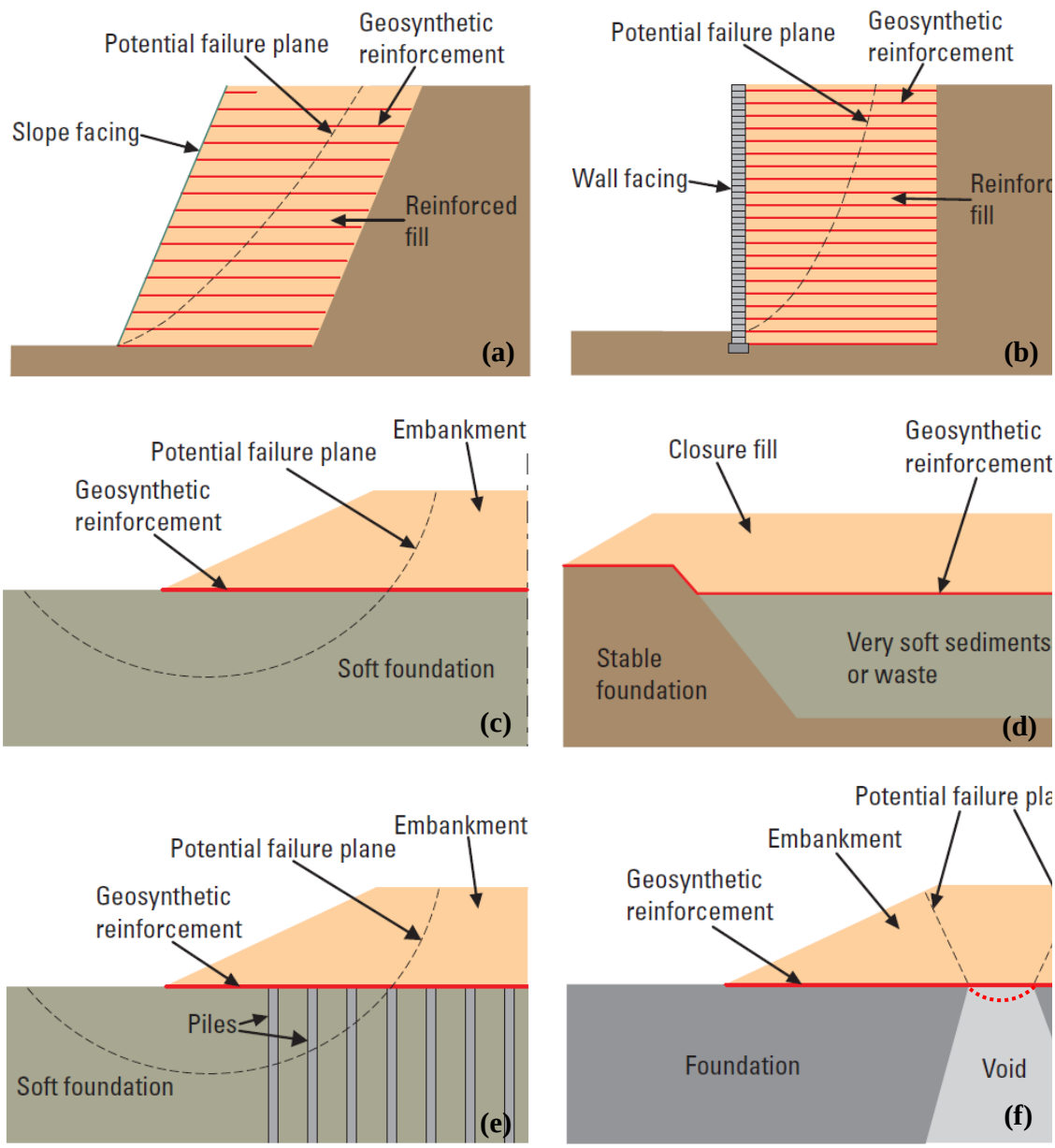

Figure 1.2. Reinforced soil applications

- ***Reinforced embankments on soft soils:*** A layer of geosynthetic reinforcement is used at the base of embankment placed over soft foundation (*Figure 1.2c*). The use of geosynthetic improves the stability of embankment and allows constructing higher and with steeper side slopes.
- ***Landfill expansion:*** geosynthetic-reinforced layer is placed over old wastes to ensure the integrity of the new water-proofing system on top of the old waste. In geotechnical terms, the objective is therefore to prevent potential differential settlements in the old wastes (*Figure 1.2d*).
- ***Pile-supported embankment solution:*** In order to reduce the settlement and improve the load transfer on the pile head, the geosynthetic-reinforced layer can be used at the base of

an embankment in the granular platform constructed over soft soil reinforced by piles (*Figure 1.2e*). A combination of geosynthetics and piles can transfer the load to the substratum and decrease the settlement of the soft soil (*Figure 1.3*).

- ***Reinforced embankment spanning cavities:*** Geosynthetic layer is placed at the base of the embankment above a platform where cavities can appear (*Figure 1.2f).* This solution limits the effect of cavities on the deformation of the surface of the embankment and stops the sinkhole.

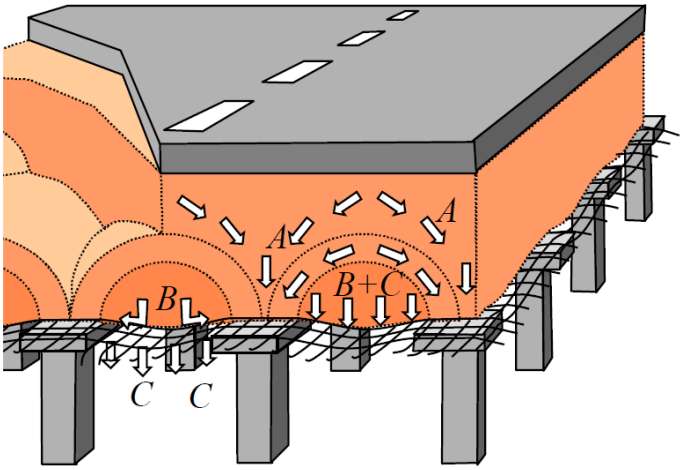

Figure 1.3. Load distribution in piled embankments (Van Eekelen, 2015)
Distribution of the vertical load is in three parts: A (arching) directly to the piles; B via the geosynthetic to the piles; C (subsoil) to the soft subsoil between the piles

1.2. OVERVIEW OF GEOSYNTHETIC-REINFORCED EMBANKMENT SPANNING CAVITIES

Nowadays the need to develop the infrastructure is increasing more and more in many areas. It leads to the rise of highways or railway line projects. The safest strategy to eliminate the risk related to a sinkhole for the transportation structures is the avoidance of the subsidence features and the potential areas (*Gutiérrez et al., 2014*). However, the constructions can have to cross-hidden underground cavities, and as a result, structures can be damaged. Unfortunately, it is not easy to detect cavities, in some cases, they can appear after the structure construction.

The cavities, also known as sinkholes, swallow holes or voids; commonly appear as a result of the chemical dissolution of carbonate rocks caused by karst processes with the presence of water in limestone, or the presence of gypsum soils. The cavities can be formed by an anthropic origin, from mining (rupture of the pile in an old mine) or solid waste activities (*Figure 1.4*).

The presence of cavities often leads to the appearance of deformation on the surface of the embankment above. In order to ensure the stability can be affected by cavities, several solutions could be applied such as evacuation and refilling voids, injection grouting, concrete slab or geosynthetic reinforcement. The filling or concrete solutions are not always able to use due to the difficulty relevant to the construction conditions, for example, the high thickness of overburden soil *(Galve et al., 2012)*.

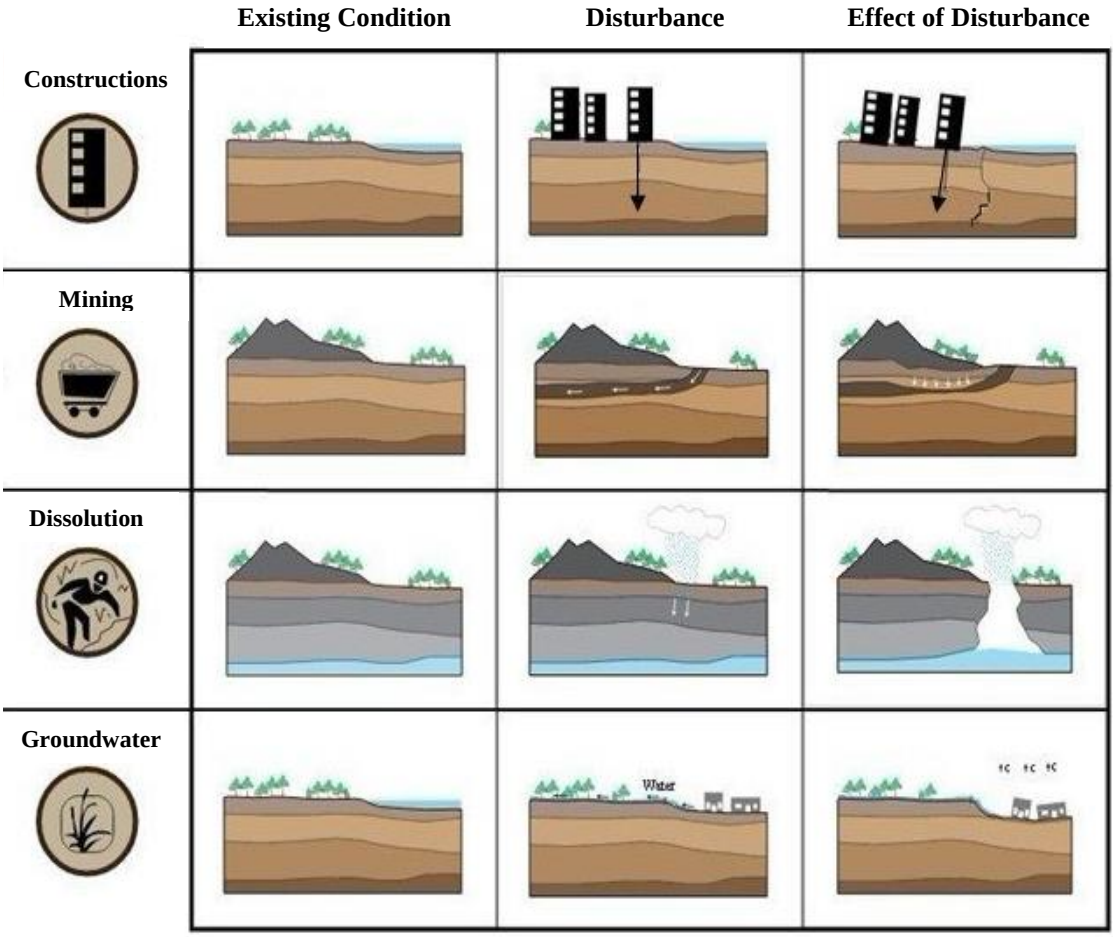

Figure 1.4. Different causes of cavities (URETEK)

At present, the use of reinforcement material, especially, the geosynthetic sheet is widespread because this solution ensures the stability and the durability of structures due to many advantages: easy installation and a small environmental impact. However, the difficulty of the optimal design of this solution is due to the misunderstanding of the behavior mechanism of geosynthetics applied over cavities.

As a “hammock”, geosynthetic reinforcement including geotextile or geogrid *(Ziegler, 2017)* can prevent the surface settlement, which can occur due to the appearance of the cavity. The solution could limit the risks effectively from sinkholes *(Blivet et al., 2002)* accordance with

many profits such as its cost or the working time of installing. The reinforcement method was also applied to bridging underground cavities (*Wang et al., 1996*) and compacted gravel mats *(Poorooshasb, 2002)*. The role of geosynthetic reinforcement applied to embankment above cavities may depend on many mechanisms occurring during the cavity opening. These complicated mechanisms contain the membrane effect of the geosynthetic sheet, the displacement of the geosynthetic in the areas around the cavity, the load transfer mechanism within the embankment and the expansion mechanism.

The load transfer mechanisms are not completely understood due to many influences such as the geometry, the applied load above embankment and the opening process of the cavity. Nevertheless, when the geosynthetic deflects that reflects on the deformation of the surface embankment, an arch may appear inside the embankment above the cavity. However, it may be not systematic because of the affluence of the collapsed material. Moreover, the expansion of soil may occur when a granular material is subjected to collapse.

Widely used as guidelines for the design of geosynthetic-reinforced embankments spanning cavities, the British Standards *BS 8006 (1995, 2010)*, the German method (*EBGEO, 2010*) and the recommendations from the French research program "RAFAEL" (*Giraud, 1997*; modified by *Villard and Briançon 2008*). Researchers are still working to improve the analytical design methods.

1.3. PROJECTS OF REINFORCED EMBANKMENT SPANNING CAVITIES

1.3.1. High-speed railway, LGV Est, Lorraine, France (Tencate, 2010)

The high-speed railway LGV Est is constructed to connect Paris with the East of France and then to connect to the German high-speed rail network with over 300 km of new track and with speed of 320 km/h *(Tencate, 2010)*. The project was constructed by GTM – Dechiron and invested by SNCF, Paris, France. During the construction, a network of cavities was discovered in a karst limestone layer below the base of the high-speed structure. Located on the upper surface of the karst layer, the width of the void varied from 0.15 m to 0.20 m.

Several design alternatives were researched in order to provide the performance of the rail structure over these cavities. Geosynthetic reinforcement was chosen as the best technique to span across any potential foundation voids and ensures the minimal settlement on the surface embankment. The French design method RAFAEL was used to maintain a solution; any problem was analyzed with the influence of the thickness of the fill materials, the geosynthetics strength, and the tensile stiffness. The maximal possible cavity diameter that could appear was

assumed as 0.5 m. As a requirement for the train speed, a maximum of 1 mm of the surface settlement was limited. Moreover, the thickness of embankment above the limestone layer was also restricted as an essential condition for the construction.

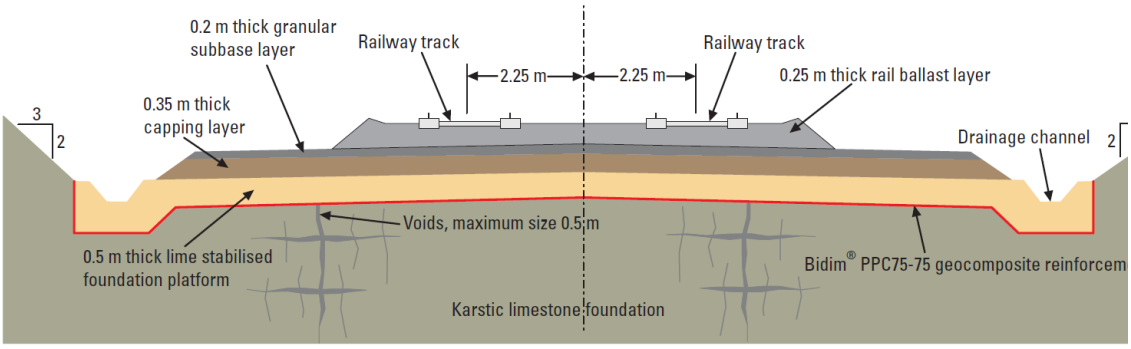

Figure 1.5. Typical cross-section through the reinforced track structure, LGV Est, Lorraine, France (Tencate, 2010)

The design method concludes that a 1.05 m of fill thickness with geocomposite reinforcement named Bidim PPC75-75 can ensure the stability and limit the surface deformation of the railway structure. The used geosynthetic has an ultimate tensile strength of 75 kN/m and is produced from high polypropylene in order to provide better long-term durability with the high pH condition of limestone.

Fill thickness contains three layers below 0.25 m of the rail ballast layer (*Figure 1.5*). A 0.5 thick lime-stabilized platform with 5% lime fine-crushed limestone was compacted across the top of the geocomposite reinforcement. This layer was constructed in order to provide maximum bond development coverage. After that, a 0.35 m of the compacted granular layer was placed over the lime-stabilized platform, and then a 0.2 m of thick granular subbase layer was constructed. Now, trains can run at 320 km/h on LGV Est between Paris and Eastern France.

1.3.2. Public park, Arras, France (Texinov, 2018a)

Located in Arras city, in the north of France, a public park was constructed over an abandoned chalk quarry that causes underground cavities with a significant diameter *(Texinov, 2018a)*. Locating from 14 to 20 m in depth, the size of the hidden cavities can reach 6 m high and 3.5 m wide.

Geosynthetic reinforcement is used to solve the risk of the occurrence of cavities, and RAFAEL design method was used with simplified assumptions. Arching effect and shear

strength were not considered for the embankment of soil over the geosynthetic sheet, and the expansion factor was selected uniformly. Moreover, specific conditions make difficulty for the design: the soil embankment has a low thickness and the local materials, which their quality was not ensured, are used to fill.

Finally, the high tensile strength geosynthetic named Geoter FPET 1800 was selected for the project. Combining woven geotextile and high tenacity polyester cables, the product has a very high tensile 1800 kN/m that secure the construction in case of cavity collapse.

1.3.3. Football field, Barcelona, Spain (Tencate, 2010)

One of the most famous football clubs in La Liga (Spain), RCD Español de Barcelona SAD planned to build a new stadium in Cornella, close to Barcelona, in 2005 *(Tencate, 2010)*. The aim of this structure is creating a safe and modern stadium, and FCC Construction, Copisa JV was chosen to construct this 4-star stadium.

The proposed stadium stability is influenced by sinkholes relevant to a stratum of anthropic material. The appearance of this human-made material could be explained by the history of using the old landfill; an old solid waste was the site as a purpose for solid industrial and construction waste. The problems relevant to collapsing, sinkholes or surface depressions subjected to groundwater were confirmed for the layers above the anthropic stratum. Due to the specific structure of the stadium, an enormous volume of water can effect to the foundation and leads to the appearance of a considerable size of sinkholes; it can be reached to 4 m of diameter.

By considering the allowable differential deformation for road pavements and high-quality football fields, the maximum deformation was limited to 2% for any sinkholes forming. Three treatment procedures were planned to ensure the stability and durability of the stadium. Firstly, a minimum of 4 m thickness of well-compacted fill has to be placed above the stratum layer (*Figure 1.6*). Then, a basal reinforced has to be used in the foundation. Finally, in order to avoid the influence of groundwater on the foundation, an impermeable layer has to be placed. The construction was carried out by following several periods.

In the first period of the construction, the anthropic material located within 4 m of the ground surface was removed, and a 0.5 m compacted clay capping layer was placed above the top of the anthropic stratum.

Secondly, on the top of the clay capping layer, a 1.2 m geosynthetic-reinforced soil platform was constructed. The aim to construct this platform is to ensure the requirement for the surface deformation of the foundation. In this platform, the geosynthetic Geolon PET 600, which has a tensile strength of 600 kN/m, was placed with two different installations. In the bottom, a couple of the geotextile reinforcement was installed orthogonally to each other, while a single sheet was placed in the upper level.

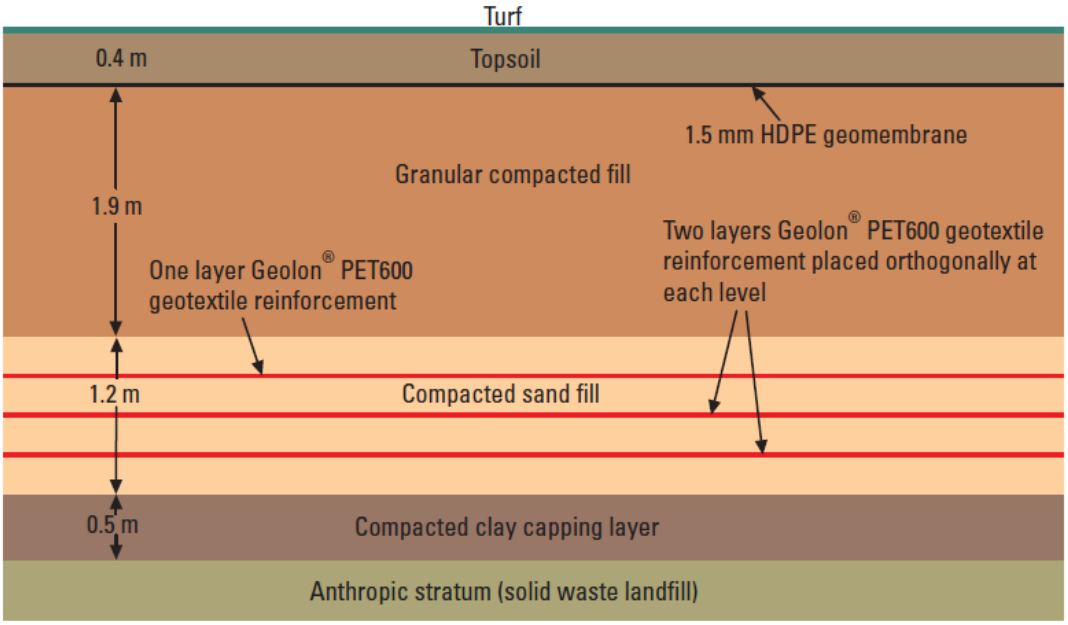

Figure 1.6. Cross section details through the reinforced foundation, Barcelona, Spain (Tencate, 2010)

Thirdly, a 1.9 m of compacted granular fill layer was installed above the reinforced platform. Then, a 1.5 mm thick of HDPE geomembrane was placed across at the top of the third layer. In order to complete the structure, a 0.4 m thick of compacted soil layer containing the football grass was finally installed on the top.

The stadium construction was finished in 2009 and becomes one of the most modern football stadiums in Spain.

1.3.4. Embankment on mining area, Estonia (Texinov, 2018b)

The discontinuous European route E20 connects roughly the West to the East though Ireland, the United Kingdom, Denmark, Sweden, Estonia, and Russia *(Texinov, 2018b)*. The project is part of the United Nations International E-road network to improve the traffic conditions and road quality. The low environmental impact is one of the critical conditions.

In Estonia, the section Tallinn-Narva designed by an Estonian public design office and constructed by SEIB Ingenieur – Consult Gmbh & Co.KG, in May 2009 (*Figure 1.7*). In the section from Kukruse to Jõhvi, a 25 m width with the average height 2 m highway was planned to construct under a 20 kPa motorway load. The main problem impact construction security is the presence of an old mining area where the cavity risk caused by bituminous schist. Geotechnical technics contains geological radar and boreholes were carried out to investigate the hidden threat. With the potential appearance of underground cavities, the solution of geosynthetic reinforcement was decided to protect the embankment over the hidden cavities.

Figure 1.7. European Route E20, Tallinn-Narva Section, Estonia (Texinov, 2018b)

The *British Standard BS 8006:1995* was chosen as a design method. As a design condition, the cavity diameter was assumed as 4 m with the acceptable surface settlement is 16 cm maximum for a 2 m high embankment within 99 years of the operating. Consequently, a high tenacity polyester geogrid named as Geoter FPET 1350/135 with the ultimate tensile strength 1350 kN/m was selected to use in 440.000 m² construction area.

1.3.5. Discussion on the design methods

The hidden cavities present a significant problem in urban construction. The standard solutions used to restrict the sinkholes risk can be noted as concrete bridges (to across the cavity areas), filling of underground voids, piles, etc. Although these methods provide durable and stabilized solutions in long-term, there are high-cost method contains several inconvenient and limitations, such as the requirements of the material quantities or cavity detection and high CO_2 emissions. Therefore, the geosynthetic solution is useful to solve the problem relevant to the risk of the hidden cavity under the embankment, and this is an economical solution.

Commonly used in many areas, high strength woven geotextiles have been shown to perform well in problematic reinforcement relevant to the underground cavities. The solution of permeable fabrics can be applied in many cavity-risk areas to ensure the stability and longevity of many structures such as highway road, railway, parking, and stadium. In Europe, two analytical design methods are commonly used: the design method resulting from the French research program entitled ‘‘RAFAEL’’ (*Giraud, 1997*) and the British standard *BS 8006* (*2010*). They are useful tools to provide rapid solutions to applied geosynthetics. However, based on many simplifying assumptions, several shortcomings are existing in the current design methods, which are mostly suggested to use for granular materials. As the main gap, the load transfer mechanism acting within the reinforced platform has not been understood completely. Moreover, the expansion mechanism of the embankment over cavities needs to be explained well.

To gain a better understanding of the mechanisms occurring during the opening of cavities under embankment reinforced by geosynthetic, many experimental and numerical works have been conducted. The current design methods including their deficiencies and the latest recommendations are presented in the next chapter of this report.

1.4. OBJECTIVES AND SCOPE OF THESIS

Based on the laboratory experiment and numerical simulation, this study tried to gain a better understanding of the mechanisms within the platform reinforced by geosynthetic over cavities.

Original laboratory equipment, with a network of tactile pressure sensors, is developed in this study, which permits to deal with load transfer mechanisms of granular platform reinforced by geosynthetics. The experimental data were analyzed, to identify the load transfer and the expansion mechanisms, the influences of the embankment material characteristics were also discussed. Also, numerical simulations based on the Finite element method were developed to compare with the experimental results.

The scope of this thesis is to focus on a series of models contain two methods of opening: a trapdoor and a progressive opening. Two geosynthetic materials were tested: a woven and a nonwoven, and three granular soils: fine sand, coarse sand, and gravel were tested as embankment materials. For each type of soil, three heights of the platform were tested for the same cavity diameter. Based on the results of the monitoring of each test consisting of the measurement of the deflection of the geosynthetic, the settlement at the surface and the stress distribution, the reinforcement mechanisms are studied.

1.5. THESIS OUTLINE

Chapter 2 presents a literature review of existing types of research on the mechanisms of geosynthetic-reinforced soils including the load transfer and expansion. Several cases study of experiment and numerical works were also described.

Chapter 3 describes the series of physical models undertaken in the PITAGOR Laboratory. The laboratory experiments aim how the cavity opening occurs with different methods and in different geometric configurations. The data of the surface settlement and the geosynthetic deflection during the opening were analyzed to clarify the influences of experimental conditions. The expansion soil was determined by a newly proposed method. The load distribution was measured and analyzed by the tactile pressure sensors.

Chapter 4 focuses on the numerical modeling. Based on the Finite element method, the software PLAXIS was used to simulate the models presented in Chapter 3. Models for each type of soils were created in order to investigate the displacement of surface soil and geosynthetics. Similar to Chapter 3, the expansion and load transfer mechanisms are also approached.

Chapter 5 highlights and discusses the fundamental results, which have been found by experimental and numerical tests.

Chapter 6 summarizes the results and presents the conclusion and then proposes the recommendations for further studies, which may improve the outcomes of the thesis.

CHAPTER 2. LITERATURE REVIEW

2.1. INTRODUCTION

Due to the difficulty to detect the small-diameter cavities, which are not possible to predict, a solution including geosynthetic reinforcement has been used to prevent the risk. The aim is to limit the surface settlement to acceptable values. Thus structures could be used until more significant repairs can be carried out. However, due to the lack of design methods considering all the complex mechanisms, this solution is sometimes not applied.

In this chapter, the definition of the soil arching is presented as a complicated mechanism that occurs within the granular embankment reinforced by geosynthetic over cavities. Several theories of the phenomenon are demonstrated and compared together. The mechanisms occurring during the cavity opening process are then presented focusing on the bending effect, the friction behavior, and the load transfer and soil expansion mechanisms.

After that, the current analytical design methods: *BS 8006 (2010)*, *EBGEO (1997, 2011)* and the French method (*Giraud, 1997*) are explained in detail. New recommendations and proposed methods are also described. The differences between them are evaluated, and the existing shortcomings and limitations are addressed.

The numerical simulations of the study area are reviewed with the comparison between two kinds of the model using the Finite or Discrete element methods. Finally, the critical studies including experimental testing and numerical works are described.

2.2. SOIL ARCHING THEORIES

2.2.1. Terzaghi

Terzaghi (1943) defined the arching effect as phenomena which known as the transfer of pressure from a yielding mass (sliding mass) of soil onto adjoining stationary parts (fixed mass). A shearing resistance along the contact between the moving and the stationary mass opposes the relative movement within the soil. Thus, the total pressure acting on the stationary masses increases by the same amount of the decreased pressure on the yielding mass, during the phenomena process (*Figure 2.1*). Terzaghi considered two vertical sliding surfaces between yielding mass and adjoining parts “ac” and “bd”.

A shear strength along sliding surfaces is defined by the Mohr-Coulomb criterion (*Eq.2.1*) with the relationship between a friction angle (φ) and the cohesion (C) of the backfill material.

$$\tau = C + \sigma.\tan\varphi \qquad \textit{Eq.2.1}$$

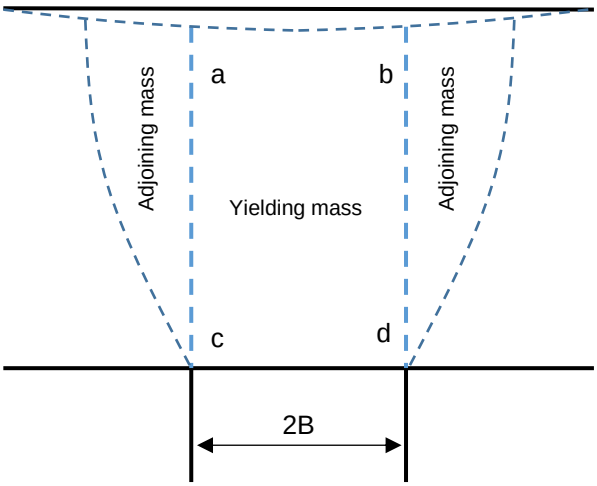

Figure 2.1. The principle of the arching effect (Terzaghi, 1943)

Taking into account the ratio of the soil pressure ratio K equal to 1.0, the equilibrium of an elementary volume of sliding mass with the thickness dz, locates at the depth z , of the width 2B can be expressed by *Eq.2.2*.

$$2B\gamma dz = 2B\sigma_z(z + dz) - 2B\sigma_z(z) + 2cdz + 2K\sigma_z(z)\tan\varphi dz \qquad \textit{Eq.2.2}$$

For a straight trench, for example, a long void, the vertical stress acting in the embankment located above the cavity at a depth z, can be expressed by *Eq.2.3*.

$$\sigma_z(z) = \frac{B\left(\gamma - \frac{2c}{B}\right)}{2K\tan\varphi}\left(1 - e^{-K\tan\varphi\frac{2z}{B}}\right) + pe^{-K\tan\varphi\frac{2z}{B}} \qquad \textit{Eq.2.3}$$

In case of a circular cavity, with the diameter D, *Eq.2.4* gives:

$$\sigma_z(z) = \frac{D\left(\gamma - \frac{4c}{D}\right)}{4K\tan\varphi}\left(1 - e^{-K\tan\varphi\frac{4z}{D}}\right) + pe^{-K\tan\varphi\frac{4z}{D}} \qquad \textit{Eq.2.4}$$

Concerning the assumption of the theory, the overload is independent of the pressure acting from the overlying soil. If a plan of the equal settlement exists, the part of the soil mass situated above this plane can act as an overload. Therefore, the accuracy of *Eq.2.3* and *Eq.2.4* needs to be validated.

According to the experimental investigations in the sand above a yielding strip, *Terzaghi (1936)* showed that the value of K is not uniform. It increases from one to maximum 1.5 following elevations vary from the centerline to approximately an amount of 2B. If elevations reach an amount of 5B, a plan of the equal settlement can exist.

Moreover, the stress acting on the trapdoor seems to be uniform in all area on the trapdoor. Note that the theory of Terzaghi considered the trapdoor problem without the presence of geosynthetic. However, this theory has been widely used in many design methods for the application of geosynthetic that are described in below sections of this study. Thus, the stress distribution calculated by this theory is needed to be validated in the specific case of the trapdoor problem, especially with the occurrence of geosynthetic reinforcement.

2.2.2. Handy

Note that the theory of Terzaghi was developed as the parameter K is the ratio between the horizontal stress and vertical stress. This assumption is not correct if the stress directions are reoriented by the arching effect. Therefore, *Handy (1985)* considered an element volume described by the path of main directions between two sliding surfaces. The resolution is similar to the others proposed by Terzaghi. The stress was assumed constant along the inverted arch in an equilibrium condition. The relevant friction is full mobilized at the sliding surfaces. The state of stress in the elementary volume is presented in Mohr's Circle in *Figure 2.2a*, and the inverted arch is described in *Figure 2.2b*. The stress σ_x and σ_z at the sliding surfaces are given by point A, with τ_{xz}, they depend on the angle resulted by $(\frac{\pi}{2} - \theta)$.

The coefficient K can be determined by *Eq.2.5*.

$$K = \frac{\sigma_x}{\sigma_z} = \frac{cos^2\theta + K_a sin^2\theta}{sin^2\theta + K_a cos^2\theta} \qquad \textit{Eq.2.5}$$

The stress applied to a width of 2B can be calculated by *Eq.2.6*.

$$p = \frac{\gamma B}{K_w tan\varphi}\left(1 - e^{-K_w tan\varphi \frac{h}{B}}\right) \qquad \textit{Eq.2.6}$$

$$K_w = 1.06(cos^2\left(\frac{\pi}{4} + \frac{\varphi}{2}\right) + K_a sin^2\left(\frac{\pi}{4} + \frac{\varphi}{2}\right)) \qquad \textit{Eq.2.7}$$

The coefficient K is concluded by *Eq.2.7*.

As an important note, the arching effect only occurs within the embankment if the thickness of the soil is six times greater than the width of the cavity (H/2B > 6). For the over thickness, the load can remain constant.

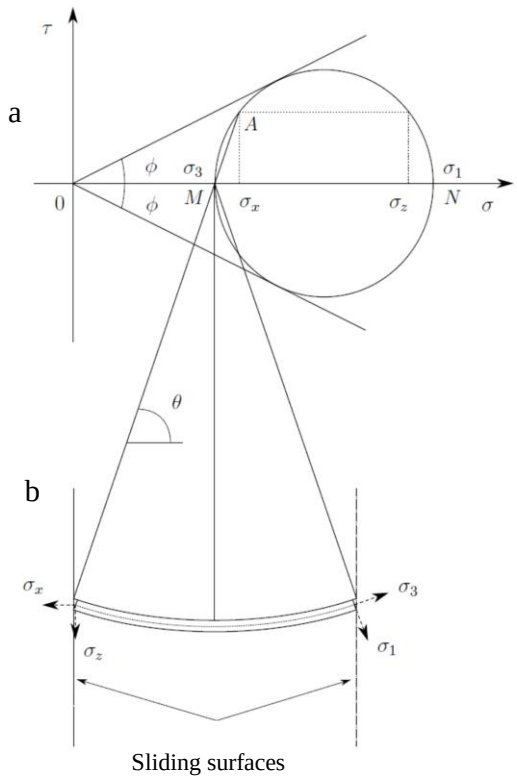

Figure 2.2. State of the stress at a boundary point of the sliding mass represented in Mohr circle (Handy, 1985)

2.2.3. Vardoulakis

Comparing to the theory of *Terzaghi (1943)*, *Vardoulakis et al. (1981)* considered a different angle of friction of the embankment material corresponding to the zones of localization of the shear deformation on both sides of the sliding surfaces. The critical angle of friction φ_c can be estimated by two different assumptions, based on Coulomb ($\varphi = \varphi_c$) or Roscoe (tan φ = sin φ_c). The ratio of the soil pressure ratio K proposed by Vardoulakis is then defined by *Eq.2.8*.

$$K_v = \frac{1 - sin\varphi_C . cos2(\frac{\pi}{2} + \beta)}{1 + sin\varphi_C . cos2(\frac{\pi}{2} + \beta)} \qquad \textit{Eq.2.8}$$

where $\tan\beta = \lambda_e - \sqrt{\lambda_e^2 - \lambda^2}$; $\lambda_e = \frac{\sin\varphi_c}{tan\varphi(1-sin\varphi_c)}$ and $\lambda = tan\left(\frac{\pi}{4} + \frac{\varphi_c}{2}\right)$

In the case of the angle of friction of soil calculated by Roscoe, the soil pressure ratio K equals to 1.0.

2.2.5. Arching theories comparison

Many other scientists proposed the earth pressure coefficient (K) by various formulas. If the method of *Terzaghi (1943)* supposedly underestimates the effect of soil arching, the formulas of *Aubertin et al. (2003)* and *Chen et al. (2010)* overestimate the effect.

In fact, these theories are applied widely in many types of research and geotechnical designs, especially the method of Terzaghi. However, these theories are proposed in the case of the trapdoor with a horizontal plane above the cavity, and their application for a geosynthetic on cavity is an approximation because the geosynthetic has a membrane shape when the cavity is opened.

Moreover, exceptionally the theory of Terzaghi, the other methods proposed the calculation process based on the limited assumption as the form of the cavity is straight, even though a circular cavity can occur as well. The limitation can make it difficult for the design.

These methods can already be compared on a trapdoor case to see the difference in the stress applied to the trapdoor. The cavity is circular, and the diameter is 0.5m. The embankment located above the cavity is assumed to fill by fine sand or coarse sand. The characteristics of filled materials are presented in *Table 2.1*. The stress applied above the cavity is calculated by each theory corresponding to height embankment varied from 0.5 m to 10.0 m.

Table 2.1. Characteristics of fill soils in the comparison

Description	***Parameter***	***Unit***	***Value***
Diameter of cavity	D	m	0.5
Unit weight of fine sand	γ	kN/m^3	18
Unit weight of coarse sand	γ	kN/m^3	20
Friction angle of fine sand	φ	°	37
Friction angle of coarse sand	φ	°	39
Surcharge	p	kN/m^2	0

Figure 2.3 indicates the stress applied to a trapdoor calculated by three methods. The vertical stress applied to the geosynthetic sheet is calculated by five methods and for two different cases of fill soils: fine sand and coarse sand.

As can be seen in *Figure 2.3*, the ratio of the soil pressure ratio K is noted in the legend of the graph for each method. The values of K obtained from Handy and Vardoulakis (Coulomb) are similar, approximately 0.4, and the ratios from Terzaghi and Vardoulakis (Roscoe) are both equal to 1.0. A comparison between results for two soil types shows that there is a slight difference in the ratio K corresponding to the difference in the friction angles of soils.

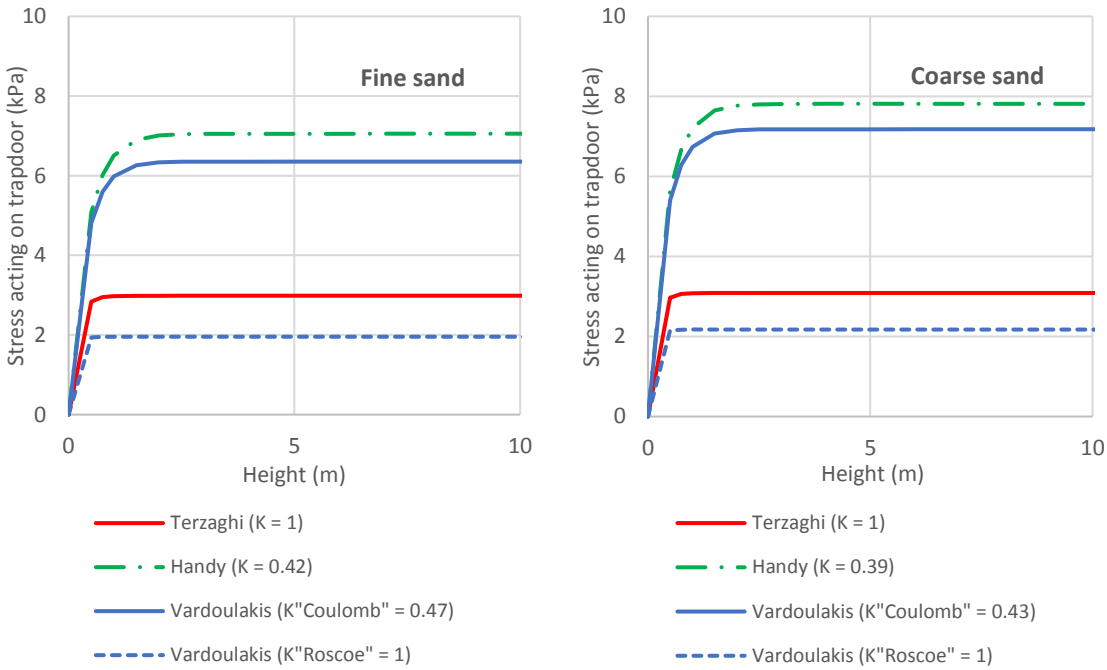

Figure 2.3. Stress applied to the cavity in different methods of calculation

The average stress computed by Terzaghi, Handy, and two methods of Vardoulakis, from the height of embankment of 1.5 m (H/D = 3), the stress tend towards a limit value. That note supposes the appearance of a stable arching within the embankment. The solution of Vardoulakis in case the ratio K calculated by Roscoe is the most optimistic whereas the hypothesis of Vardoulakis with the method of Coulomb and Handy remaining the most pessimistic. The difference between the two types of sand, in the same condition, the higher friction angle can lead to greater stress acting on the trapdoor. Generally, the theory of Terzaghi provides the most real value as it is still used mostly for the design.

It is important to note that these methods were developed for a problem of trapdoor without the use of geosynthetics. The displacement of the trapdoor is different from the deflection of geosynthetic over cavities. The methods only consider the displacement of the trapdoor, whereas the sliding surface is assumed constant. Moreover, the impact of different ways of the cavity opening including a progressive process could be dissimilar to the trapdoor process and

need to be clarified. Finally, the use of angle friction in the current methods to characterize the soils is not apparent.

2.3. REINFORCED STRUCTURE MECHANISMS

Based on theoretical considerations and experiments, various assumptions are proposed to explain the mechanisms occurring during the opening of a sinkhole under a geosynthetic-reinforced embankment:

- The membrane effect of the geosynthetic sheet,
- The displacement of the geosynthetic in the anchorage areas around the cavity,
- The load transfer within the embankment,
- The expansion of the granular material over the cavity.

2.3.1. Membrane effect and friction behavior

Geosynthetics have low bending rigidity due to their structure (*Figure 2.4*). When they are subjected to stress that is perpendicular to their horizontal plane, they take the shape of a membrane so that the tensile forces guarantee the static equilibrium of the sheet. In addition, the horizontal deflection of the sheet could increase due to the displacement of the geosynthetics in the anchorage area required to fully mobilize the friction (*Briançon and Villard, 2008*).

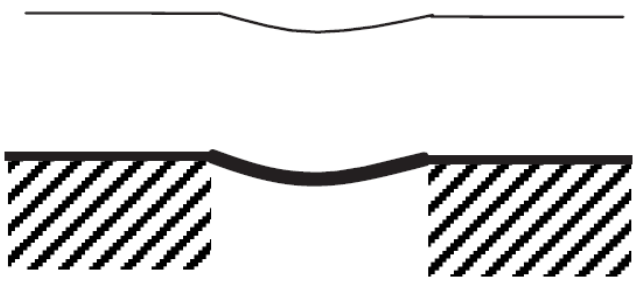

Figure 2.4. Membrane effect (Briançon and Villard, 2008)

Continuously, the friction between the sheet and soil in anchorage areas and its stretching occur with the tensioning of the sheet above the cavity. Moreover, at the edge of the cavity, the friction could equilibrate the tensile forces, includes the orientation, as a result of geosynthetics deformed by applied load, a decrease in transmitted tensile force toward the anchorage areas comparing to another directly induced by membrane effect. Based on homogeneous and isotropic sheets under simple load assumptions, a 2-D theory of membrane effect was developed by *(Giroud et al., 1990)*.

2.3.2. Load acting on the geosynthetic sheet

Taking the cavity appearance into account: the volume of subsidence soil should be considered, and it could be defined by different assumptions: the shape of collapsed soil above the cavity is widely assumed as a truncated or a cylindrical fit. In addition, if shearing mechanisms occur, an arch could appear inside the embankment over the sinkhole. The arching effect is defined by the ability of load transfer between different positions considering a relative displacement *(Briançon and Villard, 2008)*.

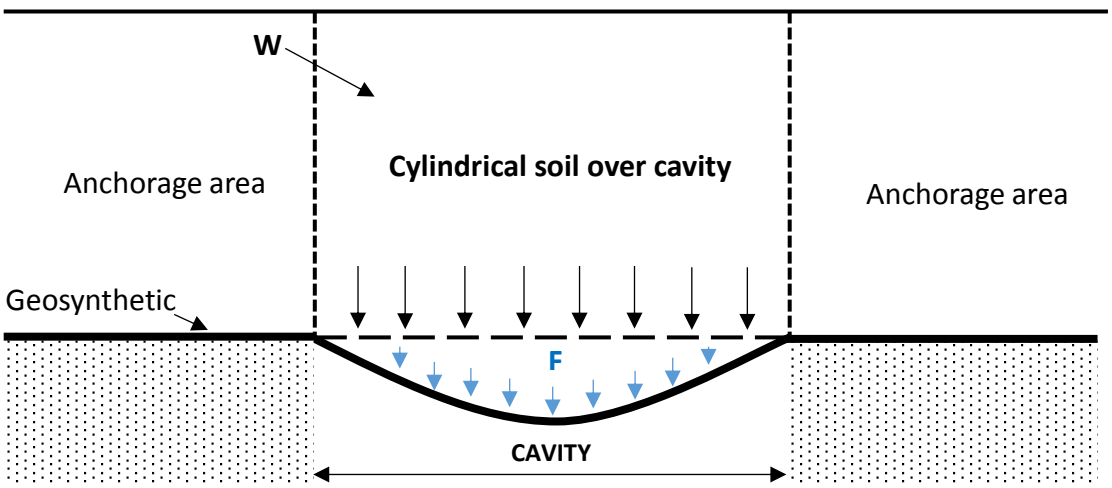

Figure 2.5. Definition of efficiency based on W_s and F_g

Even if such design methods propose to evaluate the arching effect from simplified assumptions, the arching mechanism is not well defined due to the influence of parameters such as the cavity opening mode, the geometrical conditions, geosynthetics, and the soil characteristics. To appreciate the load transfer mechanisms within the granular embankment, *Villard et al. (2016)* presented the efficiency ratio (E) which can be defined by the ratio between the load reported on the sides of the cavity and the weight W_s of the cylindrical part of the soil sited over the cavity (*Figure 2.5*). From the load acting on the geosynthetic placed above the cavity F_g, the efficiency of the load transfer within the granular embankment can be defined by $E = (W_s - F_g) / W_s$.

2.3.3. Soil expansion

Several shortcomings are still surfacing due to the simple assumptions that had been adopted *(Villard et al., 2009)* and have been continuously investigated by *Huckert el al. (2016)* and *Villard et al. (2016)*. For a granular soil layer, during the collapse, movement of particles leads to an increase in the volume of the soil above the cavity. The expansion

coefficient Ce is defined by the ratio between the final and the initial volume of soil located above the cavity (*Villard et al., 2000*). The soil expansion could appear in truncated or cylindrical soil collapse, leading to a significant reduction of the soil surface settlement. Currently, a global expansion factor has been taken into account, and this can lead to overestimation of the expansion mechanisms. In order to determine this coefficient, it is necessary to compute the volume of deformed shapes of both the soil surface and the geosynthetic deflection. Many previous types of research concluded a parabolic fit, and hence it is possible to obtain the Ce value as the ratio between the maximum deflection of geosynthetics (dg), the surface settlement (ds). Nevertheless, this assumption is not approved, because the shape of both surface soil and geosynthetic are not exactly parabolic (*Villard et al., 2016*). None method gives a relation between the expansion coefficient and the geometrical parameters of the problem (friction angle, dilatancy, etc.).

Recently, *Feng et al. (2017a)* proposed a formula to determine the expansion coefficient Ce, considering the relation between the maximum and the initial void ratios (*Eq.2.9*).

$$C_e = \frac{1 + e_{max}}{1 + e_0} \qquad \textit{Eq.2.9}$$

2.4. EXISTING ANALYTICAL METHODS

2.4.1. British Standard (2010)

2.4.1.1. Principles

The British Standard *BS8006 (2010)* proposes a design method based on several major assumptions including the soil volume of the zone of deformation is constant, there is no arching within the embankment fill, and the angle of collapsed soil is equal to the peak friction angle (*Figure 2.6*). For the depression zone, the collapsed soil is assumed as a conical shape. The procedure of design should pursue the requirements relevant to the acceptable surface deformation, the void diameter of the cavity, the allowable strain in the reinforcement and the tensile properties of the reinforcement. Due to the assumption that no soil arching occurs within the embankment, the load acting on the geosynthetic sheet is determined by the unit weight of soil and the height of the embankment ($q = \gamma . H$).

For the surface deformation, the acceptable value should correspond to the design requirements of specific structures such as truck roads, motorways, railways or overlying embankment support. In order to support the embankment, the reinforcement may be designed for a short time or whole life of the infrastructure to require the conditions established by the owner.

Regarding variation origins of cavities, the suitable design value for the void diameter could be estimated by experiences, a subterranean survey or a probabilistic approach. The geosynthetic deflection is equal to the allowable surface settlement, considering a vertical zone of extending soil from the edge of the cavity.

It is important to note that, even this design method is commonly used in Europe; it has not been validated by experimentation.

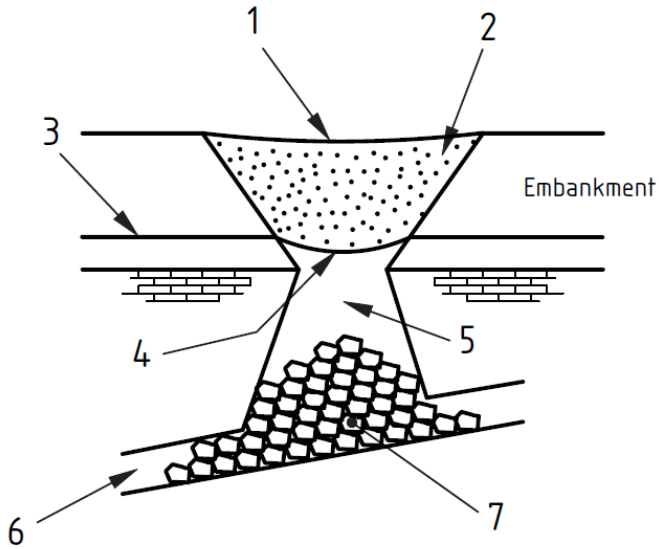

Figure 2.6. Conceptual role (BS8006, 2010)

1: Reduction depression; 2: Zone of deformation; 3: Reinforcement; 4: Depression at reinforcement

5: Void; 6: Subterranean cavern; 7: Collapsed rock

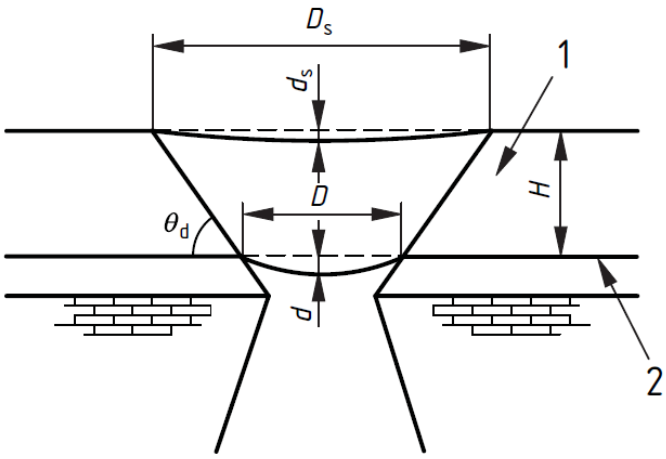

Figure 2.7. Description of parameters for design method (BS8006, 2010)

1: Embankment; 2: Reinforcement;

ds: Depression at surface; d: Depression at reinforcement

2.4.1.2. Design

The shape of the geosynthetic deflection is assumed as a paraboloid (*Figure 2.7*). The maximum allowable strain in the reinforcement could be determined by two different conditions. *Eq.2.10* is used for the axisymmetric conditions whereas *Eq.2.11* is for the plane strain conditions.

$$\varepsilon_{max} = \frac{8 \times \left(\frac{d_s}{D_s}\right)^2 \left(D + \frac{2H}{\tan\theta_d}\right)^6}{3D^6} \qquad \textit{Eq.2.10}$$

$$\varepsilon_{max} = \frac{8 \times \left(\frac{d_s}{D_s}\right)^2 \left(D + \frac{2H}{\tan\theta_d}\right)^4}{3D^4} \qquad \textit{Eq.2.11}$$

The tensile load T_{rs} can be calculated by the *Eq.2.12*.

$$T_{rs} = 0.5\lambda\left(f_{fs}\gamma H + f_g w_s\right)D\sqrt{1 + {}^{1}/_{6\varepsilon}} \qquad \textit{Eq.2.12}$$

Finally, it is necessary to calculate the minimum reinforcement bond length L_b to carry T_{rs} by *Eq.2.13*.

$$L_b \geq \frac{f_n f_p T_{rs}}{\gamma \times h \times \left(\frac{a'_1 \tan\varphi_{cv1}}{f_{ms}} + \frac{a'_2 \tan\varphi_{cv2}}{f_{ms}}\right)} \qquad \textit{Eq.2.13}$$

Table 2.2. Design parameters of British Standard (2010)

Symbol	***Meaning***	***Unit***
ε_{max}	maximum allowable strain in the reinforcement	%
d_s	surface settlement	m
d	Geosynthetic deflection	m
D_s	the diameter of surface deformation	m
D	the diameter of the cavity	m
H	the height of the embankment	m
θ_d	the angle of the collapsed soil	°
λ	Coefficient dependent on the support direction, λ = 1 (spanning one-way), λ = 0.67 (spanning two ways)	-
γ	Unit weight of the embankment material	kN/m^3

w_s	surcharge intensity	kN/m^3
f_{f_s}	partial load factor for soil	-
f_d	partial load factor for externally applied load	-
f_n	partial factor governing the economic ramifications of failure	-
f_p	partial factor applied to the pull-out resistance of the reinforcement	-
h	the average height of fill over the bond length	m
a_1'	interaction coefficient relating to the soil/reinforcement bond angle to $tan\varphi_{cv1}$ on one side of the reinforcement	-
a_2'	interaction coefficient relating to the soil/reinforcement bond angle to $tan\varphi_{cv2}$ on the opposite side of the reinforcement	-
f_{ms}	partial material factor applied to $\varphi_{cv1}, \varphi_{cv2}$	-
$\varphi_{cv1}, \varphi_{cv2}$	large strain angle of friction of the embankment fill under effective stress conditions on two opposite sides	°

2.4.2. French recommendations

2.4.2.1. RAFAEL

The first French recommendations edited in 2000 were the results of the French project called RAFAEL. During the two phases of this project, several experiments were done to verify the design method of embankment reinforced by geosynthetic subjected to localized subsidence.

The first part of the project is based on full-scale experiments and Finite element analysis corresponding to the PhD. thesis work of *Giraud (1997)*. In this study, cavities with two different diameters, 2 m, and 4m, simulated by removing clay beads, under a 1.5 m of a cohesive granular embankment and reinforced by a uniaxial geosynthetic. In the second phase of the project, the method to simulate the cavities was changed with several types of embankment materials. In this part, cavities were formed by a movable plate under a shallow embankment using hydraulic cylinders. The configuration of the experiment can be differed such as the fill materials, the types of reinforcement sheet, the height of the embankment and the diameter of cavities.

Based on the Terzaghi theory, RAFAEL method takes the limit equilibrium method in to account to calculate the vertical stress on the geosynthetic above the cavity. The method assumed that the geosynthetic is fixed at the edge of the cavity and the sheet does not move in the anchorage areas, then the deformation and tensions of reinforcement are can be calculated

in the membrane. This method also assumed that the coefficient K in the Terzaghi's formula is equal to K_a.

Comparing to the BS 8006 standard, RAFAEL does not take the scattering angle of collapsed soil into account. Therefore the shape of the subsidence zone is assumed as a cylinder, and the diameter of the surface settlement is equal to the diameter of the cavity. This design method defined an expansion coefficient Ce in the soil above the cavity to explain the difference of the vertical displacement between the geosynthetic and the platform surface.

The load acting on the geosynthetic sheet above the cavity can be calculated based on the formulation of Terzaghi (1943) (*Eq.2.14*).

$$q = \frac{\gamma L - 4c}{4K_a \tan\varphi}\left(1 - e^{-K_a \tan\varphi \frac{4H}{L}}\right) + pe^{-K_a \tan\varphi \frac{4H}{L}} \qquad \textit{Eq.2.14}$$

Where K_a is active pressure coefficient (*Eq.2.15*):

$$K_a = \frac{1 - \sin\varphi}{1 + \sin\varphi} \qquad \textit{Eq.2.15}$$

The maximum tensile force can be determined by *Eq.2.16*.

$$T_{max} = \frac{qB}{2}\sqrt{1 + {}^{1}/_{6\varepsilon_{max}}} = J\varepsilon_{max} \qquad \textit{Eq.2.16}$$

The maximal strain of geosynthetic is calculated by *Eq.2.17*, with f is geosynthetic deflection and L is the diameter of the cavity.

$$\varepsilon_{max} = \frac{8}{3}\left(\frac{f}{L}\right)^2 \qquad \textit{Eq.2.17}$$

The expansion coefficient (Ce) can be defined by *Eq.2.18* from the variation of the volume of the fill material inside the collapsed soil cylinder, with the assumption that both the shapes of the surface and geosynthetic deflections are parabolic. Due to the experimental results, the Ce values vary from 1.05 to 1.1.

$$Ce = \frac{V_f}{V_i} = 1 + \frac{V_g - V_s}{\pi . H . {}^{L^2}/_{4}} \qquad \textit{Eq.2.18}$$

$$s = f - 2H(Ce - 1) \qquad \textit{Eq.2.19}$$

The surface settlement is then calculated from the geosynthetic deflection, the height of embankment and Ce (*Eq.2.19*).

Table 2.3. Description of the design parameter of RAFAEL method

Symbol	***Meaning***	***Unit***
D	the diameter of the cavity	m
H	the height of the embankment	m
T_{max}	the maximum tensile force	kN/m
γ	the unit weight of overlying soil	kN/m^3
L	the diameter of the void	m
s	the surface settlement	m
f	the deflection of geosynthetic	m
Ce	the expansion coefficient	-
ε_{max}	the maximal strain	%
q	the load acting on the geosynthetic sheet	kN/m^2
K_a	the active earth pressure coefficient	-
p	The surcharge	kN/m^2

2.4.2.2. New recommendations XP G 38063-2

Based on the work of *Briançon and Villard (2006, 2008a, 2008b)*, new French recommendations will be proposed in 2019.

Taking into account the stretching of the geosynthetic sheet in the anchorage areas and the increase of stress at the edges of the cavity, *Briançon, and Villard (2008)* to replace the RAFAEL method. The new method was validated by a full-scale experiment *(Briançon and Villard, 2006)* and numerical simulations *(Villard and Briançon, 2008)*.

The vertical displacement of the geosynthetic sheet was noted that could be larger than the value obtained by the initial RAFAEL method, considering the displacement of the geosynthetic in the anchorage areas around the cavity. The difference in stretching of the sheet in overlapped areas and continuous sections was also highlighted, leading to an increase of surface settlement.

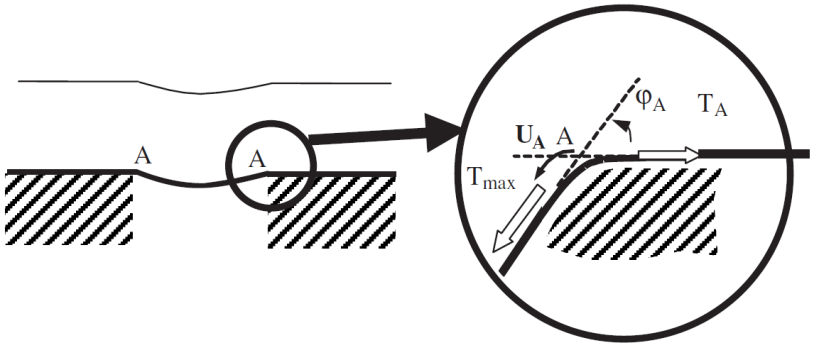

Figure 2.8. Mechanism at the edge of the cavity (Briançon and Villard, 2008)

The change in orientation of the geosynthetic sheet induces a decrease in the tension due to the friction between the sheet and the soil. *Eq.2.20* defines the tension in the geosynthetic sheet T_A (*Figure 2.8*) after the change in orientation.

$$T_A = T_{max} \times \exp(\varphi_A \times \tan\delta_{\frac{GSY}{soil}}) \qquad \textit{Eq.2.20}$$

where T_{max} is the maximum value of tension in the sheet, φ_A is the angle of the change in the orientation at the edge of the geosynthetic sheet and $\delta_{\frac{GSY}{soil}}$ is the interface friction angle between soil and geosynthetic.

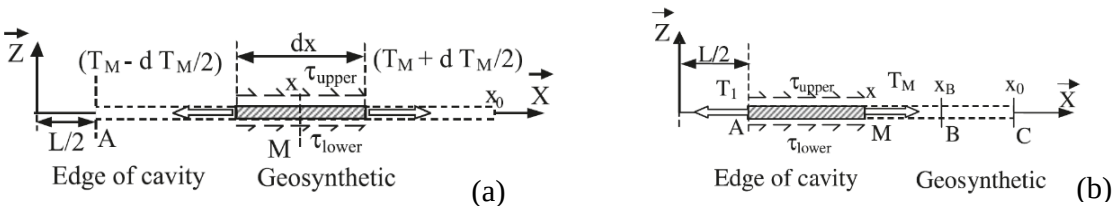

Figure 2.9. Equilibrium of an elementary section: $U_A \leq U_0$ (a) and $U_A > U_0$ (b), Villard and Briançon (2008)

Additionally, based on the analytical formulation proposed by (*Terzaghi, 1943*), the load applied to the geosynthetic sheet is assumed uniformly and perpendicularly. By taking the load transfer mechanism on the embankment into account and considering the equilibrium of a segment of the sheet, *Villard and Briançon (2008)* established a relationship between applied loads, the geometry, and characteristics of soil and geosynthetic (*Eq.2.21*). In this relation, the unknown parameter $\beta = \tan(\varphi_A)$ is a coefficient characteristic of the change in orientation of the sheet.

$$\frac{L}{4\beta}\left(\beta\sqrt{1+\beta^2}+\mathrm{ArgSh}\beta\right)-\frac{L}{2}=U_A+qL^2\frac{3+\beta^2}{12\beta J} \qquad \textit{Eq.2.21}$$

$$T_1=qL\frac{\sqrt{1+\beta^2}}{2\beta}e^{K.A\tan\beta\tan\varphi_{lower}} \qquad \textit{Eq.2.22}$$

Taking into account the displacement U_A and tensile force T_1 on the edge of the cavity, two cases are suggested: the interface friction is partially mobilized at any point of the sheet ($U_A \leq U_0$) or fully mobilized at the edge of the cavity ($U_A > U_0$) (*Figure 2.9*).

If $U_A > U_0$:

$$U_A=U_0+\frac{T_1^2-T_2^2}{2JQ_0} \qquad \textit{Eq.2.23}$$

and

$$K=1; \qquad T_2 = U_0 Jr \quad \text{and } r = \sqrt{q_0(tan\varphi_{lower}+tan\varphi_{upper})/(JU_0)}$$

If $U_A \leq U_0$:

$$U_A=\frac{T_1}{Jr} \qquad \textit{Eq.2.24}$$

and $K = U_A/U_0$.

Then, taking into account point M located at the center of the geosynthetic sheet above the cavity, the tensile force T_M, the deformation ε_M , and vertical displacement f_M can be defined by *Eq.2.25*, *Eq.2.26*, and *Eq.2.27*, respectively.

$$T_M=\frac{qL}{2\beta}\sqrt{1+\left(\frac{2\beta}{L}\right)^2} \qquad \textit{Eq.2.25}$$

$$\varepsilon_M={}^{T_M}/_{J} \qquad \textit{Eq.2.26}$$

$$f_M=\beta\frac{(4x^2-L^2)}{4L} \qquad \textit{Eq.2.27}$$

Based on the last French experiment and numerical works in this field (*Huckert et al., 2016* and *Villard et al., 2016*), the design method adopted for the French recommendations consists in the resolution of the *Eq.2.28*. This main equation is obtained by equalizing both geometric and constitutive elongation of the reinforcement; z(x) is the vertical displacement of the geosynthetic; T_H is the horizontal tensile force in the geotextile, which is constant over the cavity and can be obtained by resolving (*Eq.2.28*). Also, U_A is the geosynthetic displacement in the anchorage areas, defined as a function of the variable β *(Villard and Briançon, 2008)*.

$$\Delta L = \int_{x=0}^{x=D/2} \partial s - \frac{D}{s} = U_A + \int_{x=0}^{x=\frac{D}{2}} \varepsilon(x) \,.\, \partial s \qquad \textit{Eq.2.28}$$

with:

$$\int_{x=0}^{x=D/2} \partial s = \int_{x=0}^{x=D/2} \left[\sqrt{1 + (\frac{dz}{dx})^2} \right] dx \qquad \textit{Eq.2.29}$$

$$\int_{x=0}^{x=D/2} \varepsilon(x)\, \partial s = \frac{T_H}{J} \int_{x=0}^{x=D/2} \left(1 + \left(\frac{dz}{dx}\right)^2 \right) dx \qquad \textit{Eq.2.30}$$

$$\beta = \frac{dz}{dx}(x = \frac{D}{2}) \qquad \textit{Eq.2.31}$$

Thus, the tensile force T(x) in the geotextile is given by:

$$T(x) = T_H \sqrt{1 + \left(\frac{dz}{dx}\right)^2} \qquad \textit{Eq.2.32}$$

The consideration of new load distribution requires only changes in the definition of g(x) and z(x) linked together by the following relation *(Villard and Briançon, 2008)*:

$$\frac{q(x)}{T_H} = \frac{d^2 z}{dx^2} \qquad \textit{Eq.2.33}$$

By assuming that the total loads applied on the geosynthetics are the same, in each case results for a uniform load can be solved:

$$\begin{cases} q(x) = q \\ z(x) = \dfrac{q(4x^2 - D^2)}{8T_H} \end{cases} \qquad \textit{Eq.2.34}$$

Eq.2.28 can be resolved easily by an iterative procedure, and a numerical integration process gave the unknown value of T_H and thus the displacements and the tensile forces in the geosynthetic. The total load transfer q is calculated from the Terzaghi's formula using K = 1.0. Finally, the new French recommendations are only proposed for granular soils, for 1.03 < Ce < 1.05 and 1.5 < H/D < 3.

The last results presented by *Huckert et al. (2016)* and *Villard et al. (2016)* such as the non-uniform load distribution depending on the cavity opening mode have not been taken into account due to the complexity to define the cavity opening mode.

2.4.3. EBGEO (1997, 2011)

2.4.3.1. Principles

In order to provide recommendations for the design of geosynthetics reinforcement for overbridging systems in areas prone to subsidence, EBGEO (Recommendations for design and analysis of earth structures using geosynthetic reinforcements) incorporates the principles of several methods and results from RAFAEL, a French project.

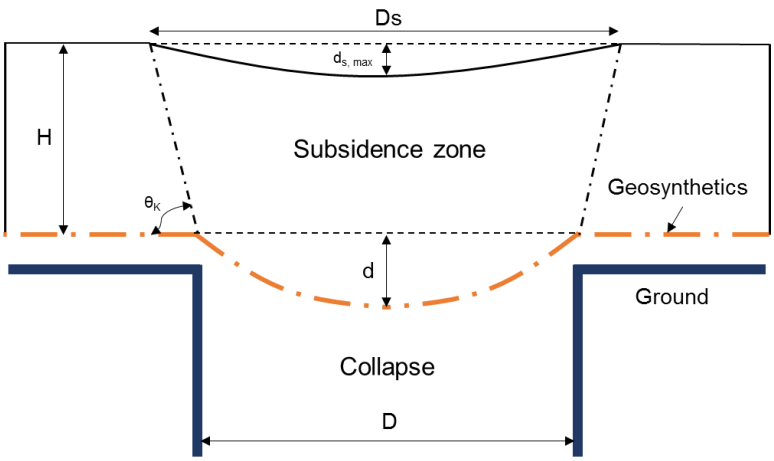

Figure 2.10. Designations

The German method separates the stabilization principle into two different types: a complete stabilization for entire designed working life, and a partial stabilization for a defined load duration. Geosynthetics are possible to install as one layer or more than two layers, and for isotropic or anisotropic geosynthetics reinforcement.

Two main structural models to analyze the collapsed soil within the embankment: a failure model, an arch model, and the ratio H/D are taken into account to select the model. In the case of the low relative density of embankment soil, the failure model without lateral reaction (H/D < 1) and with lateral reaction ($1 \leq H/D \leq 3$) can be assumed. Otherwise, for high relative density, an arching model is recommended for the analysis. In addition, similar to the BS 8006, EBGEO assumes the geometry of collapsed soil as a truncated cone, for the failure model and a spherical segment for the arch model.

Taking the load transfer into account, the tensile stress can be calculated depending on the type of geosynthetic reinforcement: isotropic or anisotropic for the biaxial model and extremely anisotropic for the uniaxial model. Several analysis methods can be used to determine the tensile forces.

Regarding the uniaxial reinforcement, EBGEO recommends the behavior of geosynthetic sheet based on the RAFAEL method. An axial stiffness ratio and the ratio of the short-term strength limit strains are taken into account as conditions in order to analyze the extremely anisotropic geosynthetic reinforcements.

2.4.3.2. Design

a. Determining the maximum depression on the road surface

Firstly, the specifications of the subsidence contours on the road surface are determined. The maximum subsidence (d_{smax}) can be estimated by the ratio between the maximum surface settlement (d_s) and the maximum diameter of the subsidence depression (D_s) (*Figure 2.10*) which depends on specified requirements for car parks, motorways, urban highways or railway.

The diameter of subsidence depression on the surface is determined by *Eq.2.35*.

$$D_s = D + \frac{2H}{\tan(\theta_k)} \qquad \textit{Eq.2.35}$$

b. Determining the allowable subsidence at the geosynthetics

The maximum allowable of geosynthetic deflection can be estimated from the expansion coefficient corresponding to the surface settlement (*Eq.2.36*); this point is similar to the RAFAEL method.

$$d_{max} = d_{s\,max} + 2H(Ce - 1) \qquad \textit{Eq.2.36}$$

Then, the maximum allowable reinforcement strain for design (ε) is selected as a minimum value of the allowable geometric strain resulting from the maximum subsidence (ε_{geo}) (*Eq.2.37*) and the maximum reinforcement strain for load duration.

$$\varepsilon_{geo} = \frac{8}{3}\left(\frac{d_{max}}{D}\right)^2 \qquad \textit{Eq.2.37}$$

The maximum value of geosynthetic deflection can be calculated from the maximum allowable reinforcement strain (*Eq.2.38*).

$$d_{max} = D\sqrt{\frac{3}{8}\varepsilon} \qquad \textit{Eq.2.38}$$

c. Determining the normal stress

In order to determine the normal stress, the three analyzed models should be selected considering the ratio H/D.

- *Failure model without lateral reaction (H/D < 1)*

$$\sigma_{v,G,k} = \gamma_K H \qquad \textit{Eq.2.39}$$

$$\sigma_{v,Q,k} = q_k \qquad \textit{Eq.2.40}$$

- *Failure model with lateral reaction (1 ≤ H/D ≤ 3)*

$$\sigma_{v,G,k} = \frac{\frac{D}{2}\left(\gamma_k - \frac{4c_k}{D}\right)}{2K_{ak}\tan\varphi_k}\left[1 - e^{-K_{ak}\tan\varphi_k\left(\frac{4H}{D}\right)}\right] \qquad \textit{Eq.2.41}$$

$$\sigma_{v,Q,k} = q_k e^{-K_{ak}\tan\varphi_k\left(\frac{4H}{D}\right)} \qquad \textit{Eq.2.42}$$

$$c_k = \frac{\gamma k.\,D}{3} \qquad \textit{Eq.2.43}$$

- *Temporary arching model (H/D > 3)*

In this case, the live load is uniformly set as q_k = 33.3 kN/m².

$$\sigma_{v,G,k} = \gamma_k h \qquad \textit{Eq.2.44}$$

- *The load component factors*

The axial stiffness ratio ω can be determined as a ratio between the transverse axial stiffness and the axial stiffness in the machine direction for an assumed strain and load duration (*Eq.2.45*). The ratio ω is set as 1.0 for an isotropic geosynthetic.

$$\omega = \frac{J_{cmd}}{J_{md}} \qquad \textit{Eq.2.45}$$

Then the load components factors for the machine (*Eq.2.46*) and cross-machine directions (*Eq.2.47*) can be calculated.

$$X_{md} = \frac{1}{1+\omega} \qquad \textit{Eq.2.46}$$

$$X_{cmd} = 1 - X_{md} \qquad \textit{Eq.2.47}$$

- *The values of horizontal tensile forces*

$$H_{md,d} = \frac{X_{md}(\gamma_G \sigma_{v,G,k} + \gamma_Q \sigma_{v,Q,k})D^2}{8d_{max}} \qquad \textit{Eq.2.48}$$

$$H_{cmd,d} = \frac{X_{cmd}(\gamma_G \sigma_{v,G,k} + \gamma_Q \sigma_{v,Q,k})D^2}{8d_{max}} \qquad \textit{Eq.2.49}$$

- *The values of actions*

The actions in the machine and cross-machine directions are calculated by *Eq.2.50* and *Eq.2.51*.

$$E_{md,d} = \frac{H_{md,d}}{\cos\alpha} \qquad \textit{Eq.2.50}$$

$$E_{cmd,d} = \frac{H_{cmd,d}}{\cos\alpha} \qquad \textit{Eq.2.51}$$

d. Anchorage length

In the case of highway construction, the geosynthetic must be anchored from the edge of the imaginary collapse. The required anchorage length is given by *Eq.2.52*.

$$L_A \geq \frac{E_d \gamma_B}{\sigma_{v,k} f_{sg,k} \times 2} \qquad \textit{Eq.2.52}$$

e. Overlap lengths

Considering the tensile force can be transferred to the respective section, the overlap lengths should be estimated by *Eq.2.53*.

$$U_L \geq \frac{E_d \gamma_B}{\sigma_{v,k} f_{sg,k} \times n} \qquad \textit{Eq.2.53}$$

Table 2.4. Design parameters of EBGEO standard (2011)

Symbol	***Meaning***	***Unit***
d_{smax}	maximum surface settlement	m
D_s	the diameter of surface deformation	m
D	the diameter of the cavity	m
H	the height of the embankment	m
θ_k	the angle of the collapsed soil	°
ε	the maximum allowable strain in the reinforcement	%
ε_{geo}	the maximum subsidence strain for load duration	%
$\sigma_{v,G,k}$	the normal stress in case of failure model without lateral reaction	kN/m²
γ_K	the unit weight of overlying soil	kN/m³
$\sigma_{v,Q,k}$	the normal stress in case of failure model with lateral reaction	kN/m²
q_k	the live loads	kN/m²
K_{ak}	the active earth pressure coefficient	-
c_k	the cohesion of overlying soil	kN/m²
ω	the axial stiffness ratio	
J_{cmd}	the transverse axial stiffness for geosynthetic cross-machine direction	kN/m
J_{md}	the axial stiffness for geosynthetic machine direction	kN/m
X_{md}	the load component factor for geosynthetic machine direction	kN/m

X_{cmd}	the load component factor for geosynthetic cross-machine direction	kN/m
$H_{md,d}$	the design value of horizontal tensile forces for geosynthetic machine direction	kN/m
$H_{cmd,d}$	the design value of horizontal tensile forces for geosynthetic cross-machine direction	kN/m
$E_{md,d}$	the design value of actions for geosynthetic machine direction	kN/m
$E_{cmd,d}$	the design value of actions for geosynthetic cross machine direction	kN/m
L_A	the anchorage length	m
U_L	the overlap length	m
α	the angle at the geosynthetic boundary can be estimated by the radius of cavity depression and the deflection of the geosynthetics	-

2.4.4. Design methods comparison

The physical characteristics of the current design methods are presented in *Table 2.5*. Overall, there are some remarkable differences between the *BS 8006 (2010)* and the other methods. The main differences are due to the two principal assumptions relevant to a constant volume of the depression zone, and no arching is considered within the embankment. As a necessary consequence, the shape of collapsed soils and the method to compute the load acting on the geosynthetic sheet are disparate with the other methods.

Table 2.5. Physical characteristics of the current design methods

Standards/ methods	***BS 8006 (2010)***	***RAFAEL***	***XP G 38063-2 (2019) based on Briançon and Villard (2008)***	***Villard et al. (2016)***	***EBGEO (2011)***
Shape of collapsed soils	Conical shape	Cylindrical shape			Conical shape, spherical segment
Load transfer model	Uniform	Uniform		No uniform	Uniform
Arching assumption	No	Yes			Yes
Expansion in collapsed soil	No	Yes			Yes
Load acting on the geosynthetic sheet	-	Based on Terzaghi with K_a	Based on Terzaghi with K = 1		Depended on ratio H/D and based on Terzaghi with K_a
Displacement of the geosynthetic in the anchorage areas	No	No	Yes	Yes	No

For the other methods, the *EBGEO (2011)* is based on the original *RAFAEL* methods. The shape of collapsed soil is assumed as a conical fit, the expansion of the depression zone and the arching effect are taken into account to calculate the load acting on the reinforced sheet. Some unique points between these methods are due to the requirements for the design such as live loads.

Considering the displacement of the geosynthetic in the anchorage areas around the cavity, the French recommendations *XP G 38063-2* have significantly modified the *RAFAEL* method. As a result, the method to estimate the designed parameters are modified and can be calculated by an iterative process. Moreover, for the determination of load applied to the geosynthetic, the French recommendations *XP G 38063-2* use the coefficient K as 1 instead of K_a.

Note that only the French recommendations *XP G 38063-2* has been validated on experimental and numerical studies (*Briançon and Villard, 2008*; *Villard and Briançon, 2008*; *Huckert et al., 2016* and *Villard et al., 2016*).

Table 2.6. Parameters for the comparison of design methods

Description	***Parameter***	***Unit***	***Value***
Diameter of cavity	D	m	2
Height of embankment 1	H_1	m	1
Height of embankment 2	H_2	m	2
Unit weight of fill sand	γ	kN/m^3	18
Cohesion of fill sand	c	kPa	0
Friction angle of sand	ϕ	°	37
Expansion coefficient	Ce	-	1.05
Interaction coefficient relating to the soil/reinforcement	a	-	0.8
Deformation criterion	d_s/H	%	5
The interface friction angle between soil and geosynthetic	ϕ	°	25
Surcharge	p	kPa	0

The current methods are applied to an example to compare the design results. As an assumption, for example, the expansion coefficient is given as 1.05 and no surcharge is applied to the embankment. In order to compare the influence of the embankment height to the design, two cases of ratio H/D are calculated: 0.5 and 1.0 corresponding to H_1 and H_2 respectively. *Table 2.6* presents the values for the design parameters.

The results of the design calculation are presented in *Table 2.7* and *Table 2.8*. According to the assumptions, the surface settlement is calculated from the deformation criterion, and then the geosynthetic deflections are determined for each method. After that, the maximum tension and strain are identified before completed with the anchorage length. It can be noted that even in a simple case, many design methods consider the arching effect but they give different results.

The *BS 8006 (2010)* are calculated in two different cases based on the degrees of the shape of collapse soil: 60° (conical shape) and 85° (cylindrical shape). As an original assumption of the *BS 8006 (2010)*, the shape of collapsed soil is set as conical, but the case of 85° of collapse is also calculated in order to compare with the other methods which the cylindrical shape are assumed. As a result, the different shape leads to a remarkable difference in the results. Most of the required parameters for the cylindrical case is higher than the conical case. For the maximum tension and the anchorage lengths, the cylindrical case is two times larger than the conical case, whereas, for the stiffness, the difference is ten times. Due to the variation of the degree of collapsed soil, the maximum strain of the cylindrical case is four times lower than the conical case.

Table 2.7. Results of design methods in case of H/D = 0.5

Methods	***Surface settlement***	***Geosynthetic deflection***	***Tension***	***Strain***	***Stiffness***	***Anchorage length***
	ds (m)	dg (m)	T_{max} (kN/m)	ε_{max} (%)	J (kN/m)	L (m)
BS 8006 (2010) conical shape	0.05	0.05	49.94	1.03	4838	3.7
BS 8006 (2010) cylindrical shape	0.05	0.05	102.92	0.23	44357	7.7
Briançon & Villard ($K = K_a$)	0.05	0.15	52.25	0.55	9382	5.1
XP G 38063-2 (2019)	0.05	0.15	32.36	0.67	4759	3.9
EBGEO (2011)	0.05	0.15	63.83	1.50	4256	2.9

Considering the critical assumption relevant to arching effect and the collapsed soil, the French recommendations *XP G 38063-2* are calculated in two cases: K ratio is set as 1 and K_a which is named as *Briançon & Villard* ($K = K_a$). Only for the maximum tension parameter, the case

of K set as 1, the estimated value is higher than the case of K_a, but there is not an enormous difference. For the other parameters, the French recommendations *XP G 38063-2* (K = 1) shows the more optimistic results on the required parameters (*Table 2.7* and *Table 2.8*).

Due to the main principle of *EBGEO (2011)* is based on the original *RAFAEL* method, the estimated values of the geosynthetic deflection and surface settlement are similar to the French recommendations *XP G 38063-2*. There is slight variation in the formula to calculate the maximum tension relevant to the obligatory assumption of the live loads and thus to lead to the higher value estimated from *EBGEO*. Among the current methods, *EBGEO (2011)* shows the most pessimistic requirement for the strain of geosynthetic whereas the requirement for the anchorage length is most confident.

Table 2.8. Results of design methods in case of H/D = 1.0

Methods	***Surface settlement***	***Geosynthetic deflection***	***Tension***	***Strain***	***Stiffness***	***Anchorage length***
	ds (m)	dg (m)	T_{max} (kN/m)	ε_{max} (%)	J (kN/m)	L (m)
BS 8006 (2010) 60° conical shape	0.1	0.1	35.44	14.38	246	2.6
BS 8006 (2010) cylindrical shape	0.1	0.1	84.55	1.48	5726	6.3
Briançon & Villard ($K = K_a$)	0.1	0.3	49.24	4.13	1191	3.5
XP G 38063-2 (2019)	0.1	0.3	22.07	4.65	474	2.7
EBGEO (2011)	0.1	0.3	55.71	6.00	929	1.3

By comparing two cases of ratio H/D, the design parameters seem to be lower corresponding to the rise of the height embankment, in the case of the deformation criterion is fixed. For each parameter, in both cases of H/D ratio, *BS 8006 (2010)* with cylindrical shape proposes the highest requirements. Whereas, the *EBGEO (2011)* method shows the most optimistic values in the design.

The calculation with the *BS 8006 (2010)* is highly influenced by the partial factors which can lead to the vast difference in the design. The French recommendations *XP G 38063-2* will

suggest the high requirements on the maximal tension force that based on some new recommendations taken from a variety of additional mechanisms of the geosynthetic sheet. Finally, yet importantly, the expansion coefficient Ce that is set as an experienced value in this example can affect profoundly to the design.

2.4.5. Other methods and summary

2.4.5.1. Specific developments

Other authors have developed a specific design method to focus on particular cases. *Feng et al. (2017a)* proposed an analytical approach to predict load acting on the geosynthetic. The shape of the soil arch is determined by combining the nonlinear Mohr-Coulomb criterion, the static equilibrium of the segmental arch and a non-associated flow rule. The load transferred from the overlying soil to the soil arch and the collapsed soil are used to determine the load applied to the geosynthetic. In this proposed method, the influences on soil expansion were also shown. The average expansion coefficient increases with decreasing stiffness of the geosynthetic whereas this factor decreases following the increment of the H/D ratio. The soil pressure acting on the geosynthetic was found as it decreases first then increases, due to the existence of an optimal subsidence width for which the soil pressure is minimal. In addition, an evaluation of the soil dilatancy was studied as this parameter increase with an increment of the void width. The proposed method also suggested using nonlinear failure criterion to describe the stress and deformations of the overlying and the geosynthetic reinforcement. However, even if the proposed method was confirmed by model tests of *Zhu et al. (2012)*, which is described in detail in *Section 2.5*, it should be validated by another experiment tests in which other parameters need to be considered. In addition, *Feng et al. (2017b)* proposed a new method considering a nonlinear Mohr-Coulomb yielding criterion, a non-associated flow rule and a static equilibrium of segmental arches through a dilatancy coefficient.

Earlier, *Feng and Lu (2015)* considered the behavior of the geosynthetic reinforcement in case of two nearby cavities. As a specific case, the movement of the geosynthetic in the direction of the line connecting the two cavities can be more predisposed to be cracked. Additionally, some parameters influencing the geosynthetic behavior were presented. Following the increase of the unit weight of the overlying soil, the maximum strain and the settlement are both increases, but they decreased with the increment of the internal frictional angle and the cohesion of the soil. The effect of the interface friction between the geosynthetic and the soil was clarified as lower angles are correlated with lesser values of the maximum strain of the geosynthetic but higher values of the settlement. Moreover, the height of the overlying soil,

tension geosynthetic strength, cavity width and the distance between two cavities are found to affect the geosynthetic behavior.

Concerning the determination of the geosynthetic strain, *Giroud (1995)* established equations due to its deflection by assuming that the shape of the deflected geosynthetic is a parabola or a circular arc. Nevertheless, the proposed solutions were not validated regarding the cause of the geosynthetic deflection, especially in the cases the material is used to reinforced embankment overlying cavities. By concerning the maximal deflection, y, and initial length, b, the uniformly distributed strain of geosynthetic can be determined by the equation below:

$$\varepsilon = \frac{8}{3}\left(\frac{y}{b}\right)^2 \qquad \textit{Eq.2.54}$$

As recommendations, several methods have been developed can be listed as a model established of *Poorooshasb (2002)*, proposed assessment for *BS8006* by *Potts and Zdravkovic (2008)*, a simplified method of *Viana et al. (2008)* or a recommendation to combine parabolic and circular expressions for the deformation of the reinforcement *(Shukla and Sivakugan, 2009)*.

2.4.5.2. Summary

It is important to note that the existing methods were established from strong simplifying assumptions that are different from the realistic mechanisms. According to the geotechnical conditions, the nature and the process of the void opening of underground cavities may be varied in different areas. In addition, the performance of the geosynthetic reinforcement could be influenced by the characteristics of the embankment material where it is used.

Many impacts can affect the surface settlement such as the method of the cavity opening, the characteristics of embankment soil and the coefficient of expansion. It is necessary to establish a test protocol to determine the expansion factor whereas the formulation to define it does not exist.

The current design methods and the new recommendation are mostly based on studies of the granular material. The effectiveness of the design method needs to be clarified with the presence of treated soils. In some applied projects, this point was ignored.

The knowledge relevant to the shape of collapsed soil above reinforcement is necessary to be improved in order to calculate the load acting on the geosynthetic sheet. Also, considering the

formulation of *Terzaghi (1946)* that used to determine the load transfer effect, the value of the ratio K_a is not indicated, and there is no experiment can be used to determine this parameter. Moreover, the assumption that at the cavity area, the stress distribution on the geosynthetic sheet uniformly seems not precisely. Many design methods considered a uniform load applied to the geosynthetic above the cavity during the opening process without any validation by experimental studies.

Most of the analytical methods assume the geosynthetic sheet is fixed at the anchorage areas of the cavity. In order to improve the *RAFAEL* method, *Villard and Briançon (2008)* and *Briançon and Villard (2008)* considered the displacement and the friction behavior of the geosynthetic sheet. A characteristic length U_0, the relative displacement from which the friction mobilization becomes maximum is considered.

2.5. KEY EXPERIMENTAL STUDIES

The technique of embankments reinforcement by geosynthetics have been investigated and developed by a variety of experimental works including full-scale and laboratory experiment. As one of the first full-scale experiments, *Kinney (1986)* performed two-dimensional sinkhole tests, to investigate the reinforcement mechanisms using low tensile stiffness geosynthetic under narrow trenches and granular embankments. After that, *Kempton et al. (1996)* and *Alexiew (1997)* accompanied circular cavities, and this sinkholes type is widespread interested in many present studies.

2.5.1. Experimental testing of arching effect by Costa et al., 2009

Costa et al. (2009) investigated failure mechanisms using an active movement of a deep rectangular trapdoor over a granular soil. The experiment was constructed within a strong box (419 × 203 mm in plane and 300 mm height), with a wall created by a transparent glass, which is allowed to monitor the model (*Figure 2.11*). The trapdoor (85 mm length and 35 mm width) was located against the glass wall, and its downward movement could be triggered by a magnet.

In this study, centrifuge modeling was used to determine the role of the stress state with the reduced-scale models were set as 15-g-ton. A 159 mm thickness of fine sand (classified as SP in USCS) was prepared into the strong box. Thus the ratio between soil height and trapdoor width (H/B) is 4.5, and this allows to compare the failure mechanism between deep (H/B >2) and shallow (H/B < 2) conditions. The failure mechanisms were investigated by monitoring

the displacements of 12 colored layers placed inside the sand. Triangular sand markers were included in the colored layers in order to calculate strains within the tested soil. The failure patterns were investigated in four sections (*Figure 2.11b*). The experiment was conducted in four different testing series, in where the gravity, the density of sand and the trapdoor displacement were varied.

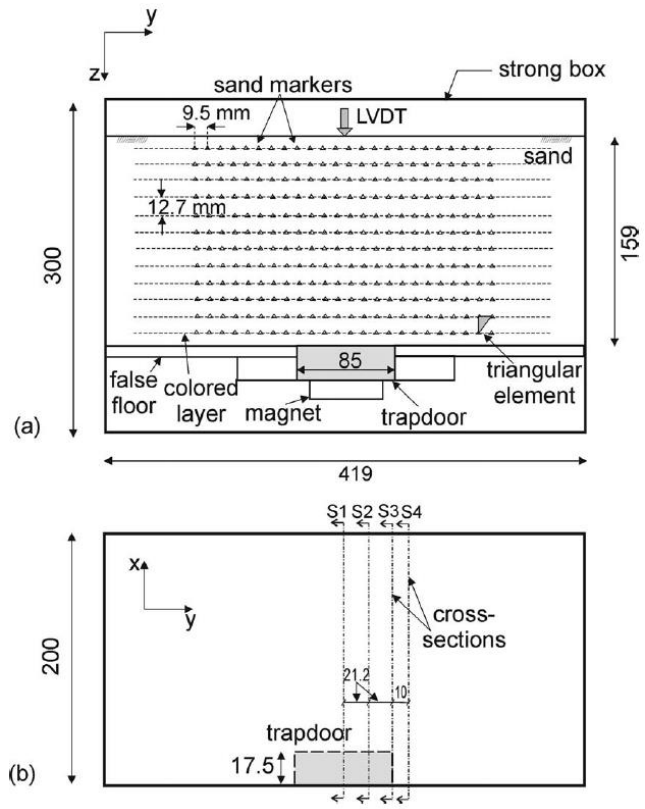

Figure 2.11. Model configuration of Costa et al. (2009)

(a): elevation view (b): plan view

An image acquisition system consists of a closed circuit camera, and a video recording device was used to analyze the pattern of failure surfaces. For the deep conditions, the study found that the failure surface becomes inclined to the vertical corresponding to the increasing downward movement of trapdoor whereas in the shallow case, the failure surface seems to be constant. Another point was concluded for the influence of the soil relative density on the settlement. In the case of the loose sand was used, the settlement was more massive three times than the case of dense sand. Moreover, the presence of inclusion (such as a pipe) placed above the trapdoor was noted to influence the pattern of the failure surfaces. The soil overinclusion is prevented from sliding into the void under the trapdoor, and hence the failure zones were developed better.

2.5.2. Arching effect study by Pardo and Sáez, 2014

An experimental and numerical study of the arching effect in the coarse sand was conducted by *Pardo and Sáez (2014)*, using a digital imaging technique. The experimental work replicated the trapdoor test of *Terzaghi (1936)* using coarse sand (classified SP in USCS). The trapdoor (10 cm of width) was placed at the bottom of a rigid box that allows monitoring the displacement by the imaging technique (*Figure 2.12*). Five load cells were also placed in different positions inside the trapdoor, in order to measure the vertical stress, with low deformations. The trapdoor was gradually moved downward to 0.6 mm per step and monitored by a high-resolution camera. Two displacement transducers were installed and compared the measurement with the imaging technique. The displacement was calculated from a series of images taken from 33 steps of the test. A numerical simulation was then performed using Finite element method using Mohr-Coulomb and Hujeux models.

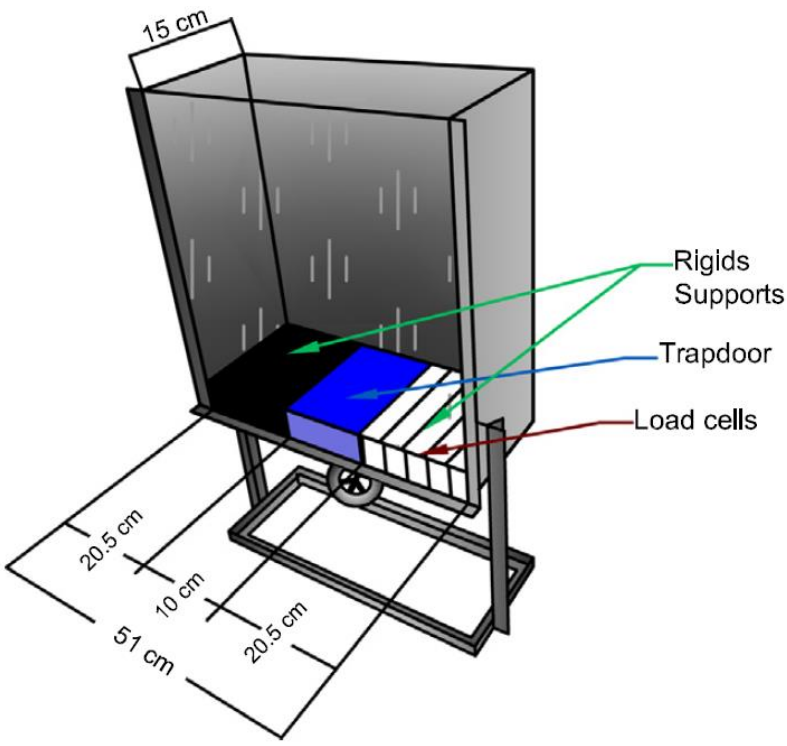

Figure 2.12. Trapdoor device scheme of Pardo and Sáez (2014)

The increment of stress on the rigid supports near the trapdoor measured by the load cells was compared with those obtained by Finite element models. Both experiment and numerical works obtained significant increasing stress close to the trapdoor. With the Hujeux model, the peak of the stress increment was represented better than the Mohr-Coulomb, whereas the less

complicated model reproduced an excellent fit with the shape of the distribution in the area far from the trapdoor (*Figure 2.13*).

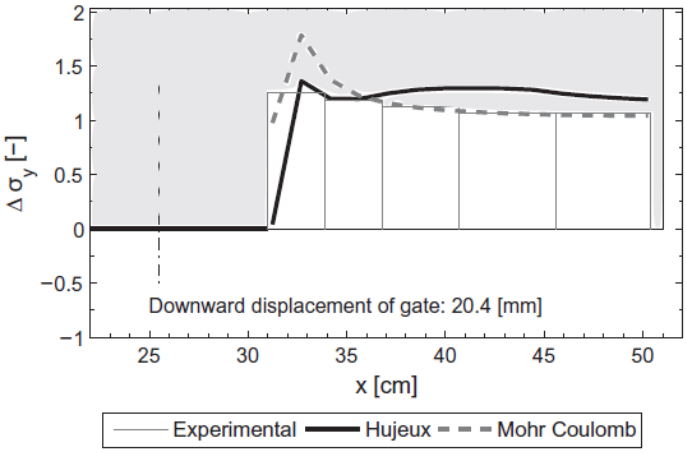

Figure 2.13. Load distribution on rigid support of the box (Pardo and Sáez, 2014)

Moreover, the shear strain pattern obtained from the imaging technology was similar to the triangular formation. Unfortunately, like many other research studies, the limit of this study is the fact that it was confined to 2-D analyzes, and the results ought to be reconfirmed in the case where geosynthetics are used to cover sinkholes.

2.5.3. Laboratory tests of soil arching by Rui et al., 2016a

A series of model tests with dense sand was conducted by *Rui et al. (2016a)*, to investigate the soil arching considering four test variables: fill height, trapdoor width, pile width and grain size of tested sand.

Inside a strain box, the tested sand was filled in a chamber (1.2 m length × 0.8 m height × 0.3 m width) (*Figure 2.14*). A series of 16 steel beams and moving components were placed at the bottom of the chamber to control the movement of the trapdoor. A pile or settling soil can be simulated by controlling the movable beam. A lift was used to move the beams downward, and a dial indicator placed below to measure the settlement. Finally, an imaging technique was used to obtain the displacement of the sand.

As a result, this study induced relation between the shape pattern and the H/B ratio (ratio of the full height embankment and the width of trapdoor), and a triangular slip surface developed after minor movements of the trapdoor. The presence of the equal settlement was confirmed in case of the ratio between the width of the trapdoor, and the pile is large enough (larger than 3).

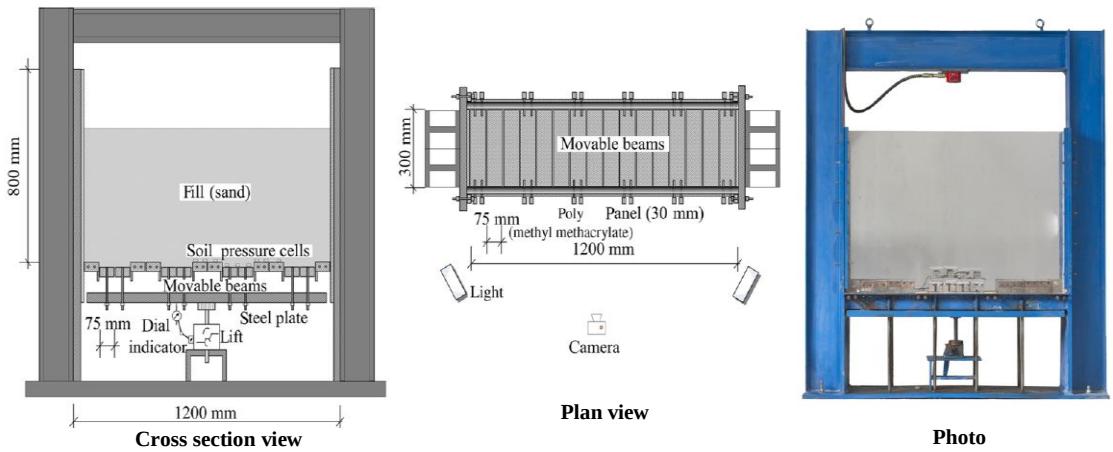

Figure 2.14. Test setup (Rui et al., 2016a)

The H/B ratio also influenced stress-distribution behavior. According to the load cells, which were placed to measure the pressure on the beams during the settlement of the soil, a decrease was obtained in the pressure on the beams whereas an increment of stress distribution on the piles was observed at the beginning of the settlement process. In the case H/B is higher than 2, the arching degree is higher than those of the lower H/B, reflecting by the stress distribution.

2.5.4. Model tests of interaction between soil and geosynthetics of Zhu et al., 2012

By using a strip trapdoor, *Zhu et al. (2012)* carried out a series of model tests to study the influence of arching effect within an overburden sandy soil and the interaction between soil and geosynthetic above the localized subsidence in landfills. As presented in (*Figure 2.15a*), the model tests were set up by a tank including two faces made by observed-toughened glasses and steel plates. In order to simulate the subsidence, a trapdoor was placed at the base of the tank, which was supported by a reductor, two pillows, and a drive chain to move up and down synchronously (*Figure 2.15b*).

The first strategy (*Figure 2.16a*) of this study is to study the effects filling height and the tensile stiffness of geosynthetics on soil arching and the interaction between soil and geosynthetics. Three different tensile stiffness of geosynthetics (4.7, 9.4 and 14.1 kN/m), four different height of sandy soils (0.4, 0.8, 1.2 and 1.6 m) were carried out for this part. The second strategy (*Figure 2.16b*) is to investigate the mechanism of strains and deflections of geosynthetics with the fill materials including 1.6 m of sandy soil and 0.04 m of compacted clay. In order to measure the soil pressures, miniature pressure transducers were placed on the geosynthetics.

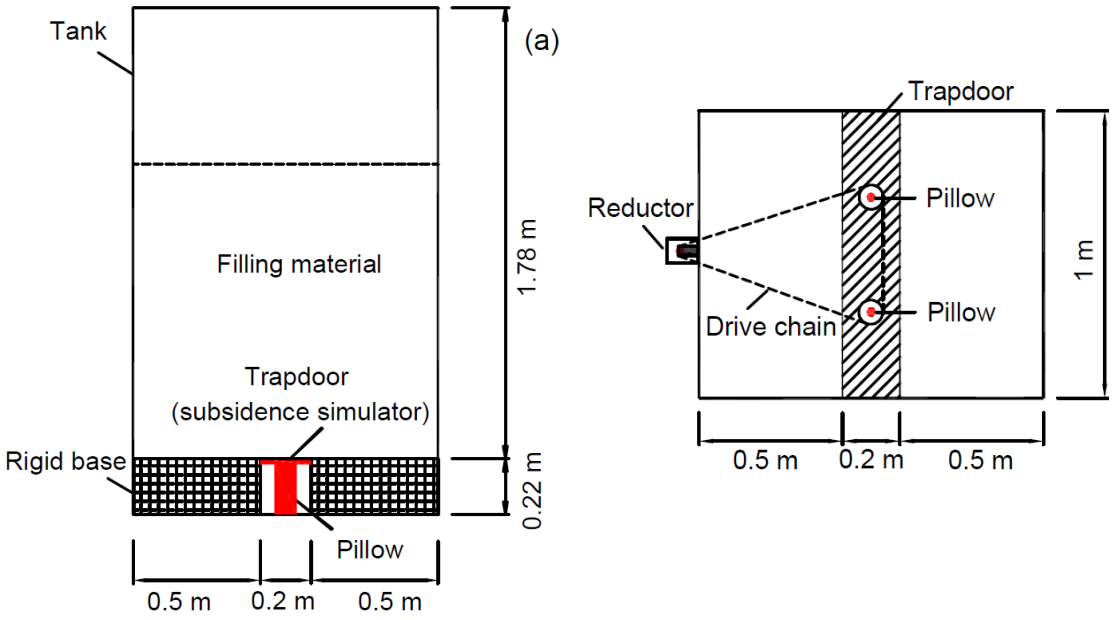

Figure 2.15. Layout of model tests (Zhu et al., 2012)

The results of the first strategy show that for the larger heights of fill soils, the soil pressure can transfer more effectively from the subsidence zone to the nearby area. Nevertheless, when the soil arching is fully formed, the soil pressures acting on the deflected geosynthetics are independent of the fill height and the stiffness of the geosynthetics. Moreover, there is not a significant difference in the deflection of geosynthetics when the height of overburden soil is varied; the deflection can be decreased by increasing the tensile strength stiffness of geosynthetic.

According to the pressure obtained by the miniature pressure transducers placed in different vertical distances from the trapdoor, the existence of the rotation of principal stress axes of the soil is confirmed. In addition, the distance between the deflected geosynthetics can affect the ratio between the horizontal and vertical stress of soil.

For the second strategy, two layers of geosynthetics were used on the top and the bottom of the compacted clay (*Figure 2.16b*). Consequently, the use of compacted clay with the geosynthetics can reduce the tensile strain and the deflections of materials as well.

Nevertheless, in the model tests, the effect of modulus of overburden materials is ignored, and the accuracy of the method to measure the deflection seem to be considered.

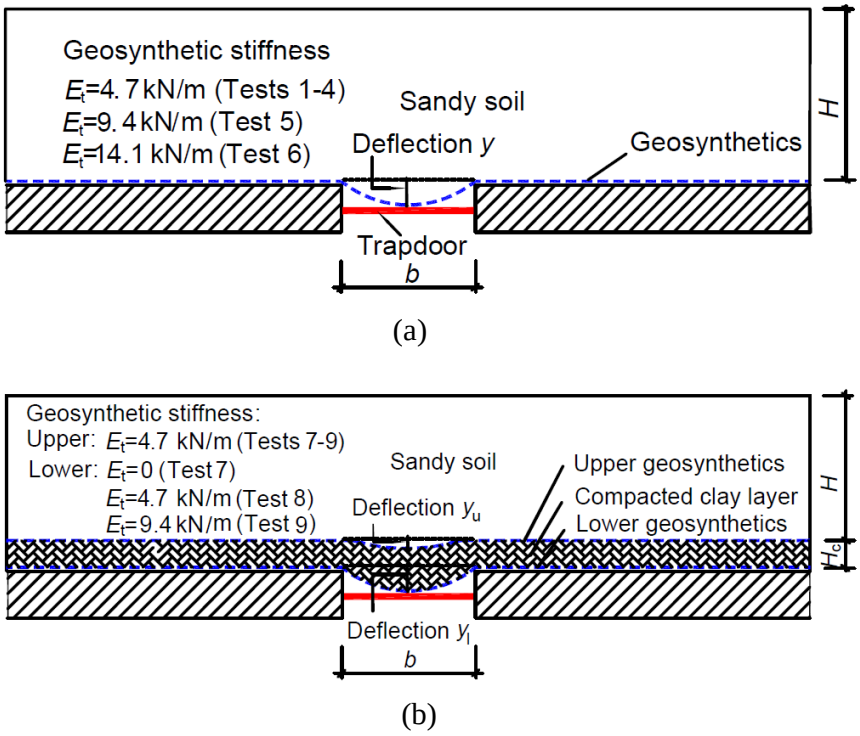

Figure 2.16. Illustration of first (a) and second (b) test strategies (Zhu et al., 2012)

2.5.5. Experimental and numerical tests on geosynthetic of Huang et al., 2015

A 2-D experimental testing and numerical simulation based on the Discrete element method were used by *Huang et al. (2015)* to model a platform of geosynthetic reinforced soil over a channel (*Figure 2.17*). This study aims to investigate the subsidence of soil, the geosynthetic deflection and the influenced impacts such as the friction angle, the overlying soil height and the particle size distribution of fill material.

An 875 mm × 650 mm × 50 mm test chamber was built with a 125 mm long of wooden blocks were installed at the bottom in order to simulate a channel. A layer of the nonwoven geotextile with the stiffness of 600 N/m was placed on the top of the wooden blocks. In this research, soil particles were simulated by aluminum cylindrical bars, which were created in a uniformly 48 mm length but in three different diameters (5.6, 12.7, 19.0 mm). Before testing, fill material was produced by mixing the bars with varying ratios to constitutive different particle size distribution. In order to allow the visual observation, the front wall of the test chamber was made by acrylic sheet, and photogrammetry was applied to track the movement of the marked bars. The experiment data was then compared with the numerical simulation with several assumptions such as the repose angles were used to approximate the internal angles of friction, which are not possible to be measured for the aluminum bars.

Figure 2.17. Photo of the test by Huang et al., 2015

By using the reference lines with the photogrammetry, the subsidence of the soil mass and the maximum horizontal displacement at different elevations within the filled material were presented with the increase of elevations the subsidence decrease while the horizontal displacement approximately reductions exponentially. The results also indicate that the friction angles influence significantly on the subsidence and tension in geosynthetic: with higher angles, the subsidence declined. In addition, corresponding to a higher overlying soil layer, the maximum subsidence increased. Otherwise, for the geosynthetic deflection, no test condition was found as the influenced impacts on the deformation shape, which was assumed as a parabolic curve. Moreover, for both soil mass subsidence and geosynthetic deflection, the different particle size distribution seems not to affect.

The research separated three different zones of the subsidence deduction. A rapid zone locating from the top of the channel to the height of 125 mm and therefore ratio between the height of soil and the diameter of the channel, H/D equals to 1.0. A slow zone locating from the height of 175 mm, H/D equals to 1.4. Between two zones, a transition zone connected them. Due to the increase of the elevation, the subsidence decreases very quickly in the rapid area, while it reduced gradually in the slow. This result confirmed the critical height of soil arching which differs from 1 to 1.87 times more substantial of the trapdoor width.

However, the results of this research may not be applied on the realistic conditions due to many shortcomings such as the difference between the shape of the soil particles and the aluminum bars, the assumption of the method to determine the angle of the internal friction and the limitation of the 2-D modeling.

2.5.6. Full-scale experiment of cavity by Huckert et al., 2016

Circular cavities under geosynthetic-reinforced embankment were simulated with granular soils, and a cohesive treated soil was used as fill materials. Three experimental sections were constructed for each fill soil. A specific device includes tubes and clay pebbles located over a trapdoor was used to create the cavities following the process of the progressive opening with three different diameters: 0.75, 1.25 and 2.2 m (*Figure 2.18*). Traffic loads were applied to the top of the embankment as a surcharge. Three types of geosynthetic were tested with two main purposes: comparing the different stiffness of the reinforced materials and adapting to the treated soil.

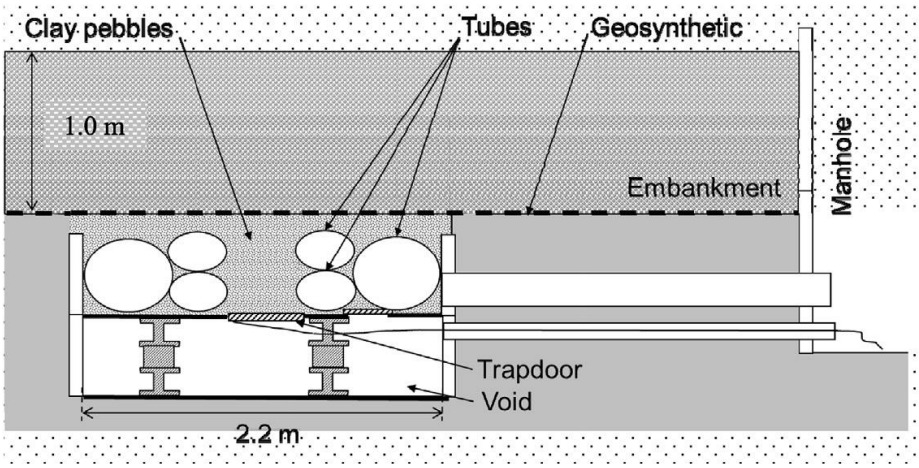

Figure 2.18. Schema of full-scale experiment (Huckert et al., 2016)

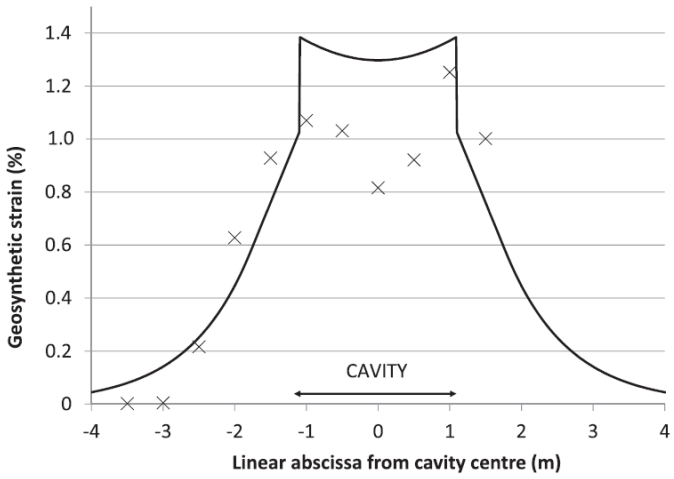

Figure 2.19. Analytical and experimental geosynthetic strain (Huckert et al., 2016)

During the tests, several monitoring devices were used to measure the data. In order to realize the load transfer, Earth Pressure Cells were placed around the cavities. For the geosynthetic, the Bragg grating optical fiber is used to measure the strain whereas the laser sensor measured

the deflection of the sheet after the cavities opening. During the process, the evolution of the deflection can be monitored by the Ground Penetrating Radar which can also be used to obtain the displacement within the embankment. The surface settlement was analyzed manually by a topographic work.

The use of a variety of the test configuration allowed the authors to confirm the variation for the collapse mechanisms between the different types of soils. For the granular materials, during the cavity opening the deformation of the embankment is progressive and the cylindrical geometry was observed whereas the opening process for the treated soil tends to decrease gradually. As an influence of the stiffness of geosynthetic, the weaker material leads to the higher surface settlement. A mean expansion coefficient Ce = 1.037 was found for the gravel. For the load transfer mechanisms, an increase of the vertical stress at the anchorage areas corresponding to the position was confirmed.

The experiment results were compared with the analytical methods for the deflection and the strain of the geosynthetics in the case of tests for granular materials (*Figure 2.19*). Even though at the anchorage areas, the results were compatible, several differences were found for the areas above the cavity relevant to the shape of load distribution. It can be explained by the assumption as a uniform distributed load on the geosynthetic sheet based on Terzaghi's formulation.

As a shortcoming, the influence of the opening process on the load transfer and expansion mechanisms has not been found in this study.

2.5.7. Other experimental studies

Firstly established by *Terzaghi (1936)*, the trapdoor system is commonly used to analyze the redistribution of stress within the granular soil, often known as arching. This phenomenon has been extensively studied for many years by many authors in both experiment and numerical works. *Iglesia et al. (2014)* developed the yielding trapdoor in an increased gravity environment, similar to that of a geotechnical centrifuge. They found that the stress distribution evolves from an initially curved shape to a triangular one. More importantly, they confirmed that if the depth of the overlying soil was less than 1.5 times the width of the trapdoor, a curved-triangular arch could not be sustained.

Paikowsky et al. (2003) conducted another research on the trapdoor (3.81 cm wide and 45.7 cm long), whereby a photo-elastic technique and tactile sensors were used to observe the

development of the stress distribution during the trapdoor test within the granular material. As a significant result, an increment of the pressure was found on the outer zone of the trapdoor, following its downward movement.

Among the studies of geotextiles reinforced embankment above cavities, *Nagy et al. (2017)* developed a full-scale experiment using a triaxial geogrid (225 kN/m of stiffness) to reinforce an elastic road system under a static load, with the presence of underground. The experimental result was then compared with a numerical simulation based on the Finite element method. It confirmed that the deformation of the road structure is significantly reduced with the use of the triaxial geogrid.

2.5.8. Summary of experimental studies

In order to investigate the arching effect within the granular soil over by trapdoor test, a 2-D photographic method has been commonly used to evaluate the displacement. However, the measurement is influenced strongly by the resolution of the image. Regarding the stress distribution analysis, the pressure cells have been usually installed, yet, the size, shape and the cost of the cell may limit the number of observed points nearby. The variance of the stress distribution in different areas along the trapdoor was observed clearly by *Pardo and Sáez (2014)* in coarse sand and *Paikowsky et al. (2003)* by using a tactile sensor.

Focus on the use of geosynthetic to reinforce the platform over cavities; many studies have improved significantly the understanding of the mechanism occurring in the soil embankment. Based on an experimental test that represents the soil particles by metallic bars, *Huang et al. (2015)* have found the influence of the soil characteristics such as friction angle on the shape of deformed geosynthetic. A relation between the soil pressures acting on the soil over a deflected geosynthetic, *Zhu et al. (2012)* showed that before the soil arching degree reaches a peak, the pressure could transfer effectively to the trapdoor area to the outer zones. Then, the soil pressures on the deflected geosynthetic are not influenced by the fill height and the material stiffness.

Notably, the expansion coefficient was taken into account in the case of large cavities to gain an understanding of the expansion behavior, primarily aiming to the estimation of the surface settlement. *Huckert et al. (2016)* executed three full-scale experimental sections to reproduce the opening of the cavities, a progressive opening was applied under the embankment, and the shape of the deflection of the geosynthetics was confirmed as a parabolic curve. In the case of treated materials, the accuracy of the design methods needs to be reviewed as reflected in this

study. According to a full-scale experiment, the collapse mechanism is different for granular materials and treated soils.

Table 2.9. Summary of main current outcomes of experiment studies

Current studies	***Main outcomes***	***Tested dimension***	***Relevant mechanisms***
Paikowsky et al., 2003	- Using tactile sensors to observe the stress distribution	2-D	Load transfer
Costa et al., 2009	- Influence of the soil density on the settlement - Pattern of the failure surfaces	2-D	Soil expansion
Zhu et al., 2012	- Effects of fill height and tensile stiffness on soil arching	2-D	Load transfer
Pardo and Sáez., 2014	- Load distribution on rigid support near the trapdoor	2-D	Load transfer
Iglesia et al., 2014	- Shape of load distribution	2-D	Load transfer
Huang et al., 2015	- Influence of friction angle of the fill on the subsidence and tension in geosynthetic	2-D	Soil expansion
	- Critical height of soil arching		Load transfer
Rui et al., 2016a	- Relation between the shape pattern and the H/D ratio - Confirms the presence of the equal settlement - Influence of H/D on the stress distribution	2-D	Load transfer
Huckert et al., 2016	- Variation of collapse mechanisms due to the types of fill (cohesive and granular soils) - Influence of stiffness of geosynthetic on the surface settlement - Mean value of expansion coefficient for gravel - Progressive mode of the cavity opening in granular materials - Cylindrical geometry of the collapsed granular soil.	3-D	Soil expansion
	- Increase of the vertical stress at the anchorage areas		Load transfer
	Strain measurement in GSY on cavity and anchorage areas		GSY behavior
Nagy et al., 2017	- Effect of geogrid on the deformation of road structure	3-D	Load transfer

As summarized in *Table 2.9*, many studies have improved the knowledge significantly on the load transfer and the soil expansion mechanisms. The analysis results do not allow for the exact determination of the behavior mechanical of geosynthetic due to the accuracy of the imaging, which is commonly used in laboratory observations. Additionally, the study on numerous instrumented tests, which could characterize load mechanisms, seems to be restricted by the high costs and the ability to change the geometrical configurations.

2.6. NUMERICAL ANALYSIS

Finite element method (FEM), Finite difference method (FDM) and Discrete element method (DEM) are useful to study the load transfer and the expansion mechanisms within the geosynthetic-reinforced soil above cavities. These models could be utilized to characterize precisely the large deformation within the granular embankment and the geosynthetic behavior. Additionally, FEM model was applied successfully to simulate the vertical stress distribution at the soil surface *(Cui et al., 2007)* and soil reinforcement for mechanically stabilized earth walls *(Yu et al., 2015)*.

Finite difference method is common to simulate the geotechnical problems considering the mechanical characteristics of geosynthetics. FLAC3D (Fast Lagrangian Analysis of Continua) is a commercial finite difference method program for continuum analyzes. The software uses an explicit finite volume formulation that solves the complex behaviors of models with an incremental constitutive law. Many geotechnical issues with the applications of geosynthetics can be reproduced: the mechanically stabilized earth walls *(Yu et al., 2015),* the inclusion of geosynthetic reinforcement above the piles (*Han and Gabr, 2002*; *Jennings and Naughton, 2012*) or the geosynthetic-reinforced embankment over cavities (*Tano et al., 2017*; *Yu and Bathurst, 2017*).

A comparison between the FLAC and PLAXIS programs was carried out by *Yu et al. (2015)* focusing on the numerical soil-structure interaction. Although the study described the conditions that give a good agreement between the two simulation methods but in the case of the soil reinforcement materials that are discontinuous in the plane-strain direction, the results can be different.

Taking into account the effect of cavity opening process to the load distribution on the geosynthetic, *Villard et al., (2016)* compared a numerical simulation coupling FEM and DEM to the experimental works to show study the behavior of granular embankments reinforced by geosynthetics. The numeric results demonstrated a significant influence of the cavity opening

process on the load transfer mechanisms along with the geosynthetic sheet and confirmed the expansion factor within the embankment is no uniform. Nevertheless, the link between the geosynthetic characteristic, the subsoil properties, and the opening process have not been clarified fully.

2.6.1. Finite element method

The Finite element method (program PLAXIS 2-D) with the user-friendly interface is widely used to solve the soil-structure problem including the behavior of geosynthetic. The behavior of soil behavior can be analyzed in an axisymmetric and plane strain modes. A variety of constitutive models with different complexity can be used for accordant applications. All constitutive models can be set in drained or undrained conditions. In this program, the strains, stress and failure states of soils could be calculated whereas the quadratic 6-node or 15-node triangular elements are available to represent the geometry.

The Finite element modeling can represent the geosynthetic reinforcements due to its advantages over experimental works. The configuration of the model can be varied easily beside the deformations of geosynthetic and soil, and the load transfer mechanisms within the platform may be invested, which limited to study in a model test.

Geotextiles, which are named in PLAXIS as geogrids, could be simulated by the use of unique tension elements. The behavior of the geosynthetic material in the surrounding soils can be represented by geogrids element combining with the interface elements. The characteristics of these elements are defined using a normal stiffness and a maximum tension force. The membrane effects are taken into account by the use of updated mesh calculations.

In PLAXIS 2-D, a basic parameter axial stiffness EA could be specified as a material property of the geosynthetic. The stiffness could be defined based on the material tension stiffnesses and the cross-section areas. The relation between the force and the strain in axisymmetric models can be defined below:

$$\begin{bmatrix} \mathrm{N} \\ \mathrm{H} \end{bmatrix} = \begin{bmatrix} \mathrm{EA}_1 & 0 \\ 0 & \mathrm{EA}_1 \end{bmatrix} \begin{bmatrix} \varepsilon \\ \varepsilon_{\mathrm{H}} \end{bmatrix} \qquad \textit{Eq.2.55}$$

where H is the hoop force, ε_H is the hoop strain.

As a joint element, the interface element could be added to geogrids elements to allow for correct modeling of soil-structure interaction. The interface could be used to simulate thin zones of intensely shearing material at the contact between the geogrid and the surrounding soils. The elements can also be created between different soils or materials. The distribution of nodes and stress points in the interface elements and the connection to soil elements is different depending on the use of 15-node or 6-node elements. In the case of 15-node soil elements, the corresponding interface elements are defined by five pairs of nodes, whereas three pairs of nodes are defined in the case of 6-node elements.

The values of interface properties in PLAXIS can be set as a single soil zone, with no thickness. Therefore, the properties of surrounding soils and interface elements could be different. The interfaces have properties of friction angle, cohesion, dilation angle, tensile strength, Young's modulus (E_i), and Poisson's ratio (v_i).

In PLAXIS 2-D, the effective normal stress applied perpendicularly on the interface could be displayed.

2.6.2. Key numerical studies

2.6.2.1. Experimentation and numerical simulation of Schwerdt et al., 2004

In order to test the geogrids placed above the cavity, *Schwerdt et al. (2004)* carried out three experimental tests, in Anhalt University of Applied Sciences, Dessau, Germany. The tests were performed with a single layer and multiple layers of geogrids, and then the results were compared with the results from numerical calculations.

In two first tests, only one layer of geogrids, with a short-term tensile strength T_{ult} of 30 kN/m and 40 kN/m were placed below the soil with a height of 0.7 m and 1.6 m respectively, and at the bottom of a test platform, a circular 1.68 m diameter subsidence was created. In the last test, the void diameter of 2.0 m was planned, two different strength of geogrids (30 kN/m and 40 kN/m) were placed under a 1.6 m of granular soil. The dynamic load was applied by four test cylinders with the maximal force of 50 kN. A 60 km/h speed of truck was simulated with overlapping more than 300 000 cycles.

For the first test, a substantial increase of strain in geosynthetic was measured after 500 cycles, and at the end of 2500 loadings, the material failed. An additional load was applied on test 2, and after 3600 cycles more, with the load was increased to 100 kN, the material failed. In the

double layers test, after 450 000 loading cycles, no cracking or damage could be found on the material, even the load increased 2.4 times of planned load for the last 150 000 cycles.

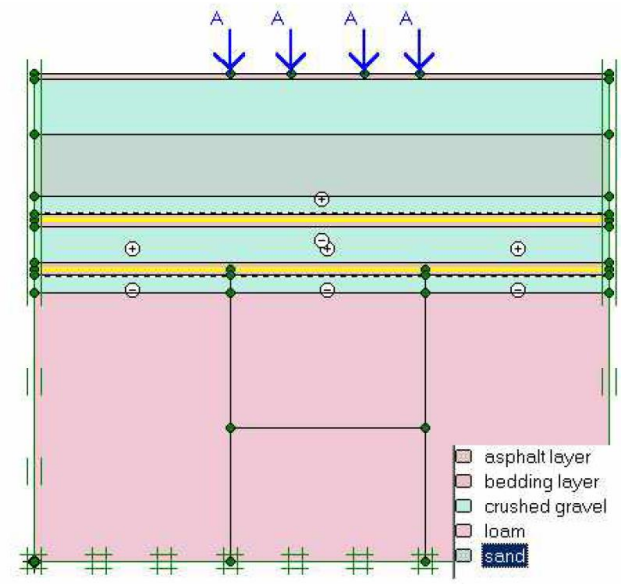

Figure 2.20. Model of the layers for the PLAXIS calculations (Schwerdt et al., 2004)

After the experimental tests, the program PLAXIS® was used to calculate the depressions of the surface and the strengths of the geogrid layers (*Figure 2.20*) and compare the results with the last test. The comparison of measured values and PLAXIS calculation was presented in *Table 2.10*.

Table 2.10. Surface settlement and material deflection values are taken from measurement and PLAXIS (Schwerdt et al., 2004)

Depressions	***Planned loading (300 000 cycles)***		***Additional loading (150 000 cycles)***	
	Measurement	***Numerical calculation***	***Experiment test***	***Numerical calculation***
ds (cm)	1.0	1.2	1.4	3.8
dg_1 (cm)	0.9	1.3	0.8	4.0
dg_2 (cm)	1.2	1.3	1.4	4.1

Based on the good correlation between numerical calculations and measured test, the void can be safe and stable under stiff and stretched geogrids if the thick of soil above the material is ensured. Moreover, the load transfers to the edges of the cavity were stabilized even if only one layer of geogrids is used. Double layer of geogrids embedded in a crushed gravel layer was particularly good application and allow the load transfer toward the edge of the cavity.

2.6.2.2. Finite element models of Potts (2007)

Using the Finite element model with a 2-D program, ICFEP, a numerical study was completed by *Potts (2007)* to investigate the influence of a range of parameters on the behavior of geosynthetic reinforced a platform over a void. The numerical work was based on a series of model tests (*Figure 2.21a*) conducted in a large box with a moveable platform which can be lowered to simulate a void. A set of transducers named as LVDT were placed at the top and the base of the test box to measure the surface settlement and the platform movement (*Figure 2.21b*). The tests were performed with and without the use of geosynthetic reinforcement, in two series: with loose and dense sand. In the first series, the reinforced tests were conducted considering the differed ratio of H/D: 0.5, 1, 2, 3, 4 and 5; whereas for those in the second series, only H/D equal to 0.5 and 1 were completed.

Concerning the numerical work, only the case that the tests where the void reinforced by geosynthetic were simulated by the Finite element method. A Mohr-Coulomb criterion was used to represent the behavior of the fill material, in plane strain conditions. A Young's modulus of 20.000 kPa and a Poisson's ratio of 0.3 have been assigned to the fill, which was assumed to have no cohesion (γ =15.5kN/m^3; φ' = 35°). For the base material representing the bottom of the box, an elastic soil model was used, and a high Young's modulus of 100.000 kPa was assigned along with a Poisson's ratio of 0.3. Concerning the geosynthetic represent, a simple elasto-plastic soil model was used with the thickness was assumed as 0.1mm, with the stiffness J = 15 kN/m/m.

According to the results of the numerical analysis, the effects of the H/D ratio were compared with the measured data. Even if the numerical simulation reproduced the same order of the surface settlement, for the high values of H/D, the maximum surface settlements were overpredicted using the Finite element model, but for the lower ratios, the settlement is underestimated.

The influences of a number of variables of the behavior of geosynthetic-reinforced embankment over a void were also investigated considering the variation of the fill height; the width and the shape of the void; and the properties of the geosynthetic and fill; the geometrical features, low ratios of H/D lead to a higher value of the settlements of the fill and the geosynthetic. The lower stiffness of the geosynthetic was clarified as it produces greater deflections, whereas the tensile strength does not influence the stress and the deflections of the geosynthetic sheet. Regarding the angle of the interface, friction was resulted not to cause

significant influences on the behavior of the geosynthetic. For the effect of the fill properties, the study illustrated that Young's modulus and the coefficient of earth pressure in the fill do not have any significant impact on the behavior of the reinforcement platform. The numerical analyses also indicated that K is independent of the fill properties and the value K = 1.0 is still appropriate to estimate the vertical stress applied on the geosynthetic.

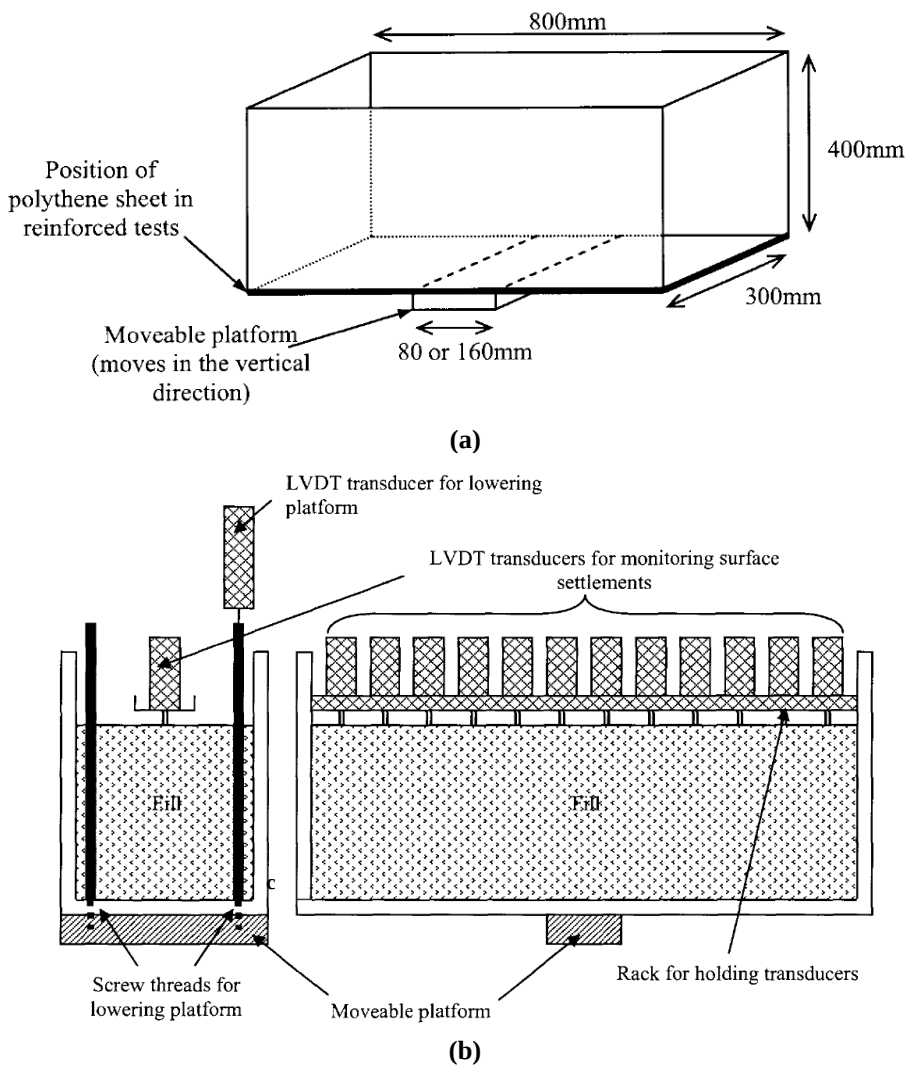

Figure 2.21. Experiment test set-up (Potts, 2007)

Moreover, the study showed that the significant influence of the friction angle of the fill material on the geosynthetic deflection. It was found that higher values of shearing resistance lead to lower values of the deflected geosynthetic, especially for the greater height of the fill. The study also confirmed a dramatic effect of the dilation angle on the surface settlement as it reduces following the increase of the dilation angle. Moreover, as the dilation angle increases, the geosynthetic deflection decreases, thereby the arching effect within the fill is enhanced.

Although many variables were considered in this study and several significant effects were clarified, other influences such as the way that the void opening and the behavior of the coefficient expansion should be investigated. Moreover, the results of the numerical analysis need to be validated with the experimental study.

2.6.2.3. Numerical approach by Villard et al. (2016)

From the results of the full-scale experiment obtained by *Huckert et al. (2016)*, a numerical model was developed to examine the load transfer mechanisms of granular embankments reinforced by geosynthetic above cavities *(Villard et al., 2016)*. A progressive opening and a gradual downward process were considered in order to understand the influence on the load distribution. The 3-D numerical model was developed combining the Finite elements method (for the geosynthetic behavior) and Discrete element method (for the granular material).

Based on the results of this study, the analytical method proposed by *Briançon & Villard (2008)* has improved with the better knowledge of the load transfer mechanisms acting within the embankment, the shape of the load distribution on the geosynthetic sheet and the determination of the expansion coefficient.

The simulation has succeeded to reproduce the geosynthetic behavior as presenting the difference in the shape of the geosynthetic deflection between both opening procedures (*Figure 2.22a*). Moreover, considering the Terzaghi‘s formulation for the calculation of the load acting on the geosynthetic sheet, the numerical results showed that the values of the soil pressure ratio could reach 1.3 when considering H/D ratios between 0.25 and 2, and the use of the active earth pressure ratio K_a is not well adapted. Moreover, the non-uniform shape of load distribution above the cavities was noted, and it is influenced by the opening process: a conical shape for the progressive opening and constant for the gradual downward process (*Figure 2.22b*). Taking into account the change in local porosities within the granular embankment, the authors also confirmed the difference in the expansion coefficients and the dependence with two opening processes. A value of 1.037 was found as the expansion factor for the gradual downward opening, and values of 1.048 and 1.036 were obtained for the progressive process.

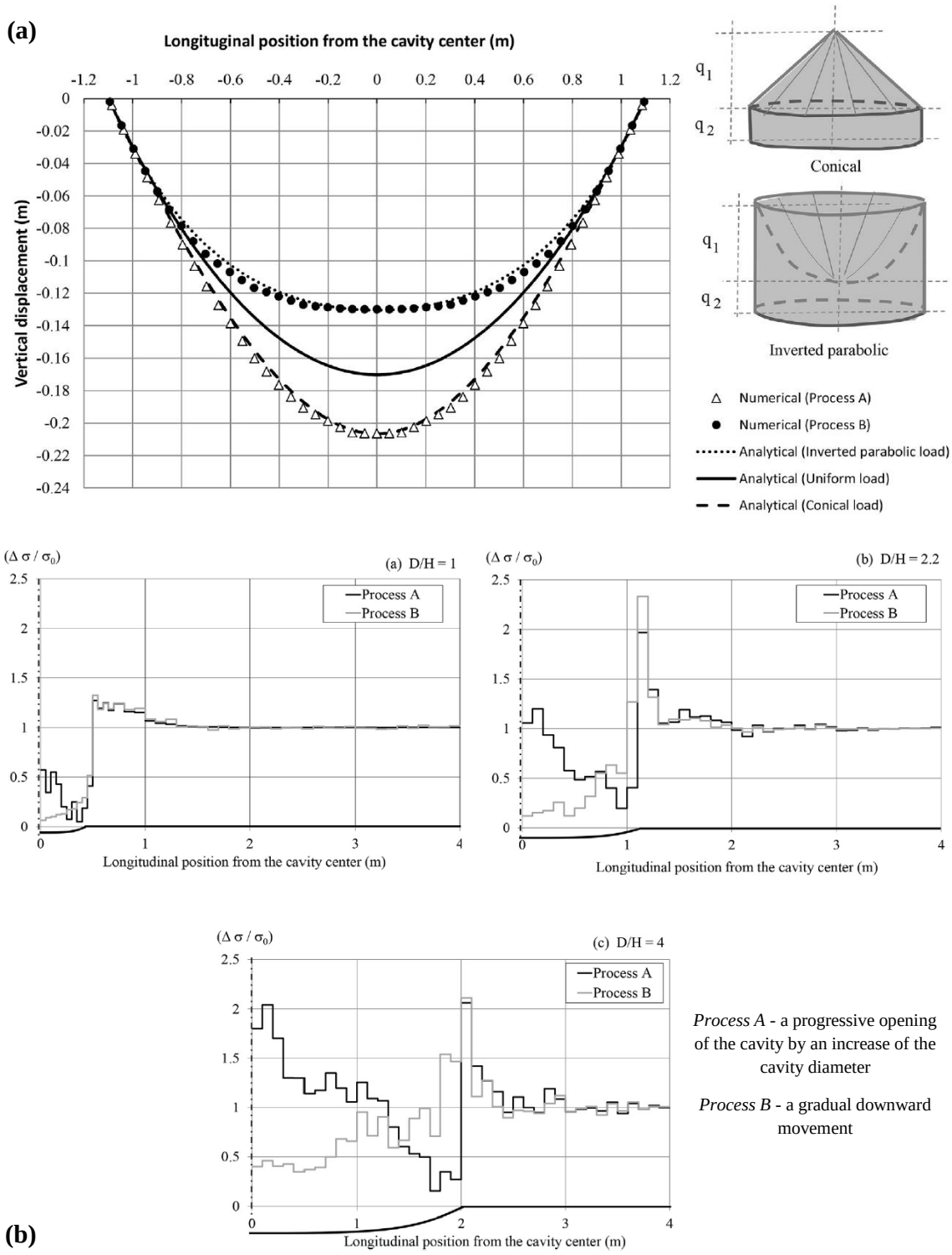

Figure 2.22. Key results of numerical simulations (Villard et al., 2016)

a: Geosynthetic deflection b: Increase in vertical stress

2.6.2.4. Numerical approach of Yu and Bathurst (2017)

The Finite difference method was used to represent a geogrid pullout test and a geotextile-reinforced soil layer over a void based on two physical tests *(Yu and Bathurst, 2017)*. In a

pullout test, geogrid sheets were placed in granular soil, inside a pullout box (*Figure 2.23a*). With three different types of geogrid, the highest stiffness is 1903 kN/m; the physical tests were performed under four different surcharge pressures (10, 25, 50 and 100 kPa). A load cell was placed near the clamp to measure the tensile load. The program FLAC version 2-D was used to simulate the test with plane strain boundary conditions and 3376 zones of soil (*Figure 2.23b*). *Figure 2.23c* presents the soil boundaries above and below the clamp, which was modeled by a single beam element.

Regarding the geosynthetic representation, 115 cable elements were used with the first one was slaved to the right beam note at the end of the clamp. The granular soil was modeled using a Mohr-Coulomb model, and due to the lack of the parameters reported in the physical tests, a parametric study was carried out. The interface between the granular soil and the geosynthetic was simulated by a grouted cable element with the frictional and cohesive shear strength calculated from a range of the strength reduction factor.

A geotextile-reinforced soil layer over a cavity was then simulated based on an experiment of *Villard and Briançon (2008)* (*Figure 2.23d and Figure 2.23e*). A geotextile sheet (J = 1100 kN/m) was placed between a gravel layer and a 0.5 m height of a void, which is created by deflating supporting airbags. The surcharge loads were processed differently at the left side (q_1) and over the void (q_2). An optical fiber sensor was used to measure the strains in the geosynthetic sheet. The numerical program also used the linear-elastic Mohr-Coulomb model for the gravel layer and the supporting soil. The interface between geosynthetic and the gravel layer or the supporting soil was selected as the reported values (30° and 25°). The interface reduction factor, R_i, was computed as 0.6 similarly for these two interfaces. Similar to the pullout test, a range of the lack-information parameter was also examined. The simulation was run in two different cases, which have the main difference is the definition of the interfaces. In the first case, two interfaces between the supporting soil, the gravel layer and the geosynthetic were defined. In the second case, only an interface between the two soils is modeled whereas the interaction between the geosynthetic and the surrounding soil was simulated by the grouted cable elements. The FLAC model was simulated to force equilibrium before the cavity opening, and after that, the model was solved to reach the force equilibrium again. Then the surcharge was applied following the procedure of the physical tests.

Based on a range of assumed soil and interface properties, a parametric study was carried out to clarify the influences on geosynthetic behavior. For both tests, the impact of Young's modulus in the range of 10 and 100 MPa can be neglected. Regarding the effect of soil

cohesion, a minor difference was found on the geogrids pullout loads when the cohesive component was varied from 1 to 5 kPa. For the void test, to have a good agreement in the geosynthetic deflection with the measurement, the cohesion of the gravel layer was obtained as 1.0 kPa whereas a value of 5 kPa was found for the supporting soil.

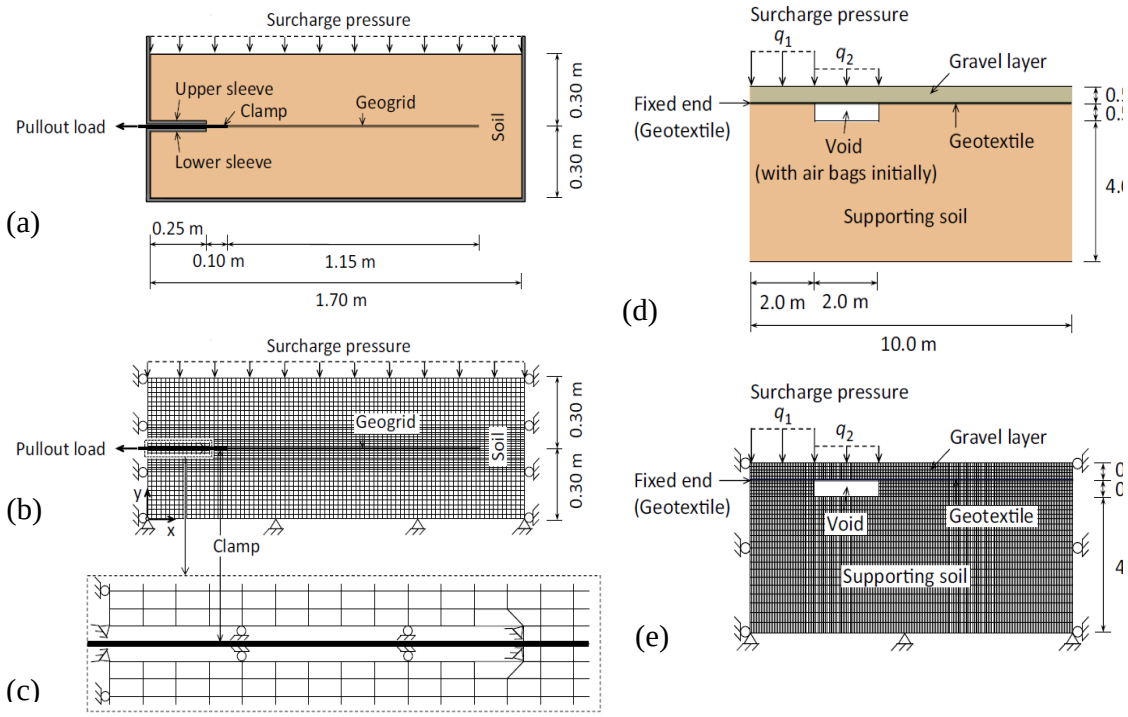

Figure 2.23. Simulation works of Yu and Bathurst (2017)

The influence of the cable-element grout stiffness on the geosynthetic pullout load has been clarified for different surcharge load, and the value of 20 MN/m/m agreed well with the experiment test. A value of 0.67 was suggested to select for the strength reduction factor of the surrounding soil. In the case of the void test, the influence of the interface stiffness and shear stiffness between soil and geosynthetic on the geotextile vertical displacement seems to be minor.

Regarding the effect of the FLAC strain mode, there is not a significant difference that found on the pullout load between the large-strain and small-strain modes, but for the geosynthetic deflection in the void test, the large-strain mode showed a good agreement with the physical examination.

Through large-strain mode, better agreement of the vertical displacement of geosynthetic over void was found with the measured data in case of the geosynthetic modeled with beam

elements instead of cable elements, whereas the similar results were found for the geotextile strains.

2.6.2.5. Other numerical studies

A few decades ago, the interface between the geosynthetic reinforced soft ground and its surrounding had been reproduced using the Finite element modeling by *Hird and Kwok (1990)*. The Finite element method is also used by *Brocklehurst (1993)* to investigate the behavior of geosynthetics considering the performance of a plane strain incorporating two layers of the soil system.

Following the study of *Potts (2007), Pizá (2009)* investigated the effects of the stress distribution within a fill reinforced by a layer of geosynthetic, considering two shapes: a circular void and a longitudinal one. Using ICFEP program based on the Finite element method, the fill material and the foundation soil were modeled as granular by elastic-perfectly plastic materials with the Mohr-Coulomb failure criterion. The geosynthetic (J = 50kN/m) was simulated by membrane elements using elastic-perfectly materials. A significant displacement analysis was used to model the effect of the geosynthetic. Concerning the load transfer mechanisms for the case of the circular void, the vertical stress applied on the geosynthetic were compared between various ratios of H/D and the hydrostatic values. A stable arch was achieved for a low H/D, and the arching behavior was identified for the H/D ratio equal to 2.2 where the stress starts to decrease after an increase. Regarding the effect of H/D ratios on the behavior of geosynthetic, the study indicated that for both two types of the cavity, a greater void width has a more deflection for the geosynthetic. The shape of deflected geosynthetic was also compared between different H/D ratios and void types. Whereas the H/D ratios seem not to affect the shape of the longitudinal void, the difference was obtained for the circular. Moreover, the similarity of the shape with a circular arc was indicated that is better than a parabolic curve, from the comparison between two different widths of voids (1.0 m and 2.0 m). Although several effects of the varied shape of voids on the geosynthetic behavior, the results need to be validated by experimental work.

Using PLAXIS 2-D, *Tahmasebipoor et al. (2010)* performed a parametric study to investigate the behavior of geotextile-reinforced soil over cavity considering the influences of used geosynthetic parameters and cavity characteristics. The Mohr-Coulomb failure criterion was applied for the soil, and a plane strain condition with 15-node triangular elements was used for the analysis. The interface elements were placed on both sides of the geosynthetic to allow its

movement inside the surrounding soil. The use of the Finite element method successes to specify that the settlement of the ground surface could be reduced following the rise of the geosynthetic stiffness. It also decreased following the increase of the reinforced layers used over the cavity. However, this study focused on a plane strain condition in the numerical model, and the results should be validated or clarified by experimental work.

The soil arching in the geosynthetic-reinforced fill above a void was investigated by a finite-element parametric study of *Potts and Zdravkovic (2010)*. Concerning the lateral earth pressure coefficient, K, in the shear zone, a new value of K = 1.0 is recommended, corresponding to significant lesser-predicted vertical stress at the bottom of the overlying soil.

Using the Finite element program PLAXIS, *Girout et al. (2014)* investigated the load transfer within a geosynthetic-reinforced platform. The numerical work is based on a centrifuge test considered the soil settlement through the downward movement reproduced by a mobile tray. As a conclusion, the 2-D axisymmetric model is possible to simulate the load transfer within the embankment. In order to describe the granular performances, even the Hardening soil and Hypoplastic models were used in the simulation, but the hypoplastic model was noted for the advantage due to the consideration of the soil density. The numerical results confirm the load transferred by arching in the granular embankment, the load distribution is mostly applied on the inclusion edge, and it can be increased by the additional load which is transferred through the geosynthetic by the membrane effect. The parametric studies were also proposed to improve the understanding of the load transfer mechanisms considering the embankment thickness, the void ratio of granular material and the displacement evolution of the tray.

Following the experimental work of *Pardo and Sáez (2014)*, *Vasquez, (2014)* used the Discrete element method to reproduce the arching effect with an active trapdoor test. Due to the results of the stress fields and the orientation of the principal stress, the arching effect phenomenon was confirmed. Comparing to the FEM simulation deduced by *Pardo and Sáez (2014)*, the DEM model predicted a similar increment of vertical stress following the displacement of the trapdoor.

More recently, *Rui et al. (2016b)* developed a 2-D DEM to simulate laboratory trapdoor tests, which have a good agreement of the deformation and stress distribution with the works presented by *Rui et al. (2016a)*. In order to calibrate the numerical models, a series of plane strain compression tests were performed. The numerical works confirmed the shape of the soil arching revolution patterns as a triangular, a tower-shape and an equal settlement pattern,

which are highly depended on the ratio between the height of the fill material and the width of the trapdoor.

In the research area, a case study in Algeria was conducted to investigate the influence of geosynthetic reinforced embankment on locally weak zones by PLAXIS program *(Benmebarek et al., 2015)*. By Considering the variety of geosynthetic stiffnesses, from 500 kN/m to 10 000 kN/m, the effects of the reinforcement material and the friction angle of the embankment soil that reduce the settlement have been confirmed.

2.6.3. Summary of numerical studies

As the most important results, the numerical work of *Villard et al. (2016)* highlighted that the shape of load distribution the load distribution is not uniform on every area on the sheet and depends on the mode of the cavity opening. Moreover, the ratio H/D was confirmed to have a significant influence on the load distribution. Additionally, in order to have a good concordance between experimental and numerical works, the value of K in the Terzaghi's formulation was suggested to use as 1.3 for the case study with given test parameters.

A summary of the primary outcomes taken from the current numerical studies is presented in *Table 2.11*. Due to the advantages of the numerical methods, numerous testing configurations were considered to improve the load transfer and soil expansion mechanism as well as the behavior of geosynthetic. Numerical methods such as FEM, FDM, and DEM have been used independently or as a combination to reproduce the behavior of geosynthetic-reinforced embankment over cavities. In many studies, the Mohr-Coulomb failure criterion has been used successfully to represent the behavior of the fill material, especially in the case of granular.

The accuracy of numerical models depends on the choice of soil and geosynthetic constitutive models selected, which may be challenging for parameters that are not available from related test documentation. Most of the numerical experiments presented above are based on the relevant experiments, however, in many cases the lack of testing parameters, for example, the soil characteristics could restrict the results of the simulation. Even if parametric studies were also performed, many other influences should be investigated to gain a better understanding of the analytical assumptions and the behavior of the structure.

Table 2.11. Summary of main current outcomes of numerical studies

Current studies	***Method***	***Main outcomes***	***Relevant improvements***
Schwerdt et al., 2004	FEM*	- Confirm the load distribution after cavity opening	Load transfer
Potts, 2007	FEM*	- Influences of friction and dilatancy angles of filling soil on the arching effect - Note for the K value equal to 1	Load transfer
		- Effects of geosynthetic stiffness - Effects of width and shape of void - Effects of geometrical properties	Soil expansion
Pizá, 2009	FEM	- Note for stable arch within filling soil as H/D = 2.2	Load transfer
		- Difference on the deflected geosynthetic between the type of voids - Influence of void width on the deflected geosynthetic - Shape of deflected geosynthetic was noted as a circular arch	Soil expansion
Tahmasebipoor et al., 2010	FEM	- Effect of geosynthetic stiffness on the surface settlement	Soil expansion
Vasquez, 2014	DEM	- Confirm the similarity between DEM and FEM simulations to reproduce the vertical load distribution	Load transfer
Villard et al., 2016	FEM & DEM*	- Used the K value as 1.3 for granular embankment - Effects of opening process and H/D ratio on the load distribution shape: Similar in anchorage areas but different in cavity area	Load transfer
		- Effect of cavity formation process on the expansion mechanism	Soil expansion
		- Displacement of GSY in anchorage areas	Geosynthetic behavior
Yu and Bathurst, 2017	FDM*	- Influence of soil parameters and strain mode calculation on the deflection and strain of the geosynthetic - Compare with FEM	Geosynthetic behavior

* *Study calibrated from experimental results*

2.7. CONCLUSIONS

Geosynthetic reinforcement solution is widely applied for the construction of the infrastructure due to many advantages such as its cost and easy installation. However, the understanding of some specific mechanisms for this solution is necessary to improve. One of the main gaps is the misunderstanding of the load transfer mechanisms acting within the embankment above cavities.

Among many theories of the arching effect in the soil, the formulas of *Terzaghi (1943)* is applied commonly for the calculation of the load on the geosynthetic above cavities. However, this method has several deficiencies due to the simplified assumptions that should be improved. In fact, the evolution of the cavity opening process may differ according to the geotechnical environment and the characteristics of the embankment material. Most of the existed theories are based on the trapdoor experiment known as a downward movement while a progressive opening process may affect differently. Concerning the formulation of the load acting on the geosynthetic sheet, there is no method exist to determine the soil pressure coefficient directly. In addition, numerous author proposed various definitions for the K value include the assumption of the rotation of the stress such as *Handy (1985).* However, the application of the method should be validated with experiment works. Moreover, according to the numerical results performed by *Chevalier et al. (2012)* and *Villard et al. (2016)*, the values of K for the granular material are strange with the usual value of K_a.

Another issue should be improved the misunderstanding of the expansion mechanism which is recommended as an essential factor in many design methods such as *RAFAEL* or *EBGEO (2011)*. A uniform expansion factor is considered to estimate the surface settlement, and due to the high cost of the full-scale experiments, the ability to determine this coefficient is restricted.

Currently, there are two viewpoints for the analytical design are used in Europe. The British Standard *BS 8006 (2010)* is based on some significant assumptions that make it different from the other methods such as *RAFAEL* and *EBGEO (2011)*. The major differences between these methods are the definition of the geometry, the behavior of the depression zone and the assumption of arching effect within the embankment above cavities. According to many studies, the existence of the arching effect is confirmed thus the assumption of no arching in the overburden soil over geosynthetic-reinforced cavities should be changed. Moreover, these methods are based on the same assumption for the geosynthetic sheet at the edges of the cavity. By taking into account, the frictional behavior of the sheet in the anchorage areas, *Briançon*

and Villard (2008) and *Villard and Briançon (2008)* have been significantly improved the *RAFAEL* method.

Many experiment works have been developed to improve the knowledge of the load transfer mechanisms in this field. Instead of many significant results have been found, especially in the full-scale experiment. However, some difficulties relevant to the costs of the instruments can restrict the number of experimental tests. In addition, the limitation of the 2-D method for the tests observation and the restraint for the fill material applied commonly in many laboratory experiments should be considered to improve the accuracy of the experimental results. The numerical works based on FEM and DEM were also carried out for this study field, and the good agreement with the experimental results was confirmed. It has been found that a reasonable agreement can be achieved between the observation and simulation of geosynthetic reinforcement in a reinforced embankment. However, the simulation should be extended with more points of view that explained as the aims of the experiment work in the thesis.

Presently, the experimental work of *Huckert et al. (2016)* and numerical study of *Villard et al. (2016)* have succeeded to validate the French recommendations. Nevertheless, due to the limitation of the latest studies, several important points should be clarified. As an essential mechanism acting within the embankment over the geosynthetic reinforcement over the cavity, the non-uniform distribution of load on the geosynthetic sheet and the influences need to be validated by experiment. In addition, the lack of experience in determining the expansion coefficient is another shortcoming. This factor should be defined considering the influences from the geotechnical parameters (for example the height of embankment or the type and density of embankment soils) and cavity characteristics (for example the size of void or the opening mode).

Last, it is a sufficiency to mention the significant developments on specific cases of the design proposed by *Feng and Lu (2015)*, *Feng et al. (2017a)* and *Feng et al. (2017b)*, due to the knowledge improvements for the soil arching, soil expansion influences or the behavior of reinforcement platform with two adjoining cavities.

CHAPTER 3. LABORATORY EXPERIMENT

Publication: Pham, M. T., Briançon, L., Dias, D., Abdelouhabd, A., 2018. Investigation of load transfer mechanisms in granular platforms reinforced by geosynthetics above cavities. Geotextiles and Geomembranes 46, 5: 611-624.

3.1. INTRODUCTION

In this chapter, novel laboratory equipment is introduced to deal with the load transfer mechanisms of the granular platform reinforced by geosynthetics. A series of physical modeling tests were carried out using two cavity opening methods, a trapdoor, and a progressive procedure, two geosynthetics, and three soils. For each type of soil, three platform heights were tested. This laboratory experiment has been pursued to complete the full-scale experiment of *Huckert et al. (2016)* and to validate experimentally the conclusions of the numerical simulations proposed by *Villard et al. (2016)* on the influence of the cavity-opening mode. The experiments permit to observe directly the deformation of the geosynthetic and the settlement at the surface during the different cavity opening processes. A plan of equal settlement *(Terzaghi, 1943)* is also predicted for each case of tested soils. Also, by using a tactile pressure sensor, the variation of stress could be measured, considering two different methods to form the embankment. From the experimental results, the load transfer mechanisms are analyzed, the soil expansion coefficient is determined, and the influences of the geometrical and physical parameters are studied.

To summarize, the laboratory tests aim to improve the understanding of the expansion and load transfer mechanisms can be expressed by the planned works, which are listed below:

- The influences of the H/D ratio
- The influences of three fill materials
- The influence of the cavity opening modes: a trapdoor and a progressive procedure
- The influence of geosynthetic stiffness
- The load distribution in two different programs of embankment formation

3.2. LABORATORY TEST

3.2.1. Description

An experimental laboratory device has been developed to simulate collapses in a geosynthetic-reinforced platform. To analyze the load transfer behavior inside granular platforms above the cavities, the laboratory tests have been set up using different conditions to create a database (displacements of soil, deflection of geosynthetics, and pressure distribution). This work was carried out for two different methods of cavity opening, two types of geosynthetics, three types of granular soils used as overlying soils, and three different types of platform heights reflected by the H/D ratio, where H is the height of the overlying soil and D is the diameter of the cavity. Some tests were carried out twice to check

the repeatability of the experiments. For each test, a new geosynthetic sheet was used, and the average soil density of the filled cylinder(s) was controlled. The unit weight was obtained with an accuracy of ± 0.01 kN/m^3.

Both nonwoven and woven geosynthetics were used for fine sand and coarse sand. Particularly, for gravel, only woven geosynthetics were used in seven tests, and the nonwoven geosynthetics were not used due to the fact that they can be damaged by the gravel particles.

In order to study the load transfer mechanisms, due to the purpose of limiting the damage to the observation sensors, only woven geosynthetic material was used for fine sand. The research studies with other tests configurations are developed based on numerical works, which are presented in the following chapters.

3.2.2. Model setup

3.3.2.1. Device

The experiment was set up on a rectangular table (1.2 m × 1.4 m), whose main function was to connect the entire set of tested items (*Figure 3.1)*. A metal 4-feet table guaranteed the balance of the platform through the testing. On the table, a round hole with a diameter of 0.5 m was located in its center. The cavity was simulated at this position. At the two opposite sides of the rigid table, several screws were used to fix the geosynthetic sheet with metallic clamps. The height of the platform can vary by setting one, two, or three metallic cylinders (inner diameter D_c = 1.0 m, H = 0.25 m) leading to three H/D ratio cases, namely 0.5, 1.0, and 1.5.

Two different methods were operated to simulate the cavity, namely the trapdoor and the progressive opening procedure. *Figure 3.2* illustrates the two opening modes. For the trapdoor procedure (Mode A), a rigid circular plate combined with a jack was used to simulate the cavity opening. For the progressive procedure (Mode B), a cone filled with sand was emptied making it possible to reproduce a concentric opening of the cavity under the geosynthetic sheet. The cone was connected under the table using screws, and the filled sand was kept in the cone by a lock. When the lock is opened, the sand can fall out of the cone vertically with the same duration for each test (500 seconds) and hence leading to the opening of the cavity.

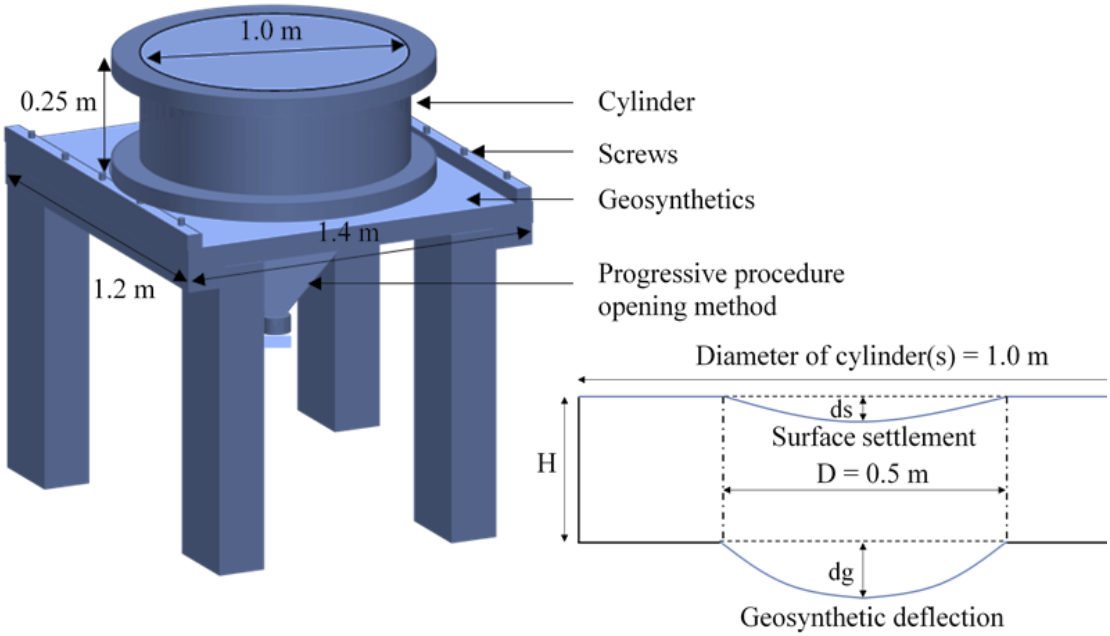

Figure 3.1. Experimental device

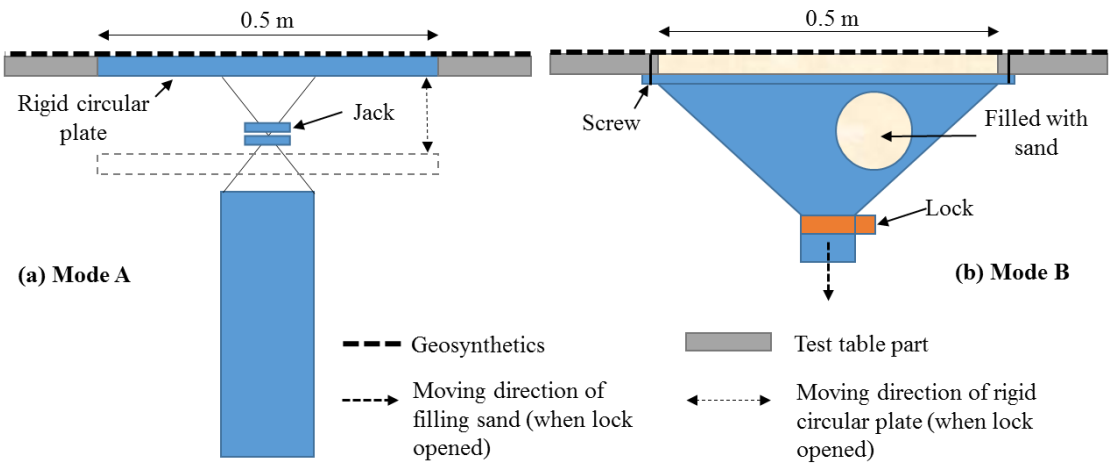

Figure 3.2. Opening methods: trapdoor procedure (a), and progressive procedure (b)

3.2.2.2. Tested soils

Several types of granular materials were used: fine sand (SF), coarse sand (SC), and gravel (G). The main characteristics of the given soils are presented in *Table 3.1*. The sand friction angles were deduced from triaxial tests at low confinement stress at 25 kPa, 50 kPa, 75 kPa, and 100 kPa, and direct shear tests were used for gravel. In order to gain an understanding of the influence of the soil in loose or dense states on the expansion and load transfer mechanisms, several tests were repeated using the same conditions but using different mass densities.

Table 3.1. Tested soil characteristics

Soils	***Unified Soil classification***	***D_{max} (mm)***	***D_{50} (mm)***	***Cu***	***Cc***	***ρ (Mg/m³)***	***ρ_s (Mg/m³)***
SF	SP	1	0.36	1.82	0.89	1.4	2.64
SC	SP	2	0.82	2.07	0.85	1.44	2.63
G	GP	10	6.1	2.52	1.36	1.32	2.62
Soils	***Unified Soil classification***	***e_{min}***	***e_{max}***	***e_0***	***D_R***	***φ' (°)***	***c' (kPa)***
SF	SP	0.59	0.98	0.89	0.23	36.5	0
SC	SP	0.48	0.85	0.83	0.05	39.7	0
G	GP	0.59	1.00	0.98	0.05	37.9	0

3.2.2.3. Tested geosynthetics

In order to simplify the comparison between tests, weak geosynthetic types with low stiffness values were chosen. To study the influence of the material characteristics, two different types of materials were used (*Figure 3.3*), namely a woven geosynthetic (W) and a nonwoven geosynthetic (N). Note that the aim to use the tested geosynthetics, especially, the nonwoven material is to obtain easily the deflection. The properties of these geosynthetics are presented in *Table 3.2*.

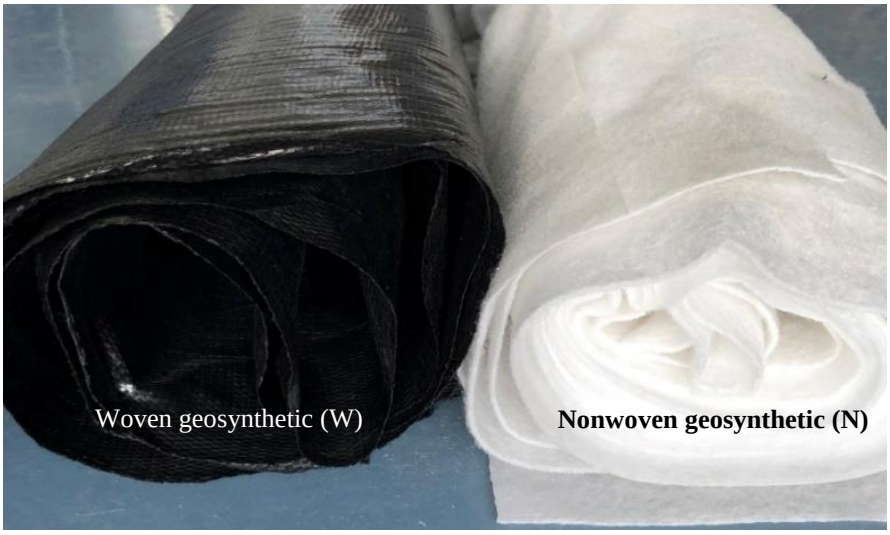

Figure 3.3. Tested geosynthetics

Table 3.2. Geosynthetic characteristics

Geosynthetics	Machine direction			Cross direction		
	ε (%)	T (kN/m)	J (kN/m)	ε (%)	T (kN/m)	J (kN/m)
Woven (W)	2	4	200	2	4	200
	5	8	160	5	8	160
	12*	15	125	12*	15	125
Nonwoven (N)	5	0.5	10	5	0.5	10
	20	2	10	20	1	5
	76*	7	5.32	88*	7.7	6.78

** Denotes rupture*

3.2.3. Monitoring

3.2.3.1. Displacement sensors

During the opening process, surface soil subsidence occurred and the geosynthetic sheet deformed at the same time. A laser sensor (VS) was used to measure the initial level of the soil surface before the cavity opening, the settlement of the soil surface, and the geosynthetic deflection after the cavity opening. The laser sensor was moved on a rail located on the upper cylinder to measure the surface settlement and under the test table to measure the deflection of the geosynthetic sheet. The laser sensor was connected to a wire displacement sensor (HS) located on the side of the rail, in accordance with its horizontal position (*Figure 3.4*). The laser sensor VS had an acquisition frequency of 1.5 kHz and a resolution of 32 µm in static states. *Figure 3.5* presents photographs of the displacement sensors in the actual experiment.

Both sensors were connected to a data logger, and the curve of surface soil displacement and geosynthetic deflection could be generated and displayed directly using specific software (*Figure 3.6*). The measurement rail could be located along with four different directions with angular differences of 45° to achieve surface settlements and along two perpendicular directions to obtain the geosynthetic deflection. In addition, references marked on the cylinders and the test table were used to set the location of the laser sensor to ensure the consistency for each test. The data collection interval of the displacement sensors was set to 0.1 seconds in order to obtain the displacement curves. At least four passages of the laser sensor had to be executed on the rail for each test to ensure the detail of the graph is good

enough. Moreover, during the cavity opening, displacement sensors were located at the middle of the measurement rail to obtain the displacement of the soil surface with time.

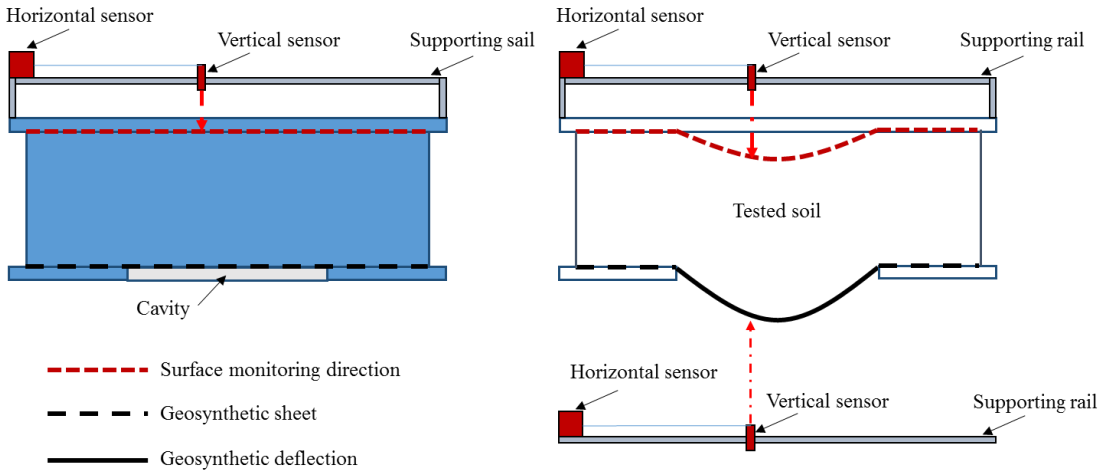

Figure 3.4. Location of displacement monitoring sensors

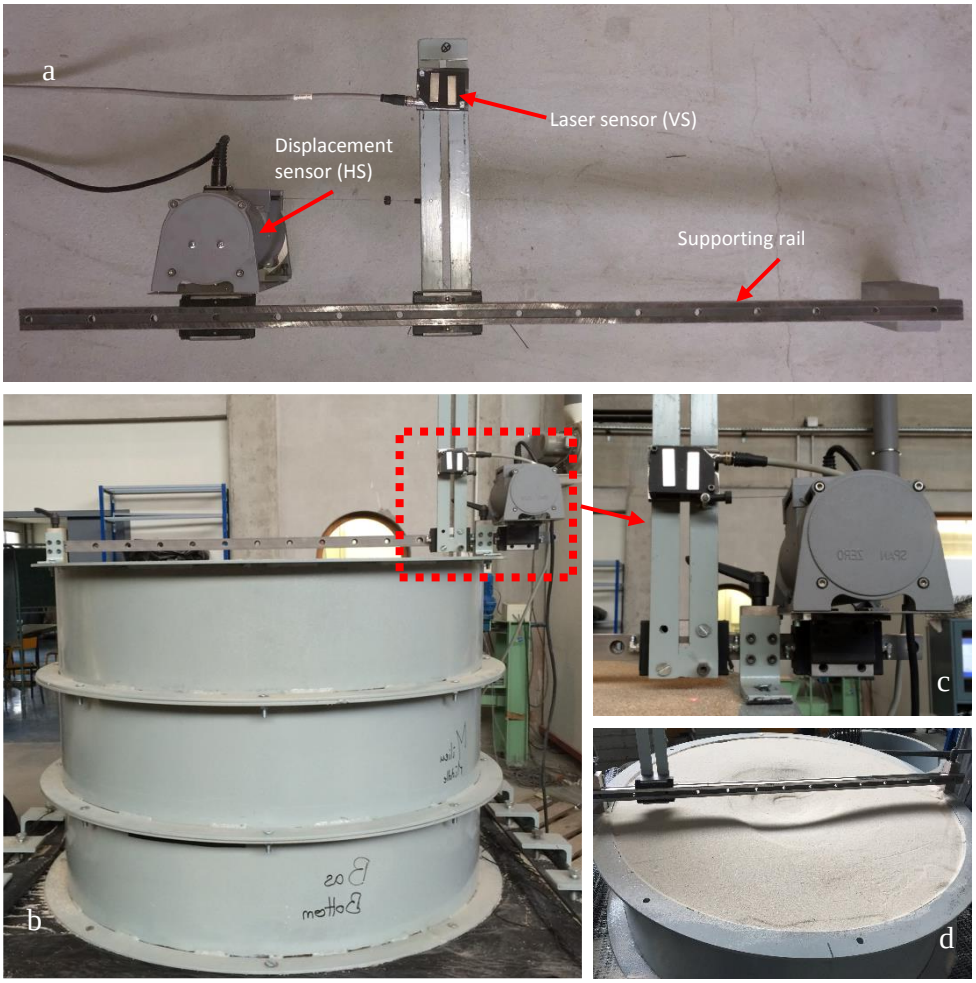

Figure 3.5. Photographs of displacement sensors

a: Arrangement of sensors on supporting rail b: Displacement sensors placed on cylinders

c: Zoom of displacement sensors d: Top view of displacement sensors

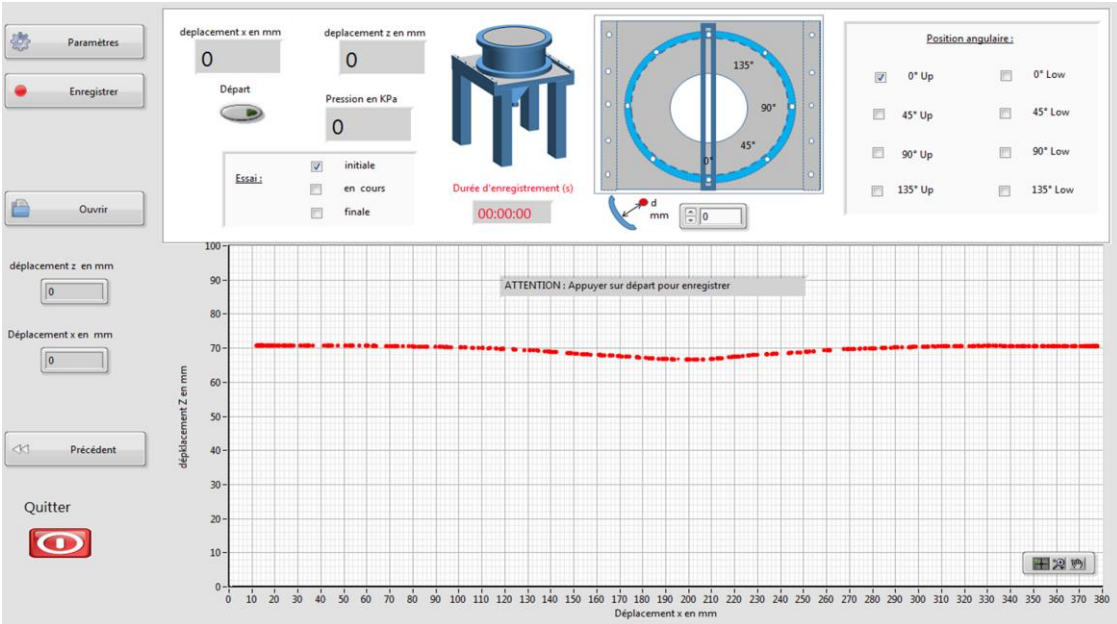

Figure 3.6. Interface of software for displacement measurement

3.2.3.2. Tactile pressure sensor

A Tactile Pressure Sensor (TPS) is a network of unit sensors enclosed in a polymeric pad that could obtain the stress distribution. The TPS has been used previously by *Paikowsky et al. (2003)* to measure the vertical stress distribution during a trapdoor test in granular material. The TPS can be used for various surface geometries but not for soil stress cells. Additionally, it has additional benefits for large surfaces, as reported previously *(Palmer et al., 2009)*. The pressure range of TPS was 69.77 kPa, and its resolution is 0.02 kPa, while the pressure sensitivity is 0.4%, and the accuracy error is less than 2%. The dimensions of the TPS sheet were 0.18 m × 0.33 m with a 1 cm × 1 cm unit sensor (*Figure 3.7*). The TPS contained 512 unit sensors placed along 16 columns and 32 rows. The data were transmitted to a data logger (*Figure 3.7*), and a software program permitted the conversion of the signals to pressures in accordance with the TPS calibration. Data could be retrieved for each element or a group of selected elements.

To capture the pressure distribution during the collapse, the TPS was placed between the rigid table and the platform to allow measurements of pressure. In order to analyze the load transfer during the cavity opening, the TPS was placed in three different locations on the geosynthetic: the anchorage, the border and the center of the cavity (*Figure 3.8*).

The movement between TPS and the geosynthetic sheet was checked before and after the cavity opening by the comparison of the marked points (*Figure 3.9*). During the tests, TPS

was always stable on the up face of the geosynthetic. In fact, the part of TPS placed on the cavity area is deflected vertically following the displacement of the geosynthetic during the opening process. Notwithstanding the vertical displacement of geosynthetics is minor near the cavity border, the deflection of TPS can be ignored.

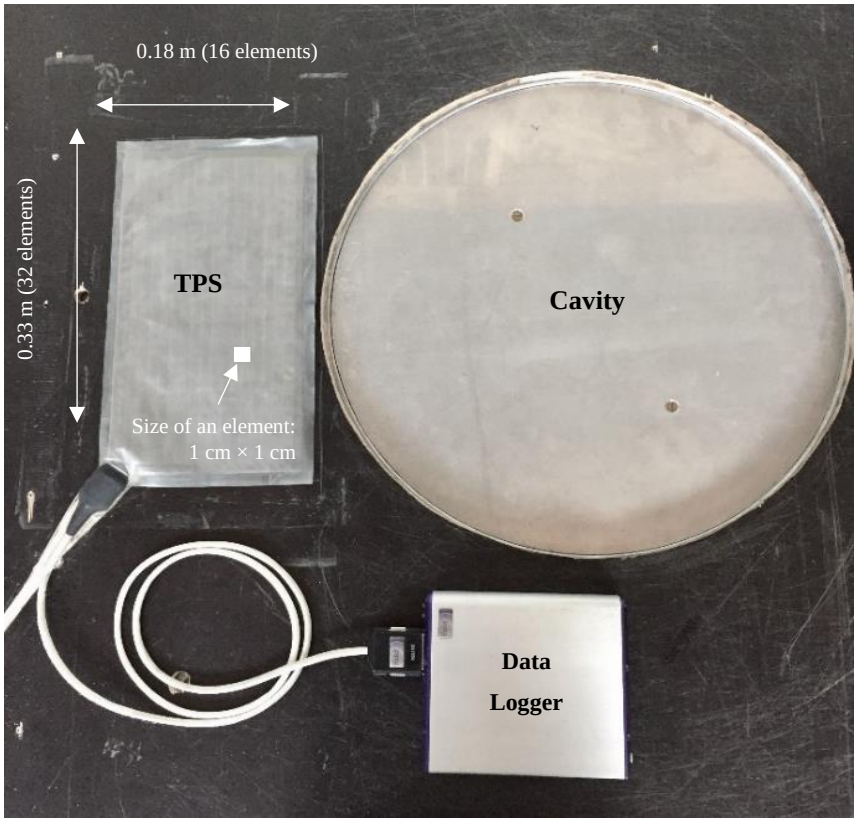

Figure 3.7. Photograph of TPS on the anchorage area of the cavity

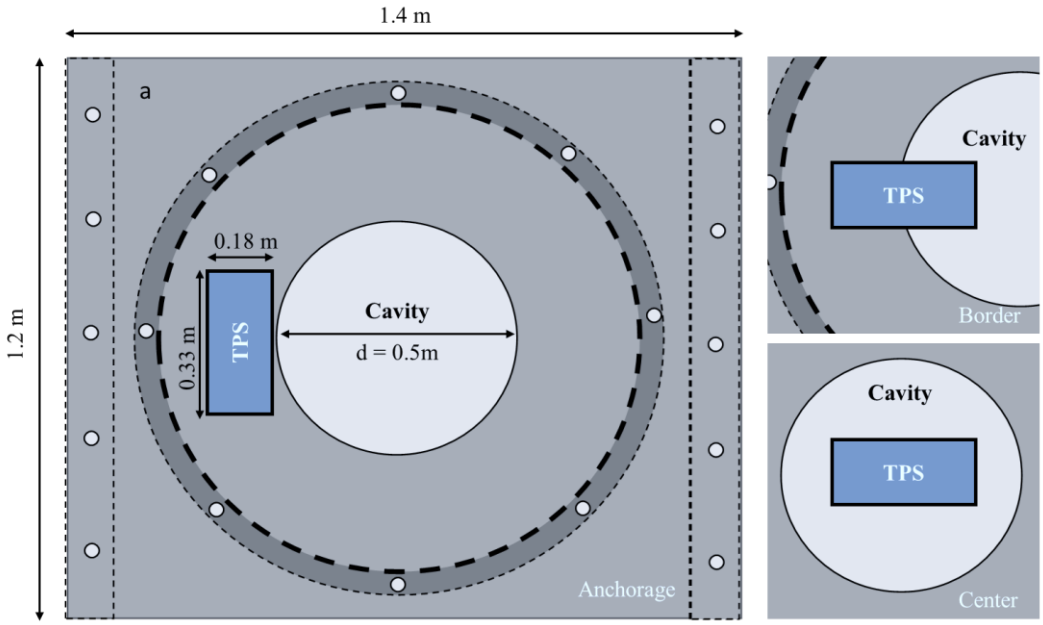

Figure 3.8. Locations of TPS at the anchorage, the border and the center of cavity

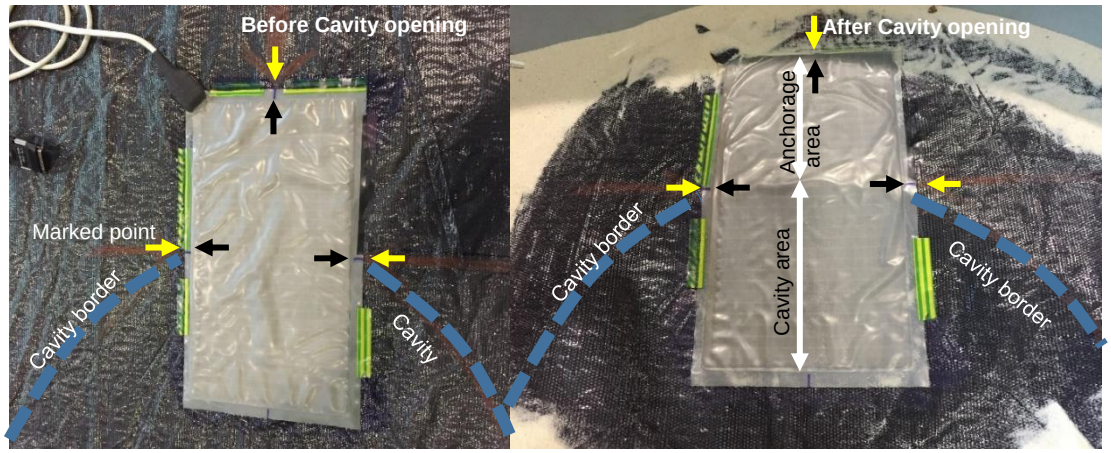

Figure 3.9. Location of TPS before and after the cavity opening

During the cavity opening, the stress is measured then the final values are compared with the initial values. After that, the analyzed stress values are linked between three locations; thus the load distribution along the geosynthetic sheet and the anchorage areas could be determined.

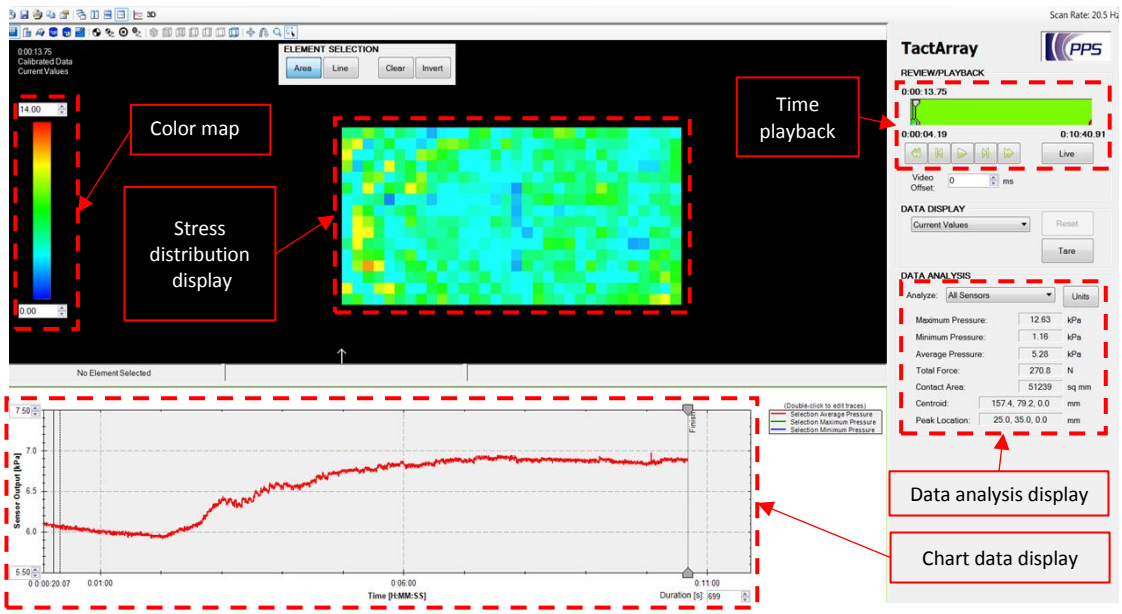

Figure 3.10. Chameleon TVP software interface

A specific program, Chameleon TVP, is used to record and analyze the measurement data observed by TPS (*Figure 3.10*). Especially, with the stress distribution display, the data can be treated in a line, a selected zone or all the sensor area. The chart data display presents the variation of stress by test time, and the time playback option supports the time management. The data analysis display shows the maximum, minimum and average pressures. Moreover, in the color map, the color scale of the stress display can be changed.

3.2.4. Test program

3.2.4.1. Platform set-up

The opening system was installed under the hole formed on the test table to create the cavity, the TPS was placed next to the cavity, and it was connected to a computer. The geosynthetic sheet was then stretched out on the test table before it was fixed on the table using screws and metallic clamps. The platform was then built, and the height of the tested soil depended on the number of cylinders used. There were three cases regarding the ratio H/D, namely 0.5, 1.0, and 1.5, leading to soil heights of 0.25 m, 0.5 m, and 0.75 m, respectively. The soil filling was completed by hand-filling a bucket to assure uniform soil density. Each soil bucket was subsequently weighted. Moreover, in order to control the density of tested soils, a vibration tamper could be used. The surface soil was then flattened to avoid any confusion in the following analysis steps.

The name of each test was regulated according to the following procedure: geosynthetics type (Nonwoven/N or Woven/W), soil type (Fine Sand/SF, Coarse Sand/SC, or Gravel/G), opening mode (trapdoor/A or progressive opening/B), H/D ratios, and density. For example, W/SF/A/0.5/1.41 means that the test was performed with woven geosynthetics and fine sand, the trapdoor procedure was used, the H/D ratio equaled 0.5, and the density was 1.41.

3.2.4.2. Displacement measurement procedure

The supporting measurement rail (*Figure 3.4*) was fixed to the upper cylinder in order to measure the initial surface condition. The cavity was then opened by the opening device. When the opening process was completed, the opening device was removed, and the surface soil settlement and the deflection of the geosynthetic sheet were measured. In order to ensure measurement reproducibility and control the symmetry of the deflection, these measurements were conducted along (at least) two perpendicular directions.

3.2.4.3. Stress measurement procedure

Considering the influence of the embankment formations on the load transfer mechanism over the geosynthetic-reinforced cavities, two different test programs were carried out: the intermittent program (Program 1) and the continuous program (Program 2). The main difference is the method to increase the embankment height concerning the open of the cavity. In Program 1, after the cavity opening, the ratio H/D was defined by the number of cylinders installed above the rigid table. Whereas in the case of Program 2, the cavity is

formed since the first cylinder is set up, and the other cylinders are then placed continuously. In that case, the data from the stress variation is monitored for each level of the embankment height.

Moreover, a comparison between two different programs could be useful to analyze the construction sequence applied to the cavity. In Program 1, the cavity is similar to an evolving void, which appears below the geosynthetic after the process of embankment construction. For Program 2, like an existing void, the cavity appears before the fill placed in layers over the geosynthetic. With Program 2, it is possible to study load transfer mechanisms in a specific case that an overload placed on embankment reinforced by geosynthetic with the presence of an existing cavity. Therefore, the existence of the stable arch within the embankment could be checked to correspond to the height of fill.

3.2.5. Analysis procedures

3.2.5.1. Soil expansion

In this study, two procedures were used to calculate the expansion coefficient. They are based on the volume variation of the granular material when the cavities appear. The differences between these two models are due to the shape assumptions. Specifically:

- ***Model 1***: the parabolic curve for both geosynthetics and surface soil
- ***Model 2***: the combination of the polynomial curve for geosynthetics and a Gaussian model for the surface soil

For Model 2, the reason to choose the functions to fit the shapes of the deformation is due to the examination for the coefficient of determination (R^2) in different functions. The selected functions have the best values of R^2.

For Model 1, taking into account the cylindrical shape of the collapse, and assuming that both the surface and geosynthetic deflections have a paraboloid shape, the variation of the volume of the granular material inside the collapsed soil cylinder leads to *Eq.3.1*, depending on an expansion coefficient Ce_1.

$$d_s = d_g + 2H \times (1 - Ce_1) \qquad \textit{Eq.3.1}$$

So far, there has been no study that permits the precise definition of a general rule leading an accurate estimation of the value of the expansion coefficient Ce. Based on the tests completed in this study, it is possible to calculate the coefficient of soil expansion Ce_1 from the measured values ds and dg assuming that the deformed geosynthetics and surface settlement have a parabolic shape.

In addition, for each test, a function is calibrated for the deflection of geosynthetics and embankment surface, and it could be named as a measurement method. Correspondingly, the deflection of the geosynthetic sheet could be approximated by a 4th order polynomial function (this type of fitting function was found as the better one for all the tests). Additionally, the deformation of the soil surface was considered as a Gaussian function.

From the Gaussian function g(z), and the polynomial function f(z) defined between the center of the cavity and its radius, it is possible to determine the volume of the soil settlement, V_s (*Eq.3.2*) and the volume of the geosynthetic deflection, V_g (*Eq.3.3*):

$$V_s = \int_0^{ds} \pi . g^2(z) . dz \qquad \textit{Eq.3.2}$$

and

$$V_g = \int_0^{dg} \pi . f^2(z) . dz \qquad \textit{Eq.3.3}$$

Thus, the expansion coefficient Ce_2 could be calculated using *Eq.3.4* as a function of the volume of the initial soil before collapse (V_i):

$$C_{e2} = \frac{V_f}{V_i} = 1 + \frac{V_g - V_s}{\pi . H . {D^2}/{4}} \qquad \textit{Eq.3.4}$$

where V_f is the final volume and V_i is the initial volume of the cylinder part of soil above a cavity. *Figure 3.11* illustrates V_i, V_f, V_s, and V_g.

In this study, a specific program, CurveExpert, was used to calculate the volume of soil. In this software, numerous models can be used to fit the curve, including the Polynomial fit and the Gaussian model.

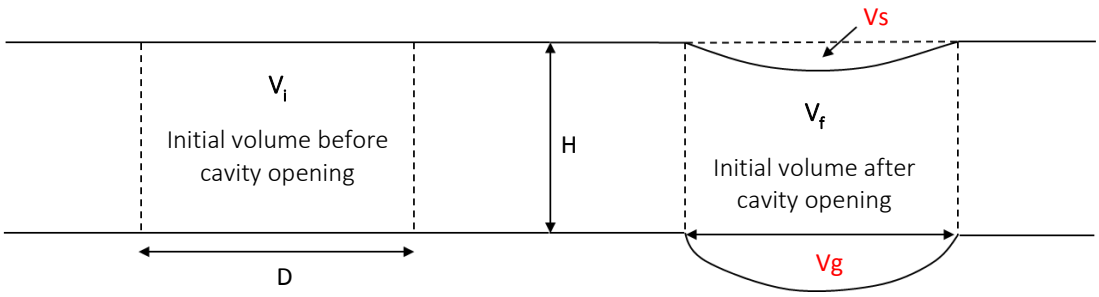

Figure 3.11. Illustration of volumes of soil settlement and geosynthetic deflection

3.2.5.2. Shape of collapsed soils

The measurement data obtained from the distance sensors are exported from specific software to Excel files. At least the data was measured in two different directions, and hence the next step is to compare the maximum values of the deformation between the directions to prevent any significant difference, which can be caused from the experimental tests. Any strangle points in the deformation curves are needed to remove. Next, the curves of the overlying soil settlement and the deflected geosynthetics are fit to prevent that a line connecting their center perpendiculars to the horizontal plane.

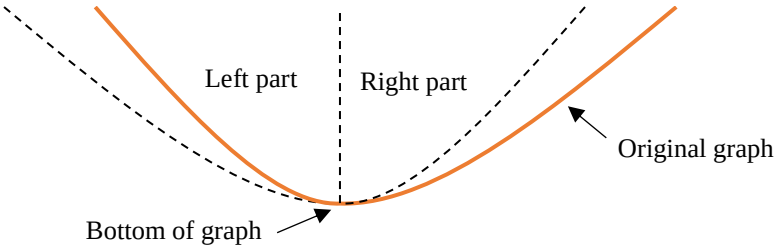

Figure 3.12. Two parts of deformation curves

After that, the program CurveExpert is used to calculate the volumes of the collapsed. For both deformed shapes of the surface of the overlying soils and the geosynthetics, at the bottom of the graphs, the curves are separated into two parts, as can be seen in *Figure 3.12*. Then for each part, by using CurveExpert, the volumes of the two parts were calculated. Thus, the expected volumes are determined as the mean values of these two volumes. Note that this procedure is applied to both curves of the surface settlement of the overlying soils and deflected geosynthetics. Thereby, the masses can be calculated rapidly with different shape assumptions.

In order to specify the shape of the collapsed soil, the variations of the surface settlement and the deflection of geosynthetics were plotted. The shape of the collapsed soil can be determined according to the following procedure. In the surface settlement curve, the inflection dots between the stable part and the settlement part must be marked, and they are

then connected to the nodes of the geosynthetic deflection curve to determine the shape of the collapsed soil (*Figure 3.13*).

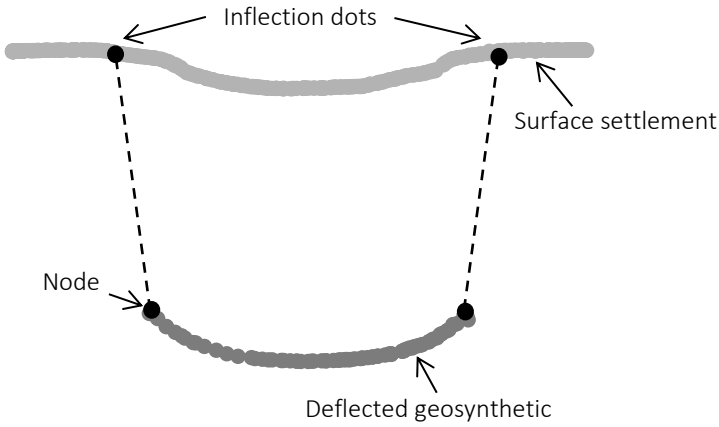

Figure 3.13. Shape of collapsed soil

3.2.5.3. Load distribution

In order to analyze the load distribution, two different processes are used depending on the locations of the TPS placed on the geosynthetics. The first process is for the tests in which the TPS placed at the anchorage areas. Note that, this process is only used for Program 1 (as described in *Section 3.2.4.3*), for Program 2, the TPS is not placed in the anchorage areas. The second process is used when the TPS placed at the cavity border and cavity center for both Program 1 and Program 2.

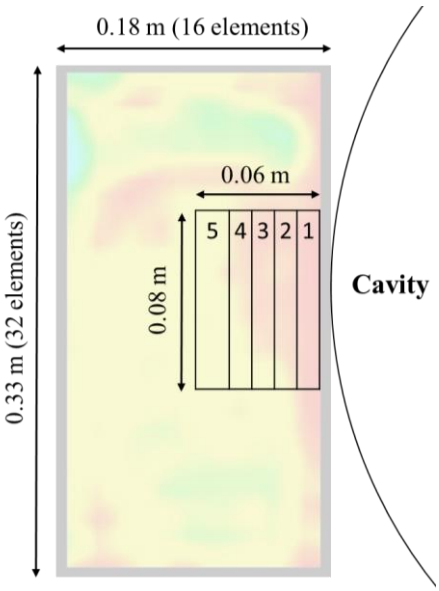

Figure 3.14. Selected areas on TPS (1-5)

Regarding the process for the anchorage areas, selected areas were defined on the TPS, which have 0.06 m length and 0.08 m wide. In this case, the load transfer was measured in five areas (*Figure 3.14*). Each area contains eight sensors except the fifth (which used 16 sensors). The reason to decide the selected areas, in this case, is due to two reasons:

- For the number of the selected areas, we have chosen 5 because we have observed that for all cases, the vertical stress on the geosynthetic is not affected by the cavity opening from the sixth area,
- For the wide of the selected areas, due to the value can be then deduced for all the anchorage areas, only the areas contain eight unit sensors in wide are focused to keep providing the accuracy of the measurement.

For each area, the variation stress was calculated based on the initial and final stress values obtained before and after the cavity opening. The load applied to each area was then determined. Based on this estimation, the total load applied to the side of the cavity could be deduced.

Concerning the tests that the TPS placed at the center and border of the cavity, it is rotated a degree of 90° as its location at the anchorage areas. Because there is no effect of the rigid cylinder, the measured regions are selected along the length of the sensor, whereas, for the wide, the size is the same as in the case of anchorage areas. Thus, in this case, the dimensions of the measured areas on the TPS are 0.08 m wide and 0.33 m length.

3.2.5.4. Efficiency of load transfer

Firstly, the variation of stress ($\Delta\sigma_i$) is determined by the stress acting on the TPS at the initial condition (before cavity opening) and the final state (after cavity opening), in the selected areas (s_i) of sensors on the TPS. Then each variation load (ΔQ_i) was calculated for the selected areas. The variation of the load, named as $\Delta Q_{anchorage}$, which acts on the anchorage areas in where TPS was placed, could be computed by the summation of ΔQ_i:

$$\Delta Q_{anchorage} = \Sigma \Delta Q_i = \Sigma\, \Delta\sigma_i \times s_i \qquad \textit{Eq.3.5}$$

Due to the assumption of the load transfer mechanisms, the decrease of the load acting on the cavity after the opening is equal to the increase of the load applied to the anchorage areas and hence $\Delta Q_{anchorage} = \Delta Q_{cavity}$.

The load acting on the geosynthetic sheet before the cavity opening could be calculated by the unit weight and the volume of the overlying soil ($Q_1 = \gamma \times V$). Due to the decrease of the load after the cavity opening, the load applied on the geosynthetic sheet above the cavity, Q_{cavity} could be computed as follows:

$$Q_{cavity} = Q_1 - \Delta Q_{cavity} \qquad \textit{Eq.3.6}$$

Finally, the efficiency of load transfer can be determined by the equation below:

$$E = (Q_1 - Q_{cavity}) / Q_1 = \Delta Q_{cavity} / Q_1 = \Delta Q_{anchorage} / Q_1 \qquad \textit{Eq.3.7}$$

3.3. RESULTS AND ANALYZES

3.3.1. Settlement and deflection

Table 3.3 and *Table 3.4* present the best results of the maximum deflection of the geosynthetics and the maximum settlement of soil for woven and nonwoven geotextiles, respectively. The other results performed are presented in *Appendix A*.

Table 3.3. Woven geosynthetic test results

Test	***ds (mm)***	***dg (mm)***	***Test***	***ds (mm)***	***dg (mm)***	***Test***	***ds (mm)***	***dg (mm)***
W/SF/A/0.5/1.41	22	32	W/SC/A/0.5/1.45	18	35	W/G/A/0.5/1.34	23	29
W/SF/A/1.0/1.38	14	32	W/SC/A/1.0/1.45	13	31	W/G/A/1.0/1.32	17	29
W/SF/A/1.5/1.39	6	27	W/SC/A/1.5/1.44	2	27	W/G/A/1.5/1.30	8	36
W/SF/B/0.5/1.41	38	50	W/SC/B/0.5/1.45	36	53	W/G/B/0.5/1.32	27	42
W/SF/B/1.0/1.40	22	41	W/SC/B/0.5/1.50	26	45	W/G/B/1.0/1.29	21	44
W/SF/B/1.5/1.39	10	44	W/SC/B/0.5/1.57	25	41	W/G/B/1.5/1.31	14	47
			W/SC/B/0.5/1.64	9	34			
			W/SC/B/1.0/1.45	13	42			
			W/SC/B/1.5/1.45	7	41			

Table 3.4. Nonwoven geosynthetic test results

Test	ds (mm)	dg (mm)	Test	ds (mm)	dg (mm)
N/SF/A/0.5/1.39	36	55	N/SC/A/0.5/1.48	32	50
N/SF/A/1.0/1.39	28	54	N/SC/A/1.0/1.47	28	52
N/SF/A/1.5/1.39	14	45	N/SC/A/1.5/1.46	18	52
N/SF/B/0.5/1.40	72	81	N/SC/B/0.5/1.49	65	84
N/SF/B/1.0/1.39	45	68	N/SC/B/1.0/1.45	27	77
N/SF/B/1.5/1.39	17	65	N/SC/B/1.5/1.45	21	75

The shape of the deflected geosynthetic is influenced significantly by the mode of the cavity opening. As a typical comparison is presented in *Figure 3.15*, an inverted parabolic curve can fit the shape of Mode A and a conical shape can be adopted for Mode B.

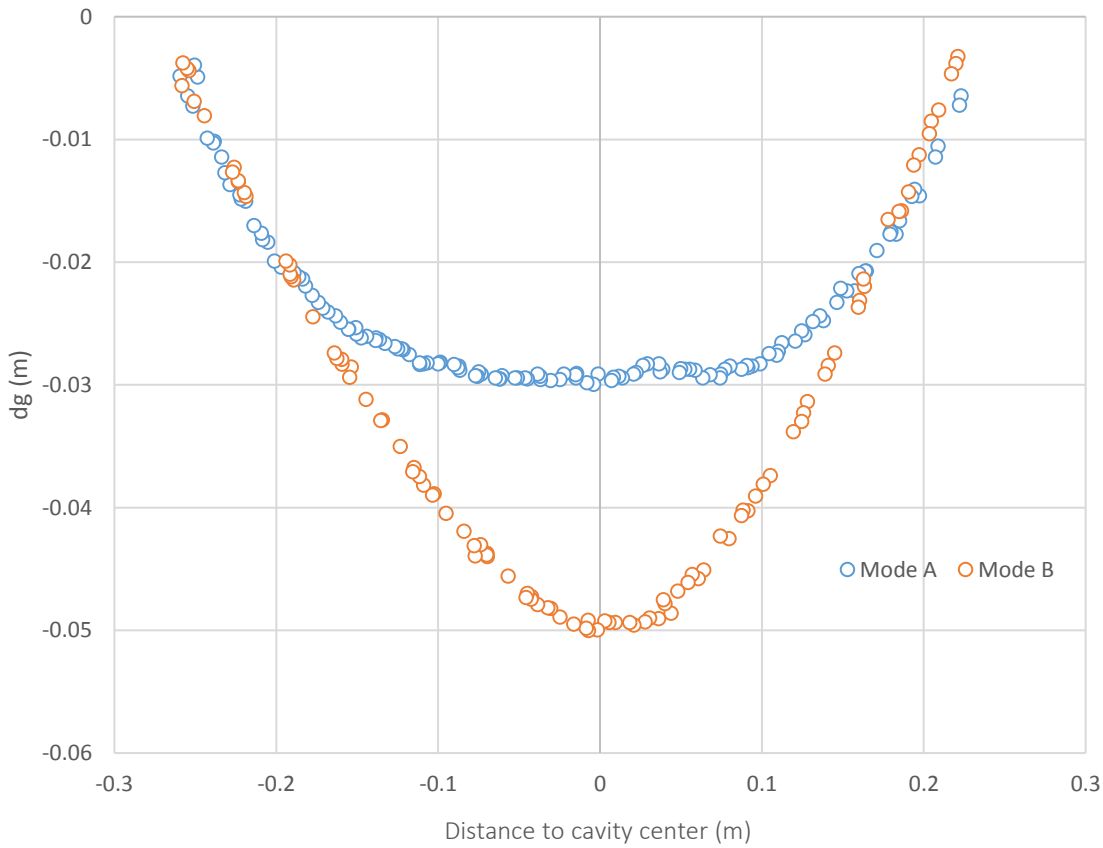

Figure 3.15. A typical comparison of deflected geosynthetic (Fine sand & Woven GSY)

3.3.2. Influence of experimental conditions

3.3.2.1. Repeatability

Several tests were conducted with fine sand and coarse sand in the same configuration (*Table 3.5*) in order to check the repeatability of the tested procedure. The monitored values had an accuracy that varied from 0 – ± 1.5 mm for the surface settlement and from ± 1.0 – ± 2.5 mm for the geosynthetic deflection. The difference could be explained by the difficulty to install the geosynthetics in the same way for each test.

Table 3.5. Repeatability tests

Test	ds (mm)		dg (mm)	
W/SF/A/0.5/1.41	22		32	
		20.5 ± 1.5		31 ± 1.0
W/SF/A/0.5/1.40	19		30	
W/SF/B/0.5/1.41	38		50	
		38 ± 0		47.5 ± 2.5
W/SF/B/0.5/1.41	38		45	
W/SC/A/1.0/1.50	14		28	
		12.5 ± 1.5		30.5 ± 2.5
W/SC/A/1.0/1.50	11		33	
W/SC/B/0.5/1.64	9		34	
		10 ± 1.0		35 ± 1.0
W/SC/B/0.5/1.64	11		36	

3.3.2.2. Opening methods

The values of maximum deflection (dg) of geosynthetics for the two opening modes and the different geometrical configurations for the three tested soils are shown in *Figure 3.16* and *Figure 3.17* for the nonwoven and woven geosynthetics. The trapdoor procedure (Mode A) systematically led to lower vertical displacements than those obtained under the same conditions for the concentric opening (Mode B). This observation confirmed the results of the numerical study proposed by *Villard et al. (2016)*. The settlement at the surface (ds) was also impacted by the opening mode (*Figure 3.18* and *Figure 3.20*) yielding similar trends of variation, but consistent differences in the monitored values due to the soil expansion.

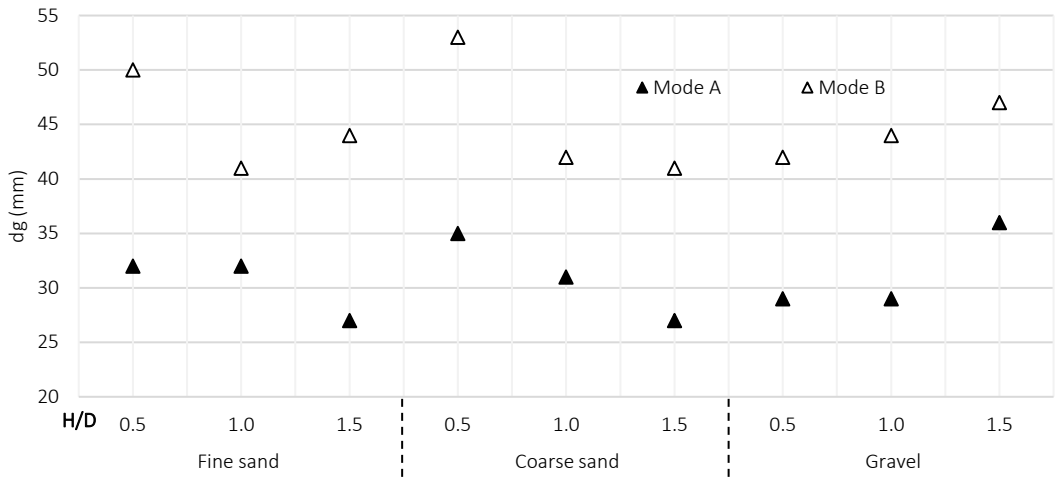

Figure 3.16. Geosynthetic deflection of woven geosynthetic tests

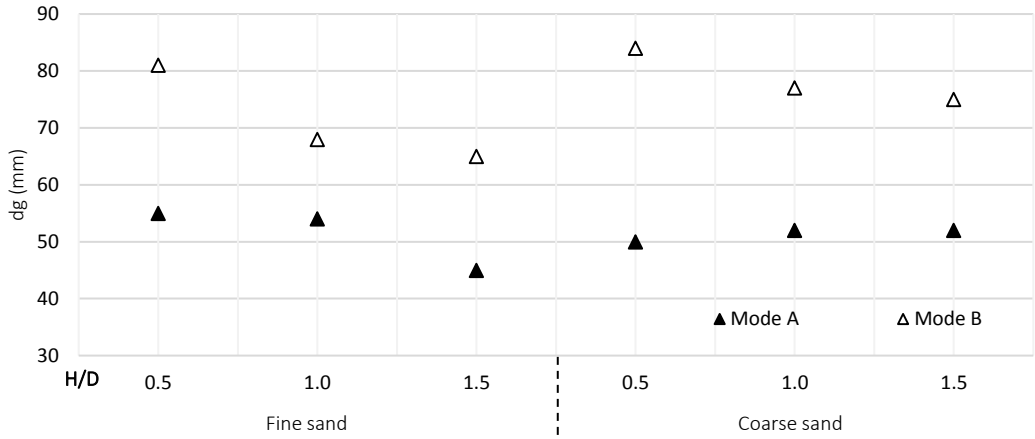

Figure 3.17. Geosynthetic deflection of nonwoven geosynthetic tests

3.3.2.3. H/D ratio

Figure 3.18 presents the influence of the ratio H/D on the surface settlement (ds) for the woven geosynthetic tests. In both cases of the opening processes, the surface settlement decreased with an increase in embankment height at a given diameter. This trend was also observed for the nonwoven geosynthetic tests (*Figure 3.20*). This result was similar to the analytical method proposed by *Briançon and Villard (2008)* and could be explained by the expansion of the soil located above the cavity.

Considering that the settlement at the surface decreases linearly with the increase in the values of H/D (*Figure 3.18* and *Figure 3.20*), it is possible to evaluate the "equal settlement plane" (*Figure 3.19* and *Figure 3.21*). The equal settlement plane could be achieved for H/D values in the range of 1.6 and 2.6, for the woven geosynthetic (*Figure 3.19*), it means that in

case of the height of filled soil in the field of 0.8 m and 1 m for a cavity diameter equal to 0.5 m, the settlement can get zero. For the nonwoven geosynthetic (*Figure 3.21*), the deduced H/D varied from 1.8 and 2.2, corresponding to the height of filled soil of 0.9 m and 1.1 m for a cavity diameter equal to 0.5 m. These differences are due to the fact that we tried to summarize results from different soils, different processes to create cavities and different geosynthetics. This applies to all configurations except one configuration relevant to gravel. Due to the soil expansion, the influence of H/D was slighter on the deflection of geosynthetics.

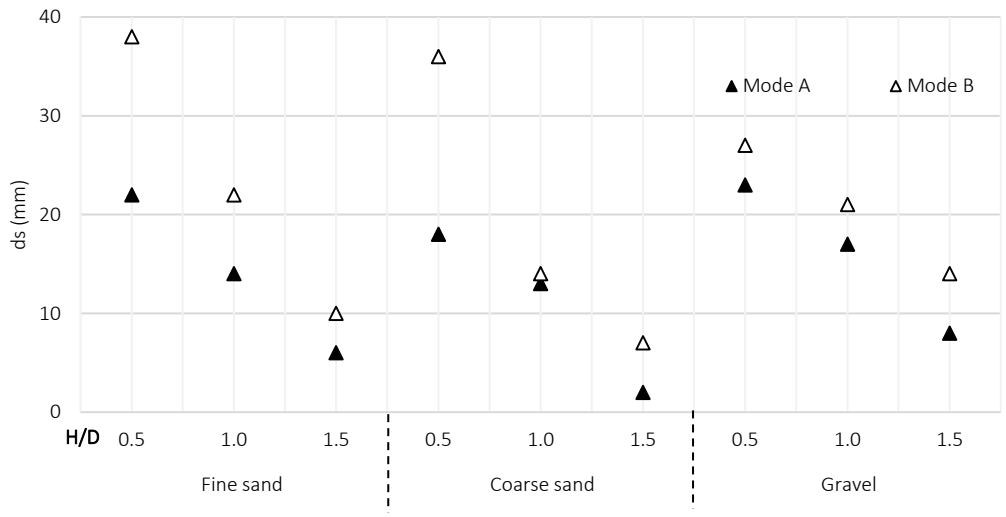

Figure 3.18. Surface settlement of woven geosynthetic tests

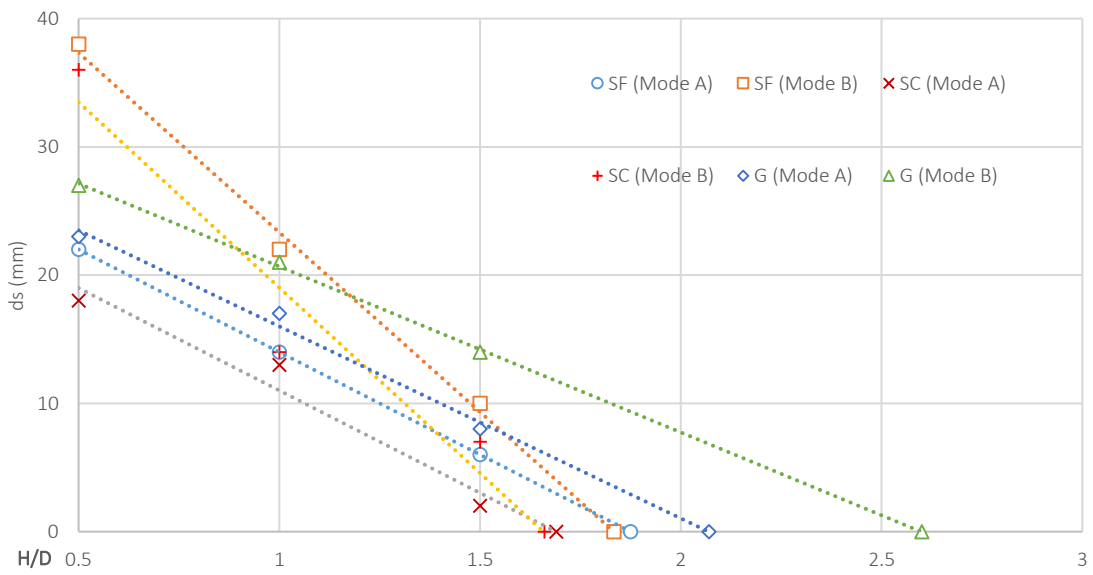

Figure 3.19. Estimation of equal settlement plane for woven geosynthetic

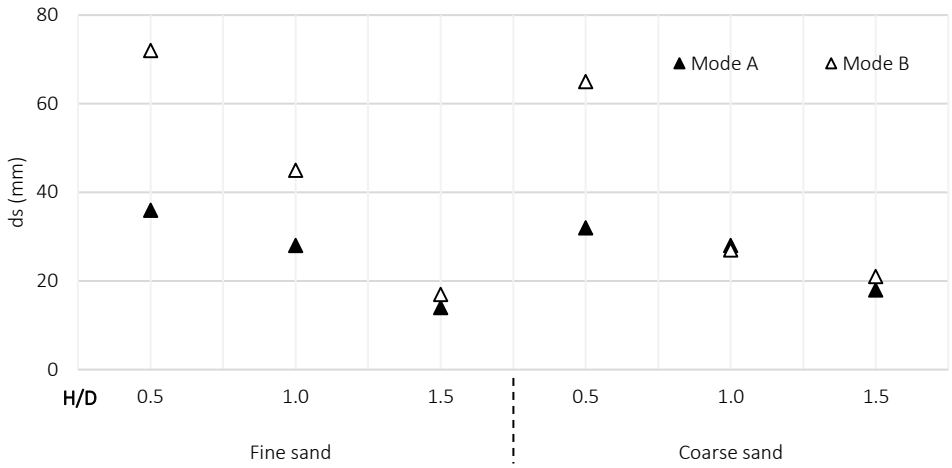

Figure 3.20. Surface settlement of nonwoven geosynthetic tests

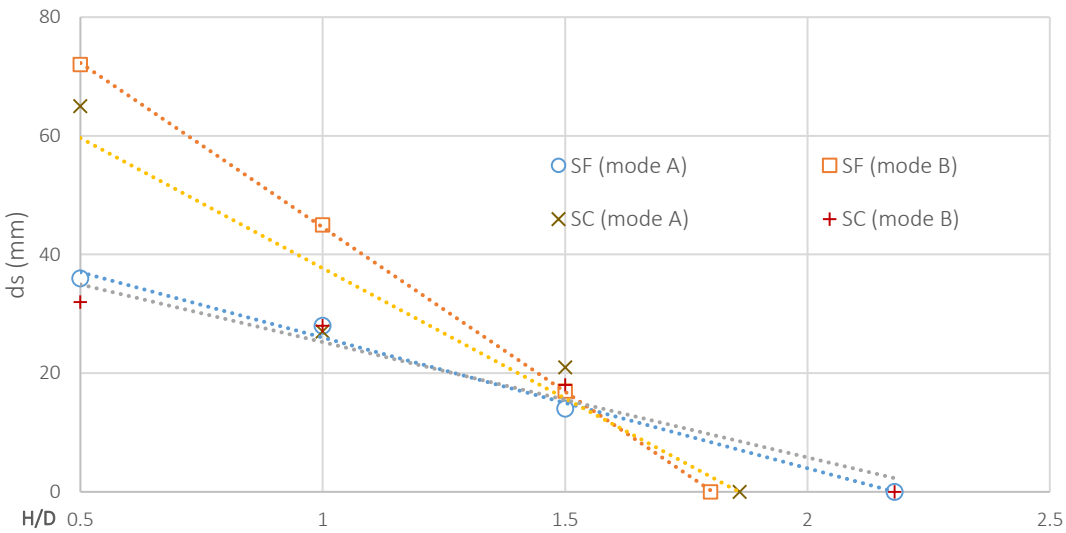

Figure 3.21. Estimation of the equal settlement plane for nonwoven geosynthetic

Nevertheless, the "equal settlement plane" was estimated by a simple assumption as a settlement decreasing linearly with only three ratios of H/D. These other factors such as the geosynthetic deflection and the embankment height (larger than 0.75 m) are not possible to consider in the experimental works. Thus, these results should be confirmed by numerical simulations.

3.3.3. Expansion analysis

3.3.3.1. Shape of deformed zone

For woven geosynthetics, the results showed that in 80% of the tests, the shape of the volume of soil above the cavity, and after the opening of the cavity, is cylindrical. For the other test

of the woven (experiments using low H/D values) and for all the nonwoven geosynthetics tests, a truncated form can be observed. Nevertheless, the opening of the cone remained low (α < 10°). *Figure 3.22* presents the possible shapes of the embankment after the opening of the cavity.

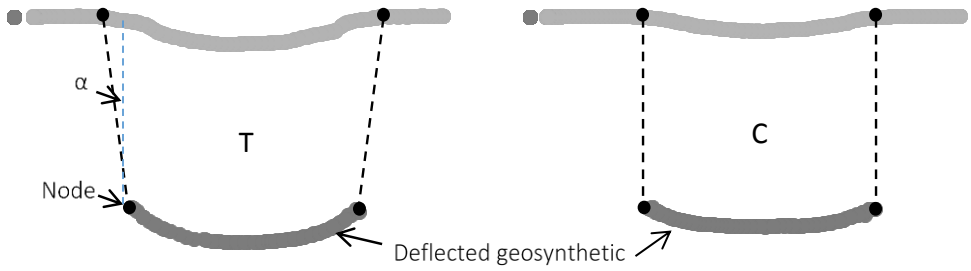

Figure 3.22. Shape forms of embankment: T – truncated shape, C – cylindrical shape

3.3.3.2. Comparison of coefficients estimated by different methods

The two models parabolic and measures methods are applied to fit the curves of the measurement data for both the deflected geosynthetic and surface settlement. As presented in *Figure 3.23*, shapes fit by two models are somewhat similar in the case of geosynthetic deflection, due to the shape of the deflected geosynthetic is symmetric. Whereas, a significant difference can be noted for the settlement curves. It is evident that the model 2, based on a Gaussian curve provides a better fit to the measurement data. The values of the coefficient determination from several tests are presented in *Table 3.6* as proof for the accuracy of the measurement model over the parabolic model.

Table 3.6. Coefficient of determination comparison between two models

Test	***Curves***	***Coefficient of determination (R^2)***	
		Parabolic method	**Measurement method**
W/SF/B/0.5/1.41	Settlement	0.869	0.996
	Geosynthetic deflection	0.908	0.992
W/SF/B/1.0/1.40	Settlement	0.888	0.994
	Geosynthetic deflection	0.990	0.997
W/SC/B/0.5/1.45	Settlement	0.839	0.991
	Geosynthetic deflection	0.993	0.995
W/SC/B/1.5/1.45	Settlement	0.848	0.942
	Geosynthetic deflection	0.980	0.989

W/G/A/0.5/1.34	Settlement	0.790	0.949
	Geosynthetic deflection	0.974	0.998
W/G/A/1.0/1.32	Settlement	0.824	0.970
	Geosynthetic deflection	0.969	0.998
N/SF/A/0.5/1.39	Settlement	0.907	0.969
	Geosynthetic deflection	0.998	0.999
N/SF/B/0.5/1.40	Settlement	0.771	0.997
	Geosynthetic deflection	0.991	0.994

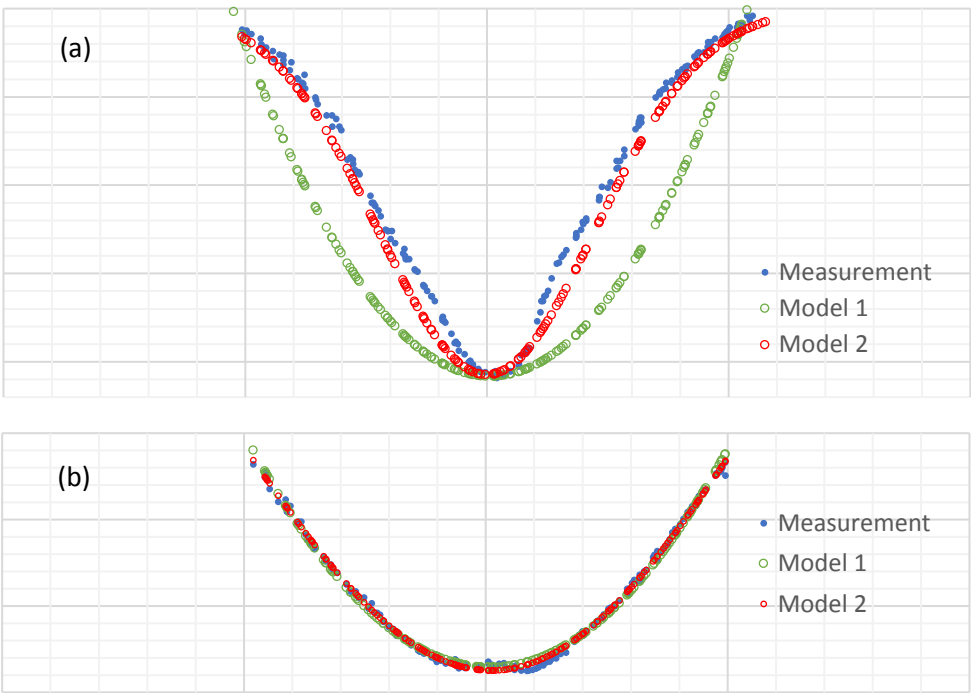

Figure 3.23. Comparison between two models to fit the curves of measurement data

a: surface settlement b: deflected geosynthetic

Figure 3.24 and *Figure 3.25* show the results of Ce computed using two methods. In some tests, the shape of the collapsed soil is conical, especially in the case of nonwoven geosynthetic, but Model 1 is still be applied because the opening of the collapsed soil is low and a cylindrical shape can be considered for the analysis. The values of the coefficient of soil expansion calculated using the parabolic method vary between 1.01 and 1.05, which constitute commonly adopted values for estimating the dimensions of the cavity for these types of materials. This is remarkable given the difference between the coefficients obtained by the parabolic method, and the values determined from the measurement method. On 20 tests among the 30, the proposed method yielded higher values for the expansion coefficient

compared to the parabolic method. Nevertheless, the variation is not essential, and the highest difference value is equal to 3%.

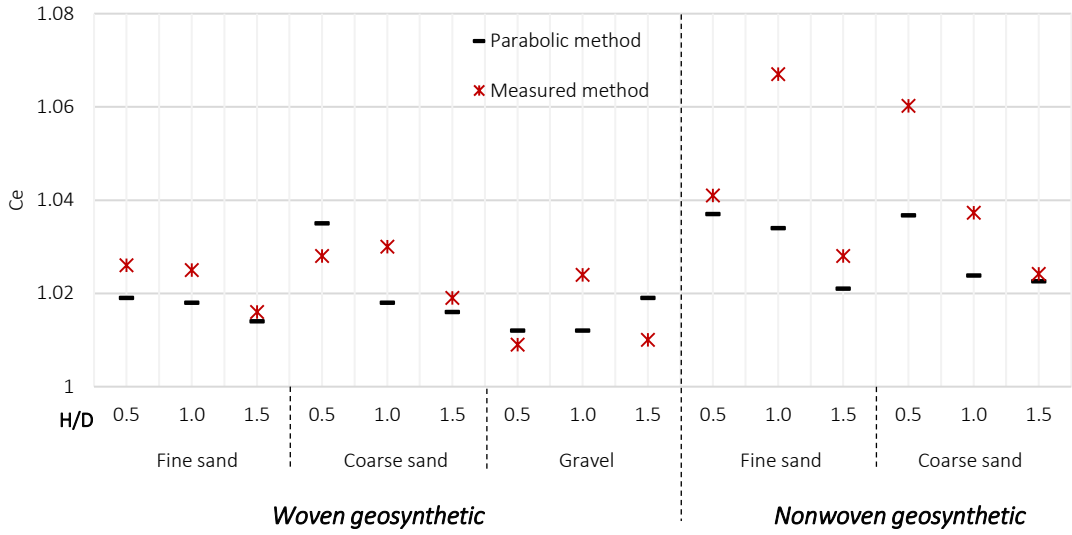

Figure 3.24. Comparison of Ce values estimated using two different methods for Mode A tests

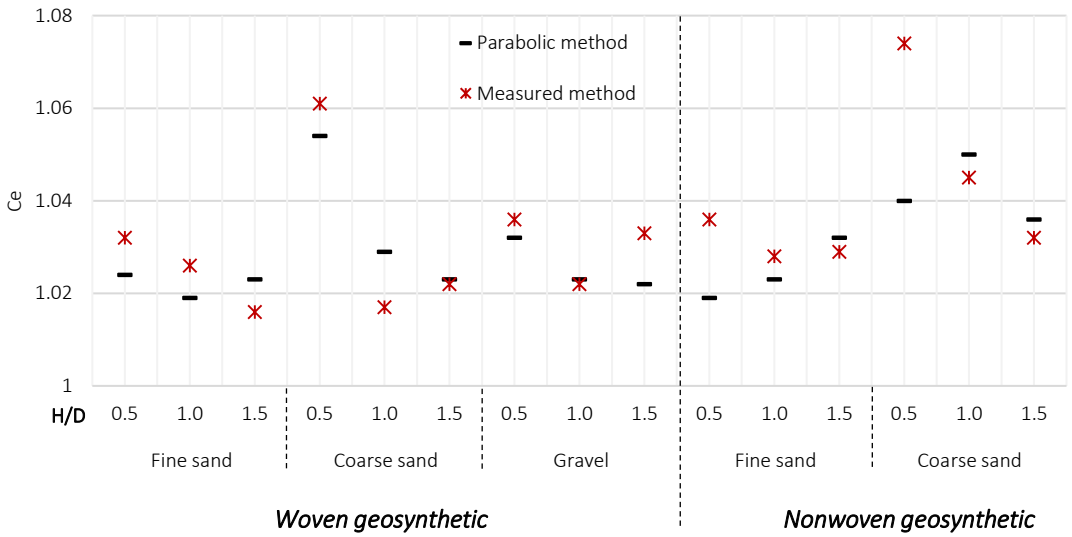

Figure 3.25. Comparison of Ce values computed using two different methods for Mode B tests

3.3.3.3. Influence of density

The influence of density was studied based on the tests with coarse sand (SC) for a progressive opening (Mode B), and an H/D value of 0.5 (*Figure 3.26*). By controlling the mass of the soil, tests were performed using the same conditions with four respective density values, namely 1.45, 1.50, 1.57, and 1.64, and with relative densities D_R of 0.03, 0.29, 0.49,

and 0.71, respectively ($D_R = e_{max} - e/e_{max} - e_{min}$). As *Figure 3.26* shows, the values of the coefficient of expansion develops with the density increases, except for the Ce_1 case and the density of 1.57. This observation seems to be logical since the dense soil has a higher capacity to increase its volume.

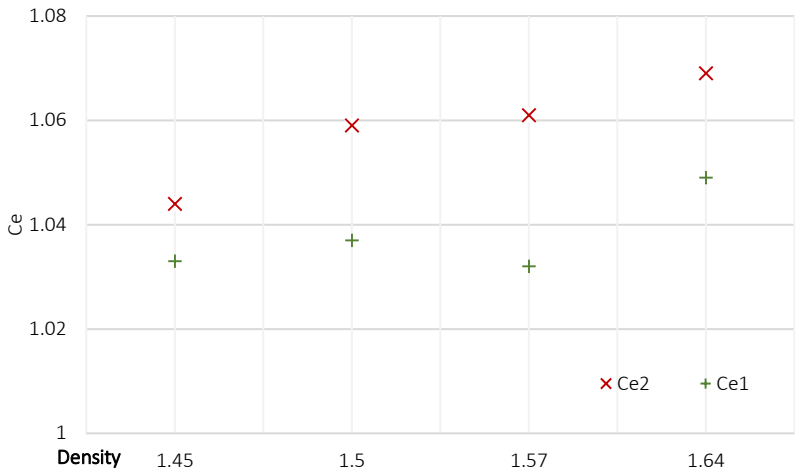

Figure 3.26. Ce values of coarse sand tested Mode B, H/D = 0.5, and woven GSY

In addition, the influence of the soil density on the expansion coefficient can be explained by the fact that if the soil is denser, its porosity is lower, and this could tend to a lower value of the surface settlement. This point is similar to the result obtained from the trapdoor test of *Costa et al. (2009)*: the settlement was more extensive in the loose filled soil than in the densely filled soil. Moreover, the higher value of the soil density could allow the increase in the dilatancy angle *(Lee and Salgado, 2002)*; this point suggests an idea for further studies in which the influence of the porosity or dilatancy can be investigated, considering the deflection of the geosynthetic.

3.3.3.4. Conclusion on the expansion coefficient

The parabolic method is based on an assumption regarding the surface settlement shape and geosynthetic deflection. Therefore, the estimation based on the expansion coefficient Ce_1 is more appropriate. This method can be used for the design but needs to be improved by taking into account the density of soil for the determination of the expansion coefficient.

3.3.4. Load transfer mechanisms over evolving cavity (Program 1)

3.3.4.1. Load transfer on anchorage areas

The results are presented in *Table 3.7* and *Table 3.8* for two modes of cavity opening (Mode A – trapdoor and Mode B – progressive procedure), woven and nonwoven geosynthetics, and at the three H/D ratios. In some tests, the initial stress values measured by TPS did not correspond to the theoretical stress computed from the mass of the soil filling the cylinders. This issue could be explained based on the unit sensors and the accuracy of the used TPS, which seems to be no optimal at low pressures. Nevertheless, except for one test (test W/SF/A/1.0/1.40), a remarkable stress variation can be observed in *Table 3.7* and *Table 3.8* during the cavity opening. This confirms the essential assumption that the load could transfer from the embankment to the anchorage areas.

Table 3.7. Stress variation in fine sand tests calculated from anchorage areas tests

Test	***Theoretical stress (kPa)***	***Monitoring***	
		Initial stress (kPa)	***Final stress (kPa)***
W/SF/B/0.5/1.40	3.50	2.97	4.48
W/SF/B/0.5/1.57	3.90	5.10	7.07
W/SF/B/1.0/1.40	7.10	6.01	7.37
W/SF/B/1.5/1.40	10.40	5.80	10.1
W/SF/A/0.5/1.40	3.50	4.30	5.20
W/SF/A/0.5/1.57	3.90	3.99	5.35
W/SF/A/1.0/1.40	7.20	4.45	7.06
W/SF/A/1.5/1.40	10.70	5.20	9.94
N/SF/B/0.5/1.40	7.00	6.12	7.95
N/SF/B/1.5/1.40	10.40	10.43	11.41
N/SF/A/1.0/1.40	7.00	7.63	7.7
N/SF/A/1.5/1.40	10.40	9.68	10.87

A comparison between the tested materials could be performed for each H/D value. The efficiency values for woven geosynthetic materials are higher than the values for nonwoven materials. This result is undoubtedly due to the lower displacement achieved by the woven

geosynthetics, which has a higher stiffness than the nonwoven geosynthetic. In the present study, it was difficult to identify the influence of the opening mode or the importance of the H/D value on the efficiency due to the difficulty to measure low stress with the TPS. The influence of the density was more natural to be observed (*Figure 3.27*), and the efficiency of dense sand was higher than that for loose sand.

Table 3.8. Stress variation in coarse sand tests calculated from anchorage areas tests

Test	***Theoretical stress (kPa)***	***Monitoring***	
		Initial stress (kPa)	***Final stress (kPa)***
W/SC/B/0.5/1.57	3.90	4.22	5.02
W/SC/B/0.5/1.64	4.10	6.17	8.40
W/SC/B/0.5/1.64	4.10	5.39	7.40
W/SC/A/0.5/1.45	3.60	4.88	5.85
W/SC/A/1.5/1.45	10.90	4.50	9.28
N/SC/B/0.5/1.50	3.70	5.48	6.09
N/SC/B/1.5/1.45	10.90	9.81	12.34
N/SC/A/0.5/1.45	3.70	6.90	7.28
N/SC/A/1.0/1.45	7.30	6.55	8.15
N/SC/A/1.5/1.45	10.90	9.61	10.39
N/SC/A/1.5/1.45	10.90	8.79	12.13

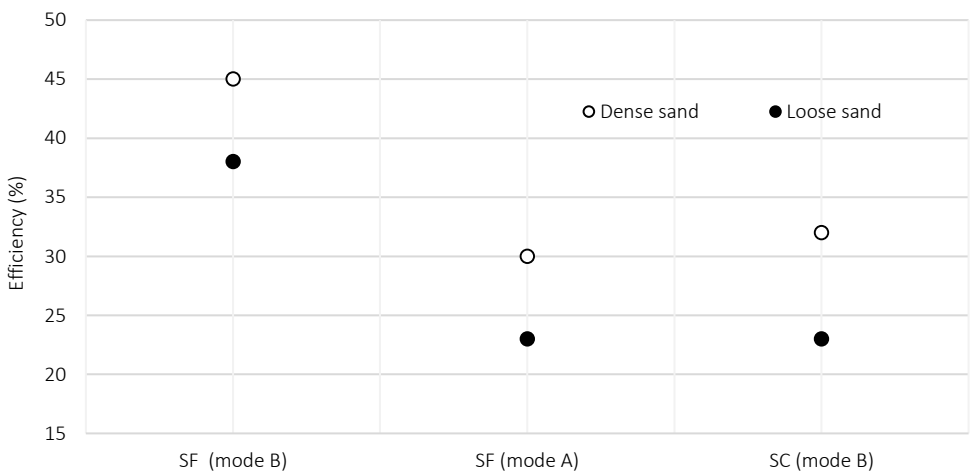

Figure 3.27. Efficiency of tests with an H/D value of 0.5 and woven geosynthetics

3.3.4.2. Comparison between cavity area and anchorage area

Note that the most important purpose for the stress measurement is to confirm the load distribution at the cavity area. Therefore, the TPS was moved to the border of the cavity to compare the load transfer during the opening process between the anchorage and cavity area (*Figure 3.28a*). *Figure 3.28b* and *Figure 3.28c* illustrate the difference of the stress measured by the TPS at the beginning (b), and the end of the opening (c). Higher stress is indicated by green colors, whereas blue colors illustrate lower stress. As can be observed, the stress increase in the anchorage area and decrease at the cavity area after the cavity opening. This variation is clearly shown at the locations located near the cavity border.

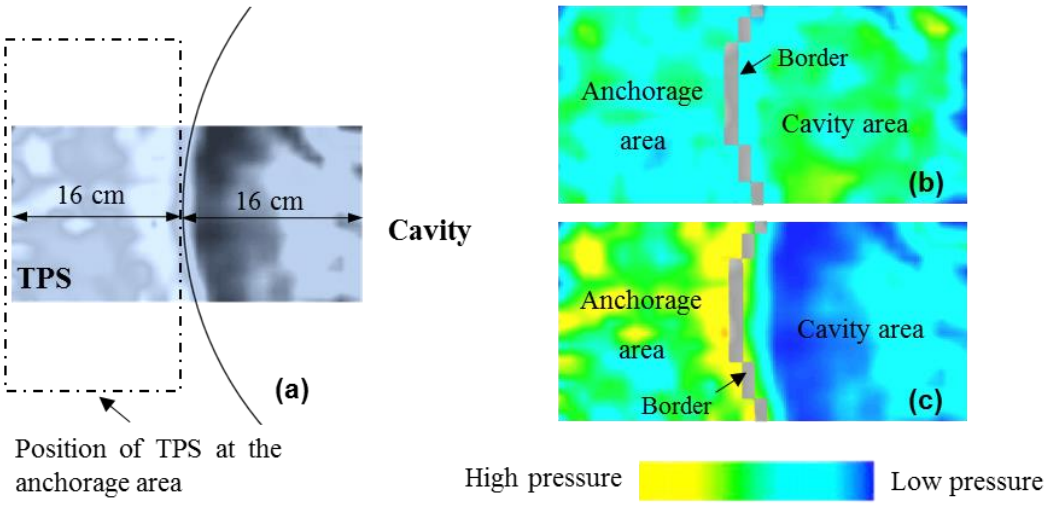

Figure 3.28. TPS located at the border of the cavity

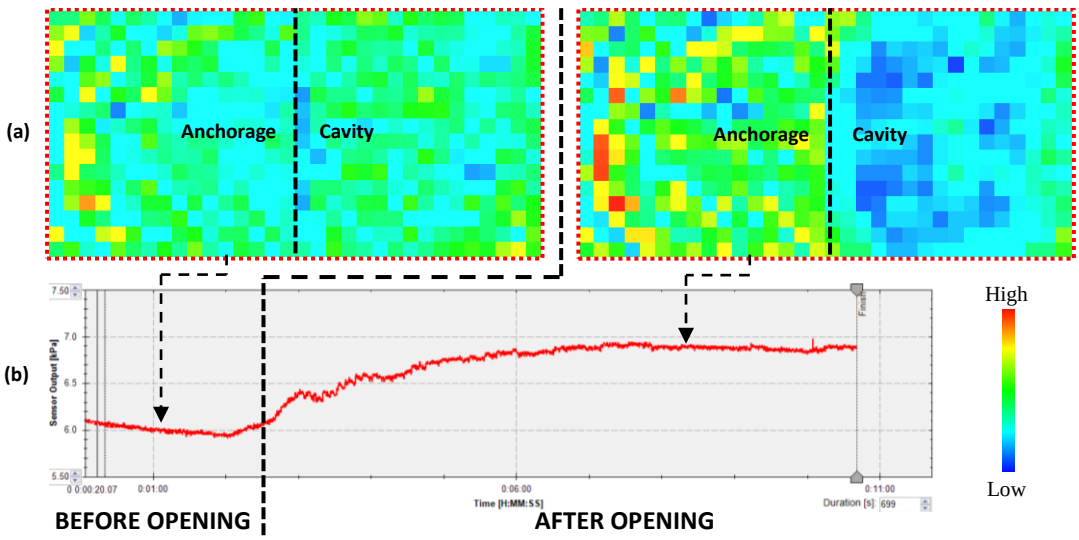

Figure 3.29. Stress variation measured by TPS placed at cavity border

a: Stress map b: Chart data display

Finally, the TPS was moved to the center of the cavity, and the stress distribution could be analyzed along the cavity as well as the anchorage area. *Figure 3.29* and *Figure 3.30* present the stress variation on the geosynthetics during the cavity opening process considering the difference between the three locations of the TPS. On the left of the figure, the stress obtained before the opening of the cavity is presented; whereas, the observations after the opening are presented in the right. In *Figure 3.29a*, the TPS located at the cavity border, associating with the *Figure 3.29b*, it can be seen that before the cavity opening, the stress measured on the sensor seems constant but after that, the stress increases in part located at the anchorage area, and the decrease in the cavity area. In *Figure 3.30a*, where the TPS placed at the cavity center, the tendency of the load distribution can be noted as a decreasing trend in the whole sensor areas. Otherwise, an increasing trend is presented in the tendency of the stress, when the TPS placed at the anchorage area (*Figure 3.30b*).

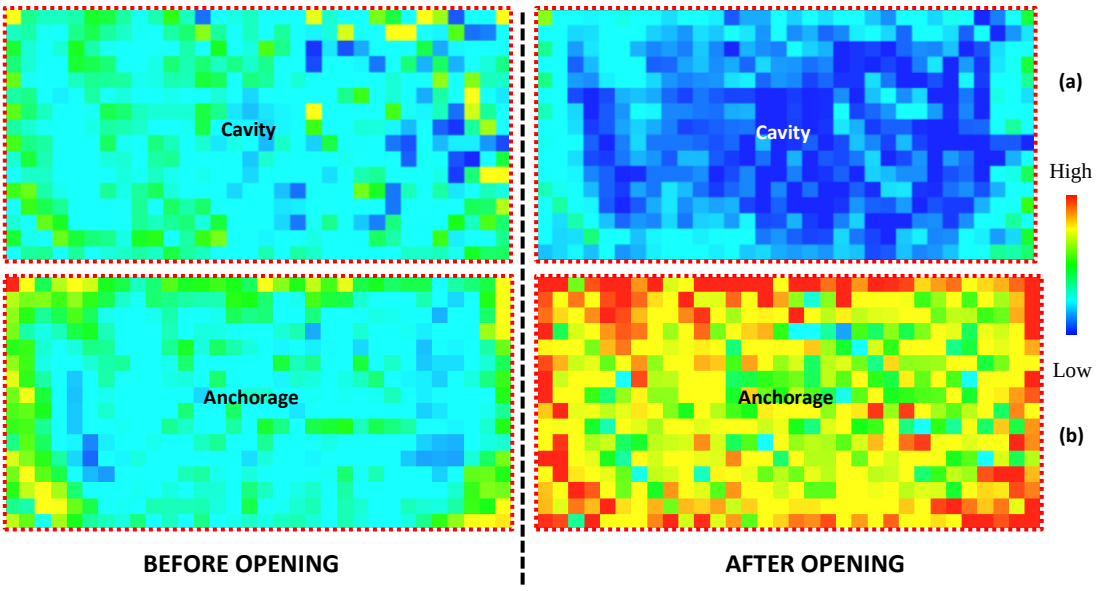

Figure 3.30. Stress variation measured by TPS comparing to different locations
a: TPS placed at cavity center b: TPS placed at anchorage areas

The increases of stress, as defined by the ratio between the final and initial stress acting on the TPS during the cavity opening (σ_f/σ_i) are calculated in both models of the cavity opening for each ratio of H/D. In *Figure 3.31*, the results are separated into two zones: the anchorage and the cavity areas to show the trend of the increase of the stress. A remarkable point can be confirmed: after the cavity opening, the load distribution is non-uniform along the geosynthetic and the anchorage area. An increment of stress is observed for all locations in the anchorage area. The load distribution reaches a more significant value in the locations

near the border, and it decreases corresponding to the development of the distance to the border. The same trend can be noticed for both opening models and three H/D ratios.

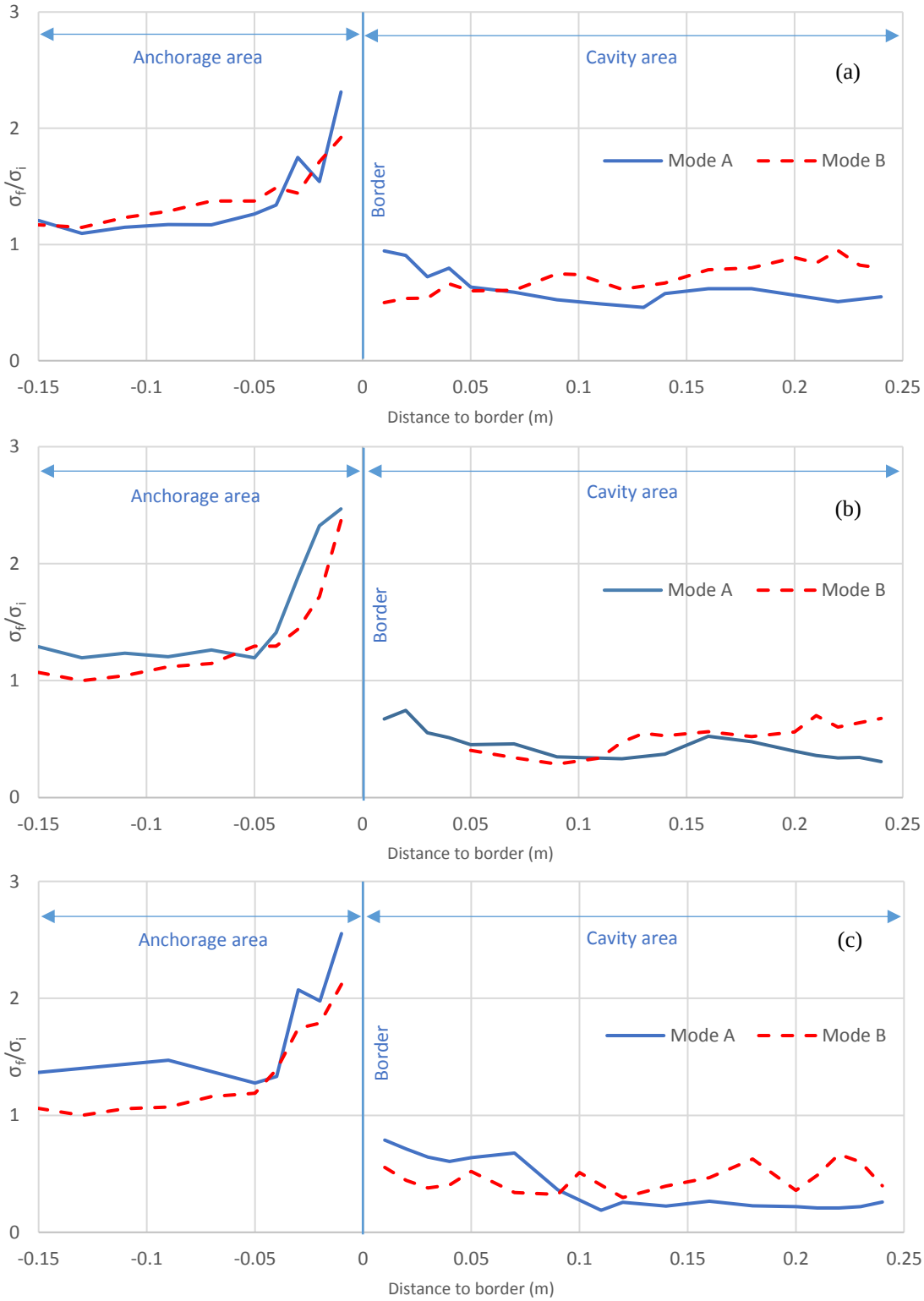

Figure 3.31. Increase of stress after cavity opening (Program 1)

(a) H/D = 0.5 (b) H/D = 1 (c) H/D=1.5

On the other hand, focusing on the cavity area, it is important to note that at all analyzed locations, the load acting on the geosynthetics reduced after the cavity opening reflecting by the values of σ_f/σ_i are entirely lower than 1.

The shapes of the load distribution are different considering the model of the cavity opening. The trend of Mode A tends to decline near the cavity center; it is confirmed for each ratio of H/D, whereas the shape of the load distribution seems to be inverse for the Mode B. Concerning the distance from the cavity border to the center, a slight growth can be seen, especially in case of the H/D ratios are equal to 0.5 and 1.0. For the 1.5-H/D ratio, the direction of the stress variation tends to fluctuate.

The efficiency of load transfer is recalculated combining the stress measured by TPS, which was placed in three different positions on the test table (*Figure 3.28*). For both modes of cavity opening, the load can transfer more efficient corresponding to the increase of H/D ratios. Moreover, the efficiency of load transfer calculated in Mode B is slightly higher than in Mode A, but the difference is not significant.

Table 3.9. Efficiency of load transfer

H/D	Mode A	Mode B
0.5	32%	35%
1.0	51%	51%
1.5	51%	57%

The results are very similar to the numerical simulation of *Villard et al. (2016)*. The difference in load distribution in the cavity area can be explained by the influence of the cavity opening process. In the cases of Mode A, the load transfer mechanisms occurring inside the embankment seems to be stable due to the cavity is processed gradually; whereas, with Mode B, this phenomenon is disturbed due to the increase of the cavity diameter during the opening process. The impact of the opening mode can be seen clearly in case of a great height of the embankment is placed over the cavity, as presented in case of 1.5-H/D test where the shape of the curve looks like a wave.

3.3.5. Load transfer mechanisms over existing cavity (Program 2)

In order to analyze the stress distribution for the test series of Program 2 and compare it with Program 1, a stress ratio $\sigma_{f_n}/\sigma_{f_{0.5}}$ is defined as a relation between the final stress measured after the second or third cylinder is placed and those of the first cylinder, thus "n" corresponding to 1.0 or 1.5. Similarly, a load ratio $F_{f_n}/F_{f_{0.5}}$ is defined for the relation of the final load between the test of H/D = 0.5 and the tests with a higher ratio of H/D.

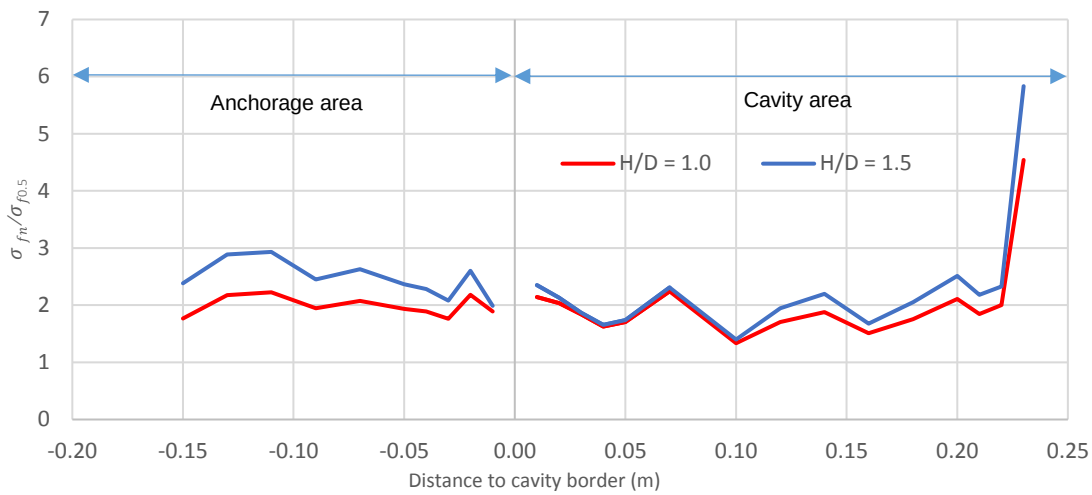

Figure 3.32. Comparison of stress ratio between Program 2 (Mode A)

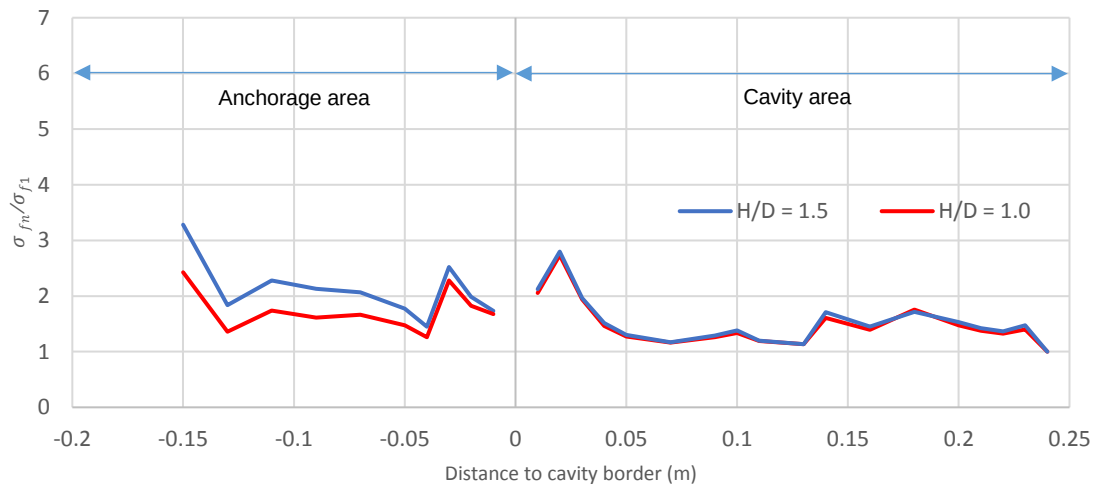

Figure 3.33. Comparison of stress ratio between Program 2 (Mode B)

Figure 3.32 and *Figure 3.33* present the stress ratio $\sigma_{f_n}/\sigma_{f_{0.5}}$ analyzed in Program 2 for two modes of the cavity opening. A different trend of the stress distribution can be seen between the anchorage and cavity areas, for both models of the cavity opening. Considering the stress variation of the tests with H/D ratios equal to 1.0 and 1.5 from the H/D = 0.5 tests, at the cavity center, the stress seems constant, especially in case of Mode B, whereas a significant

increase can be observed at the anchorage area. *Figure 3.34* and *Figure 3.35* also clarify this point, considering the load distribution, in where the load ratios at the cavity area seem to be constant between H/D = 1.0 and 1.5 whereas a significant increase can be seen for the anchorage area.

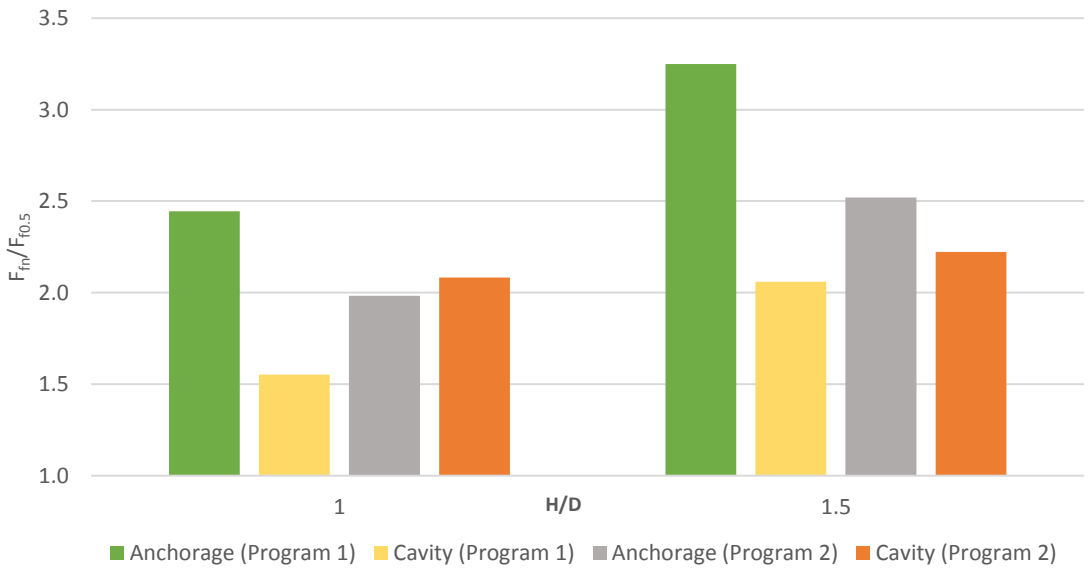

Figure 3.34. Comparison of load distribution between Program 1 and 2 (Mode A)

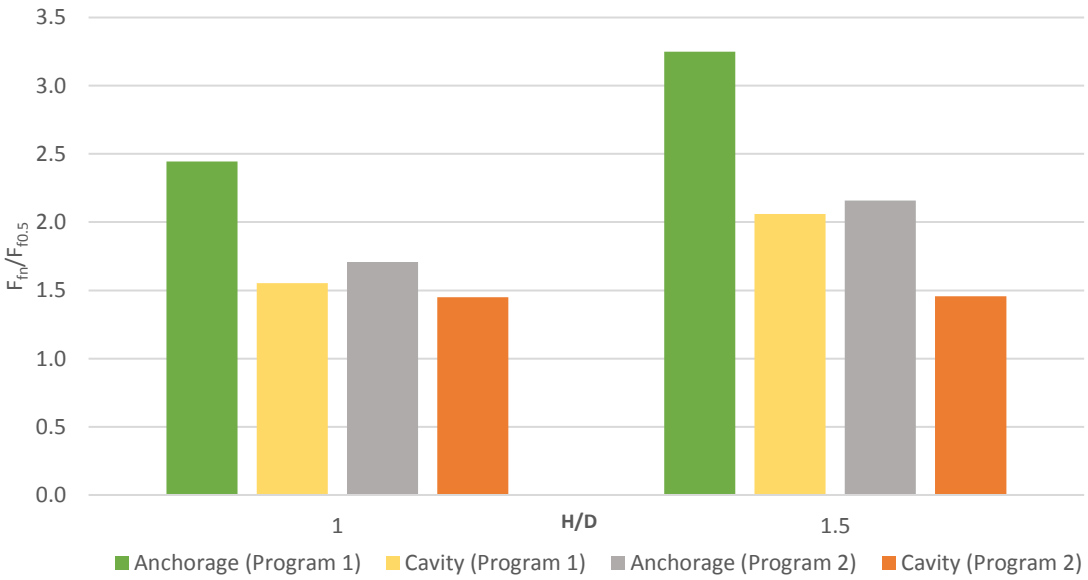

Figure 3.35. Comparison of load distribution between Program 1 and 2 (Mode B)

In *Figure 3.34*, the results of Program 2 are also compared with Program 1 for Mode A, and Mode B is considered in *Figure 3.35*. The same trend can be seen for Program 1, and both modes of the cavity opening as the load distribution ratios at the anchorage and the cavity areas are both increases between H/D ratios = 1.0 and 1.5. In the cases of Program 2, the final

loads applied on the cavity area are constant or increase a minor amount, whereas, for the anchorage areas, the increments of applied load are observed more significantly. Note that, the comparison is given when H/D ratio changes from 1.0 to 1.5.

Figure 3.36 presents the shape of the deflected geosynthetic obtained from the tests of Mode B and Program 2. It can be seen that the geosynthetic deflected in the same form, and the maximum vertical deflections between three tests have not a significant difference. This point agrees with the results obtained with the stress measurement, as the load applied on the cavity seems to be constant during the test of Program 2. Regarding Program 1, the same shape of geosynthetic deflection was presented in *Figure 3.15*, but the maximal deflections between three H/D ratios are different as present in *Section 3.3.1*.

Regarding the arching effect, even if there is a minor difference between the three ratios of H/D (*Figure 3.36*), the deflection of geosynthetic increases following the increase of the embankment height. It means that for the highest ratio of H/D = 1.5, a stable arch is not formed. It agrees with the results of the equal plane estimated in *Section 3.3.2.3* of the present study.

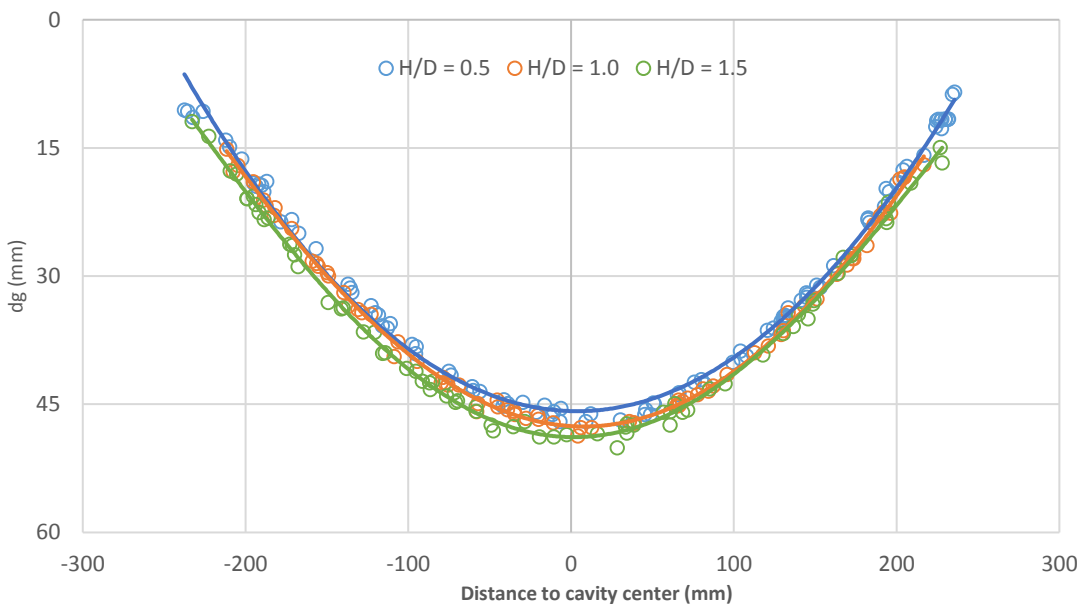

Figure 3.36. Shapes of deflected geosynthetic of Mode B (Program 2)

Finally, it can be noticed for Program 2: when the aching occurs for H = 0.25 m, the load of the added embankment is transferred on the anchorage areas, on cavity considering the second layer, and only on the anchorage considering the third layer. Therefore, the results confirm the effect of arching within the embankment reinforced by geosynthetic over the

cavity. The load could be transferred to the anchorage area even the fill provides a new overload applied on the geosynthetic after the presence of the cavity. Moreover, by comparing two test programs, it can be noted that the efficiency of load transfer of Program 2 is higher than Program 1.

3.4. IMPROVEMENT TO BRING TO THE EXPERIMENTATION

Even if a new laboratory experiment has been developed with the main advantage known as the ability to vary the test configurations, some difficulties exist during the experimental operation.

Firstly, regarding the stretching of the geosynthetics on the test table. Although screws are used to keep the geosynthetic sheet, it is difficult to prevent the stretch of the geosynthetic uniformly in all tests. This problem (*Figure 3.37*) can influence the maximum deflection of the geosynthetic after the opening of the cavity.

Secondly, concerning the method to open the cavity. The difficulty is owing to the operation of the trapdoor and the progressive cone. For the trapdoor, which is made of the metallic material, its shape can be influenced by the environmental temperature. Thus, the rounded shape of the trapdoor can difficult for the downward movement when it is connected to the test table, which is also made from a metallic material. Moreover, when the devices are connected, the movement is also restricted because sand particles can move to the split between the trapdoor and the test table. In order to solve this problem, a thin plastic film was used in this case; it can protect the metallic devices without any influence on the behavior of the geosynthetics. Regarding progressive cone, even if a degree of the opening is marked on the lock, but it is not easy to open the cone uniformly for every test. This problem can affect the velocity of the movement of the filling sand inside the cone. Therefore, it affects the acceleration of the cavity opening.

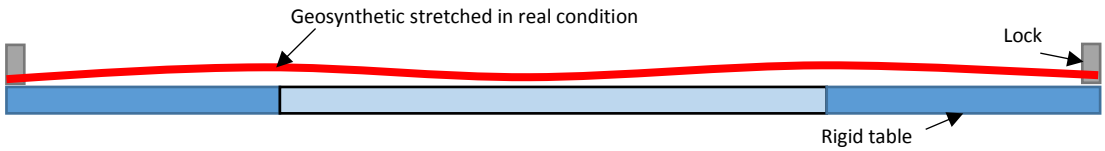

Figure 3.37. Stretching of geosynthetics on test table

Thirdly, the overlying soils are filled inside cylinders by a hand-filling in order to keep the soil density is uniform and avoid any difference on the arrangement of the filled soil

within the cylinders for each test. However, it is such challenging work and takes much time to prepare the experimental tests, especially for the trials with three cylinders.

Nevertheless, these issues only influenced the operation of laboratory devices. Measurement results are almost unaffected due to these concerns; available solutions are given to solve the problems. The most significant effort is it takes time to implement the solutions.

3.5. CONCLUSIONS

A new device was designed and developed to simulate cavities under a granular platform reinforced by a geosynthetic sheet. With the use of this apparatus, the height of the filling soil can be varied, and two procedures for the measurements of cavity openings have become available. In this study, over 80 tests were carried out on two types of geosynthetic sheets and three granular soils with different densities. The repeatability of the experiments seemed to be correct. In order to validate previous numerical studies (*Villard et al., 2016*), the influences of the cavity opening modes on the deflection of the geosynthetic sheet were presented. In the case where the trapdoor was used as an opening mode, the surface settlement and deflections of geosynthetics were lower than those of the progressive mode for both woven and nonwoven geosynthetics.

Regarding the calculation of the expansion coefficient, a precise measurement was used for the surface settlement and geosynthetic sheet deflection. It is possible to use the method that combined a Gaussian method and the 4th-degree polynomial formulation with the current parabolic hypothesis to fit the settlement and geosynthetic deflection shapes to determine the expansion coefficient. The results elicited by the new method were higher than those elicited by the current method were; thus the current method was safe and can be used. However, a new relationship between the expansion coefficient and the granular platform characteristics cannot yet be proposed from the obtained results. This study confirmed the influence of the impacts of the geosynthetic stiffness and the soil density on the expansion coefficient.

A network of tactile pressure sensors placed on and at the edges of the cavity enabled the measurement of the load distribution during the cavity opening. The differences in behavior for two opening processes were obtained based on the comparisons of the efficiency values following the stress variation, and the results confirmed findings from previously published numerical studies.

Finally, the load transfer mechanisms were studied considering the difference in the construction sequence: the cavity appears before and after the formation of the embankment. It is seen that the efficiency of load transfer in case of the existing cavity (Program 2) is higher than the evolving cavity (Program 1).

Although the experimental works have succeeded to improve the knowledge of the geosynthetic-reinforced embankment above cavities, it is limited to investigate all the aspects, due to the stint of the testing method. Hence, numerical simulation is an essential suppleness for this study to explore the other elements such as the rotation of the principal stress direction and the stress ratio. Moreover, the understanding of the influences on the geosynthetic-reinforced embankment above cavities could be developed; besides, uncertain results can also be clarified by the numerical simulations, for example, the equal settlement plane.

CHAPTER 4. NUMERICAL SIMULATIONS

Publication: Pham, M. T., Briançon, L., Dias, D., 2019. Physical and numerical tests of load transfer mechanisms in geosynthetic-reinforced granular embankments above voids. Geotextiles and Geomembranes. Submitted.

4.1. INTRODUCTION

This chapter aspires to validate the developed numerical modeling with the former experimental works, which are presented in *Chapter 3*. Then the numerical models are able to bring more information on the overall behavior of such systems.

The primary purposes are to simulate the reinforced systems above cavities for different configurations and to compare the results of the surface settlements of overlying soil, vertical geosynthetics deflection, and the load distribution that were found by the experimental tests. Note that for the load distribution which was observed by the TPS, only the case of the fine sand and woven geosynthetics were studied. Thus, the primary research strategy is to simulate the experimental tests in different configurations as presented below:

- Overlying soil modeled as fine sand and coarse sand
- Three H/D ratios of 0.5, 1.0 and 1.5
- Cavity opening modes as trapdoor (Mode A) and progressive procedure (Mode B)
- Tested geosynthetics selected as woven and nonwoven materials

At the end of the research strategy, the surface settlements of the overlying soil, the maximum deflection, and the shape of the deflected geosynthetics are determined. An equal settlement plane is also estimated. The expansion coefficient within the overlying soils is analyzed and compared to the results from the experimental tests. By using a parametric study, the parameters which have an influence on the system are investigated, and their effects on the expansion mechanism are presented.

Then, the load distribution on the geosynthetic sheet is determined for both anchorages and cavity areas. The efficiency of the load transfer is computed considering different tested configurations. Moreover, the effect of the cavity diameter and surcharges are also analyzed.

4.2. FINITE ELEMENT ANALYSIS

4.2.1. Numerical modeling

4.2.1.1. Basic concept

The PLAXIS 2-D program, (*PLAXIS, 2016*) was used to model the experimental tests, which are presented in *Chapter 3*. The numerical modeling was carried out using a 2-D axisymmetric configuration in drained conditions. The cavity area is represented at the area located from the origin coordinates to its radius (0.25 m). Two opening modes were

considered: Mode A – downward opening and Mode B – progressive opening. For the first opening mode is modeled by applying a prescribed movement and an increased diameter opening in the second mode is simulated by a deactivation process. For each possibility, the trapdoor and the test table are assumed as metallic materials. The geosynthetics are located between the overlying soils and the rigid bodies. The height of the tested soils is dependent on the ratio of H/D, which is considered for each test.

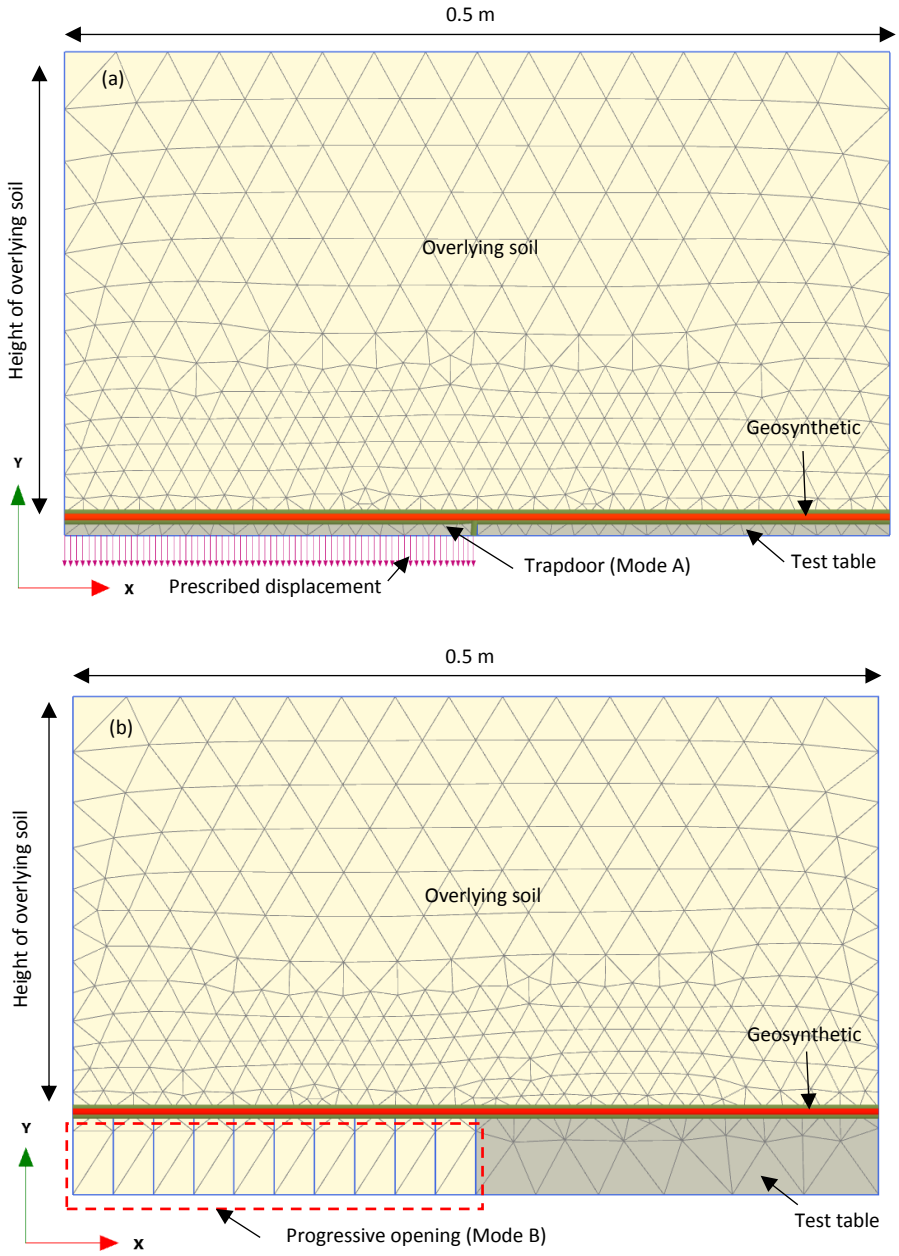

Figure 4.1. Geometrical configuration for the numerical calculation
(a): Mode A; (b): Mode B

Considering the symmetric assumption, a quarter of the mesh has to be modeled. The dimension of the model and the number of elements depend on the height of the overlying soils and the cavity width. The mesh is made considering 15-node triangular elements and based on the symmetric assumption (*Figure 4.1*). Generally, the relative element size factor is used as 0.67 as the element distribution is set as a fine level. Moreover, the mesh refined near the cavity area and it is updated at the beginning of each phase to consider deformation from the previous incremental displacement.

4.2.1.2. Soil constitutive models

The overlying soils were modeled by using two different soil constitutive models: the linear elastic-perfectly plastic (Mohr-Coulomb shear failure criteria) named MC and the Hardening soil model named HS. The Mohr-Coulomb failure criterion is recommended to use as a first-order model as it can describe well the effective stress states at the failure. The HS model depends principally on the internal friction angle φ, which is constant during the computation. In the research field related to the present study, MC and HS constitutive models have been used successfully by *Potts (2007)*, *Pizá (2009)* with Finite element simulations and especially, by *Tahmasebipoor et al. (2012)* and *Girout et al. (2014)*. Therefore, these two constitutive models are selected to develop numerical modeling with the former experimental works.

As a first analysis of the problem, the MC constitutive model is primarily used. This model can describe well the effective stress states at failure. Using this constitutive model induces some drawbacks: the non-linearity of Young's modulus due to the strain and confinement pressure levels, dilatancy before failure cannot be taken into account. The first simulations are then based on an elastic-perfectly plastic material with a Mohr-Coulomb failure criterion given by *Eq.4.1*:

$$\tau = c' + \sigma_n \tan \varphi' \qquad \textit{Eq.4.1}$$

The Hardening soil constitutive model *(Schanz et al., 1999)* can be used as an advanced model to simulate the behavior for both soft soils and stiff soils. The main meaning for the formulation of the Hardening soil constitutive model is the hyperbolic relationship between the deviatoric stress, q, and the vertical strain, ε_1 in primary triaxial loading. Once subjected to primary deviatoric loading, soil shows a reducing stiffness and simultaneously irreversible plastic strains develop.

Table 4.1. Parameters for the Mohr-Coulomb constitutive model

Parameter	***Value of fine sand***	***Value of coarse sand***	***Unit***
γ	14.0	14.5	kN/m^3
E	10	15	MPa
φ'	36.5	39.7	°
ψ	11	15	°
c’	0	0	kPa
υ	0.3	0.3	-

In the present study, all overlying soils are dry. Most of the soil parameters used in both soil model are determined by a series of triaxial tests. For MC, both fine and coarse sand are considered with the soil parameters are using as the values presented in *Table 4.1*. Whereas, for the Hardening soil, only the fine sand (*Table 4.2*) is considered to compare the two soil models. The parameters were determined using triaxial tests.

Table 4.2. Parameters for the Hardening soil constitutive model for fine sand

Parameter	***Value***	***Unit***
γ	14.0	kN/m^3
E_{50}	10	MPa
E_{oed}	10	MPa
E_{ur}	30	MPa
φ'	36.5	°
c’	0	MPa
υ	0.3	-
m	0.5	-

In order to determine the other parameters with their influences, which are not obtainable in the triaxial tests such as the dilatancy angle or earth pressure coefficient, a series of parametric finite element analyses were performed in the following section.

4.2.1.3. Materials

The Trapdoor (Mode A), which is used to open the cavity according to the test program, and the test table are assumed as the metallic material. The Linear Elastic model is used to model the metallic material in this study. The thickness of the solid bodies is equal to 0.01 m. During the model calculation process, the solid bodies, which are used to provide the test table, are fixed in all the directions.

Regarding the properties of the solid materials, the model involves two elastic parameters: Young's modulus E_Y and Poisson's ratio v. In this study, these parameters are fixed by the values of 210 GPa and 0.3, respectively for E_Y and v.

4.2.1.4. Geosynthetics elements

The geosynthetics reinforcement is modeled using the geogrid element already implemented. A linear elastic constitutive model $T = J.\varepsilon$ is used to model the geosynthetic behavior. The only material property of the geosynthetics is the elastic axial stiffness, EA. Thus, the tested geosynthetic property in the numerical models corresponds to the values of the experimental tests. The stiffness of the two tested geosynthetics used in the laboratory tests is presented in *Table 3.2*.

However, it seems difficult to monitor the variation of the geosynthetic strain during the cavity opening. On the other hand, the numerical simulations are performed to be compared with the experimental tests and hence to deal with the difficulty that how to stretch the tested geosynthetics uniformly on the test table, as described in *Section 3.4*. It was necessary to decrease the stiffness of the geosynthetics, especially for the woven material, as the influence of material stretching is higher than the nonwoven sheet. Therefore, in the numerical models, the stiffness of the woven geosynthetic was equal to 120 kN/m, whereas the value for the nonwoven geosynthetic in the numerical simulations is set as 10 kN/m.

4.2.1.5. Interface elements

In this study, interface elements are used to model the contacts between soils, steel, and geosynthetics. Interfaces were placed on both sides of the geosynthetics, allowing the sheet to move independently of the adjacent soils. The movement of the geosynthetics is allowable along with the interface.

The interface properties were selected based on the properties of fill soils with the modification of the friction angle (*Table 4.3*). The interface friction angles between geosynthetic and soils or metallic material were obtained from inclined tests, following the procedure proposed by *Briançon et al. (2011)*. Regarding the geosynthetics, two different interface elements were set. The first one is the interface between geosynthetics and overlying soils, named as Soil/GSY. The second one, GSY/Steel, is the interface between the metallic material (trapdoor or test table) and the geosynthetics. The properties of these interfaces depend on the characteristics of the closer soil or solid material, whereas the

friction angles are selected from inclined tests, the value of 25°. *Figure 4.2* presents the positions of the interface elements used in the numerical modeling for Mode A and Mode B. In the cases of Mode A tests, an interface named as Steel/Steel is defined in order to allow the movement between the test table and the trapdoor, and the stiffness inside that interface is set as very low.

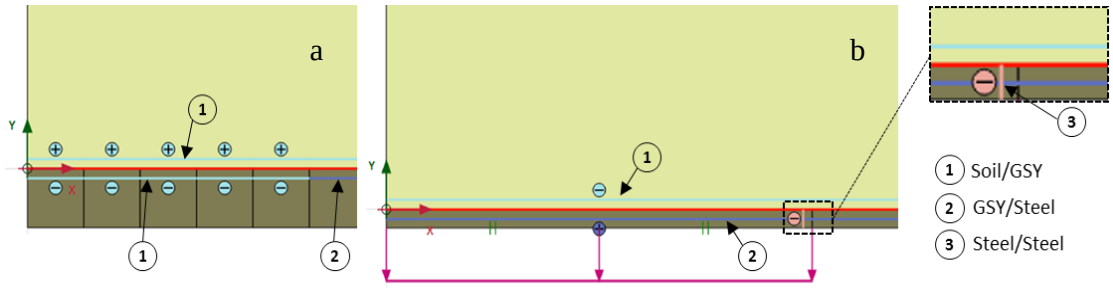

Figure 4.2. Positions of interface elements used in the numerical modeling
(a): Mode A; (b): Mode B

Table 4.3. Parameters for interfaces elements

Elements	***Soil/GSY***		***GSY/Steel***		***Steel/Steel***	
Material model	Mohr-Coulomb		Mohr-Coulomb		Linear elastic	
	SF	SC				
E *(MPa)*	10	15	10×10^{-3}	15×10^{-3}	10×10^{-3}	10×15^{-3}
φ' *(°)*	25	25	-	-	-	-
c' *(kPa)*	0	0	0	0	-	-
υ	0.3	0.3	0.3	0.3	0.3	0.3

4.2.2. Numerical analysis of the physical model

Based on the definition of the numerical modeling corresponding to the results of the parametric analysis, the numerical studies of the geosynthetic-reinforced embankment above cavities have been developed.

4.2.2.1. Initial and boundary conditions

Vertical movement is acceptable along with the models, whereas the boundary conditions do not allow any horizontal movement U_{rr} on the axisymmetric axis and on the model side during the opening of the cavity. The bottom of the numerical model is fixed in the horizontal and vertical direction. The lateral earth pressure coefficient at rest K_0 is defined using the coefficient: $K_0 = 1 - \sin\varphi$.

4.2.2.2. Cavities opening methods

In order to compare the numerical models with the experimental tests, which are presented in *Chapter 3*, two different modes to open the cavity are considered: a trapdoor (Mode A) and a progressive procedure (Mode B). Therefore, two different configurations are used in order to reproduce these two opening modes, see *Figure 4.1*.

Concerning Mode A, the trapdoor is modeled as a metallic plate, which is placed in the cavity area, below the position of the geosynthetics. The base is made of steel with the same characteristic of the test table. In order to reproduce the downward movement of the trapdoor, a prescribed movement is applied. The trapdoor movement is limited to a maximum value of 1.0 m.

For Mode B, the cavity is opened by increasing the cavity diameter. In this case, the cavity-opening mode is modeled by a series of ten soil polygons, which have the same dimensions. Although in the experimental test, fine sand was filled inside the cone to form the progressive procedure, the soil polygons are modeled as a metallic material to avoid any deformation of each polygon. Since the calculation begins, each polygon is deactivated step by step, thereby; an increased diameter process permits to reproduce in a simplified way the cavity opening.

4.2.2.3. Calculation phases

For each case, the first phase applied is the initial stress conditions. After this initial phase, a large deformation analysis is used. The calculation phases are defined due to the use of the opening modes. If Mode A is considered, the second phase corresponds to the movement of the trap to reproduce the sudden opening of the cavity. For Mode B, a series of the continuous phases consist of the deactivating process to model the increasing-diameter evolution of the cavity.

4.2.3. Sensitivity analysis of input parameters

Even if geotechnical tests can be used to determine most input parameters for the numerical simulations, some of them, such as the dilatancy angle and the earth pressure coefficient, were not determined experimentally. Therefore, a series of parametric analyses were performed in order to investigate the influence of these parameters on the expansion mechanisms. Moreover, by varying the geosynthetic stiffness, the impact of the parameter on the effectiveness of the geosynthetic-reinforced soil over cavities has been clarified. The

investigated parameters included the cavity diameter, which was varied with the increase of the height of the overlying soil to consider the effect of the geometrical configuration.

Indeed, the dilatancy of soils has received a great attention in many early works. Bolton (1986) considered the stress-strain behavior of sands and illustrated that the strength of soil could reach a peak before the critical state. Indeed, in the present study, the soils do not achieve a critical state, therefore; the angle of dilation of fill soil need to be increased.

Regarding the other important parameters of soils such as the friction angle, the density, the effects have clarified completely by the experimental tests. Whereas, the Poisson's ratio and Young's modulus are not considered in this chapter due to the fact that these parameters are determined directly by the triaxial tests. Moreover, Potts (2007) and Pizá (2009) have shown that varying Young's modulus does not have any significant effect on the behavior of the reinforced system.

4.2.3.1. Overlying soil characteristics

In order to investigate the effects of the dilatancy angle and the earth pressure coefficient on the surface settlement and the geosynthetic deflection, a series of tests were performed for the fine sand with two ratios of H/D (0.5 and 1.0) and both modes of cavity-opening. In *Figure 4.3*, four series of tests are used to present the maximal vertical displacement. In each series, the two first tests illustrate the results considering two values for the earth pressure coefficient of 0.4 and 1.0 (initial values of the fill, after the cavity opening). The two last tests present the results of displacements regarding the variation of the soil dilatancy angle, which is set equal to 11° and 15°. *Figure 4.4* presents the variation of the expansion coefficient corresponding to the variety of these two parameters.

Figure 4.3, shows that the earth pressure coefficient does not have a significant effect on the surface settlements and geosynthetic deflection. The maximum difference on the surface settlement is of only 1 mm. This can be obtained for both modes of cavity opening and H/D ratios. Therefore, as can be seen in *Figure 4.4*, the expansion coefficient seems to be unaffected. Otherwise, higher dilatancy angles have a high impact in terms of reducing the surface settlements, whereas for the geosynthetic deflection the decrease is lower. Due to the influence of the soil dilatancy angle on the surface settlement, the expansion coefficient increases with the increase of this parameter. It is evident that the dilatancy angle and the

earth pressure coefficient are parameters of overlying soil and it is normal that they do not affect the geosynthetic deflection.

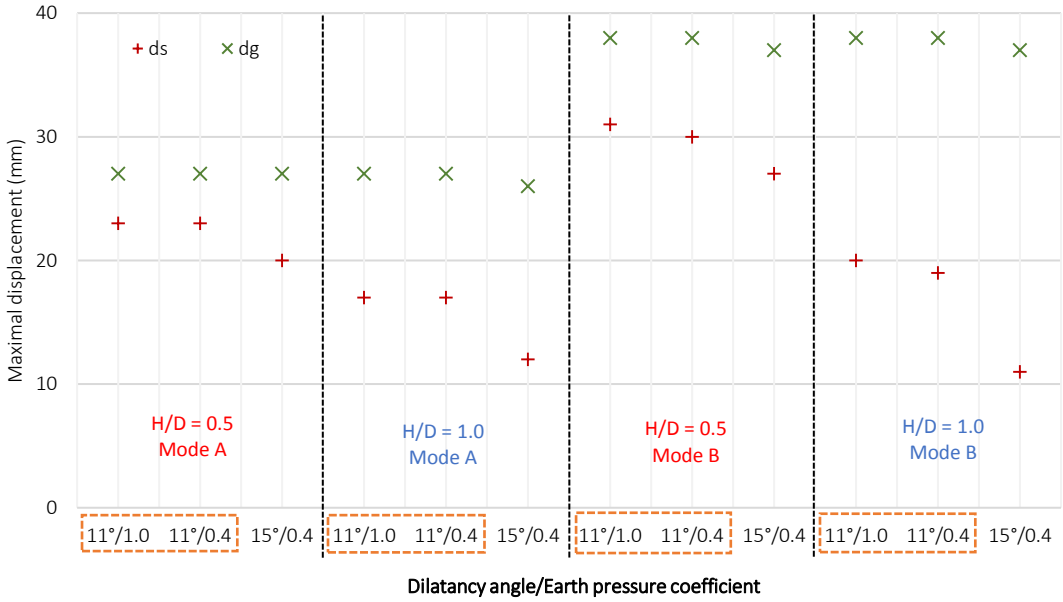

Figure 4.3. Variation of surface settlement and deflected geosynthetics due to changing of dilatancy angle and earth pressure coefficient

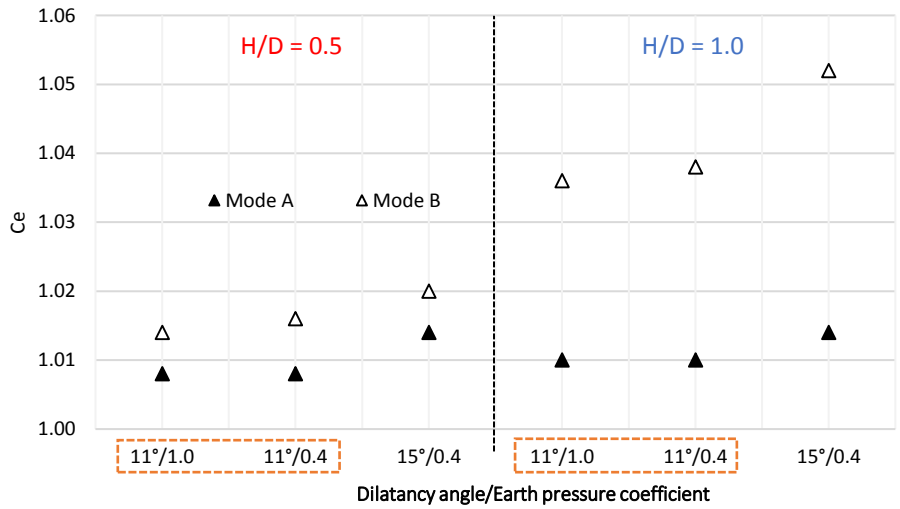

Figure 4.4. Variation of Ce due to changing of dilatancy angle and earth pressure coefficient

4.2.3.2. Tensile stiffness of geosynthetics

The tensile stiffness effect of the reinforced materials on the surface settlements and geosynthetic deflections has been considered for different values from 80 to 160 kN/m. *Figure 4.5* presents the surface settlements and the geosynthetic deflections. It can be noted that both surface settlements and geosynthetic deflections are reduced due to the fact that the load carried by the reinforcement sheet in proportional to the stiffness. This conclusion is not

affected by the variation of the H/D ratio or the mode of the cavity opening. The results are in agreement with the results obtained by *Potts (2007)*, *Pizá (2009)* and *Tahmasebipoor et al. (2012)*.

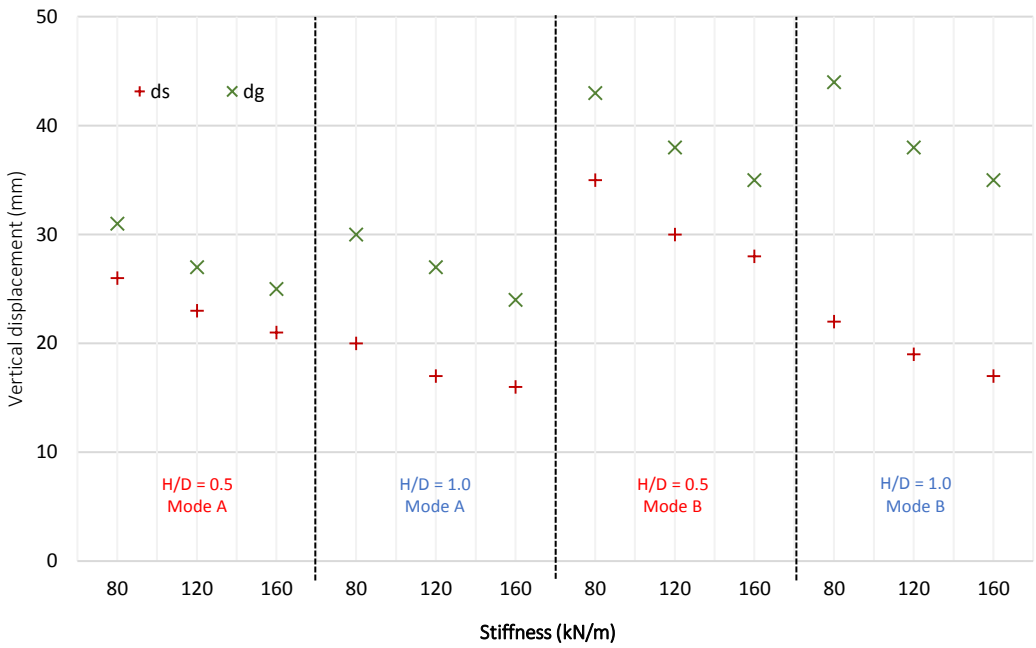

Figure 4.5. Variation of surface settlement and deflected geosynthetics due to changing of geosynthetic stiffness

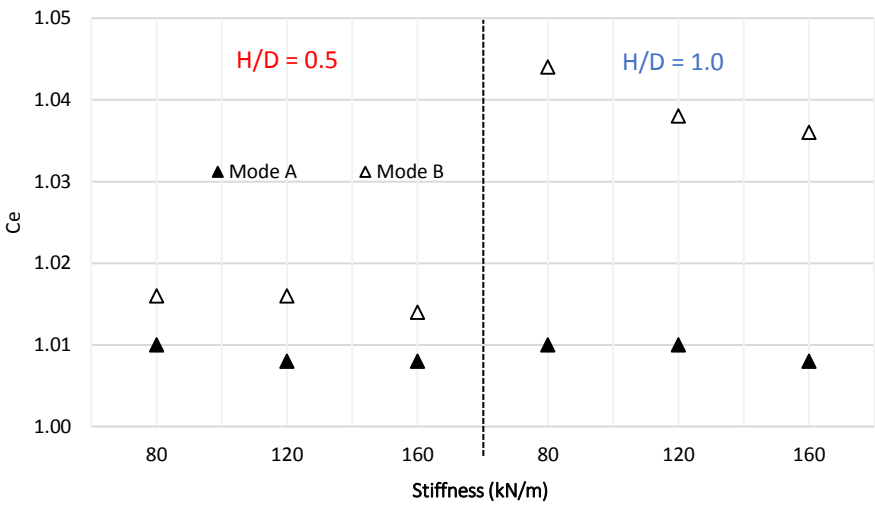

Figure 4.6. Variation of Ce due to changing of geosynthetic stiffness

Consequently, varying the tensile stiffness of the geosynthetic material has a substantial effect on the expansion coefficient *(Figure 4.6)*. The Ce values estimated with the lower stiffness materials are higher than the stiffer one. This point agrees with the results from the comparison between the woven and nonwoven geosynthetics, which are presented in *Section 4.3.3*.

4.3. KINEMATIC ANALYSIS OF EMBANKMENTS

4.3.1. Surface settlement

Figure 4.7 presents the shape of the numerical surface settlements for several soils; (see *Appendix B* for the other results). By plotting the settlements for both cavity-opening modes and comparing them with the experimental results, it can be concluded that the numerical simulations seem to reproduce with a good accuracy the surface settlements shapes and the deflected geosynthetics.

The results of the maximum surface settlements are presented in *Figure 4.8* covering a combination of three different H/D ratios, two cavity-opening modes, two different geosynthetics, and two tested soils. Corresponding to a same H/D ratio, the settlements obtained in the woven geosynthetic cases are lower than in the nonwoven geosynthetic case. Whereas, the estimated results of Mode A are lower than for Mode B.

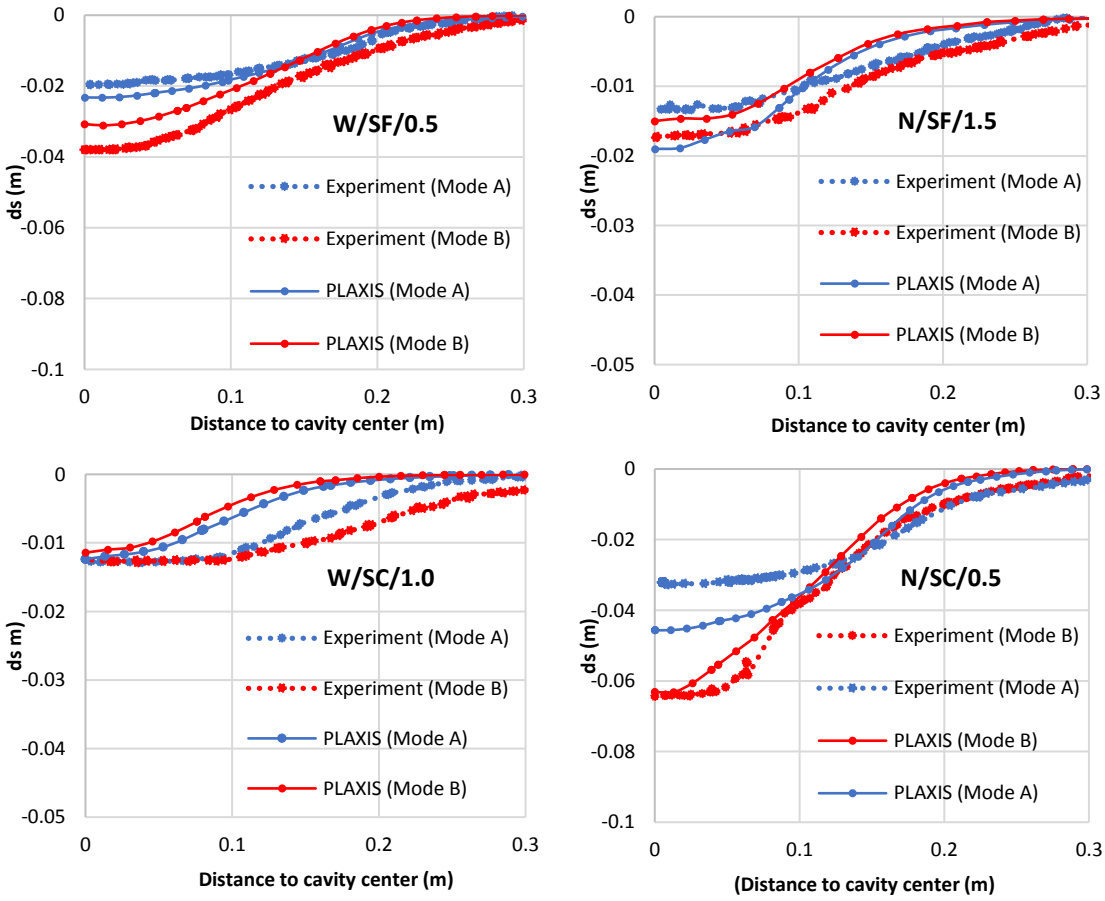

Figure 4.7. Comparison of surface settlement between experimental and numerical results

To compare the numerical and experimental results, in some cases, additional experimental tests, which were conducted to verify the repeatability, are presented. It can be noted that the

surface settlements decrease with the increment of H/D which is obtained by the experimental tests is also found by the numerical models. For the series of woven geosynthetic (*Figure 4.8a*), the results obtained for Mode A by the numerical modeling are very close to the experimental results.

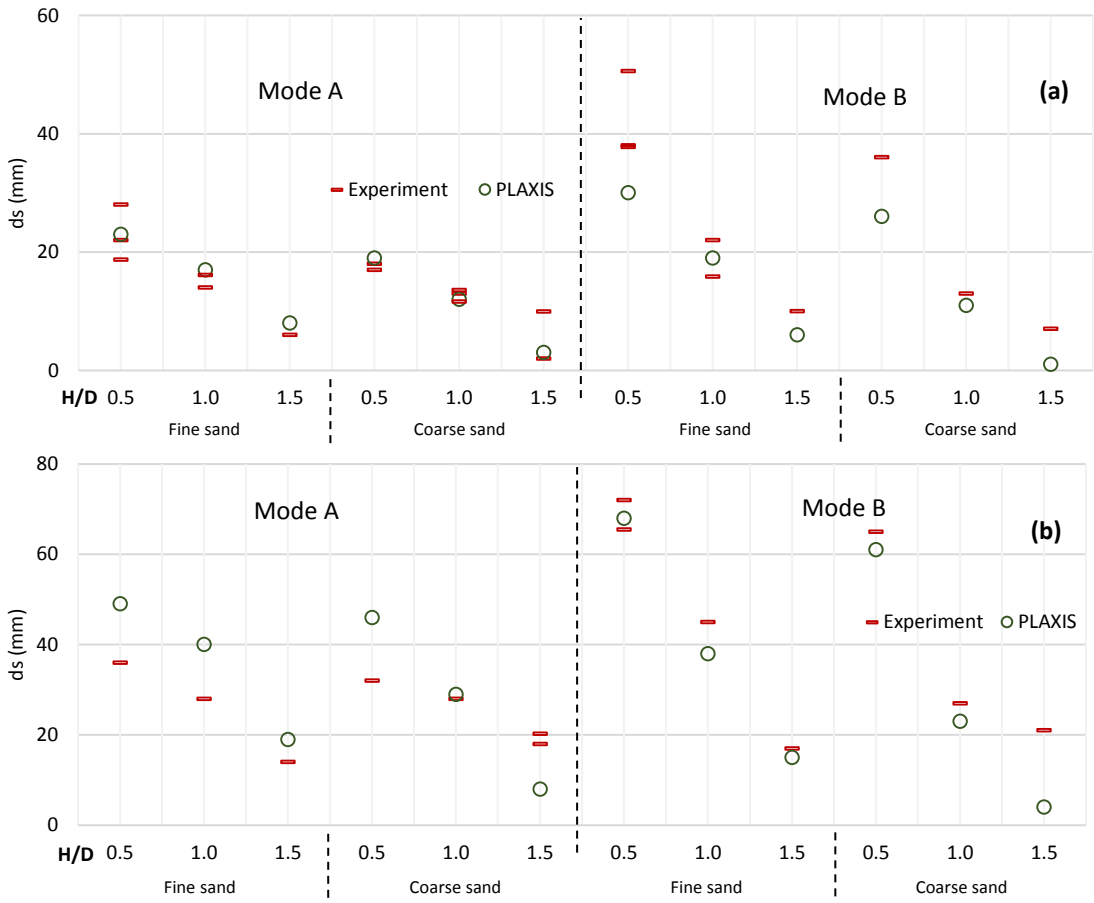

Figure 4.8. Comparison of surface settlement between experimental and numerical results (a): Woven GSY (b): Nonwoven GSY

For Mode B, even if there is a minor variation in several tests, but for the cases of H/D = 1.0, the results are precisely similar. Concerning the nonwoven geosynthetic tests (*Figure 4.8b*), numerical modeling provides higher settlements than the laboratory tests, in most cases Mode A, meanwhile, for Mode B, the results are lower. Generally, a more significant difference between the experimental and numerical results for Mode B. This can be explained by the simplified technique used to reproduce the Mode B process in the numerical models. Even if a group of ten polygons is generated to simulate a progressive opening, the speed of the sand flowing out of the cone cannot be completely reproduced.

Concerning the difference between the fine and coarse sand surface settlements, which can illustrate the soil friction angle effect, both numerical models and experiments present a

similar behavior. The same trend is obtained for each group of tests where the vertical displacement of fine sand is higher than for the coarse sand.

In the numerical modeling, uniform parameters are used for tested soils, whereas the uniformity of the soil parameters can be affected by the experiment conditions due to the difficulties regarding the stretching of the geosynthetics, which are discussed in *Section 3.4*.

4.3.2. Geosynthetic deflection

The deflections of the geosynthetics are numerically calculated and compared with the experimental tests. *Figure 4.9* presents the typical curves of the geosynthetic deflection for respectively fine and coarse sand tests. Similarly to the laboratory tests, the deflection of woven geosynthetic is lower than for the nonwoven in every test. The numerical simulations succeeded to represent the behavior of the two tested geosynthetics using the two different modes of cavity opening, where the nonwoven geosynthetic deflection is greater than the woven one. Moreover, the numerical models confirm the influence of the cavity opening process, which is illustrated in *Figure 3.15*, as the shape in the cases of Mode A can be well fit by an inverted parabolic and a conical shape can be seen in the cases of Mode B.

It can be seen that the maximum numerical geosynthetics deflection matches well with the experimental tests, for different values of H/D, two tested geosynthetics and the two types of tested soils.

Figure 4.10 presents the maximum geosynthetics deflection obtained from the experimental tests and numerical modeling. Nevertheless, when H/D ratios increase, a slight reduction can be seen for the vertical displacements of geosynthetic obtained by experimentation, for the numerical calculation, it is evident that a uniform deflection is obtained for each group for the three H/D ratios. The geosynthetics deflection with the woven material is lower than for the nonwoven one due to the effect of the tensile stiffness. Whereas, in the cases where the cavities are opened progressively (Mode B), the deflection of the geosynthetics are higher than in the cases of the downward opening (Mode A). These tendencies confirmed the results of the experimental tests. The other results are presented in *Appendix B*.

Concerning the differences between the numerical modeling and the laboratory tests, for the woven geosynthetic tested in both Mode A and Mode B, the maximum deflection are almost underestimated with the numerical simulations. Whereas, for the nonwoven geosynthetic, the numerical results overpredicted the deflection. For the variation of the three H/D ratios, at

least for one test, the numerical prediction matches with the experimental result. The influence of the experimental conditions can be seen for the geosynthetic deflection. As discussed in *Section 3.4* (see *Figure 3.37*), in the laboratory tests, a uniform strain of the geosynthetics when stretching them on the test table cannot be provided. Therefore, in some experimental tests, the deflection of the geosynthetic seems to increase a bit corresponding to the expansion as soon as the cavity-opening device is beginning. Whereas, the stretching difficulty does not affect the simulation as the tested geosynthetics is reproduced uniformly.

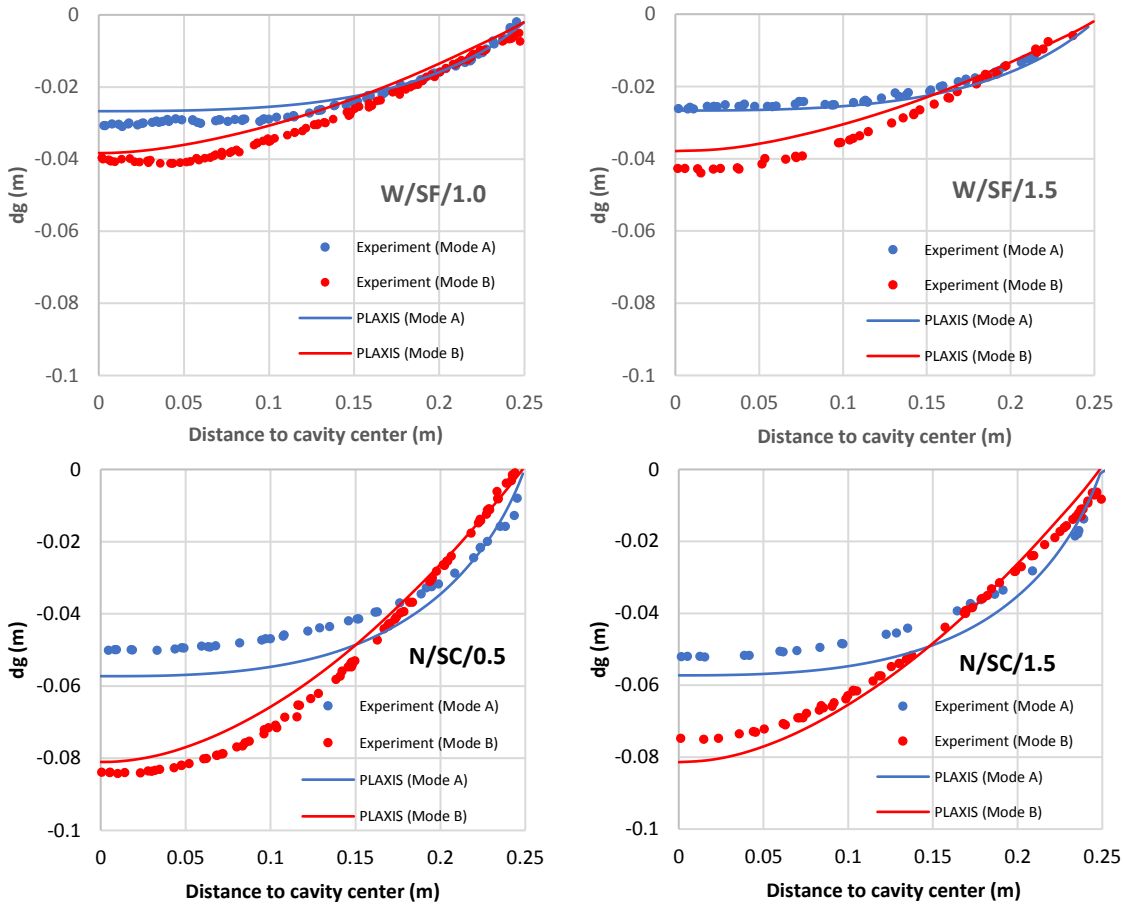

Figure 4.9. Comparison of deflected geosynthetics between experimental and numerical results

For the friction angle effect, in terms of geosynthetic deflection, while the results of coarse sand are slightly lower than those of fine sand, the experimental results trend is not clear. Thus, according to the numerical simulations, the ratio H/D seems not to affect the geosynthetic deflection.

By comparing to the results of other studies, the main differences on the surface settlement sand geosynthetics deflection obtained for Mode A and Mode B are in good agreement with the results of the numerical works performed by *Villard et al. (2016)* in which the DEM method was used to investigate a stiffer geosynthetic.

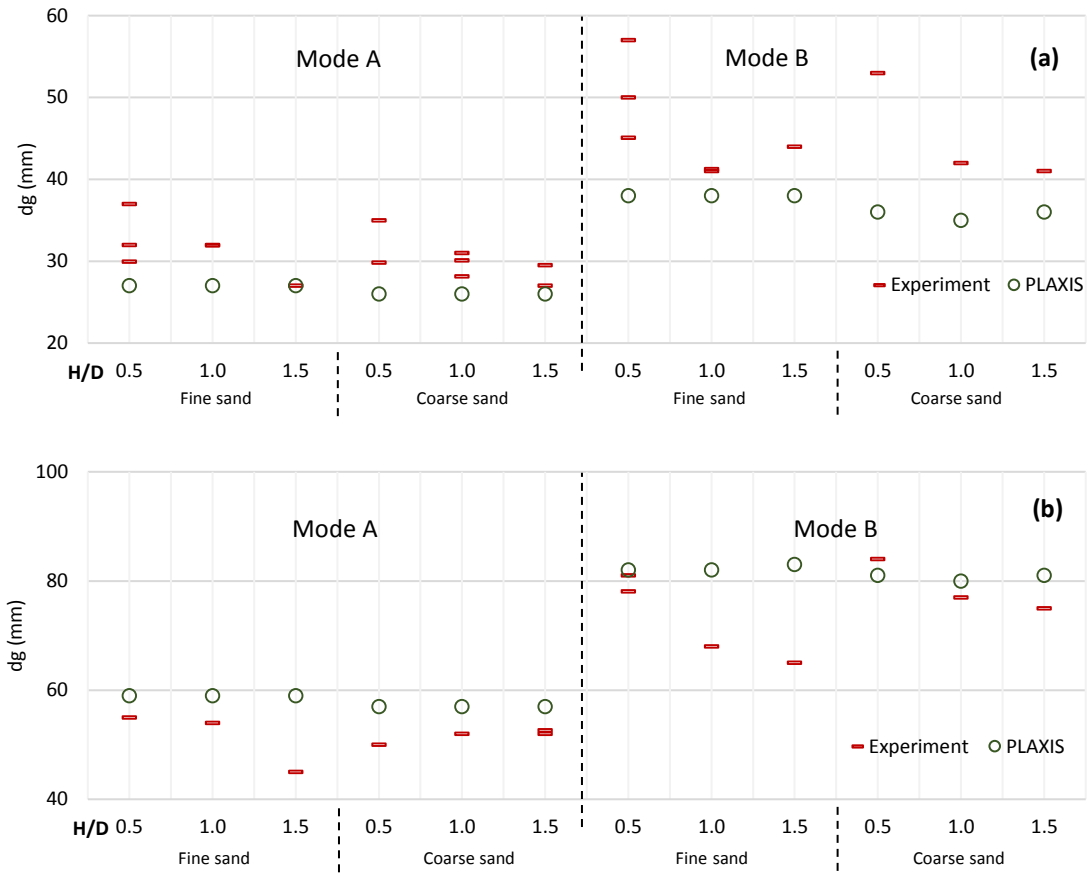

Figure 4.10. Comparison between experimental and numerical results for the maximum geosynthetics deflection

(a): Woven GSY (b): Nonwoven GSY

Figure 4.11 presents the numerical geosynthetic strains for the cases of fine sand and woven geosynthetic, considering two methods of calculation: from the average value. The average values of the geosynthetic strains are also estimated by the method proposed by *Giroud (1995)*. It can be seen that at the cavity center, the strains calculated for Mode B are higher than for Mode A. This can be explained by the assumption of the analytical method, where the shape of the deflected geosynthetic is considered a parabolic one, whereas, in the case of Mode B, the considered shape is conical. Thus, the analytical method could be improved considering the effect of the cavity-opening mode: downward or progressive procedure on the geosynthetic deflection.

Compared to the average strains calculated by the numerical results, in the case of Mode A, the geosynthetic strains at the location near the cavity center are very similar. Whereas, for Mode B, the numerical results underestimate the results calculated by *Giroud (1995)*. On the

other hand, it could be noted that the average strains calculated numerically are lower than the experimental results due to the geosynthetic deflection values.

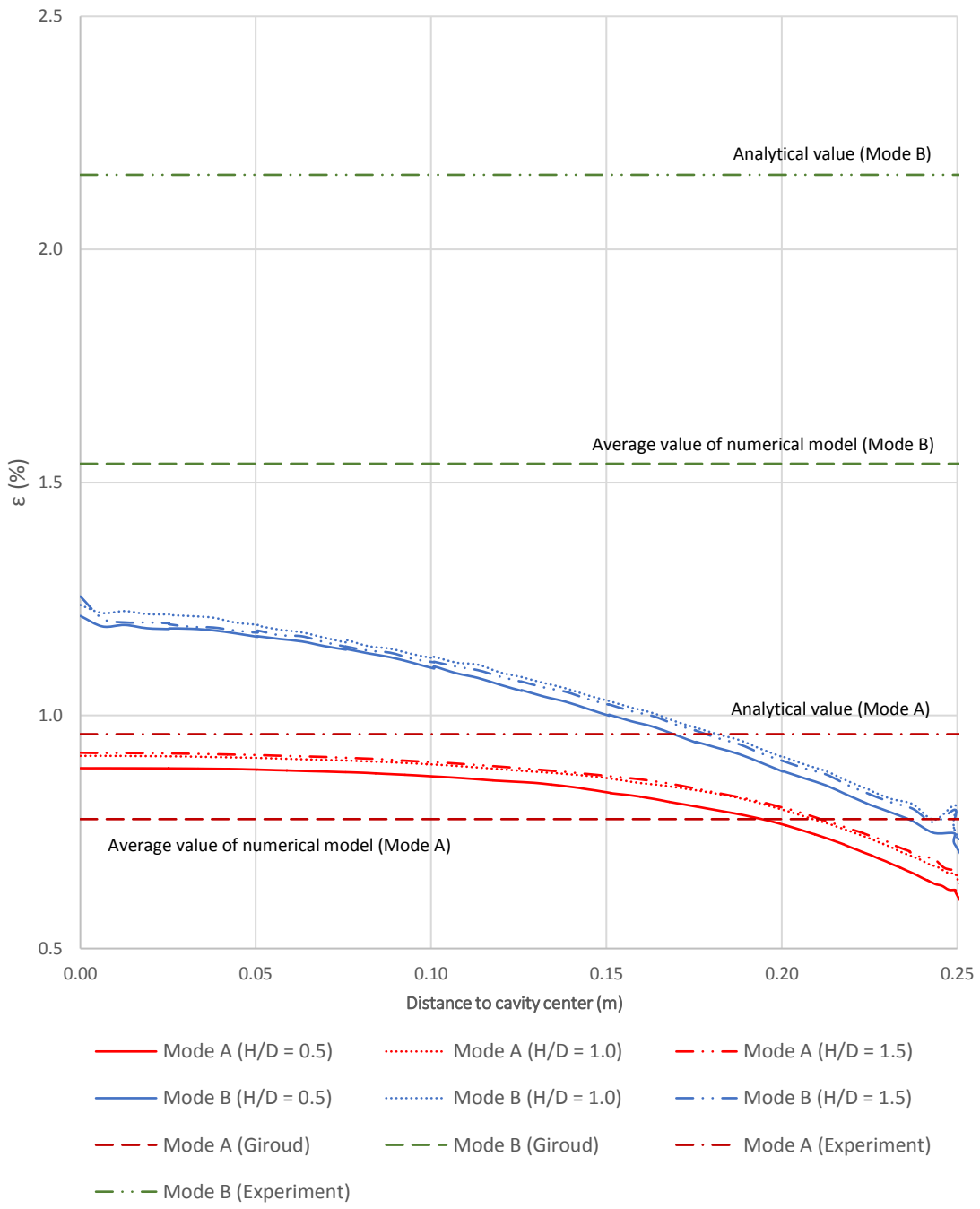

Figure 4.11. Comparison of geosynthetic strains at cavity area between two modes of cavity opening (Fine sand and Woven geosynthetic)

Figure 4.12 presents the equal settlement plane estimated by the numerical simulations. For the woven geosynthetics, the equal settlement plane could be achieved approximately for H/D values varying from 1.8 to 2.5 whereas for the nonwoven geosynthetics the H/D values

are in the range of 2 to 2.5. These results are slightly higher than the estimations obtained from the experimental tests, which are presented in *Section 3.3.1*. The difference can be explained by the assumption to estimate the height of the embankment, which the settlement is equal to zero. Like that, a simple linear used for the decreasing tendency of the settlement for the experimental results is not an accurate assumption. According to the numerical results, the surface settlements reduce gradually as the H/D ratios reach higher values than 1.5.

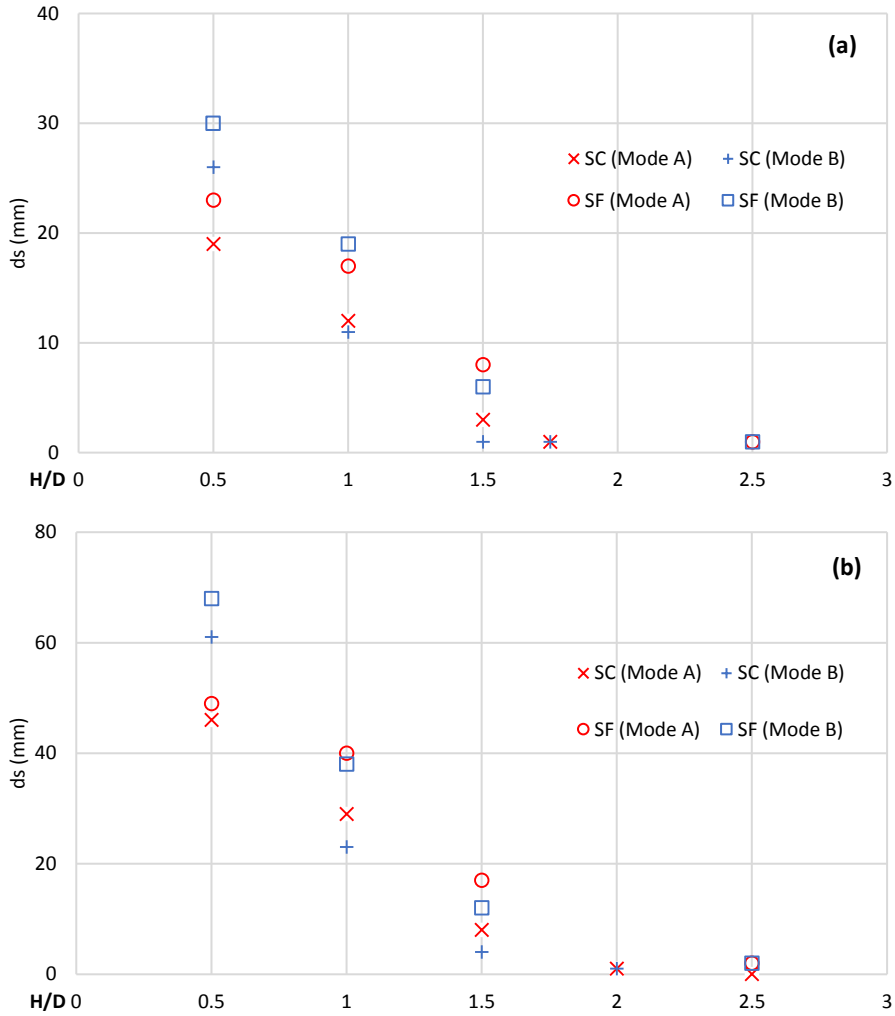

Figure 4.12. Equal settlement plane calculated by PLAXIS

(a): Woven GSY (b): Nonwoven GSY

4.3.3. Influence of the soil constitutive model

In order to verify the reliability of the numerical model for the vertical displacement of the soil surface and geosynthetics, the Hardening soil constitutive model is used to simulate the fine sand. A comparison between the two soil constitutive models, Mohr-Coulomb and Hardening soil, have been conducted for the test series of fine sand and two types of reinforced geosynthetics. *Figure 4.13* compares the difference of the maximal vertical

displacements of surface settlement and geosynthetics between the two models and the experimental results.

It is seen that both used soil models reproduced precisely the geosynthetic deflection, dg, as the variation with the experimental results are minor, except for the two first cases of nonwoven tests. Concerning the surface settlement, ds, the two soil models show the same results, and even there is a difference with the experiment. To conclude, the use of Mohr-Coulomb is reasonable and sufficient for the studied cases, because it yields no significant difference with the Hardening soil constitutive model. The MC constitutive model will be used for the following presented results.

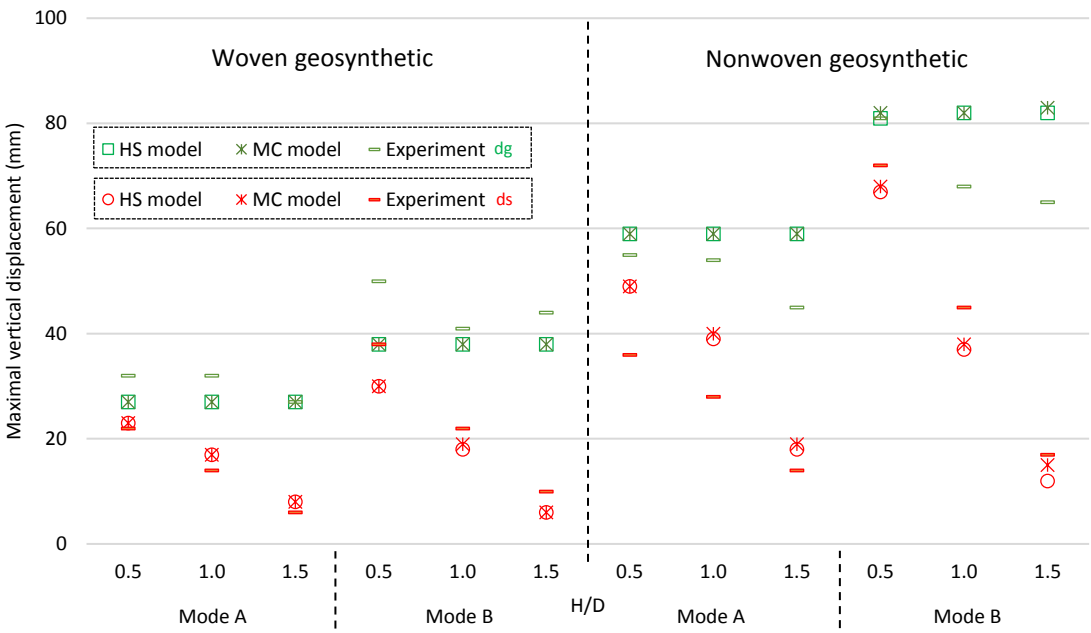

Figure 4.13. Difference of the maximal vertical displacements of surface settlement and geosynthetics

4.4. SOIL EXPANSION ANALYSIS

4.4.1. Expansion coefficient

Figure 4.14 presents the expansion coefficient and the comparison with the experimental results. It can be seen that the trend of Ce variation obtained by the numerical and experimental works is not similar. Whereas in the laboratory tests, Ce value seems to reduce as H/D increases, the numerical results show a reversed tendency, because the geosynthetic deflection tendency is different, but the surface settlements are alike.

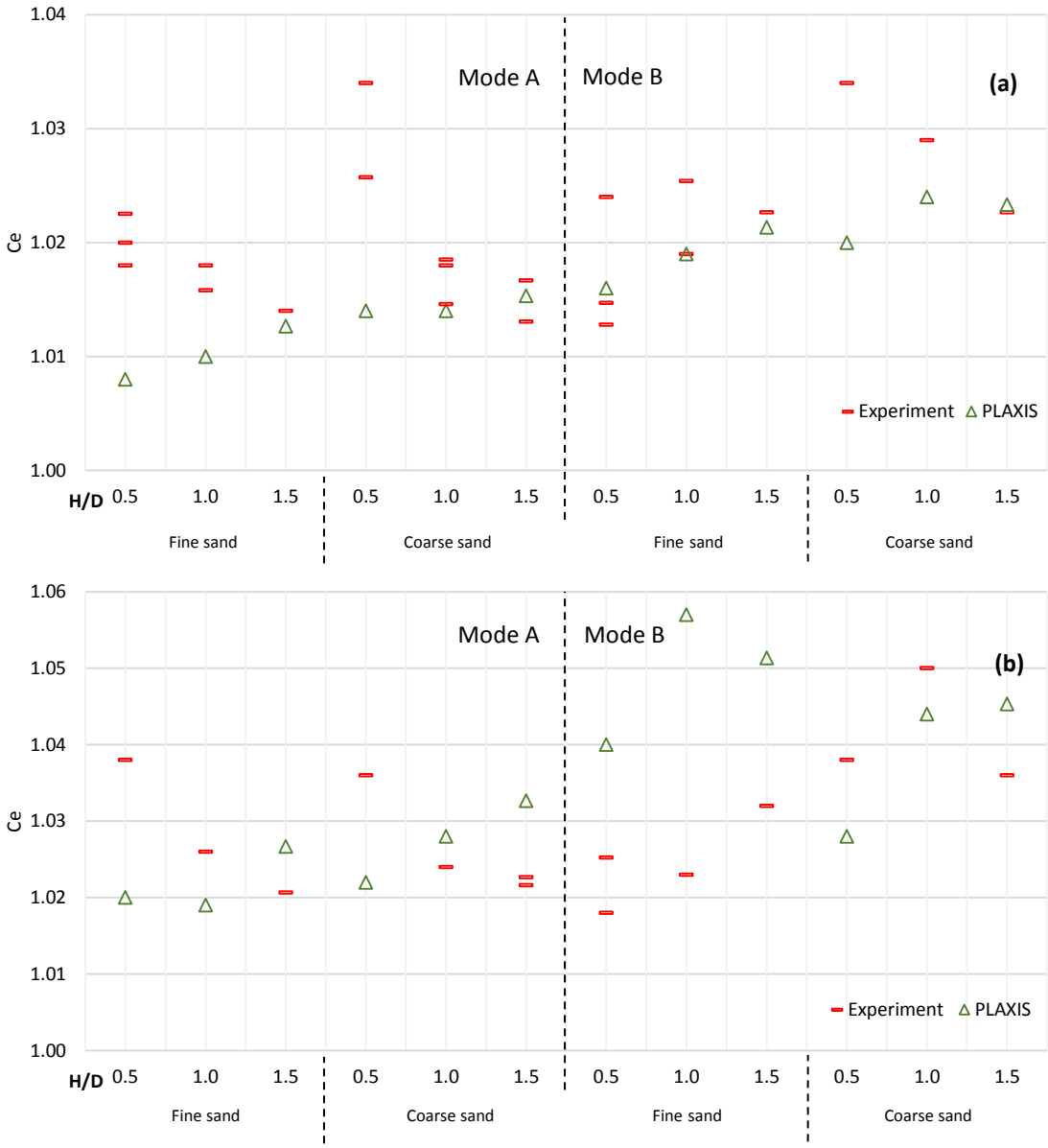

Figure 4.14. Comparison of Ce between experimental and numerical results

(a): Woven GSY (b): Nonwoven GSY

Table 4.4 summarizes the values for each series of tests. The variation is not significant. Ce values in the cases of Mode B are higher than for Mode A, as well as the values with the nonwoven are higher than for the woven, except for a test series of the nonwoven geosynthetic with fine sand. The values calculated by both methods are closer. Especially in the case of Mode A, coarse sand, and nonwoven, the coefficient values are equal. It can be concluded that the friction angle influence of the overlying soils is minor reflecting similar results between coarse and fine sand. Indeed, the difference in the Ce values between the two modes of the cavity opening is in agreement with the numerical results performed by *Villard et al. (2016)*. According to the study of *Feng et al. (2017a)*, the expansion coefficient can

also be determined as $Ce_{e\text{-}max}$ considering the relation between the maximum and the initial void ratios (*Eq.4.9*).

Table 4.4. Values of Ce calculated by numerical and experiment tests

Tested soils	***Geosynthetics***	***Opening modes***	***H/D***	***Ce*** $_{PLAXIS}$	***Ce*** $_{Experiment}$	***Ce*** $_{e\text{-}max}$	***Ce*** $_{e\text{-}average}$
Coarse sand	Woven	A	0.5	1.014	1.034	1.011	1.023
			1.0	1.014	1.018		
			1.5	1.015	1.017		
		B	0.5	1.020	1.034		1.036
			1.0	1.024	1.029		
			1.5	1.023	1.023		
	Nonwoven	A	0.5	1.022	1.036	1.011	1.042
			1.0	1.028	1.024		
			1.5	1.033	1.023		
		B	0.5	1.040	1.038		1.076
			1.0	1.057	1.050		
			1.5	1.051	1.036		
Fine sand	Woven	A	0.5	1.008	1.020	1.048	1.017
			1.0	1.010	1.018		
			1.5	1.013	1.014		
		B	0.5	1.016	1.024		1.028
			1.0	1.019	1.019		
			1.5	1.021	1.023		
	Nonwoven	A	0.5	1.020	1.038	1.048	1.027
			1.0	1.019	1.026		
			1.5	1.028	1.021		
		B	0.5	1.028	1.018		1.053
			1.0	1.044	1.023		
			1.5	1.047	1.032		

The effect of the cavity opening processes on the expansion mechanism can be shown by means of the void ratios changing within the overlying soils. As presented in *Figure 4.15*, even if for both cavity-opening processes, a significant increase of the void ratio can be seen near the cavity edge. The change in void ratio is not uniform between the two modes of the cavity opening. It reflects the presence of a disturbed zone. In the case of a progressive opening (Mode B), an increment of the void ratio can be seen along the deflected geosynthetic whereas, for the downward opening (Mode A), an increase can only be seen at

the areas near the cavity edge. This can be explained for the downward opening (Mode A), the collapsed soil seems to move gradually. Henceforth the disturbed zone appears mainly at the area between the anchorage and cavity areas, whereas for the zone near the cavity center, the soil seems to be not affected. For the progressive opening, the soil is disturbed along with the cavity areas, due to the influence of the cavity diameter increase.

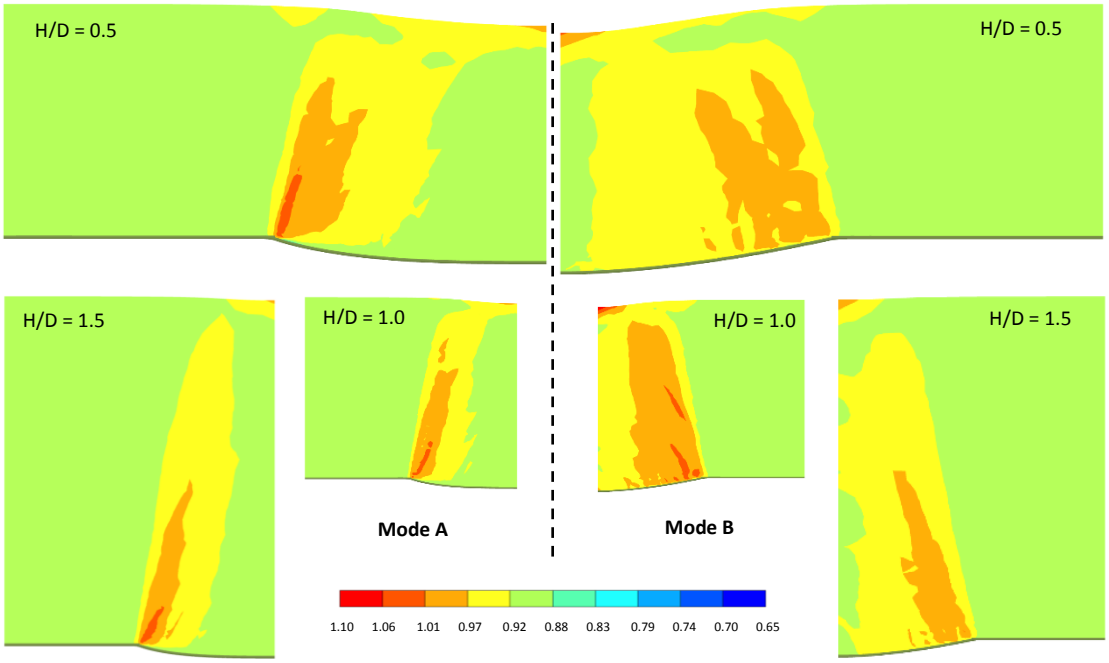

Figure 4.15. Change in void ratio within the overlying soils over reinforcement systems (Fine sand & Woven GSY)

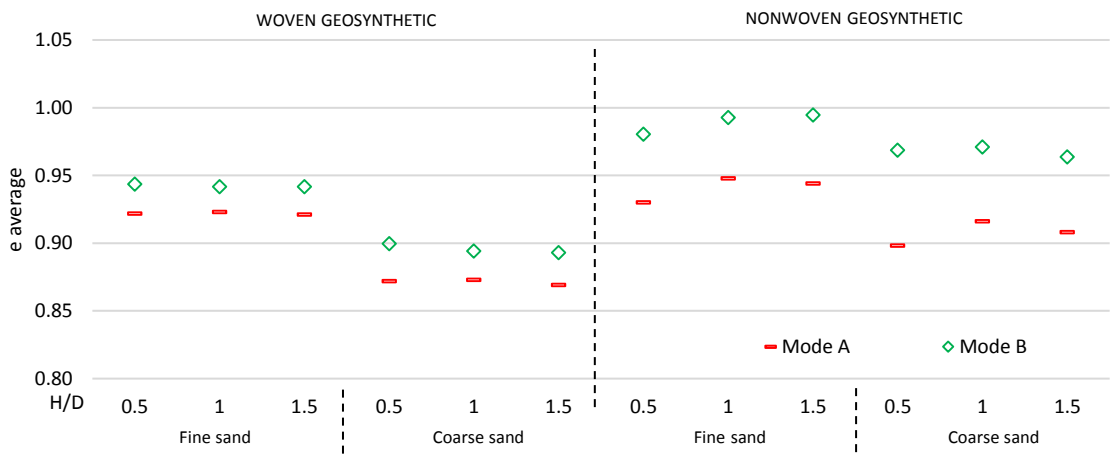

Figure 4.16. Average values of void ratio in the collapsed soil

The soil void ratio average values in the collapsed areas are calculated and presented in *Figure 4.16*. The average values of Mode B are higher than those obtained for Mode A in each case of the different test configurations. This result is associated with the values of the

expansion coefficient that have been calculated previously. The graph also shows that the mean values of the void ratio of fine sand are higher than the ones of coarse sand, whereas, the results with woven are higher than for nonwoven geosynthetics. Nevertheless, the differences are not significant.

After that, the expansion coefficient can be calculated from the void ratios. As presented in *Table 4.4*, the values obtained from the maximum void ratios (the initial value before the cavity opening) are different from those calculated using the numerical and experimental works for the deformation method. Nevertheless, if the maximum void ratios values are replaced by the average values obtained numerically after the cavity opening (*Eq.4.2*), $Ce_{e\text{-}average}$, the results become closer. Especially in the cases of the cavity opening Mode A, the results of $Ce_{e\text{-}average}$ and those of the experimental tests are very similar.

$$Ce_{e-average} = \frac{1 + e_{average}}{1 + e_0} \qquad Eq.4.2$$

The change of the total deviatoric strain γ_s is presented in *Figure 4.17*. Similar to the change of the void ratio, the tendency along the geosynthetic sheet is different for the two processes of the cavity opening due to the areas, which are influenced. Nevertheless, in both processes, at the cavity border, a significant increase can be noticed.

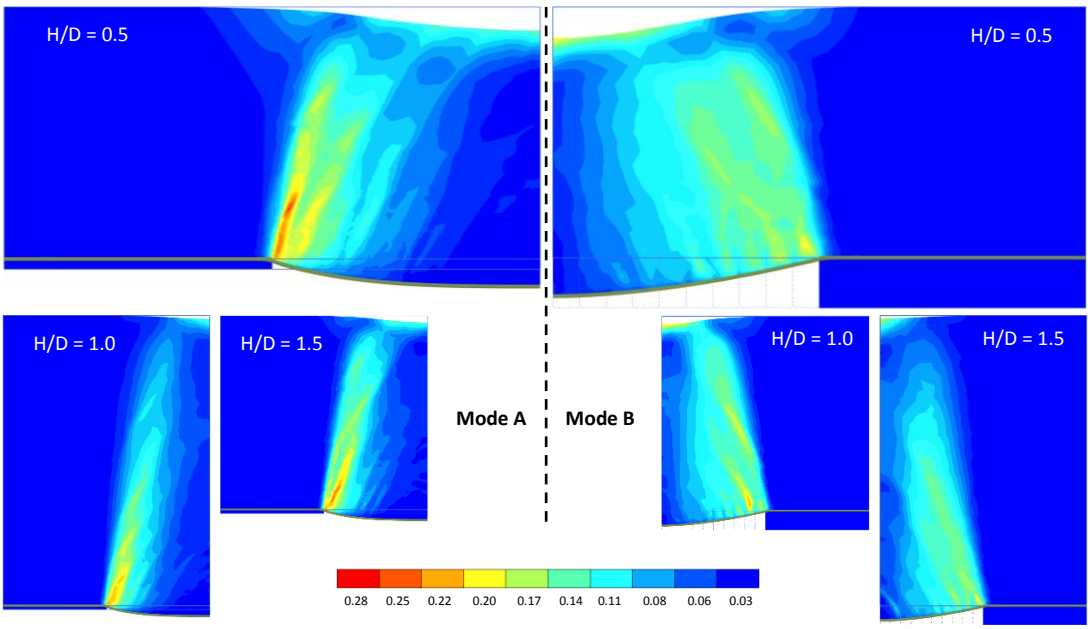

Figure 4.17. Change in deviatoric strain within the overlying soils over reinforcement systems (Fine sand & Woven GSY)

4.4.2. Effect of geometrical configurations

In order to investigate the impact of the H/D ratios in the case of larger cavity diameters, several models were performed for the cases of fine sand and the woven geosynthetic. The height of the overlying soils and cavity diameter are higher, but the H/D ratio is constant. The H/D ratios are considered in the range from 0.25 to 2.0. *Figure 4.18* presents a comparison between the surface settlements and the geosynthetic deflection for the two modes of the cavity opening.

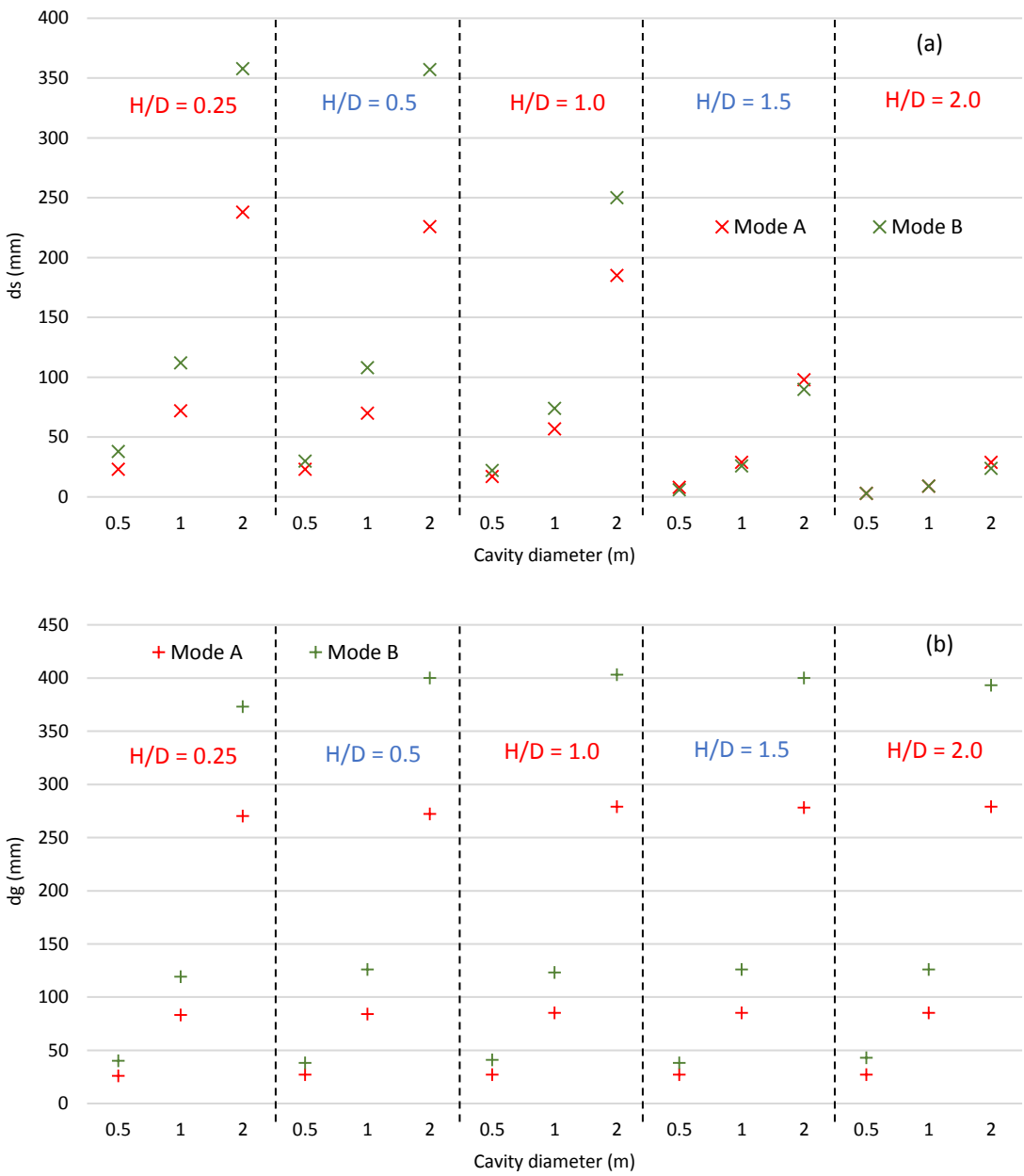

Figure 4.18. Variation of surface settlement (a) and deflected geosynthetics (b) due to changing of cavity diameter, cases of fine sand

It is seen that in each case of the H//D ratio; higher values of both surface settlements and geosynthetic deflection are obtained above the wider cavities. The maximal vertical displacements increase significantly when the cavity diameter expands from 1 to 2 m. It can be explained by the fact that when the load of the overlying soil increases for higher geometrical configurations and the geosynthetic capacity is unchanged, the vertical displacement is developed. For larger load values, the influence is higher. Except for the cases of H/D = 1.5 and 2.0, when the cavity diameters vary from 1 m to 2 m, the surface settlements increase is lower. It can be explained by the fact that the height of the overlying soils seems to reach the equal settlement plane.

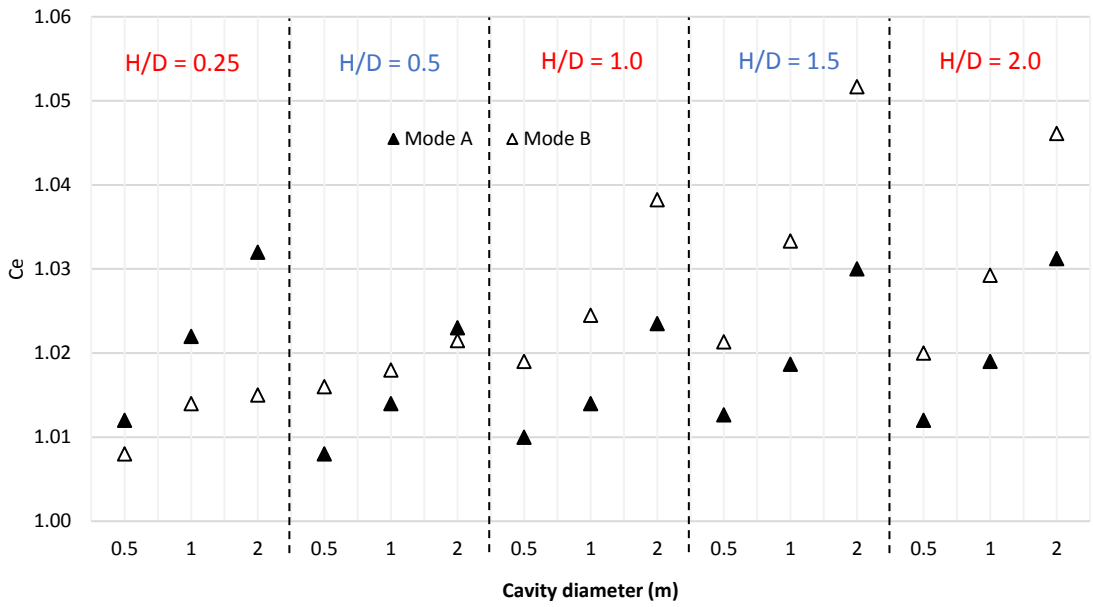

Figure 4.19. Variation of Ce due to changing of cavity diameter

The variation of the expansion coefficient due to the cavity diameters variation is presented in *Figure 4.19*. An increase of Ce can be noted for wider cavities. On the other hand, the values of Ce seem not to be influenced by the H/D ratio for Mode A. Whereas for Mode B, a significant difference between the H/D ratios is obtained, especially in the cases where low H/D ratios are considered (0.25, 0.5 and 1.0). The values of Ce in the cases of Mode B are greater than Mode A is also confirmed, excepted for the case of the H/D ratio of 0.25. Excepted for a series of tests (Mode B and H/D = 0.25), a linear tendency can be noted.

As noted in the previous section, a uniform tendency has not been seen between the experimental and numerical results, considering H/D ratios: 0.5, 1.0 and 1.5. Indeed, when the considered H/D ratios are added as 0.25 and 2.0, the uniform trend can also be noticed. A specific example can be seen for Mode A in *Figure 4.19*, Ce decreases when H/D ratio

changes from 0.25 to 0.5, after increases with the H/D ratio of 1.5, then seems to remain at H/D = 2.0. Thus, it can be concluded as the ratio H/D has not influenced significantly on the expansion coefficient.

4.5. LOAD TRANSFER ANALYSIS

4.5.1. Load transfer on cavity area

The stress applied on the geosynthetic sheet and obtained by the numerical models is analyzed for a series of 24 tests considering different configurations: two modes of the cavity opening, three ratios of H/D, two tested soils and both woven and nonwoven geosynthetics. In the numerical models. For each group of tests, the stress distribution is calculated, and the efficiency of the load transfer within the overlying soils is determined. The variation of the final stress with the initial values can be seen considering the ratio σ_f/σ_i. The analysis procedures are applied as presented in *Section 3.2.5*.

Figure 4.20 and *Figure 4.21* present the stress applied to the geosynthetic, which are respectively obtained for the fine and coarse sand. At the cavity areas, reduced stresses are obtained in most areas, whereas an increment of stress is obtained in the anchorage areas. These trends can be confirmed for both tested soils, the three ratios of H/D and the two modes of the cavity opening. Therefore, similar to the results obtained by the laboratory tests, the load transfer from the cavity area to the anchorage areas after the cavity opening is confirmed.

Regarding the stress variation at the anchorage areas, an important increase can be seen at the locations near the cavity border. Thus, the stress increase reaches a peak at the anchorage area near the cavity border. For further areas, the stress seems to rise slightly.

Concerning the cavity areas, an important difference between the two modes of cavity opening is observed. The reduction stress tendency in the Mode A cases seems to decrease from the cavity border to the center, whereas in the Mode B cases, the trend seems to increase. This phenomenon can be observed for both coarse and fine sand. Regarding the results for fine sand tests, they confirmed the experimental results, which are obtained by the TPS (see *Section 3.3.4*). The results are also in agreement with the DEM simulation performed by *Villard et al. (2016)*.

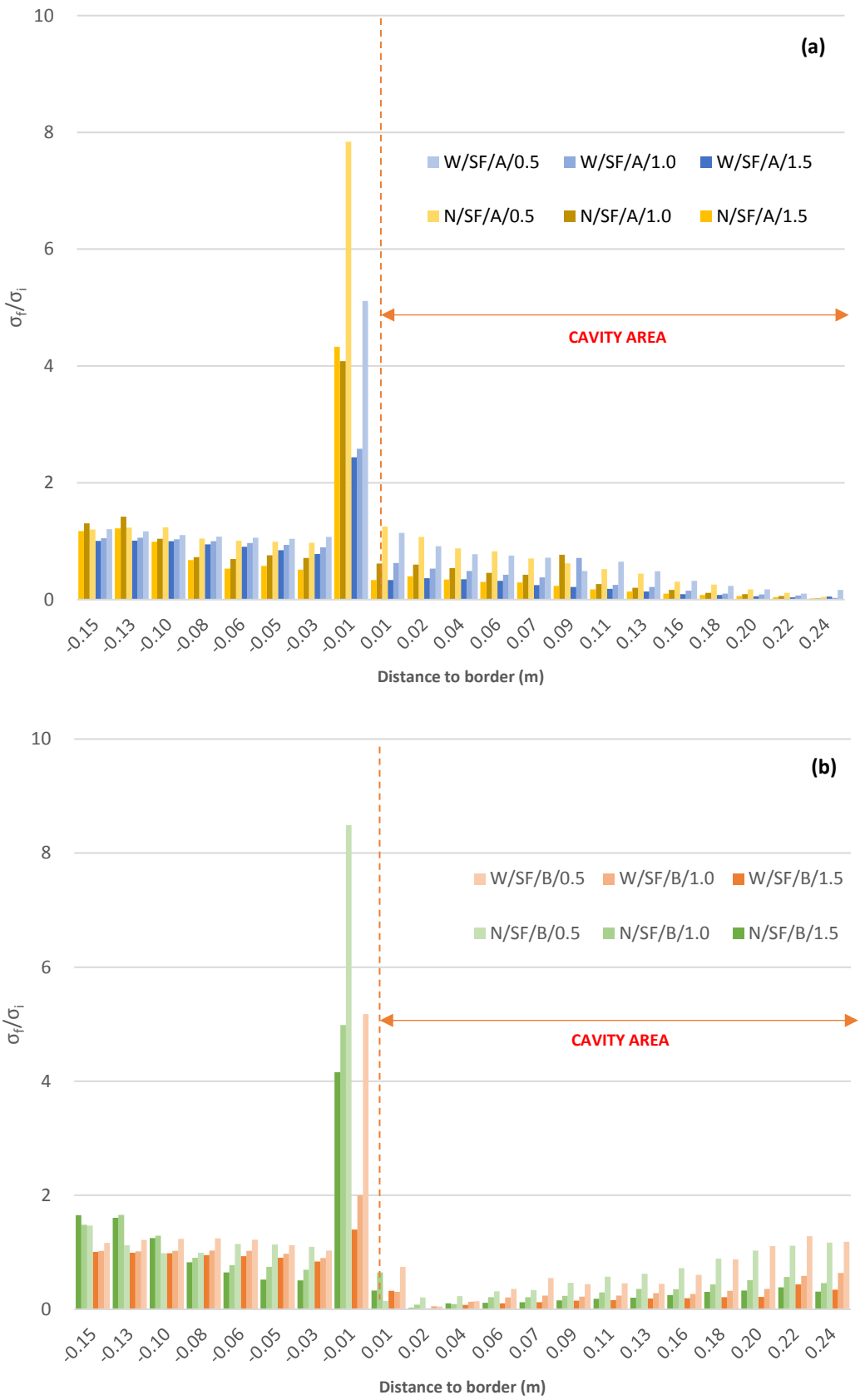

Figure 4.20. Numerical load distribution on cavity calculated for fine sand tests (a): Mode A; (b): Mode B

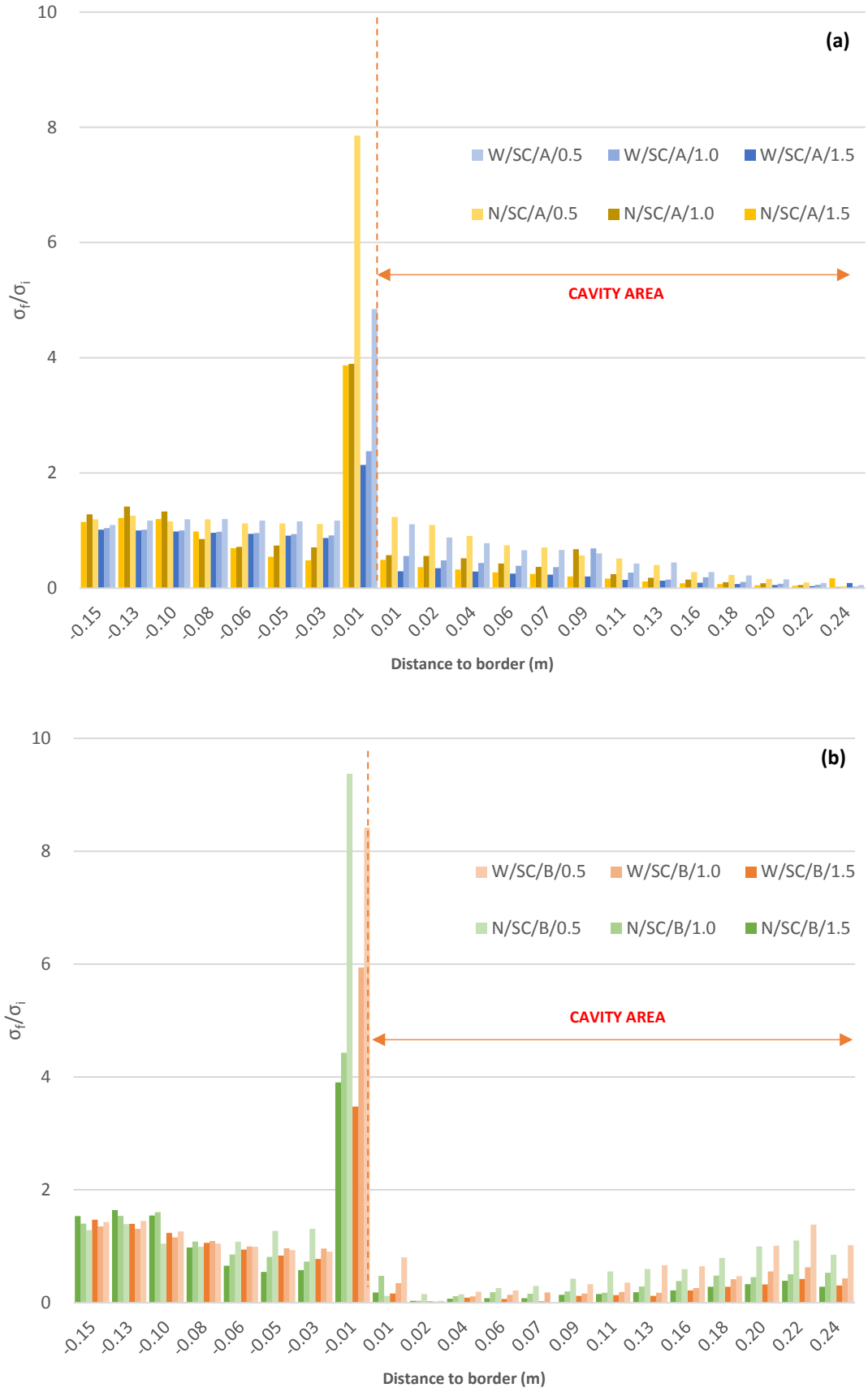

Figure 4.21. Numerical load distribution on cavity calculated for coarse sand tests (a): Mode A; (b): Mode B

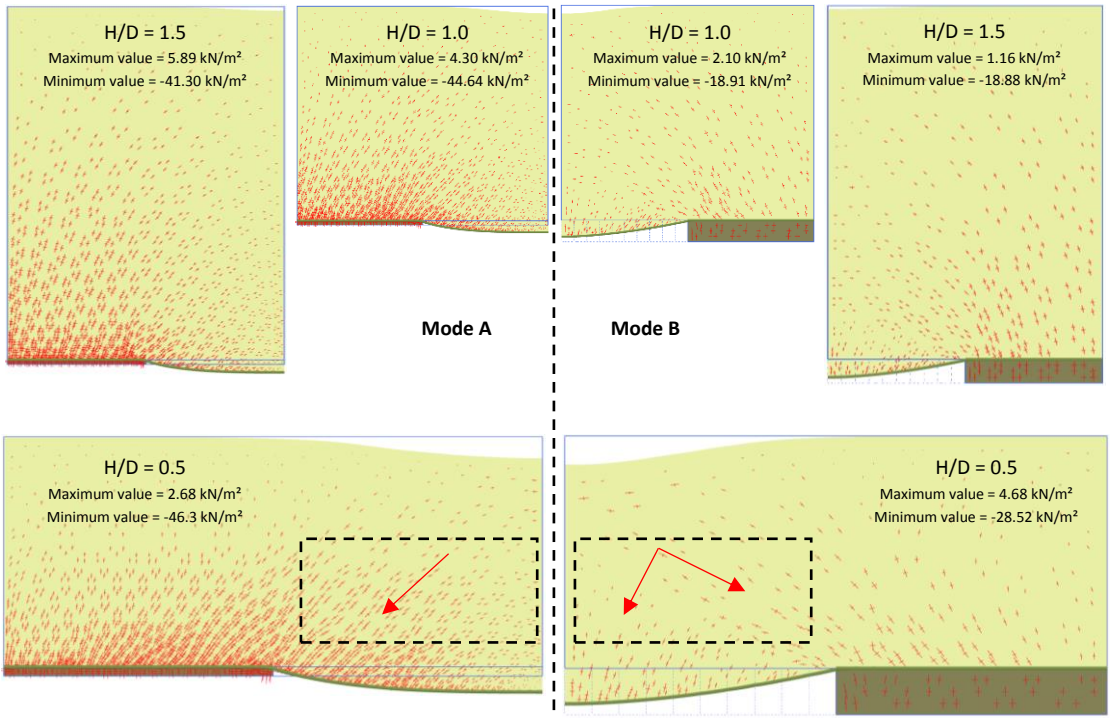

Figure 4.22. Principal stress within the fine sand over woven geosynthetic

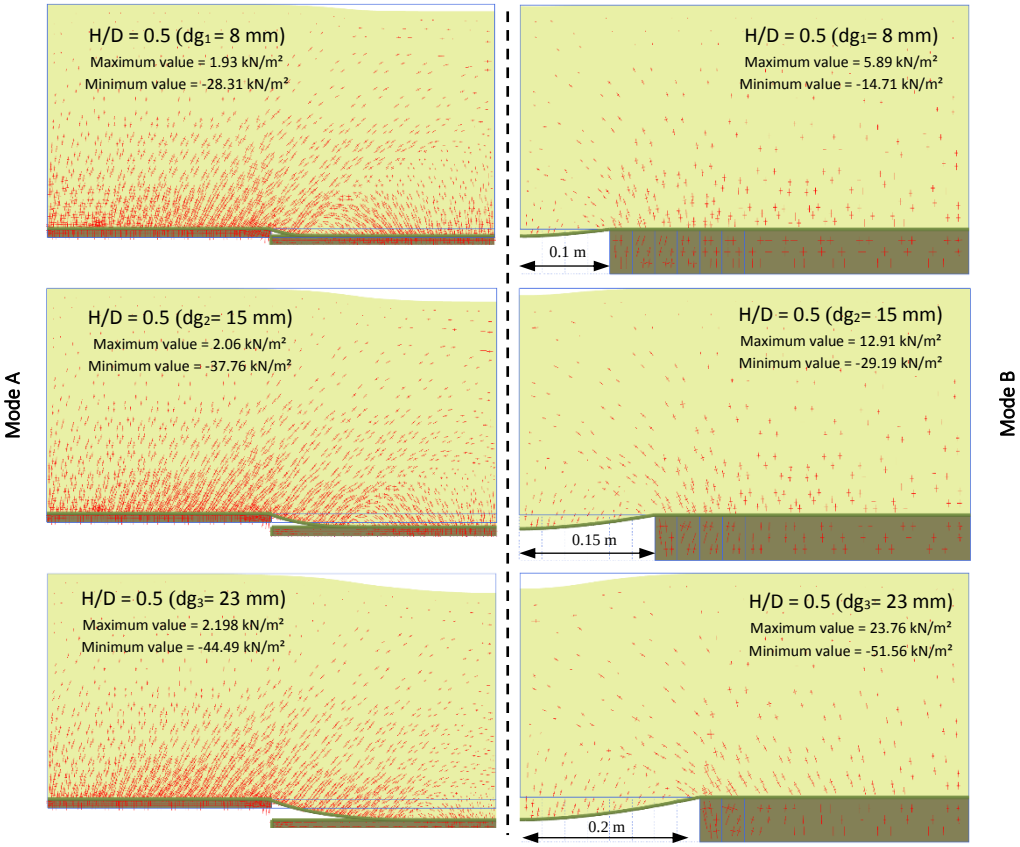

Figure 4.23. Principal stress within the fine sand over woven geosynthetic with evolutions of the two cavity opening

Figure 4.22 presents the principal stress tensors within the overlying soils above the reinforcement systems for various H/D ratios and two cavity-opening modes. Whereas, for

the cases of H/D = 0.5 (*Figure 4.23*), the principal stresses are presented considering an evolution of the deflected geosynthetic, in where dg_1, dg_2 dg_3 are the deflection values equal to respectively 8 mm, 15 mm and 23 mm. Indeed, a change in orientation of the stress can be seen in each case, since the cavity starts opening. Hence, this confirms the load transfer mechanism considering both processes of the cavity opening. It can also be seen that a significant difference of the principal directions can be obtained above the cavity area, meanwhile at the anchorage areas; the directions are the same.

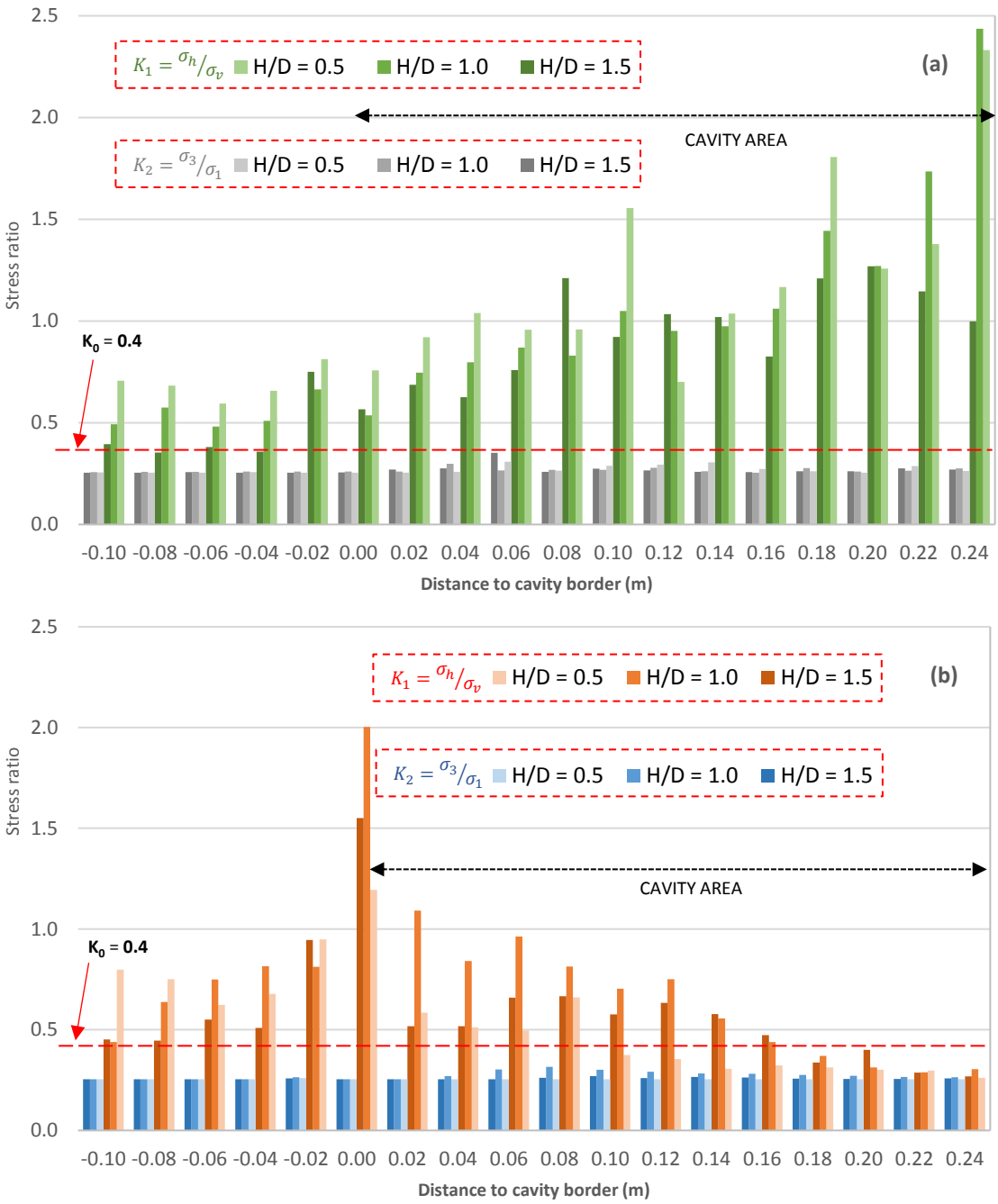

Figure 4.24. Estimation of the stress ratios of fine sand over GSY after cavity opening

(a) Mode A (b) Mode B

Figure 4.24 presents the earth pressure coefficient values just above the geosynthetic sheet, for the cases of fine sand and woven geosynthetic with three ratios of H/D. Two different stress ratios are considered, the first one is calculated by a ratio of $K_1 = {\sigma_h}/{\sigma_v}$ and the second is from $K_2 = {\sigma_3}/{\sigma_1}$. Note that before the cavity opening, these two values are equal to K_0, which is identical to a value of 0.405 in all the fine sand cases.

In both cases of the cavity opening mode, the values of K_1 are higher than K_0, whereas, those of K_2 are lower, especially at the anchorage area. Whereas the values of K_2 are rather constant through the geosynthetic areas, K_1 varied due to the cavity opening modes and the locations for the cavity area. At the anchorage areas, in both cases (modes A and B), K_1 seems to be constant. Whereas, an inverse tendency can be seen at the cavity areas. The significant difference between the two modes is while K_1 values increase significantly at the cavity center for the downward opening, these values are reduced in the cases of the progressive opening. This is also consistent with the findings based on the orientation of the principal stresses. The results confirm that the stress ratio of the overlying soil is changed during the cavity opening and it is influenced significantly by the opening mode.

4.5.2. Efficiency of the load transfer

The load transfer mechanism within the overlying soil reinforced by geosynthetics above cavities can be characterized by the efficiency E, which is defined by the ratio between the final load acting on the cavity area after the cavity opening and its initial value (see *Section 2.3.2*). The analysis procedure is the same as used in *Chapter 3*. It was described in details in *Section 3.2.5.4*.

The results of 24 computations performed concerning two cavity-opening modes and two tested geosynthetics are presented in *Figure 4.25* for fine sand and in *Figure 4.26* for coarse sand. As can be seen, the efficiency increases with the H/D ratio are similar to the results of *Villard et al. (2016)*. This tendency can be obtained in each test series for the two opening processes, two tested geosynthetics, and both coarse and fine sand. Indeed, this can be observed in *Figure 4.27*, which presents the loads applied to the geosynthetics at the anchorage and cavity areas. The loads applied on the cavity areas in each test series are rather constant, whereas at the anchorage areas the load increases systematically. This is also consistent with the results obtained for the geosynthetic deflection (as presented in *Section 4.3.2*). The geosynthetic deflection is uniform when the H/D ratios vary from 0.5 to 1.5.

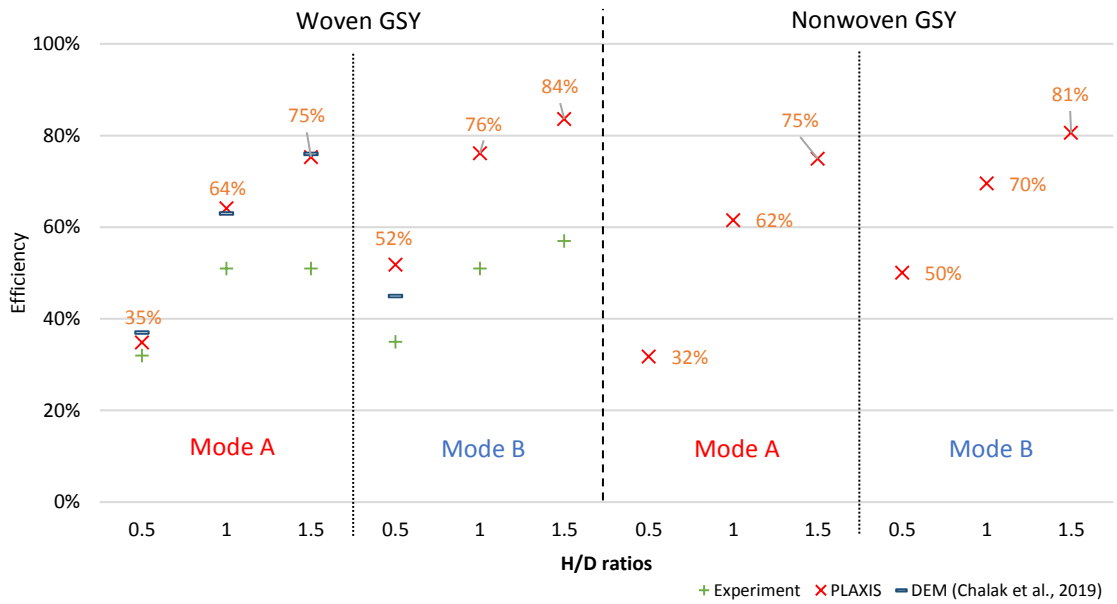

Figure 4.25. Comparison of the load transfer efficiency between experimental, DEM and FEM results, cases of fine sand tests

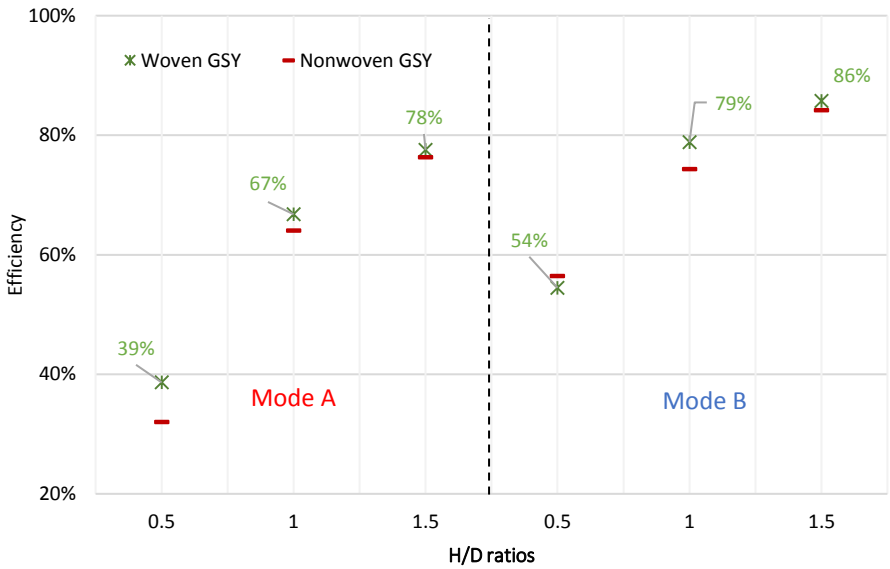

Figure 4.26. Numerical load transfer efficiency, cases of coarse sand tests

It can be concluded that the cavity opening process influences the load transfer mechanisms. Indeed, the efficiencies calculated for Mode B are higher than Mode A when the same ratio H/D is considered. This is different from the results of *Villard et al. (2016)*, which was conducted based on the relevant full-scale experiments. Indeed, the differences in the tested geosynthetics or fill materials may be the reason for these differences. Moreover, it can be seen that the geosynthetic stiffness does not have a significant effect on the load transfer efficacy.

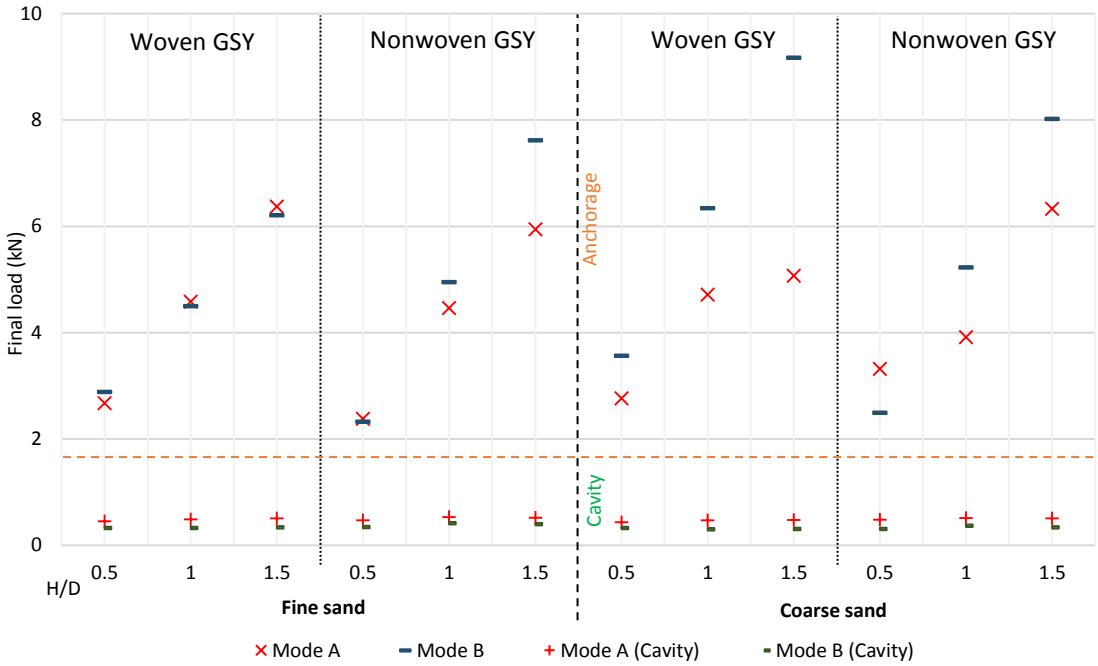

Figure 4.27. Comparison of final load applied on geosynthetics between anchorage and cavity areas

Concerning the test series on fine sand and woven geosynthetics, an efficacy comparison between the experimental, FEM and DEM (*Chalak et al., 2019*) results is presented (*Figure 4.25*). For the smaller H/D ratios, the efficiencies obtained from the three methods in the case of the downward opening are the same, and they are rather similar in the case of a progressive opening. Nevertheless, for the higher H/D ratios, while the efficiencies obtained from the experimental tests seems to remain, these FEM and DEM results provide notably the same values, and they increase with the higher ratio of H/D.

4.5.3. Effect of the cavity diameter

In order to evaluate the stress increase considering the cavity diameter variation in the cases where H/D ratios are constant, the relation between (σ_f/σ_i) and the ratio between the distance to the border and the cavities diameter are presented in *Figure 4.28* and *Figure 4.29* (respectively for Mode A and Mode B). In each case, three different diameters (0.5 m, 1.0 m and 2.0 m) are investigated with two H/D ratios: 0.5 and 1.0.

As can be seen in *Figure 4.28* and *Figure 4.29*, the stress variation tendencies are similar to the presented results, which are presented in *Chapter 3* and *Section 4.4.1*. Even if the cavity diameter increases, an increasing trend can be seen in the anchorage areas, and a decrease of the inclination occurs in the cavity areas. The tendencies, increase or decrease, seem to be constant without any influence with the cavity diameters, even if the values can be different.

Moreover, as it has been found in *Section 4.4.1*, significant stress increases can be seen at the anchorage areas near the cavity border.

Additionally, comparing the two modes of the cavity opening, similar to the previous conclusions and the DEM simulation of *Villard et al. (2016)*, both conical shape obtained for the cases of the downward opening (Mode A) and the inverted shape in the cases of the progressive opening are uniform with the cavity diameter variation.

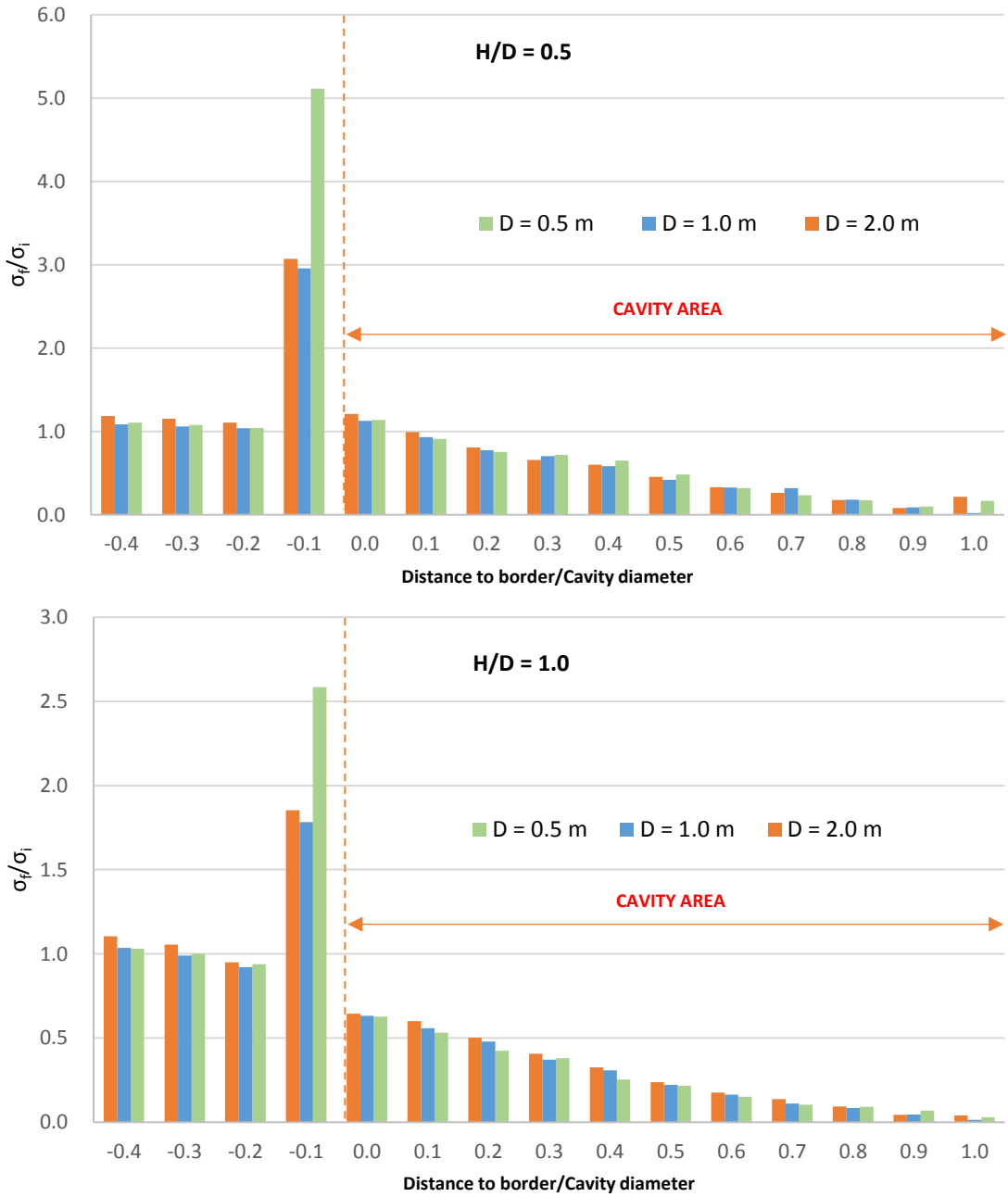

Figure 4.28. Variation of the load distribution due to the cavity diameter variation: Mode A

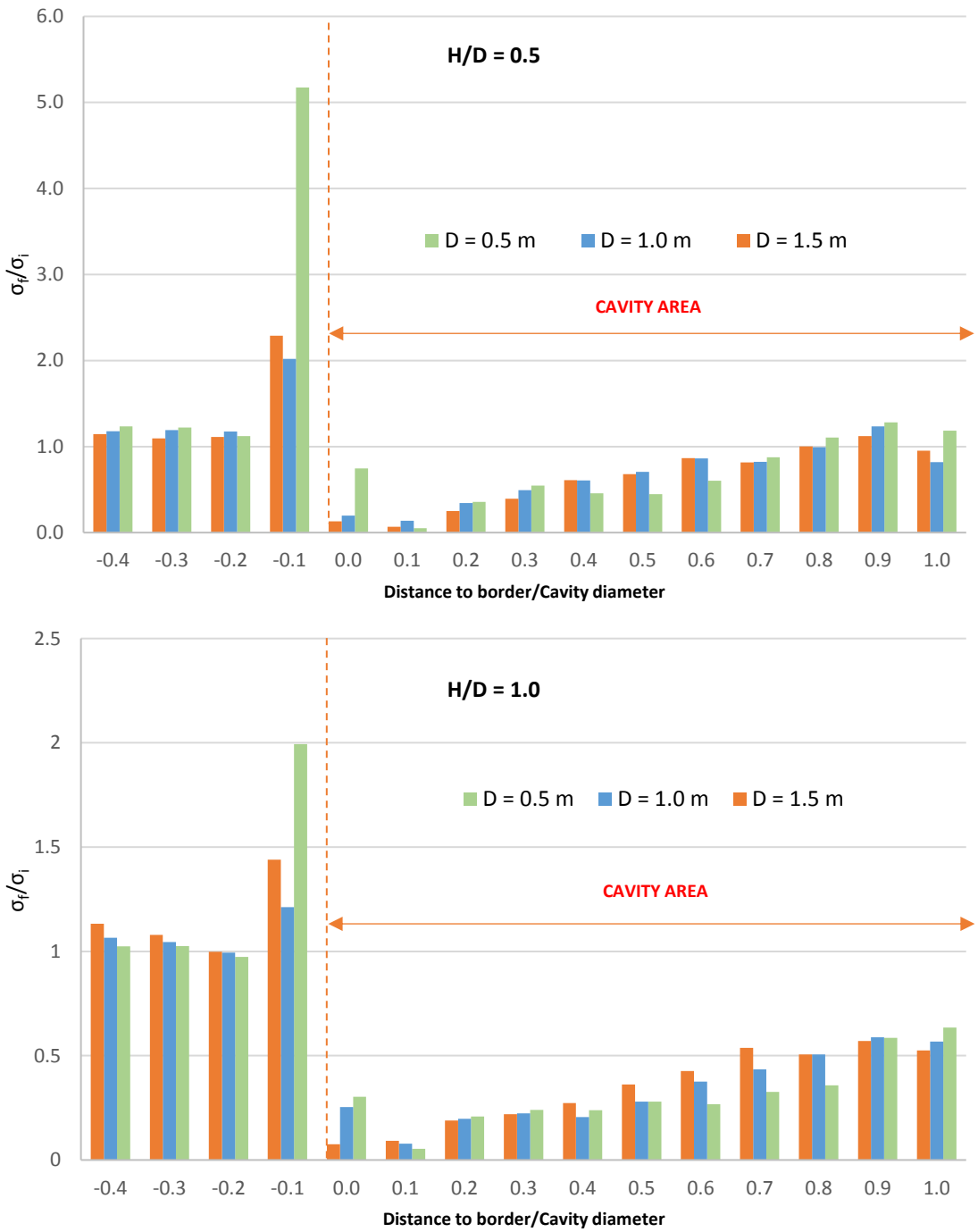

Figure 4.29. Variation of the load distribution due to the cavity diameter variation: Mode B

The load transfer efficiencies are also computed (*Figure 4.30*). The results can also be obtained for the wider cavities. Indeed, for Mode A, the load transfer efficiencies remain stable around 35% and a slightly higher than 60% for H/D = 0.5 and 1.0. These values are higher in cases of Mode B, where the values increase to 50% and 75% respectively for H/D = 0.5 and 1.0.

In conclusion, when the ratio of H/D ratio is constant, the cavities diameter variation did not affect the load transfer mechanisms, due to the fact that the stress distribution and the load transfer efficiency are not modified.

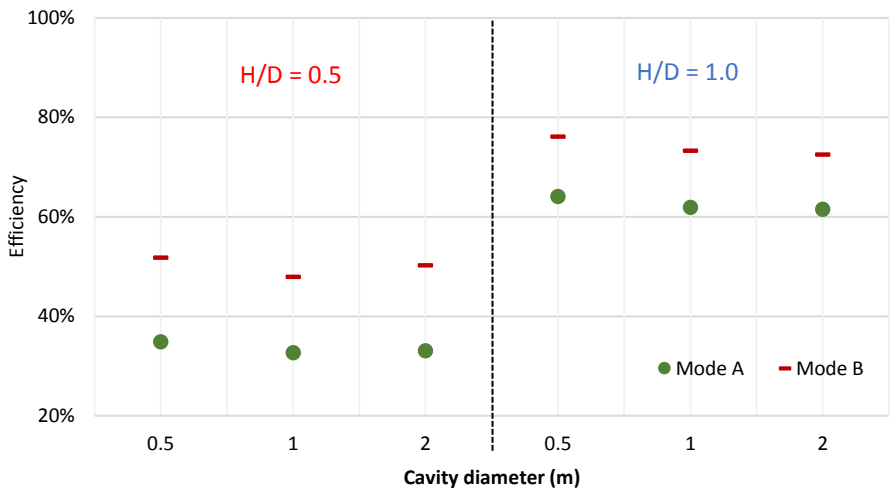

Figure 4.30. Variation of the load transfer efficiency due to the cavity diameter variation

4.5.4. Effect of the surcharges

In *Section 3.3*, a comparison between two different test programs of the embankment formation considering the load distribution has been completed. The first test program (Program 1) can be noted as the primary object of this study, in which the embankment is formed as the overlying soils are setup before the cavity is opened. For the second test program (Program 2), only the case of H/D = 0.5 is performed. The embankment height is increased continually to the higher ratio of H/D ratios when the cavity is existing below the system. Indeed, the behavior of the reinforcement system in the second tested program is similar to the case in which a surcharge is applied.

To improve understanding the effect of the surcharge when the cavity exists, with the numerical models, a surcharge is applied on the surface of the overlying soil after the cavity opening (*Figure 4.31*). The numerical calculation considers the load distribution in the case of fine sand on both the two cavity-opening processes. The additional load is applied as values of 3.52 kPa and 7.05 kPa, which are equivalent to the load increase when H/D ratios reach 1.0 and 1.5, respectively.

Figure 4.32 presents a comparison between the loads applied to the geosynthetic after the surcharge application. The increase of the final loads can be seen for both cavity opening

processes, but the increment value is different between the anchorage and cavity areas. This confirms that the arching effect, which leads to the load applied on the geosynthetic, can be transferred from the cavity to the anchorage areas even if the surcharge is applied above existing cavities.

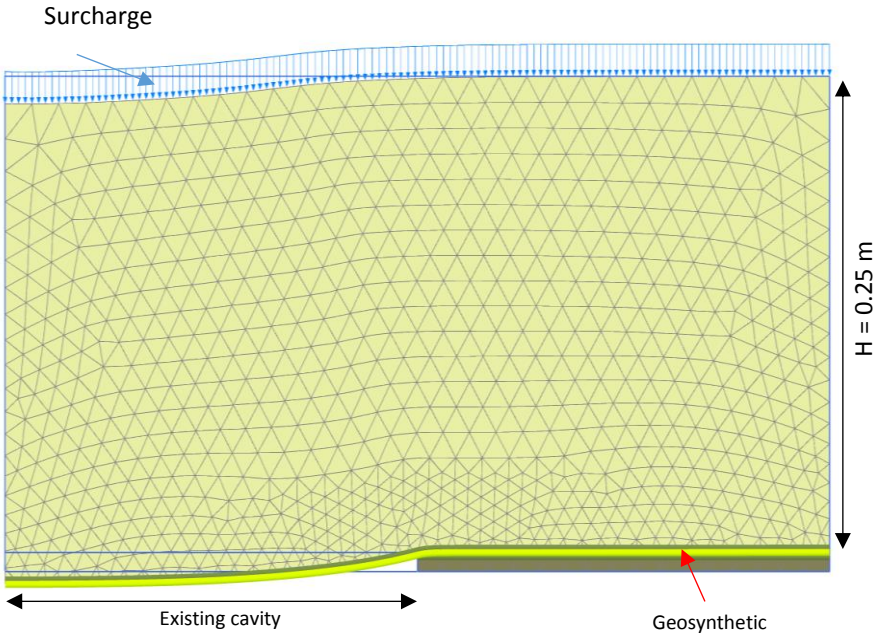

Figure 4.31. Surcharge applied on overlying soil above existing cavity

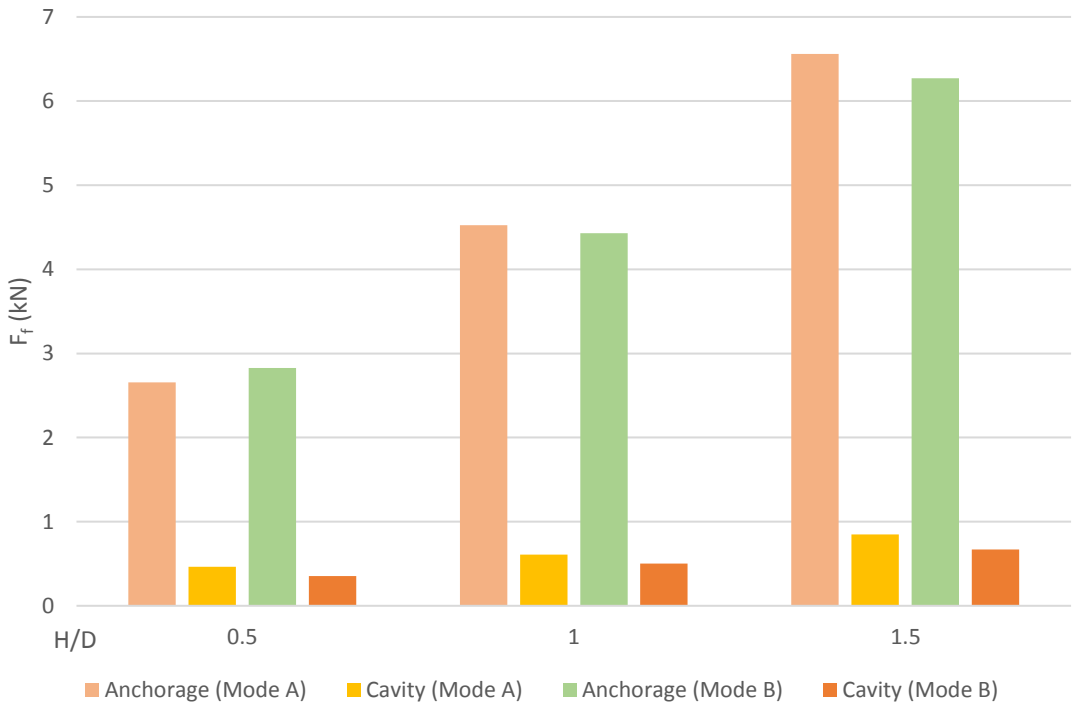

Figure 4.32. Comparison between the final load acting on geosynthetic (Fine sand and Program 2)

Figure 4.33 shows the load ratios ($F_{fn}/F_{f0.5}$) defined as the final loads after the after new surcharges added and the final load of the test with H/D = 0.5. Although the load transfer exists with the presence of the surcharge, it can be seen that the efficacy of the tests of Program 1 are higher than the one of Program 2, for both cavity-opening processes. Indeed, at the cavity areas in Program 1, the load ratios are rather constant whereas an increment can be seen for the others.

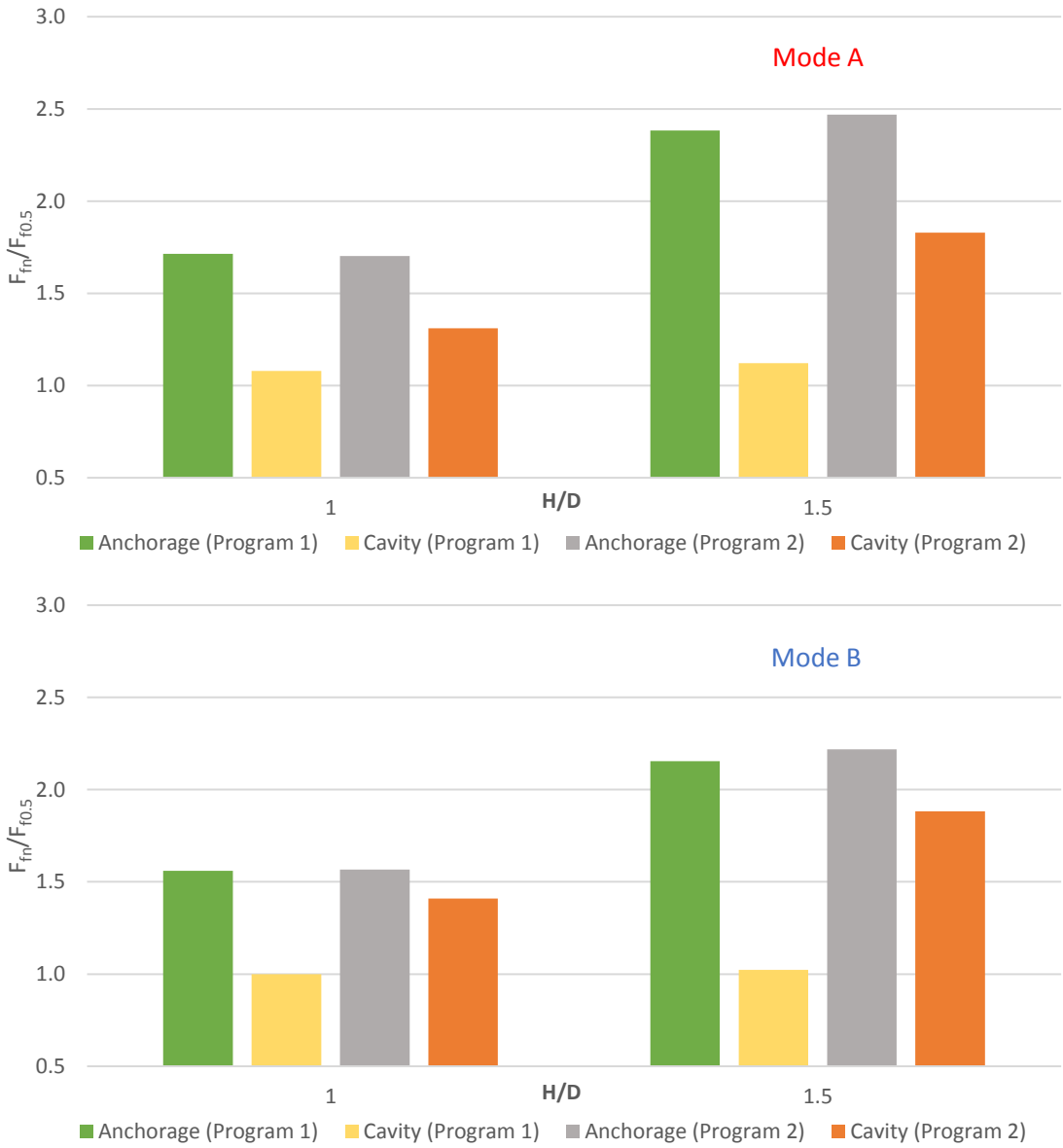

Figure 4.33. Comparison of the load distribution obtained by the numerical models between Program 1 and Program 2

The results are not repeated as the experimental results described in *Section 3.3.5*. This is due to the fact that in the experimental tests, after the cavity opening, the surcharge is formed

by adding an overlying soil, which the shearing can occur inside. Thereby, the load distribution within the additional soil cylinders is not considered in the numerical models and hence limits the load transfer efficiency at the cavity area.

The effect of surcharge in this section can be an addition for the results of the load transfer over the existing cavity, which are found by the experimental works. This leads to a consequence for a load transfer efficacy considering the way to apply surcharge: when a surcharge is due to a granular embankment, the load applied at the cavity area can be transferred more effectively than in the case of a concentrated load, existing from a solid structure, for example.

4.6. CONCLUSIONS

Based on the Mohr-Coulomb failure criterion and the Hardening soil constitutive model, a series of numerical models has been performed in order to investigate the expansion and load transfer mechanisms within the granular embankment reinforced by geosynthetic above cavities. The numerical works considered a variety of tested configurations like two types of overlying soil, two different geosynthetics, and three ratios of H/D considering the downward and progressive opening of the cavity. By comparing the soil constitutive model, there is no any significant variation between the two models, and it can be noted that the Mohr-Coulomb model is adapted to reproduce the behavior of the overlying soils over the geosynthetic-reinforced cavity.

According to the comparison with the experimental results, the numerical works have succeeded to simulate the surface settlement and the shape of the overlying soils above the reinforcement system. The same surface displacement behavior between the experimental and numerical works is obtained considering the effect of H/D ratios, the stiffness of geosynthetics, cavity opening modes, and the different soils. The equal settlement planes are estimated based on the numerical models, and the results are higher than those estimated from the experimental tests assuming a linear trend.

The other mechanisms that the numerical works have well simulated are the load transfer within the granular embankments. The presence of the load transfer from cavity areas to the anchorage areas during the opening is confirmed for both fine sand and coarse sand. The load distribution tendency considering the cavity opening processes effect has been confirmed with the results of the experimental works and other numerical simulations (*Villard et al.,*

2016). Indeed, the load distribution shape at the cavity areas is inverted between the two modes of the cavity opening and it is not affected by the cavity diameter variation. Moreover, the earth pressure coefficient developed after the cavity opening is also investigated. The load transfer efficiency is computed and compared with those obtained from the laboratory tests and DEM simulation performed by *Chalak et al. (2019)*. The FEM results confirm the experimental results in the cases of H/D = 0.5, moreover, a remarkable agreement has been found with the DEM results in each fine sand case. The higher values of the H/D ratio can increase efficiency, whereas the downward opening of the cavity leads to the lower effectiveness of load transfer than the progressive process. Moreover, applying a surcharge do not influence the presence of the load transfer. A complement could be proposed for the results of the experimental work as in the cases of the cavity existing before the presence of a concentrated surcharge, and the load applied at the cavity area can be transferred less effectively than in the case of additional fills.

On the other hand, the maximal vertical deflections of the tested geosynthetics have not well simulated by the FEM simulations. In fact, the numerical works showed a uniform geosynthetic deflection considered different H/D ratios. Note that the support of PLAXIS for simulating geosynthetic is not really plentiful, as only stiffness value can be used to reproduce the geosynthetic characteristic. Nevertheless, the shape of the deflected geosynthetics found by numerical models is the same as the experiment. Additionally, several behaviors of the reinforced materials found in the laboratory test can be confirmed such as the deflection depended on the cavity-opening mode. Moreover, even the rough size of Ce is obtained by numerical simulations, the effect of H/D ratio and the cavity opening on the expansion mechanisms has not been clarified as the trends of laboratory tests, and numerical models are not the same. Nonetheless, due to the parametric studies, several parameters could affect the expansion mechanisms. The soil dilatancy angle can influence the vertical displacement of the system and the expansion coefficient significantly, whereas, the effect of the earth pressure coefficient and cavity diameter seem minor.

Last, as a contribution, the numerical simulation also allows studying the parameters, which are not possible to investigate by the experimental tests. Indeed, the void ratios, the change of the stress ratio after the cavity opening and the deviatoric strain of the collapsed soils are investigated to prove the difference between the two cavity opening processes.

CHAPTER 5. RESULTS DISCUSSION

5.1. INTRODUCTION

The understanding of the load transfer mechanisms in the geosynthetic-reinforced embankments overlying hidden cavities was enhanced by laboratory experiments and numerical models. Due to a large number of experimental strategies, various significant results have been found, and this allows the improvement of the current design methods. This chapter summarizes the major points demonstrated through the study scheme that can be used or integrated into the design methods. Specifically:

- The displacement performance of the subsidence zone within the embankment, reflecting by its shape, the surface settlements, the behavior of the reinforced geosynthetic,
- The determination of the expansion coefficient within the embankment,
- The load distribution acting on the geosynthetic considering the shape, the load transfer efficiency and the earth pressure coefficient.

Especially, regarding the expansion coefficient, several proposed relations have been introduced that could be used for resulting referenced values. The accordance of the common arching theory as *Terzaghi (1946)* considering the use of geosynthetic is also discussed.

5.2. LOAD DISTRIBUTION

5.2.1. Shape of the load distribution

The existing design method could also be improved by taking into account the non-uniform load applied to the geosynthetics placed above the cavity.

The cavity opening process has a significant influence on the shape of the load distribution acting on the geosynthetic sheet. Based on both the experimental work conducted by the TPS and the numerical simulations, the shape of the load distribution is clearly analyzed considering the cavity opening effect. There is no significant difference at the anchorage areas, whereas, at the cavity area, the load distribution tendencies are different: a cone-shape in the cases of the progressive process and the shape is reverse for the downward opening. According to the parametric study conducted by numerical simulations, the change of H/D ratios or the cavity diameter has no effect on the shapes of the load distribution.

5.2.2. Earth pressure coefficient

The different behaviors of the reinforced systems for the two opening methods are also be confirmed by the comparisons of the principal stress within the overlying soils, as well as the earth pressure coefficient, which is estimated after the cavity opening.

The formulation of the load acting on the geosynthetic sheet proposed by *Terzaghi (1943)* is difficult to use due to the definition of the earth pressure coefficient, K. According to the numerical work presented in the present study, it is evident to note that K is not uniform in the overlying soil above the geosynthetic as well as it strongly influenced by the mode of the cavity opening. The values of K can reach 2.5 at the center and the edge of the opened cavity. Moreover, the earth pressure coefficient defined as $K_0 = 1 - sin\varphi$ in the numerical modeling could be initially used to reproduce the load distribution within the overlying soils above the geosynthetic.

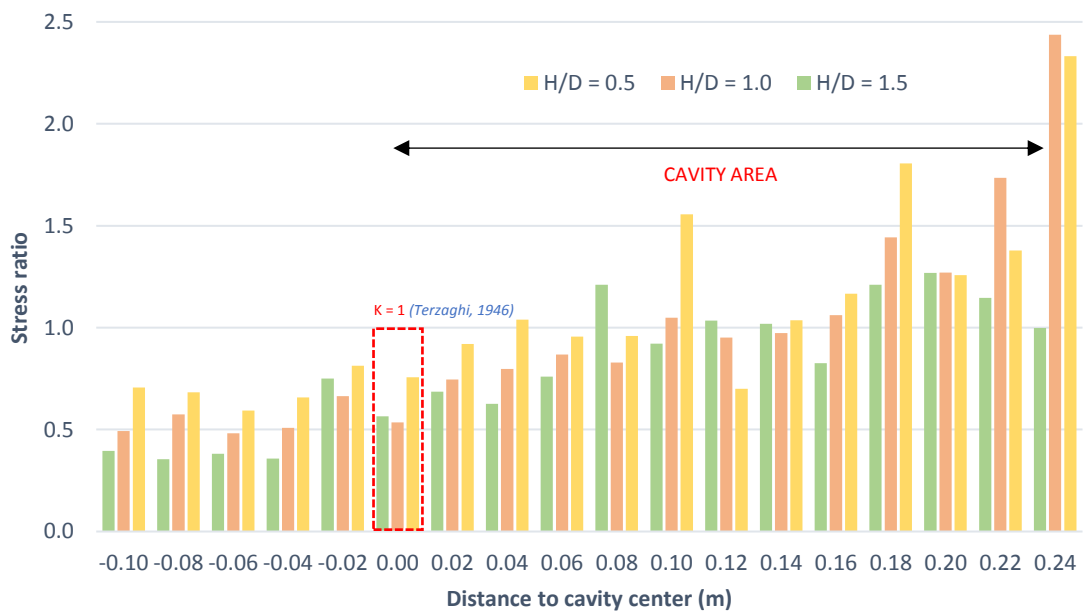

Figure 5.1. Comparison of stress ratios between the experiment of Mode A and Terzaghi's theory

Considering different processes of the cavity opening, *Figure 5.1* shows the comparison between the earth pressure coefficient obtained from the typical numerical simulations and the constant value, $K = 1$, suggested by *Terzaghi (1946)*. Note that the referenced value of *Terzaghi (1946)* is only considered at the edge of the trapdoor; the geosynthetic reinforcement was not be used, and the shearing surface was assumed as a straight line. In the case of the present study, the geosynthetic is used above the trapdoor. As combining with the movement of trapdoor, the formation of cavity seems to be similar as a decreasing-

diameter evolution and as increasing-diameter evolution in the cases of Mode B. Thus, the shearing surface within the overlying soil in the cases presented in the present study can be complicated, as it is different between the two cavity opening modes considered in the experiments. This point explains why the results obtained in the study are different and not uniform as the referenced value of stress ratio.

5.2.3. Load transfer efficiency

Table 5.1 summarizes the influences that could affect the load transfer efficiency. The load transfer efficiency tendency within the embankment over the geosynthetic-reinforced cavity is clarified by the numerical simulations. It can be noted that the load can transfer more effective with the increases of the H/D ratios and the friction angle of the overlying soils. Whereas, the change of the geosynthetic reinforcement or the cavity diameters has no significant effect on this phenomenon. The cavity opening influenced the load distribution considerably: in the cases of the progressive process, the load could transfer from the cavity area to the anchorage area more than the cases of the downward opening.

Table 5.1. Summary of influenced factors on load transfer efficiency

Impacts		***Influences***
Cavity opening modes		Mode B > Mode A
H/D ratios		Efficiency increases when H/D increases
Cavity diameter (with given H/D ratios)		No effect
Geosynthetic stiffness		No effect
Surcharge	Fill	Program 2 > Program 1
	Load	Program 1 > Program 2

In the present study, the experimental tests, as well as numerical simulations, have approached the surcharge effect on the geosynthetic reinforcement behavior above a granular embankment. Both studies considered uniform loads applied on the embankment when the beneath cavity already exists, even if the principle is not precisely similar. In the experimental tests, the surcharge is formed by adding cylinders in which is filled by sand. Due to the fact that the arching effect occurs within the additional soil fills, the efficiency of the load transfer is greater than the usual tactic of the embankment formation. In the

numerical study, the additional load is simulated as a surcharge without the effect of arching; thus, the load transfer in Program 2 is less effective than Program 1.

5.3. DEFLECTION BEHAVIORS

5.3.1. Shape of subsidence zone

The forms of the subsidence zones in the embankment have been investigated considering the curves of the surface settlements and the geosynthetic deflections. The subsidence zones have a cylindrical shape, with a low opening-angle. A new method has been proposed to fit the shape of the surface settlements and geosynthetic deflections as a Gaussian model and a 4th-degree polynomial fit, respectively. Although this method is better to match the shapes, the current method requires a rapid calculation procedure and provide safer values for the design.

5.3.2. Influences on vertical displacements

The surface settlements of overlying soils decrease for an increase of H/D ratios. The values in the case of Mode A are lower than Mode B. Using a stiffer reinforced material can lead to lower vertical displacement, whereas the progressive opening of the cavity causes a greater deflection of the geosynthetics.

5.3.3. Geosynthetic strain

The geosynthetic strain after the cavity opening was computed by the numerical models and compared with the analytic values obtained from the method of *Giroud (1995)*. The difference due to the cavity-opening mode was also illustrated as in the case of the downward opening. The analytic results are in good accordance with the numerical results, whereas an overestimation can be noted for the progressive opening. Therefore, an assumption of the analytical method relevant to the shape of the deflected geosynthetic needs to be developed more precisely.

Moreover, the influence of the cavity-opening mode on the shape of the geosynthetic deflections has been illustrated in the study. An agreement between the laboratory tests and the numerical simulations has been provided as in the cases of the gradual downward opening, the shape of the geosynthetic deflections can be modeled an inverted parabolic, and a cone shape can be seen on the cases of the progressive opening.

5.3.4. Equal settlement plane

According to the arching theory of *Terzaghi (1946)*, a plane of the equal settlement exists when the H/D ratio reaches 2.5. When the embankment height is larger than a given value as a critical height, H_c, the stress distribution is not affected by the presence of the underneath void. However, as the present study illustrated, H_c is not uniform, and it can be affected by many parameters. Indeed, the experimental tests demonstrated that H_c values are strongly dependent on the cavity opening process, the granular soils used. The numerical modeling has permitted to correct the procedure to determine the H_c used in the experimental analysis. The H/D ratios values, which the equal settlement plane can occur, varied from 1.8 to 2.5, and are lower than the suggestion of *Terzaghi (1946)*. As a significant result, the surface settlement behavior and H/D ratios is not linear, and the type of filling soil is very important.

5.4. SOIL EXPANSION COEFFICIENT

No formulation has been established to determine precisely the value of the soil expansion coefficient due to the fact that this parameter depends on many influences. The soil expansion mechanism with the opening process has been significantly illustrated by the results of both numerical and experimental studies. In fact, the soil expansion mechanisms are not uniform within the granular embankment. They depend on cavity appearances and various geometric characteristics. The average values of the expansion coefficient, for a cavity diameter of 0.5 m is presented in *Table 5.2*.

Table 5.2. Average expansion coefficient with the cavity diameter = 0.5 m

Soils	***Fine sand***		***Coarse sand***	
Cavity opening	*Mode A*	*Mode B*	*Mode A*	*Mode B*
Higher-stiffness GSY	1.014	1.020	1.019	1.026
Lower-stiffness GSY	1.025	1.032	1.028	1.045

The Ce values calculated for Mode A seem to be lower than for Mode B, the conclusions are confirmed by taking into account the different tested configurations such as the geosynthetics and soil types. By considering the change in the void ratios and the deviatoric strain within the soils overlying, the cavity opening modes influence is also illustrated. The H/D ratios seem not to affect the soil expansion; the behavior is not demonstrated clearly, as it fluctuated between the experimental tests.

Comparing to the two-tested geosynthetics, the use of stiffer materials reduce the expansion coefficient values.

Moreover, the density effect is illustrated by the experimental works, as dense soils could reduce the surface settlements. Additionally, a significant agreement between numerical and laboratory tests can be illustrated considering the positive relevance between the density (experiment) and dilatancy angle (numerical tests) of soil. The increase in both parameters values allows the expansion coefficient to increase.

Additionally, the experimental works considered two different models to determine the expansion coefficient. The values of Ce_2 found by the measurement method was systematically higher than the coefficient Ce_1 used in the existing design methods: *RAFAEL (Giraud, 1997)*, *EBGEO (1997, 2011)*. The assumption of parabolic shapes for the geosynthetic deflection and the soil settlement could be applied since it leads to a safe design, but it has to be improved to take into account the granular layer characteristics.

5.5. DESIGN PROCEDURE

According to the results illustrated in the study, regarding the recommendations suggested by *Villard et al. 2016*, a proposed procedure could be followed to design the geosynthetic reinforcement granular embankment overlying the cavity could be proposed. Three main steps consist:

- Cavity characteristics estimation
- Mechanical parameters measurement
- Geosynthetic tensile stiffness determination

The proposed values for the design such as the surface settlement or tensile force are necessary to compare with the allowable values. With the popularity and the ability to investigate most necessary parameters, numerical simulations can figure out results fast and will allow various attempts until finding the most elegant solution.

5.5.1. Cavity characteristics estimation

The purpose of the first step is to investigate or estimate the void expressions: a plane strain or an axisymmetric configuration, the cavity opening process, the possible embankment height and the size of the cavity, where the diameter should be considered, the accurate estimation could be prevented by engineering geological investigations or geologic data.

As significant results obtained from the study, the cavity opening process is one of the most considerable influences on the deformations of the embankment, the geosynthetic deflection, and the load distribution. The main result of the experimentation is that a progressive opening leads to a more critical settlement compared to the trapdoor. Thus, it is recommended to consider this cavity-opening mode, which is more conservative for the design, even if it was demonstrated that this opening mode could not occur.

Regarding the effect of the width of the circular cavity, it can be noted that considering only H/D ratio is not sufficient to estimate precisely the expansion coefficient as this parameter can be varied when the cavity becomes wider.

5.5.2. Mechanical parameters measurement

A variety of mechanical parameters can influence the mechanisms or behaviors of the geosynthetic-reinforced embankments above the cavity as the main results of the present study. For the main parameters characterized for fill materials, laboratory tests could be used. Otherwise, for the other parameters, which cannot be determined by functions or experimental tests, such as the expansion coefficient and the stress ratio, referenced values proposed by the present study could be selected.

5.5.3. Geosynthetic tensile stiffness determination

The last design step is to determine a required value of the geosynthetic tensile stiffness. Based on the analytical method proposed by *Villard and Briançon (2008)* with the suggestions presented by *Villard et al. (2016)* and new improvements from this study, the determination of the required parameter should be considered such as the cavity opening process as it can be affected by the shape of the load distribution and the deflected geosynthetic.

CHAPTER 6. CONCLUSIONS

6.1. EXPERIMENTAL APPROACH

The system of an embankment reinforced by geosynthetic above voids has been simulated by a novel laboratory device. As an essential benefit, the design of the apparatus allows for changing many configurations for laboratory testing. More than 80 tests were performed considering the variation of the embankment height, the properties of fills, the kind of geosynthetics and the methods to process the cavity. This study is one of the first research considering a precise method for monitoring the vertical displacement of surface soil and geosynthetic, by using specific distance sensors. This is also the primary investigation that the load distribution along the geosynthetic sheet can be observed directly by a tactile pressure sensor.

A variety of influences has been found to improve the knowledge of the expansion and load distribution mechanisms. The process of the cavity opening, which is not considered in any conventional methods, is being proven as the most crucial factor that can affect the subsidence zone in the embankment. This influence also effects on the feature of the load distribution on the geosynthetic after the cavity opening, as well as the efficiency of the load transfer.

In many design guidance, the expansion coefficient is assumed as a uniform factor. This is negated due to this factor is impacted by most experimental elements. The different methods to calculate the expansion coefficient of soil has been taken into account. It is shown that the assumption of the deformation shapes can change the value of the soil expansion coefficient. Using the tactile sensor at different places on the geosynthetic illustrates that after the opening, the load acting on the sheet is not uniform. Especially, to improve the understanding of the load distribution, two test programs were tested considering different processes to procedure the embankment above the cavity. This suggests the difference in the behavior of the existing and evolving cavity under the load formed by the embankment.

As a less significant influence, the ratio H/D defined by the embankment and the cavity diameter can affect the settlement of the surface soils. The other impact factors can be listed as the geosynthetic stiffness and the density.

6.2. NUMERICAL APPROACH

A computer program, PLAXIS 2-D has been used in the numerical part of this thesis. In order to clarify and develop the results obtained from the laboratory part, a series of numerical

models has been performed using the Mohr-Coulomb failure criterion and the Hardening soil constitutive model. The essential element, the cavity-opening processes, which the influence has been found by the laboratory tests, have been reproduced successfully in the Finite element models. Based on the benefit of the program computing as reducing the trial time and the ability to vary the test configurations, additional parameters that can influence on the behavior of the study systems were investigated, in particular, the void ratio of filled soils or the kind of embankment material.

Most conclusions remarked in the experimental part, such as the cavity opening, the H/D ratios, the geosynthetic stiffness, the friction angle of overlying soil have been confirmed by the numerical study as the kinematic behavior of the embankment and the load distribution on the geosynthetic. In addition, due to the parametric study, many other parameters have been illustrated for their influences on the considered mechanisms in the study, such as the cavity diameter, the dilatancy of overlying soil, the pressure ratio or the surcharge.

As a limit of the present work, the precise relation between Ce and the properties of the overlying has not yet proposed. Although the rough values of expansion coefficient of soil computed numerically are not far from those obtained by the laboratory tests, the tendency in changing with H/D ratios has not yet imitated for this factor, as the values are not homogenous. This shows the complexity to simulate the experimentation for the coefficient in PLAXIS perfectly.

Nevertheless, the success of using FEM program on simulating the laboratory tests may provide a useful tool for designing the geosynthetic reinforcement in this field. Thereby, the shortcomings of the existing analytical design methods, which was demonstrated in the thesis, could be solved.

6.3. RECOMMENDATIONS

The problematic of the embankment reinforced by geosynthetic above void includes the complex interaction of many factors such as the arching effect, the characteristics of the overlying soil, the properties of the cavity, the response of geosynthetic materials and any interaction occurs within the embankment. Even the knowledge of the complex mechanisms existing within the platform of the geosynthetic-reinforced over hidden cavity has been improved significantly in this study, a new function to determine the expansion coefficient from the granular material characteristics cannot yet been proposed. Advance laboratory tests

ought to be performed with more different kinds of overlying soils. In addition, the suitability of the apparatus with treated soils could be considered. Additional influenced parameters, which have been illustrated in the numerical part, in particular, the effect of the cavity diameter should be validated by the laboratory device. For further studies to improve the load distribution understanding, a more precise tactile sensor, which can deal with lower stress, can be considered.

The numerical results showed the similarity of the results with the different method based on DEM, even if the simple models were applied to simulate the behavior of the overlying soils. Notwithstanding, other complex soil models, which can reflect more accurately the behavior of the granular fill may be used to improve the analysis results, especially the expansion mechanisms. Another numerical method, the Finite difference method, for example, can be an interesting technique in order to clarify the present numerical results, with a different perspective.

REFERENCES

Alexiew, D. A., 1997. Bridging a sinkhole by high-strength high-modulus geogrids. In: Proceedings of the Geosynthetics'97 Conference, Long Beach, California, USA, vol. 1, pp. 13-24.

Aubertin, M., Li, L., Arnoldi, S., 2003. Interaction between backfill and rock mass in narrow stopes, in: Soil and Rock America. pp. 1–8.

Benmebarek, S., Berrabah, F., Benmebarek, N., 2015. Effect of geosynthetic reinforced embankment on locally weak zones by numerical approach. Comput. Geotech. 65, 115–125.

Bolton, M. D., 1986. The strength and dilatancy of sands. Géotechnique 36, No. 1, 65-78.

Blivet, J. C, Gourc, J. P, Villard, P., Giraud, H., Khay, M., Morbois A., 2002. Design method for geosynthetic as reinforcement for embankment subjected to localized subsidence. Geosynthetics State of the art recent developments. Proceeding of the seventh international conference on geosynthetics. 7 ICG-Nice, France. 1, 341–344.

Briançon L., Villard P. 2006. Dimensionnement des renforcements géosynthétiques de plates-formes sur cavités. Revue Française de Géotechnique, n° 117, 4° trimestre 2006, pp 51-62.

Briançon, L., Girard, H., Gourc, J. P., 2011. A new procedure for measuring geosynthetic friction with an inclined plane. Geotext. Geomembranes 29, 472–482.

Briançon, L., Villard, P., 2008. Design of geosynthetic-reinforced platforms spanning localized sinkholes. Geotext. Geomembranes 26, 416–428.

Brocklehurst, C. J., 1993. Finite element studies of reinforced and unreinforced two-layer soil systems. PhD Thesis, University of Oxford, UK.

British Standard Institute, 2010, BS8006 - Code of practice for strengthened/reinforced soils and other fills, 2010.

Chalak, C., Briançon, L., Villard, P., 2019. Coupled numerical and experimental analyses of

load transfer mechanisms in granular-reinforced platform overlying cavities. Geotext. Geomembranes, article in press.

Chen, R. X., Zhu, B., Chen, Y. M., Chen, R. P., 2010. Modified Terzaghi loosening earth pressure based on theory of main stress axes rotation. Rock Soil Mech. 31 (5), 1402-1406. (In Chinese)

Chevalier, B., Combe, G., Villard, P., 2012. Experimental and discrete element modeling studies of the trapdoor problem: Influence of the macro-mechanical frictional parameters. Acta Geotech. 7, 15–39.

Costa, Y., Zornberg, J., Bueno, B., Costa, C., 2009. Failure mechanisms in sand over a deep active trapdoor. J. Geotech. 135, 1741–1753.

Cui, K., Défossez, P., Richard, G., 2007. A new approach for modelling vertical stress distribution at the soil/tyre interface to predict the compaction of cultivated soils by using the PLAXIS code. Soil Tillage Res. 95, 277–287.

EBGEO, 1997. Empfehlungen für bewehrungen aus geokunststoffen. Deutesche Gesellschaft für Geotechnik (Hrsg). Verlag Ernst Sohn, Berlin.

EBGEO, 2011. Recommendations for design and analysis of earth structures using geosynthetic reinforcements, ISBN 978-3-433-60093-1.

Feng, S. J., Ai, S. G., Chen, H.X., Xie, H. J., 2017. An analytical method for predicting load acting on geosynthetic overlying voids. Geotext. Geomembranes 45, 570–579.

Feng, S. J., Ai, S. G., Chen, H.X., 2017. Estimation of arching effect in geosynthetic-reinforced structures. Comput. Geotech. 87, 188–197.

Feng, S. J., Lu, S. F., 2015. Deformation analysis of a geosynthetic material subjected to two adjacent voids. Geotext. Geomembranes 43, 317–331.

Galve, J. P., Gutiérrez, F., Guerrero, J., Alonso, J., Diego, I., 2012. Optimizing the application of geosynthetics to roads in sinkhole-prone areas on the basis of hazard models and cost-benefit analyses. Geotext. Geomembranes 34, 80–92.

Giraud, H., 1997. Renforcements des zones d'effondrement localisé - Modélisations physique et numérique. PhD Thesis, University of Grenoble, France.

Giroud, J. P., Bonaparte, R., Beech, J. F., Gross, B. A., 1990. Design of soil layer-geosynthetic systems overlying voids. Geotext. Geomembranes 9, 11–50.

Giroud, J. P. 1995. Determination of geosynthetic strain due to deflection. Geosynthetic International, Vol. 2, n°3, pp 635-641.

Girout, R., Blanc, M., Dias, D., Thorel, L., 2014. Numerical analysis of a geosynthetic-reinforced piled load transfer platform - Validation on centrifuge test. Geotext. Geomembranes 42, 525–539.

Gutiérrez, F., Parise, M., De Waele, J., Jourde, H., 2014. A review on natural and human-induced geohazards and impacts in karst. Earth-Science Rev. 138, 61–88. 2

Han, J., Gabr, M., 2002. Numerical analysis of geosynthetic-reinforced and pile-supported earth platforms over soft soil. J. Geotech. Geoenvironmental Eng. 128, 44–53.

Handy, R. L., 1985. The Arch in Soil Arching. J. Geotech. Eng. 111 (50), 302–318.

Hird, C. C., Kwok, C. M., 1990. Finite element studies of interface behaviour in reinforced embankments on soft ground. Comput. Geotech. 8, 111–131.

Huang, J., Le, V., Bin-Shafique, S., Papagiannakis, A. T., 2015. Experimental and numerical study of geosynthetic reinforced soil over a channel. Geotext. Geomembranes 43, 382–392.

Huckert, A., Briançon, L., Villard, P., Garcin, P., 2016. Load transfer mechanisms in geotextile-reinforced embankments overlying voids: Experimental and analytical approaches. Geotext. Geomembranes 44, 442–456.

Iglesia, G.R., Einstein, H.H., Whitman, R.V., 2014. Investigation of Soil Arching with Centrifuge Tests. J. Geotech. Geoenvironmental Eng. 04013005, 1–13.

IGS (International Geosynthetics Society), 2018. Geosynthetics classification, prepared by R.J. Bathurst. Technical note. The International Geosynthetics Society.

Jennings, K., Naughton, P. J., 2012. Similitude Conditions Modeling Geosynthetic-Reinforced Piled Embankments Using FEM and FDM Techniques. ISRN Civ. Eng. 2012, 1–16.

Kempton, G.T., Lawson, C.R., Jones, C.J.F.P., Demerdash, M., 1996. The use of geosynthetics to prevent the structural collapse of fills over areas prone to subsidence. In: De Groot, Den Hoedt, Termaat (Eds.), Proceedings of the First European Conference on Geosynthetics: Applications, Design and Construction, Maastricht 1996. Balkema, pp. 317-324.

Kinney, T. C., 1986. Reinforced roads bridging vVoids. In: Proceedings of the Fourth International Conference on Cold Regions Engineering, ASCE, Anchorage. American Society of Civil Engineers, New York, pp. 320-329. February 24-26 1986.

Lee, J., Salgado, R., 2002. Estimation of footing settlement in silty soils. Int. J. Geomech. 2, 1–28.

Nagy, A. C., Moldovan, D. V., Ciotlaus, M., Muntean, L. E., 2017. Evaluation of experimental and numerical simulation of triaxial geogrid reinforcement on the strength of road structures. Procedia Eng. 181, 472–479.

Paikowsky, S. G., Rolwes, L. E., Tien, S. H., 2003. Visualization and measurements of stress around a trap door. Proc. Soil Rock Am. 1, 22–26.

Palmer, M. C., O'Rourke, T. D., Olson, N. A., Abdoun, T., Ha, D., O'Rourke, M. J., 2009. Tactile pressure sensors for soil-structure interaction assessment. J. Geotech. Geoenvironmental Eng. 135, 1638–1645.

Pardo, G.S., Sáez, E., 2014. Experimental and numerical study of arching soil effect in coarse sand. Comput. Geotech. 57, 75–84.

Pizá, C.G., 2009. Geosynthetic reinforced fill to bridge voids. Master Thesis, Imperial College London, UK.

PLAXIS, 2016. PLAXIS 2-D Manuals. ISBN-13: 978-90-76016-20-7, Netherlands.

Poorooshasb, H.B., 2002. Subsidence evaluation of geotextile - reinforced gravel mats

bridging a sinkhole. Geosynth. Int. 9, 259–282.

Potts, J., 2007. Geosynthetic reinforced fill as a load transfer platform to bridge voids. PhD Thesis, University of London, UK.

Potts, V.J., Zdravkovic, L., 2010. Finite-element study of arching behaviour in reinforced fills. Proc. Ice-gr. Improv. 163, 217–229.

Potts, V. J., Zdravkovic, L., 2008. Assessment Of BS8006:1995 Design method for reinforced fill layers above voids. EuroGeo4 1–7.

Rui, R., Van Tol, A. F., Xia, Y. Y., Van Eekelen, S. J. M., Hu, G., 2016. Investigation of soil-arching development in dense sand by 2D model tests. Geotech. Test. J. 39, 415–430.

Rui, R., van Tol, F., Xia, X. L., Van Eekelen, S., Hu, G., Xia, Y. Y., 2016. Evolution of soil arching; 2D DEM simulations. Comput. Geotech. 73, 199–209.

Schanz, T., Vermeer, P. A., Bonnier, P. G., 1999. The Hardening soil model: Formulation and verification. Estud. Front. 281-296.

Schwerdt, S., Naciri, O., Jenner, C. G., 2004. Performance of aggregates in geogrid-reinforced soils used for protection against surface collapse into underground voids, in: 3rd European Geosynthetics Conference. pp. 483–487.

Shukla, S. K., Sivakugan, N., 2009. A general expression for geosynthetic strain due to deflection. Geosynth. Int. 16, 402–407.

Tahmasebipoor, A., Noorzad, R., Shooshpasha, E., Barari, A., 2010. A parametric study of stability of geotextile-reinforced soil above an underground cavity. Arab. J. Geosci. 5, 449–456.

Tano, B. F. G., Stoltz, G., Touze-Foltz, N., Dias, D., Olivier, F., 2017. A numerical modelling technique for geosynthetics validated on a cavity model test. Geotext. Geomembranes 45, 339–349.

Tencate, 2010. Reinforced soil case studies. Technical note. TenCate Corporate.

Texinov, 2018a. Sécurisation de terrain sur carrière souterraine. Technical note. Texinov Company.

Texinov, 2018b. Earthfill over mine areas. Technical note. Texinov Company.

Terzaghi, K., 1936. Stress distribution in dry and saturated sand above a yielding trap-door. Proc., 1st International Conference on Soil Mechanics and Foundation Engineering, Cambridge, Mass., 307–311.

Terzaghi, K., 1943. Theoretical soil mechanics. John Wiley Sons, Inc.

Van Eekelen, S. J. M., 2015. Basal reinforced piled embankments, experiments, field studies and the development and validation of a new analytical design model. PhD Thesis, Technische Universiteit Delft, Netherlands.

Vardoulakis, I., Graf, B., Gudehus, G., 1981. Trap-door problem with dry sand: A statical approach based upon model test kinematics. Int. J. Numer. Anal. Methods Geomech. 5, 57–78.

Vasquez, A. F. S., 2014. Numerical study of the arching - Effect using the discrete element method. Master Thesis, Pontificia Universidad Catolica De Chile, Chile.

Viana, P. M. F., Bueno, B. S., Paulo, S., Carlos, S., Costa, Y. D., Rural, F., 2008. A Simplified Method to Predict Vertical Displacements , Deformations and Tensile Stress in Geosynthetics Overlying Voids, in: The First Pan American Geosynthetics Conference & Exhibition. pp. 1218–1226.

Villard, P., Briançon, L., 2008. Design of geosynthetic reinforcements for platforms subjected to localized sinkholes. Can. Geotech. J. 45, 196–209.

Villard, P., Chevalier, B., Le Hello, B., Combe, G., 2009. Coupling between finite and discrete element methods for the modelling of earth structures reinforced by geosynthetic. Comput. Geotech. 36, 709–717.

Villard, P., Gourc, J. P., Giraud, H., 2000. A geosynthetic reinforcement solution to prevent the formation of localized sinkholes. Can. Geotech. J. 37, 987–999.

Villard, P., Huckert, A., Briançon, L., 2016. Load transfer mechanisms in geotextile-reinforced embankments overlying voids: Numerical approach and design. Geotext. Geomembranes 44, 381–395.

Wang, M. C., Feng, Y. X., Jao, M., 1996. Stability of geosynthetic-reinforced soil above a cavity. Geotext. Geomembranes 14, 95–109.

XP G 38063-2, 2019. T2 Renforcement de la base de remblais sur zones à risques d'effondrements. being proposed.

Yu, Y., Bathurst, R. J., 2017. Influence of selection of soil and interface properties on numerical results of two soil-geosynthetic interaction problems. Int. J. Geomech. ASCE 17, 1–16.

Yu, Y., Damians, I. P., Bathurst, R. J., 2015. Influence of choice of FLAC and PLAXIS interface models on reinforced soil-structure interactions. Comput. Geotech. 65, 164–174.

Zhu, B., Gao, D., Li, J., Chen, Y., 2012. Model tests on interaction between soil and geosynthetics subjected to localized subsidence in landfills. J. Zhejiang Univ. Sci. A 13, 433–444.

Ziegler, M., 2017. Application of geogrid reinforced constructions: History, recent and future developments. Procedia Eng. 172, 42–51.

APPENDIX A

Table A.1. Results of displacements and expansion coefficient

N°	***Test notation***	***H/D***	***Density***	***Opening mode***	***ds (mm)***	***dg (mm)***	***Ce (Model 1)***	***Ce (Model 2)***
Test 30	W/SF	0.5	1.41	B	51	57	1.013	1.027
Test 32	W/SF	0.5	1.41	B	38	50	1.024	1.032
Test 33	W/SF	0.5	1.41	B	38	45	1.015	1.035
Test 54	W/SF	0.5	1.56	B	10	35	1.050	1.071
Test 5	W/SF	1.0	1.40	B	22	41	1.019	1.026
Test 57	W/SF	1.0	1.43	B	16	41	1.025	1.042
Test 31	W/SF	1.5	1.39	B	10	44	1.023	1.016
Test 29	W/SF	0.5	1.41	A	22	32	1.019	1.026
Test 37	W/SF	0.5	1.41	A	28	37	1.018	1.043
Test 14	W/SF	0.5	1.40	A	19	30	1.023	1.044
Test 15	W/SF	1.0	1.38	A	14	32	1.018	1.025
Test 16	W/SF	1.5	1.39	A	6	27	1.014	1.016
Test 55	W/SF	0.5	1.57	A	17	23	1.013	1.035
Test 56	W/SF	1.0	1.44	A	16	32	1.016	1.029
Test 26	N/SF	0.5	1.40	B	72	81	1.019	1.036
Test 27	N/SF	0.5	1.42	B	65	78	1.025	1.041
Test 41	N/SF	1.0	1.39	B	45	68	1.023	1.028
Test 43	N/SF	1.5	1.39	B	17	65	1.032	1.029

Test 28	N/SF	0.5	1.39	A	36	55	1.037	1.041
Test 45	N/SF	1.0	1.39	A	28	54	1.034	1.067
Test 44	N/SF	1.5	1.39	A	14	45	1.021	1.028
Test 11	W/SC	1.0	1.5	B	13	42	1.029	1.017
Test 12	W/SC	0.5	1.5	B	26	45	1.037	1.059
Test 35	W/SC	0.5	1.6	B	25	41	1.032	1.061
Test 39	W/SC	0.5	1.6	B	9	34	1.049	1.069
Test 40	W/SC	0.5	1.6	B	11	36	1.049	1.059
Test 34	W/SC	0.5	1.5	B	36	53	1.033	1.044
Test 13	W/SC	1.5	1.4	B	7	41	1.023	1.022
Test 36	W/SC	1.0	1.5	A	13	31	1.018	1.030
Test 20	W/SC	0.5	1.5	A	18	35	1.035	1.028
Test 53	W/SC	0.5	1.4	A	17	30	1.026	1.031
Test 22	W/SC	1.0	1.5	A	14	28	1.015	1.026
Test 51	W/SC	1.0	1.5	A	12	30	1.019	1.028
Test 23	W/SC	1.0	1.5	A	11	33	1.022	1.032
Test 21	W/SC	1.5	1.4	A	2	27	1.016	1.019
Test 52	W/SC	1.5	1.5	A	10	30	1.013	1.043
Test 42	N/SC	0.5	1.5	B	65	84	1.040	1.074
Test 46	N/SC	1.0	1.5	B	27	77	1.050	1.045

Test 47	N/SC	1.5	1.5	B	21	75	1.036	1.032
Test 48	N/SC	0.5	1.5	A	32	50	1.037	1.060
Test 49	N/SC	1.0	1.5	A	28	52	1.024	1.037
Test 50	N/SC	1.5	1.5	A	18	52	1.023	1.024
Test 6	W/G	0.5	1.35	B	27	46	1.036	1.055
Test 38	W/G	0.5	1.32	B	27	42	1.032	1.036
Test 7	W/G	1.0	1.29	B	21	44	1.023	1.022
Test 8	W/G	1.5	1.31	B	14	47	1.022	1.033
Test 17	W/G	0.5	1.34	A	23	29	1.012	1.009
Test 18	W/G	1.0	1.32	A	17	29	1.012	1.026
Test 19	W/G	1.5	1.30	A	8	36	1.019	1.028

APPENDIX B

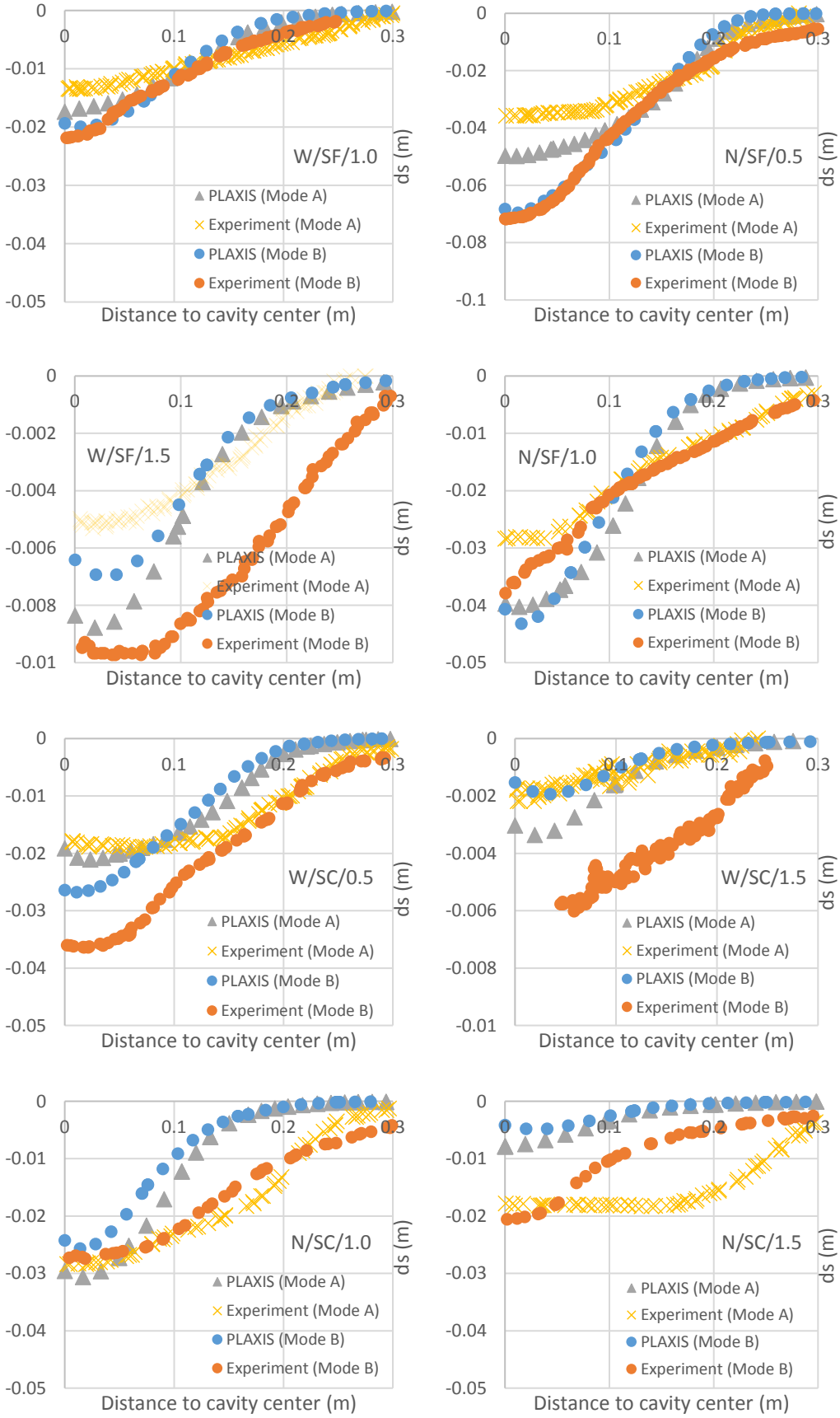

Figure A.1. Surface settlement: Experimental and numerical results

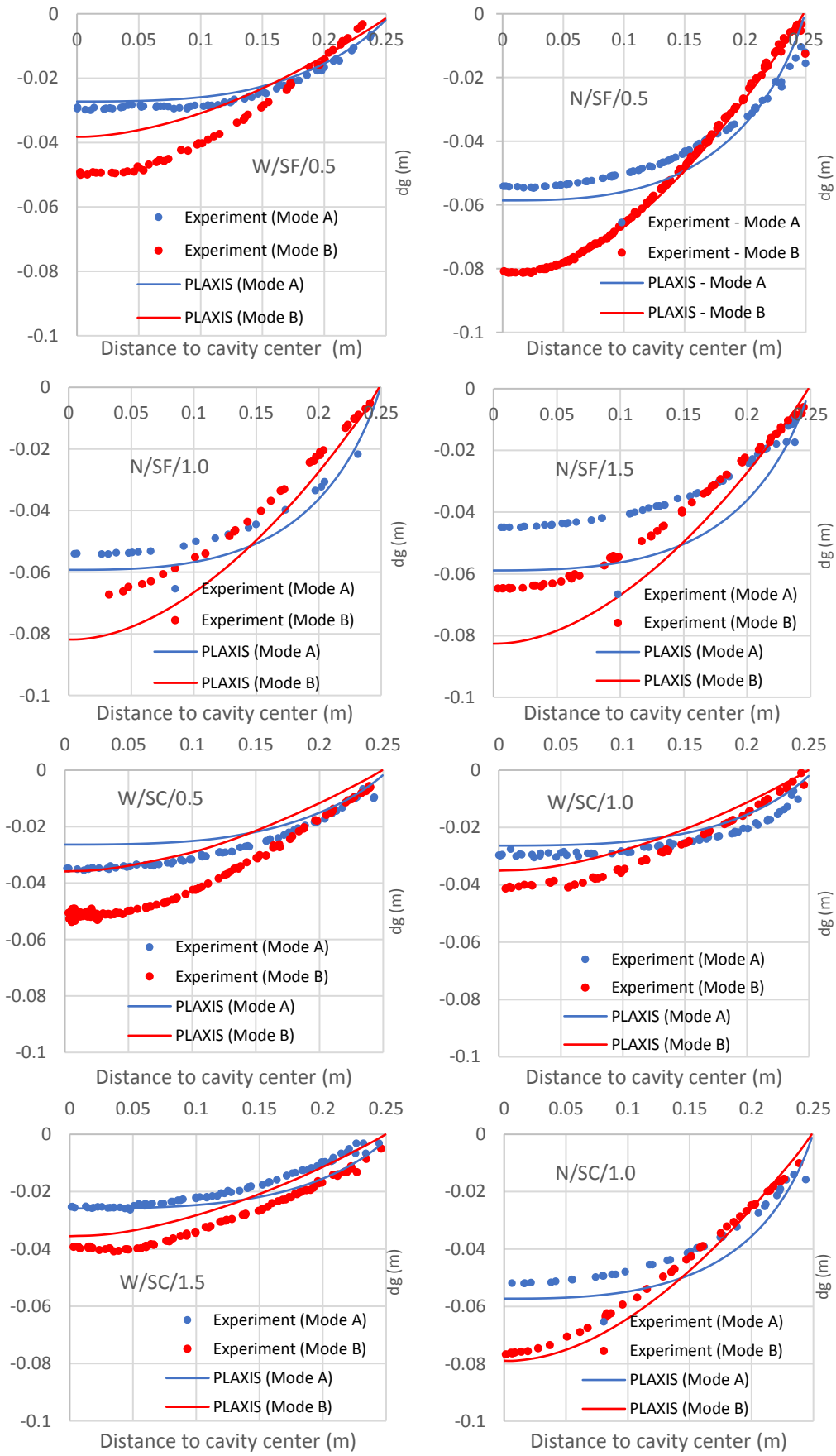

Figure A.2. Deflected geosynthetics: Experimental and numerical results